COVID-19 GLOBAL PANDEMIC: ANALYSIS OF SECONDARY METABOLITES FROM NATURAL PRODUCTS TO AID THE ENGINEERING OF DRUGS

A THESIS SUBMITTED TO THE

CENTRAL DEPARTMENT OF CHEMISTRY

INSTITUTE OF SCIENCE AND TECHNOLOGY

TRIBHUVAN UNIVERSITY

NEPAL

FOR THE AWARD OF

DOCTOR OF PHILOSOPHY

IN CHEMISTRY

BY

ASMITA SHRESTHA

AUGUST 2024

COVID-19 GLOBAL PANDEMIC: ANALYSIS OF SECONDARY METABOLITES FROM NATURAL PRODUCTS TO AID THE ENGINEERING OF DRUGS

A THESIS SUBMITTED TO THE

CENTRAL DEPARTMENT OF CHEMISTRY

INSTITUTE OF SCIENCE AND TECHNOLOGY

TRIBHUVAN UNIVERSITY

NEPAL

FOR THE AWARD OF

DOCTOR OF PHILOSOPHY

IN CHEMISTRY

BY

ASMITA SHRESTHA

AUGUST 2024

TRIBHUVAN UNIVERSITY

Institute of Science and Technology

DEAN'S OFFICE

Kirtipur, Kathmandu, Nepal

Reference No.:

Institute of Science & Technology
Dean's Office
Kirtipur 2045

EXAMINERS

The Title of Ph.D. Thesis: "COVID-19 Global Pandemic: Analysis of Secondary Metabolites from Natural Products to Aid the Engineering of Drugs"

Name of Candidate: Asmita Shrestha

Internal Examiner:

Dr. Bindra Shrestha
Tri-Chandra Multiple Campus
Tribhuvan University, NEPAL

External Examiners:

(1) Prof. Dr. Rajendra Joshi
School of Science
Kathmandu University
Dhulikhel, NEPAL

(2) Dr. Pankaj Wadhwa
School of Pharmaceutical Sciences
Lovely Professional University
Punjab, INDIA

(3) Dr. Sailesh Malla
Strain Improvement Department
Copenhagen, DENMARK

September 04, 2024

(Dr. Surendra Kumar Gautam)
Asst. Dean

DECLARATION

Thesis entitled **"COVID-19 Global Pandemic: Analysis of Secondary Metabolites from Natural Products to Aid the Engineering of Drugs"** which is being submitted to the Central Department of Chemistry, Institute of Science and Technology (IoST), Tribhuvan University, Nepal for the award of the degree of Doctor of Philosophy (Ph.D.) is a research work carried out by me under the supervision of Prof. Dr. Niranjan Parajuli of Central Department of Chemistry, Tribhuvan University and co-supervised by Dr. Salyan Bhattarai affiliated with Paraza Pharma, Inc., Montreal, Canada and Assoc. Prof. Dr. Khaga Raj Sharma of Central Department of Chemistry, Tribhuvan University. This research is original and has not been submitted earlier in part or full in this or any other form to any university or institute, here or elsewhere, for the award of any degree.

Asmita Shrestha

RECOMMENDATION

This is to recommend that **Asmita Shrestha** has carried out research entitled **"COVID-19 Global Pandemic: Analysis of Secondary Metabolites from Natural Products to Aid the Engineering of Drugs"** for the award of Doctor of Philosophy (Ph.D.) in **Chemistry** under our supervision. To our knowledge, this work has not been submitted for any other degree. She has fulfilled all the requirements laid down by the Institute of Science and Technology (IoST), Tribhuvan University, Kirtipur for the submission of the thesis for the award of a Ph.D. degree.

.....

Prof. Dr. Niranjan Parajuli
Supervisor
Professor
Central Department of Chemistry, Tribhuvan University,
Kirtipur, Kathmandu, Nepal

Central Department of Chemistry
T.U., Kirtipur

.....

Dr. Salyan Bhattarai
Co-Supervisor
Scientist
Paraza Pharma, Inc.
2525 Avenue Marie-Curie Montreal, QC, Canada

.....

Associate Prof. Khaga Raj Sharma
Co-Supervisor
Associate Professor
Central Department of Chemistry, Tribhuvan University,
Kirtipur, Kathmandu, Nepal

August 2024

त्रिभुवन विश्वविद्यालय
TRIBHUVAN UNIVERSITY
विज्ञान तथा प्रविधि अध्ययन संस्थान
Institute of Science and Technology
रसायन शास्त्र केन्द्रीय विभाग
CENTRAL DEPARTMENT OF CHEMISTRY
कीर्तिपुर, काठमाडौं, नेपाल
Kirtipur, Kathmandu, NEPAL

Central Department of Chemistry
T.U., Kirtipur

पत्र संख्या:
Ref. No.:

LETTER OF APPROVAL

Date: 04/09/2024

On the recommendation of Prof. Dr. Niranjan Parajuli (supervisor), Dr. Salyan Bhattarai (co-supervisor), and Associate Prof. Dr. Khaga Raj Sharma (co-supervisor), this Ph.D. thesis submitted by Asmita Shrestha, entitled **"COVID-19 Global Pandemic: Analysis of Secondary Metabolites from Natural Products to Aid the Engineering of Drugs"** is forwarded by Central Department Research Committee (CDRC) to the Dean, IoST, T.U.

Bhattarai
.....

Prof. Dr. Jagdeesh Bhattarai

Professor

Head

Central Department of Chemistry

Tribhuvan University

Kirtipur, Kathmandu, Nepal

Tel.: 977-1-4332034, Fax No.: +977-1-4330537, http://www.cdctu.edu.np e-mail: head@cdc.tu.edu.np

ACKNOWLEDGEMENTS

I'm extremely pleased and honored that I was able to capture some of the most memorable experiences during the work and study of my Ph.D. I would like to thank all the innumerable people whose love and support have enabled me to do this work. I owe a debt of gratitude to Prof. Dr. Niranjan Parajuli, my research supervisor and the professor of the Central Department of Chemistry, for allowing me an opportunity to complete my doctoral program under his careful supervision and guidance. His unmatched and exceptional advice, continuous inspiration, gracious collaboration, unwavering patience, constructive criticism, and boundless passion allowed me to finish my dissertation, for which I am incredibly grateful. My sincere gratitude to Dr. Salyan Bhattarai, my research co-supervisor and the scientist of Paraza Pharma, Canada for his constant support and advice. And I am thankful to Associate Prof. Dr. Khaga Raj Sharma, my thesis co-supervisor, associate professor of the Central Department of Chemistry for his guidance and support. Warm praises to Prof. Dr. Jagadeesh Bhattarai, Head of the Central Department of Chemistry, for his kind support. I am very grateful to the University Grants Commission (UGC) for providing me with financial support (Fellowship Award no.: Ph.D. -78/79-S&T-06) to carry out this research work. The part of this research was also funded by the UGC, Grant number CoV-76/77-02, so I am thankful to Prof. Dr. Ram Chandra Basnyat (PI). My deep sense of appreciation goes to Mr. Rishab Marahatha, Mr. Siddha Raj Upadhyaya, Mr. Bimal Kumar Raut, and Mr. Rabin Budhathoki for their inspiration and support. My sincere gratitude to Mr. Saroj Basnet for his guidance during my initial days.

It gives me great pleasure to express my profound gratitude, love, and respect to my parents (Mr. Sovit Lal Shrestha and Mrs. Tika Kumari Shrestha) and parents-in-law (Mr. Jit Bahadur Silwal and Mrs. Shanta Silwal) for their everlasting faith and pantheism, which have given me the courage and fortitude to confront the world fearlessly. With great pleasure, my beloved husband Mr. Manoj Silwal deserves special thanks for his unconditional love, inspiration, support, and prayers that helped me at every step of the road and enabled me to finish the research work on time. I am deeply grateful to my son, Master Samyak Silwal, for bringing joy and light into my life during this journey. Your laughter and love provided me with the motivation and resilience needed to navigate through the challenges of research and study. I am grateful to all my family members and friends for their constant support and inspiration during this journey.

Asmita Shrestha

सोध शार

कोभिड–१९ (COVID–19) रोगको सङ्क्रमण सार्स–कोभ–२ (SARS–CoV–2) नामक भाइरसको कारणले हुन्छ । जसले विश्वमा सन् २०१९ को अन्त्यबाट जटिल स्वास्थ्य समस्या सिर्जना गरेको थियो । पछिल्लो समय कोभिड–१९ को जोखिम विश्वमा कम भएता पनि यसको पुर्ण निवारण वा निर्मुल भएको अवस्था छैन । विभिन्न कारणले गर्दा सार्स–कोभ–२ मा म्युटेशन (एमिनो एसिडमा बदलाब हुने रसायनिक क्रिया) भई यसको नयाँ स्वरूपहरु (Variants) संसारमा देखा परिरहेका छन् । भाइरसको नयाँ स्वरूपले यसबाट हुने सङ्क्रमणको जोखिम कायम नै राखेको छ । त्यसैले यस विषयमा थप वैज्ञानिक अनुसन्धानको आवश्यकता रहेको देखिन्छ । सार्स–कोभ–२ मा हुने यस्तो म्युटेसनले चिकित्साशास्त्रका क्षेत्रमा थप चिन्ता र चासो थपेको छ । त्यसैले भरपर्दो एन्टिभाइरल औषधी वा खोपको विकास तर्फ अझै प्रगती गर्नु पर्ने देखिएको छ । वनस्पतीबाट भाइरस नियन्त्रणको लागि औषधीजन्य गुण भएका यौगिक पत्ता लगाउनु यस अनुसन्धानको प्रमुख उदेश्य हो किनकी वैज्ञानिकहरूले गरेका यस अगाडीका शोधले पनि त्यस्तो संभावना प्रष्टाएको छ ।

त्यस्ता यौगिकले सार्स–कोभ–२ को प्रोटिनमा के कस्तो रसायनिक गुण देखाउछ, सोको गहन खोजमा यो अध्ययन केन्द्रित गरिएको छ । जसको लागि यस अनुसन्धानमा फार्माकोकाइनेटिक्स अध्ययन (Pharmacokinetics study), मलिक्युलर डकिङ् (Molecular docking), मलिक्युलर सिमुलेशन (Molecular Dynamics Simulation), र डेन्सिटी फङसन सिद्धान्त (DFT) मा आधारित विश्लेषण विभिन्न कम्प्यूटेशनल सफ्टवेयरको माध्यमबाट गरिएको छ । यस अनुसन्धानमा वनस्पतीबाट निकालिएका १९१ वटा यौगिकमा सार्स–कोभ–२ को स्पाइक प्रोटिन (Spike Protein) र आरएनए–डिपेन्डेन्ट–आरएनए–पोलिमरेज (RdRp) मा कम्प्यूटेशनल अध्ययन गरिएको छ । मलिक्युलर सिमुलेशन नामक कम्प्युटेशन अनुसन्धानले यसको थप पुष्टी पनि गरेको छ । यस्तो सैध्दान्तिक अनुसन्धानलाई थप वैज्ञानिक आधारहरू प्रदान गर्न प्रयोगशालामा आधारित प्रोटिन एस्से (Protein assay)पनि गरिएको छ ।

इन सिलिको (*In silico*) अनुसन्धानको आधारमा, टिनोस्पोरा प्रजातिहरूबाट (*Tinospora species*)चयन गरिएका २६ secondary मेटाबोलाइटहरूमध्ये कर्डिफोलियोसाइड ए लाई (cordifolioside A) सबैभन्दा शक्तिशाली मानिएको छ । यसले (-२५.०९ kcal/mol) को उचित binding free energy, महत्त्वपूर्ण गोल्ड (GOLD) फिटनेस स्कोर, प्रतिक्रियाशीलता, उपयुक्त

फार्माकोकाइनेटिक प्रोफाइल (pharmacokinetic profile) र SARS–CoV–2 को लक्ष्य S1–RBD सँग पर्याप्त स्थिरता देखाएको छ । यस बाहेक, *Tinospora cordifolia* कच्चा एक्स्ट्रयाक्ट प्रयोग गरी इन भिट्रो (*in vitro*) सञ्चालन गरिएको थियो किनभने यसमा कर्डिफोलियोसाइड ए को उपयुक्त मात्रा हुन्छ, यसले SARS–CoV–2 को S1–RBD सँग मानव एन्जियाटेन्सिन रूपान्तरण गर्ने इन्जाइम 2 (ACE2) लाई लगभग १.२५ mg/mL को एकाग्रतामा ५० % ले बाइन्ड गर्न रोक्छ ।

३६ फ्लेभोनोइडहरू मध्ये, cyanidin, यसको पर्याप्त फार्माकोकाइनेटिक प्रोफाइल, उचित अन्तरक्रियाको साथ binding free energy (-२५.०९ kcal/mol) , ५१.९१ को गोल्ड फिटनेस स्कोर, S1–RBD संग यसको कम्प्लेक्सको उपयुक्त स्थिरता, र पर्याप्त प्रतिक्रियाशीलता। थप रूपमा, रातो अंगूर (*Vitis vinifera*) मा साइनिडिन (cyanidin) पाइने भएकोले, यसले SARS–CoV–2 को S1–RBD सँग मानव एन्जियोटेन्सिन रूपान्तरण गर्ने इन्जाइम 2 (ACE2) लाई लगभग १.२५ mg/mL को एकाग्रतामा ५० % ले बाइन्ड गर्न रोक्छ।

स्क्रिन गरी चयन गरिएका ७९ एल्कालोइडहरूमध्ये नेफेरिन (neferine) SARS–CoV–2 को RdRp र S1–RBD को अवरोधक भएको पाइयो । RdRp संग bind हुँदा neferine ले उपयुक्त स्थिरता र प्रतिक्रियाशीलता प्रदर्शन गर्यो, –५.०८३ को S-स्कोर र -९.१ kcal/mol को binding energy प्रदर्शन गर्दै नेफेरिनले SARS–CoV–2 Omicron भेरियन्टको S1–RBD मा मुख्य एमिनो एसिड अवशेषहरूसँग (amino acid residues) -७.६ kcal/mol को binding energy को साथ उल्लेखनीय अन्तरक्रिया पनि प्रदर्शन गऱ्यो र नेफेरिनको इन भिट्रो परीक्षणले S1-RBD सँग ९९.६० + ०.३२८ μg/mL को IC_{50} सँग स्वीकार्य बाइन्डिङ देखाउँछ ।

५० ट्रपिनहरू (terpenes) मध्ये, क्रिप्टोटानशिनोन (cryptotanshinone) S1–RBD ओमिक्रोन भेरियन्टको बलियो अवरोधकको रूपमा पत्ता लगाइएको छ, जसले स्थिरता, उचित फार्माकोकाइनेटिक प्रोफाइल, र लक्ष्य प्रोटीनको साथ राम्रो बन्धन सम्बन्ध (–७.६ kcal/mol) प्रदर्शन गर्दछ । इन सिलिको विश्लेषणको नतिजालाई प्रमाणित गर्दै २५.५ + ०.४६३ μg/mL को IC_{50} सँग, क्रिप्टोटान्सिनोनले SARS–CoV–2 Omicron भेरियन्टको S1–RBD सँग hACE 2 को बाइन्डिङ्लाई रोक्न सक्षम छ ।

यस अनुसन्धानले कोभिड–१९ को औषधी विकास गर्न प्रभावकारी र सुरक्षित उपचारहरूको खोजीमा महत्वपूर्ण योगदान प्रस्तुत गरेको छ ।

ABSTRACT

SARS-CoV-2 (Severe acute respiratory syndrome coronavirus 2), the pathogenic agent of Coronavirus (CoV) disease-19 (COVID-19), has wreaked havoc around the world since the end of 2019, underscoring the need for effective COVID-19 treatment. Even though COVID-19 is no longer a pandemic, research should still be done to find effective treatments for these potentially lethal CoVs because new and deadly CoVs can appear at any time and represent a threat of spreading new CoV pandemics. The frequent unfolding of new mutants of the virus may impose serious concerns again regarding the efficacy of therapeutic agents, therefore any advancement toward the development of potent antiviral medications is always critical. Since secondary metabolites have been used to cure several ailments, they could be useful in managing COVID-19. Quantitative understanding and characterization of dynamic molecular processes are key issues in modern biology and need sophisticated computational experimental methodologies to get molecular-level information on ligand-binding configurations, interactions, and dynamic conformational landscapes.

To better understand the basis of the activity of secondary metabolites with biological activity, this research incorporated the pharmacokinetics study, molecular docking, molecular dynamics simulations, binding free energy (BFE) calculation, and density functional theory (DFT) analyses utilizing different computational tools followed by spike protein assays. The study began with the selection of a diverse library of 191 metabolites relying on their antiviral properties known for their potential bioactivities. These metabolites were screened against key viral proteins: S1-RBD of spike (S) protein and RNA-dependent-RNA-polymerase (RdRp); involved in the viral entry, replication, and infection processes of SARS-CoV-2.

Based on *in silico* investigation, cordifolioside A was identified to be the most potent of the 26 secondary metabolites selected from *Tinospora* Species. It showed proper binding free energy of -25.09 kcal/mol, significant GOLD fitness score (58.27), reactivity, suitable pharmacokinetic profile along with considerable stability with target S1-RBD of SARS-CoV-2. Furthermore, the *in vitro* experiment using *Tinospora cordifolia* crude extract, which was conducted because it contains an appropriate quantity of cordifolioside A, revealed that it inhibits the binding of human angiotensin

converting enzyme 2 (hACE2) with S1-RBD of SARS-CoV-2 by 50 % at a concentration of approximately 1.25 mg/mL.

Of the 36 flavonoids, cyanidin was determined to be the more potent due to its adequate pharmacokinetic profile, binding free energy (-25.09 kcal/mol) with proper interactions, GOLD fitness score of 51.91, appropriate stability of its complex with S1-RBD, and sufficient reactivity. Additionally, as cyanidin is present in red grapes (*Vitis vinifera*), *in vitro* investigation is carried out on it and the findings indicate that it significantly interferes by 50 % at a concentration of approximately 1.25 mg/mL to the interaction of hACE2 with S1-RBD of SARS-CoV-2.

Neferine, an alkaloid, was found to be an inhibitor of RdRp and S1-RBD of SARS-CoV-2 among screened 79 selected compounds. Neferine exhibited the appropriate stability and reactivity when complexed with RdRp, exhibiting an S-score of -5.083 and a binding energy of -9.1 kcal/mol. Neferine also demonstrated notable interactions with key amino acid residues in S1-RBD of the SARS-CoV-2 Omicron variant, with a binding energy of -7.6 kcal/mol and *in vitro* assay of neferine shows its acceptable binding with S1-RBD accompanied by IC_{50} of 99.60 ± 0.328 µg/mL.

Among the 50 terpenes, cryptotanshinone was discovered to be a strong inhibitor of the S1-RBD Omicron variant, exhibiting stability, proper pharmacokinetic profile, and good binding affinity (-7.6 kcal/mol) with target protein. With an IC_{50} of 25.5 ± 0.463 µg/mL, cryptotanshinone was able to inhibit the binding of hACE 2 with S1-RBD of the SARS-CoV-2 Omicron variant, validating the results of the *in silico* analysis.

In conclusion, this thesis offers a comprehensive computational study for the identification of secondary metabolites with potential inhibitory effects against SARS-CoV-2. The results present a significant contribution to the search for effective and safe treatments for COVID-19. Further preclinical investigation is necessary to validate and optimize these promising metabolites as potential COVID-19 therapeutics.

Keywords: *Secondary Metabolites– DFT– Protein assays– Molecular docking– Pharmacokinetics Study– Molecular Dynamics Simulations*

LIST OF ACRONYMS AND ABBREVIATIONS

2D	: Two Dimensional
$3CL^{pro}$	: 3-Chymotrypsin-like Protease
3D	: Three Dimensional
ACE2	: Angiotensin-Converting Enzyme 2
ADMET	: Adsorption, Distribution, Metabolism, Excretion, and Toxicity
ARDS	: Acute Respiratory Distress Syndrome
BBB	: Blood Brain-Barrier
BFE	: Binding Free Energy
CADD	: Computer-Aided Drug Designing
CBV	: Coxsackie Virus
CNS	: Central Nervous System
COVID-19	: Coronavirus Disease 2019
CTD	: C-Terminal Domain
DENV	: Dengue Virus
DFT	: Density Functional Theory
EC_{50}	: Half-Maximal Effective Concentration
ELISA	: Enzyme-Linked Immunosorbent Assay
EV	: Enterovirus
FDA	: Food and Drug Administration
GOLD	: Genetic Optimization for Ligand Docking
HBA	: Hydrogen Bond Acceptor
HBD	: Hydrogen Bond Donor
H-Bond	: Hydrogen Bond
HBV	: Hepatitis B virus
HCoVs	: Human Coronavirus
HIV	: Human Immunodeficiency Virus
HOMO	: Highest Occupied Molecular Orbital
IC_{50}	: Half-Maximal Inhibitory Concentration
ICTV	: International Committee on Taxonomy of Viruses

LBDD	: Ligand-Based Drug Designing
LD_{50}	: Lethal Dose 50
LUMO	: Lowest Unoccupied Molecular Orbital
MD	: Molecular Dynamics
MERS-CoV	: Middle East Respiratory Syndrome Coronavirus
MM/GBSA	: Molecular Mechanics/Generalized Born Surface Area
MOE	: Molecular Operating Environment
M^{pro}	: Main Protease
NTD	: N-Terminal Domain
ORF	: Open Reading Frames
PDB	: Protein Data Bank
PDBQT	: Protein Data Bank, Partial Charge (Q), and Atom Type (T)
PL^{pro}	: Papain-like Protease
RB	: Rotatable Bonds
RCSB	: Research Collaboratory for Structural Bioinformatics
RdRp	: RNA Dependent RNA Polymerase
Rg	: Radius of Gyration
RMSD	: Root Mean Square Deviation
RMSF	: Root Mean Square Fluctuation
SARS-CoV	: Severe Acute Respiratory Syndrome Coronavirus
SARS-CoV-2	: Severe Acute Respiratory Syndrome Coronavirus 2
SASA	: Solvent Accessible Surface Area
SBDD	: Structure-Based Drug Designing
SBVS	: Structure-Based Virtual Screening
S-RBD	: Spike Receptor Binding Domain
TCM	: Traditional Chinese Medicine
TPSA	: Topological Polar Surface Area
VDss	: Steady State Volume Distribution
VOCs	: Variant of Concerns
WHO	: World Health Organization

LIST OF SYMBOLS

α	: Alpha
μM	: Micromolar
Å	: Angstrom
mL	: Millilitre
nm	: Nanometer
ns	: Nanosecond
ps	: Picosecond
β	: Beta
γ	: Gamma
δ	: Delta
Δ	: Delta

LIST OF TABLES

LIST OF FIGURES

TABLE OF CONTENTS

CHAPTER 1

1. INTRODUCTION

1.1 Severe Acute Respiratory Syndrome 2 (SARS-CoV-2)

The sudden emergence of SARS-CoV-2, which is responsible for the Coronavirus Disease 2019 (COVID-19), occurred in late 2019 in Wuhan, China. The global spread of the virus resulted in a pandemic, that profoundly affected public health, economies, and daily life worldwide. The major mode of transmission is through respiratory droplets, which are released when an infected individual coughs, sneezes, talks, or breathes heavily near others in proximity. COVID-19 symptoms range in severity and may consist of fever, cough, shortness of breath, fatigue, loss of taste or smell, sore throat, body aches, and in severe instances, pneumonia and organ failure. Generally, older adults and persons with pre-existing abnormal health conditions are at high risk of experiencing severe illness. To control the spread of the virus, various measures have been implemented, such as widespread testing, contact tracing, quarantine, and isolation protocols, social distancing, wearing masks, and the development and distribution of vaccines.

Previous epidemics of the 21st century were caused by viruses such as severe acute respiratory syndrome coronavirus (SARS-CoV) in 2002 and Middle East respiratory syndrome coronavirus (MERS-CoV) in 2012 hurting health and economy (Lvov *et al*., 2020) and now prevailing is SARS-CoV-2 emerged at the end of 2019. The disease was officially named COVID-19 by WHO on 12 February 2020 and the virus was named SARS-CoV-2 by the International Committee on Taxonomy of Viruses (ICTV), the Coronaviridae Study Group (CSG) of the International Committee on Taxonomy of Viruses, 2020. Since the disease originally arose in the seafood and animal market of Wuhan city, animal-human transmission was suspected but then gradually the infection was observed in the population outside the city and then in other countries as well. This creates a huge stir on its transmission route and human-human transmission was speculated (Habibzadeh & Stoneman, 2020). The cases soared through many countries over a few months, and on March 11, 2020, WHO declared COVID-19 as a global pandemic. Most of the patients caused by COVID-19 are susceptible to acute respiratory distress syndrome (ARDS). The disease is highly transmissible. Most of the countries

imposed a lockdown and travel was almost banned internationally and internally as well for months. According to WHO, as of 21 July 2024 over 775 million confirmed cases and more than seven million deaths have been reported globally https://www.who.int/publications/m/item/covid-19-epidemiological-update-edition-167.

1.1.1 SARS-CoV-2, Viral Etiology, and History

According to numerous investigations, SARS-CoV-2 was claimed as the group of *coronaviruses*, which has the largest single-stranded RNA virus genome to date measuring approximately 32 kilobases (kb). Coronaviruses are classified as part of the family Coronaviridae, subfamily Coronavirinae, and order Nidovirales. Coronavirinae comprised four different type of α-coronavirus, β-coronavirus, γ-coronavirus, and δ-coronavirus. It is believed that these groups of coronaviruses diverged from each other around 2400-3000 BC (Woo *et al*., 2012) and tend to infect distinct groups of animals (**Figure 1**) (Singh, D. & Yi, S. V. 2021). In 1937, coronavirus was first discovered in hens. Before the severe acute respiratory syndrome (SARS) outbreak in February 2003 (Fouchier *et al*., 2003), it was not regarded as being particularly dangerous to people. Before that, those with weakened immune systems were most commonly affected by the mild infections produced by the coronaviruses that humans spread (Su *et al*., 2016; Vaheri *et al*., 2013) (Zhou *et al*., 2018). Since 2002, β-coronaviruses have been responsible for three zoonotic outbreaks in China, including severe acute respiratory syndrome coronavirus (SARS-CoV) in 2002, Middle East respiratory syndrome (MERS-CoV) in 2012 (Zaki *et al*., 2012), and the most recent outbreak of SARS-CoV-2 at the end of 2019 (Cui *et al*., 2019). Apart from the mentioned ones, there are four additional human coronaviruses: HCoV-229E, HCoV-OC43, HCoV-NL63, and HKU1.

SARS-CoV-2 is a novel β-coronavirus sharing the same subgenus as SARS-CoV and MERS-CoV and sharing gene sequence similarity less than 90% with them (Chan *et al*., 2015). The SARS-CoV-2 spike (S) protein exhibits significant sequence similarity, up to 98%, with the bat coronavirus (RaTG13) (Li *et al*., 2003).

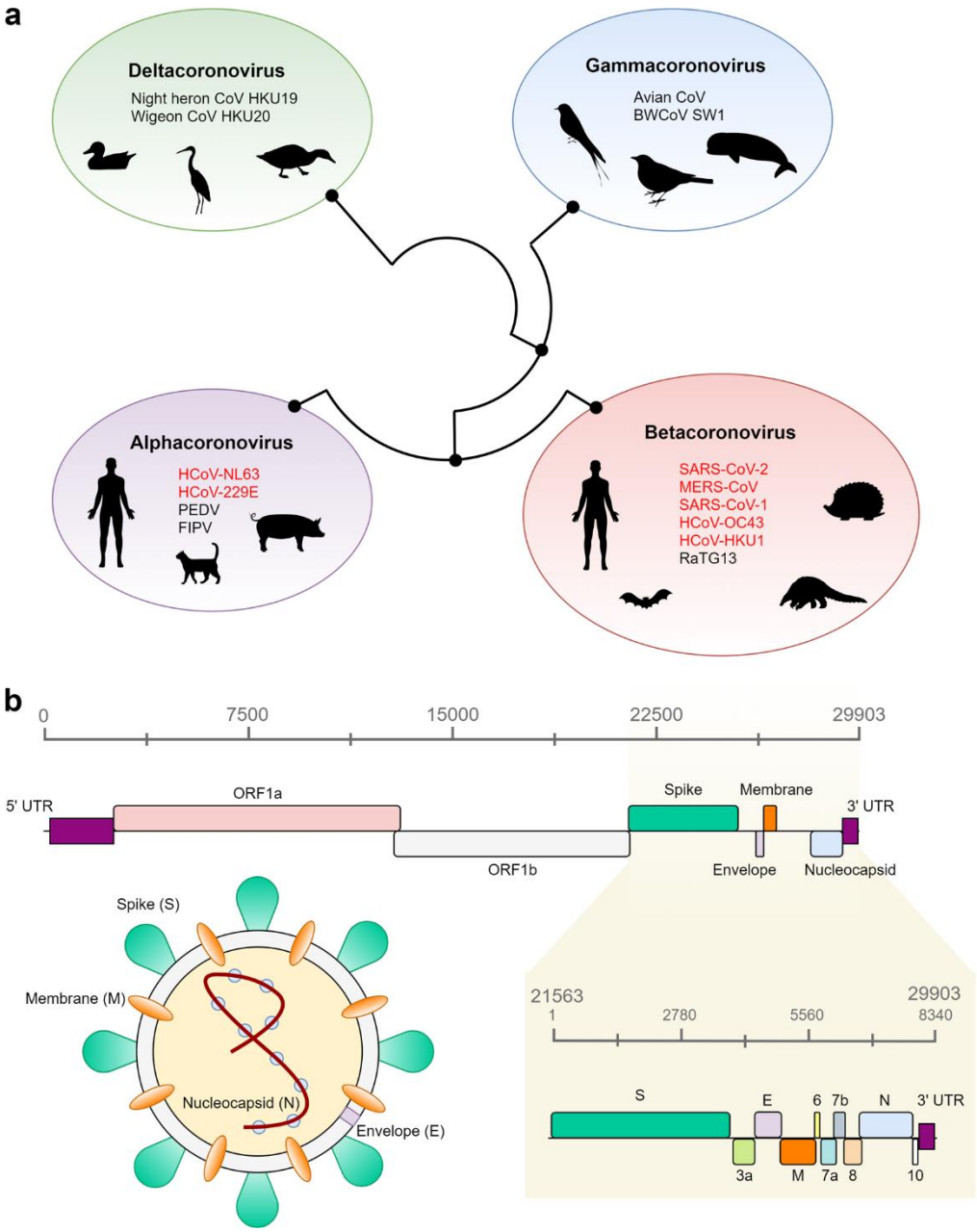

Figure 1: a. Schematic depiction of the four genera of coronaviruses, their evolutionary relationship, and their animal hosts. b. Genomic distribution of all open reading frames (ORFs) across the 29,903 bp SARS-CoV-2 genome (Singh, D. & Yi, S. V. 2021).

1.1.2 Framework of SARS-CoV-2

Its genomic size is ~ 32 kb and is the largest viral RNA genome known containing 14 reading frames (Khater & Nassar, 2021). Open reading frames ORF1a and ORF1b are found at the 5′ end of the SARS-CoV-2 genome and encode polyproteins that are then processed by proteolytic cleavage into non-structural proteins including 3-chymotrypsin-like protease ($3CL^{pro}$) or main protease (M^{pro}), papain-like protease (PL^{pro}), RNA dependent RNA polymerase (RdRp) and so on (**Figure 2**). The viral

genome's 3′ end contains open reading frames that encode for structural proteins, including spike (S), nucleocapsid (N), envelope (E), and membrane (M) proteins (Paraiso *et al*., 2020). The S protein is comprised of two subunits namely S1 and S2, where S1 aids in receptor-binding whereas S2 affiliates membrane fusion after proteolytic activation (Walls *et al*., 2020). The S1 subunit accommodates the N-terminal domain (NTD) and C-terminal domain (CTD) which is also known as the receptor-binding domain (RBD) that is mainly accountable for recognizing host receptor angiotensin-converting enzyme 2 (ACE2) (Lan *et al*., 2020). The SARS-CoV-2 S CTD binding surface has more buildups that straightforwardly correlate with the receptor ACE2 than does SARS-RBD (21 versus 17), and a bigger surface region is covered with SARS-CoV-2 S CTD in complex with ACE2 than with SARS S-RBD (Huang *et al*., 2020).

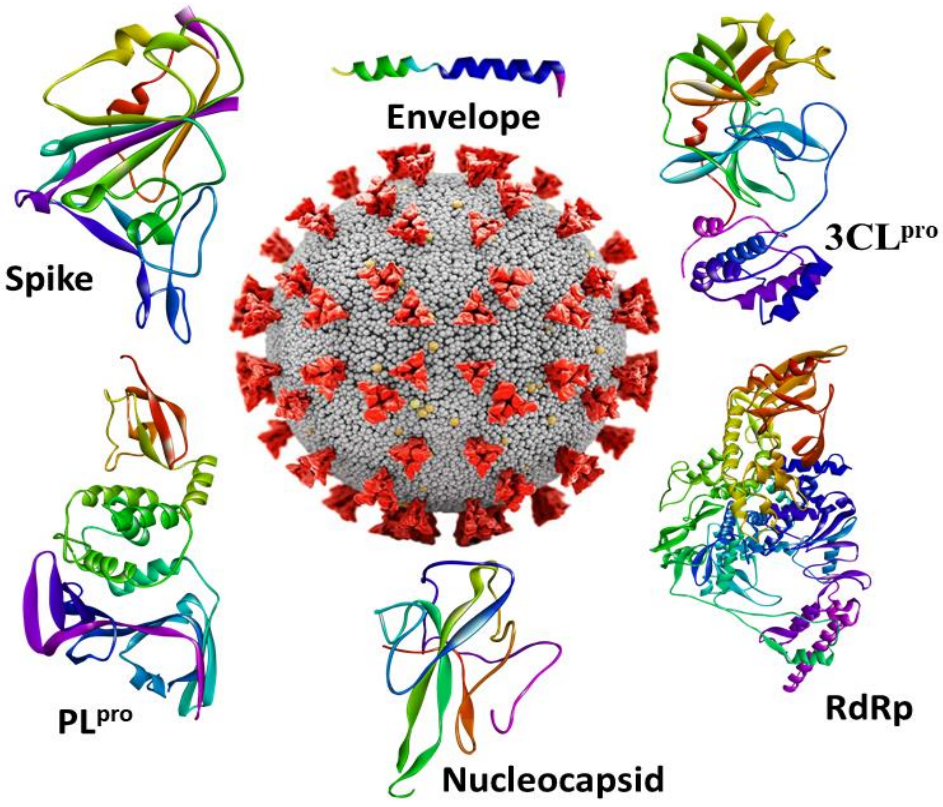

Figure 2: SARS-CoV-2 with some of its structural and non-structural proteins.

Human angiotensin-converting enzyme 2 (hACE2) has a ten times higher affinity for S-RBD of SARS-CoV-2 than that for S-RBD of SARS-CoV making hACE2 a plain receptor responsible for attachment of virus into the cell (Choudhary *et al*., 2020). SARS-CoV-2 has been rapidly transmitting worldwide and the factors aid leading to so

could be correlated to greater receptor binding affinity, presence of a higher number of alternate host cell receptors as well as more susceptibility to proteases.

- **Spike Protein**

  A substantial amount of glycosylated S proteins coat the surface of SARS-CoV-2, mediating viral cell entrance by binding to the host cell receptor ACE2 (Letko *et al*., 2020). The S protein is 180-200 kDa in size and is made up of an intracellular short unit called the C-terminal segment, an extracellular N-terminus, and a transmembrane (TM) domain that is anchored in the viral membrane (Bosch *et al*., 2003). The S protein typically has a metastable, prefusion conformation; nevertheless, when the virus interacts with the host cell, it undergoes significant structural changes that enable the virus to fuse with the host cell membrane.

  The total length of the S protein is 1273 amino acid residues and consists of a signal peptide (1-13) located at the N-terminus; the S1 subunit (14-685), and the S2 subunit (686-1273) are responsible for the receptor binding and membrane fusion (Xia *et al*., 2020). The S protein is an inactive precursor in its original form. Target cell proteases cleave the S protein into S1 and S2 subunits during viral infection (Bertram *et al*., 2013), which is required for activating the membrane fusion domain after viral entry into target cells (Hoffmann *et al*., 2020). Receptor recognition is a key factor in determining viral entrance and a target for therapeutic design since the binding of virus particles to the host cell receptors initiates viral infection. In the aminopeptidase N region, the RBD found in the S1 subunit interacts with the cell receptor ACE2 mediating viral attachment to the host cell in the form of trimer (Wrapp *et al*., 2020).

- **M^{pro}**

  NSP5, also known as M^{pro} cleaves polyproteins automatically, resulting in a mature protein at first. The downstream NSPs of pp1a and pp1ab are then cleaved by M^{pro}, resulting in the release of NSP 4-16. M^{pro} is crucial for the maturation of other NSPs and increases viral biosynthesis (Zhang & Tang, 2021).

- **PL^{pro}**

  As a protease, PL^{pro} (Papain-like-protease) may cleave the replicase polyprotein's N-terminus and release NSP1, NSP2, and NSP3. Furthermore,

PL^{pro} is required for viral replication correction, it plays a critical role in coronavirus replication and infection of host cells (Costanzi *et al*., 2021).

- **RdRp**

  NSP12, also known as RNA-dependent RNA polymerase (RdRp) is always conserved in coronaviruses, and the C-terminal of RdRp contains an important polymerase domain (Subissi *et al*., 2014). NSP8 functions as a primer in RNA synthesis, and the NSP7-NSP8 complex boosts NSP12 activity, resulting in increased binding of NSP12 to RNA (Imbert *et al*., 2006). RdRp is a crucial protease in the coronavirus replication/transcription complex.

1.1.3 Variants of SARS-CoV-2

All viruses could alter their genetic makeup and such genetic change is referred to as a mutation. As with DNA, when nucleotide sequence of the RNA strand changes, mutation happens. SARS-CoV-2 has also experienced several mutations or changes in its genetic sequence relative to the reference sequence. Changes in the genomic sequence of SARS-CoV-2 can be brought about by random mutations followed by selection and recombination (Rahimi *et al*., 2021). Many mutations have been found in SARS-CoV-2, and if those mutations are the cause of the protein structure change, it will result in a variety of variants. Each variant might differ from the others and the reference type, and the extent depends on the mutated residue, and they exert different characteristics too. The variants of the virus are categorized into different classes, with one such class known as Variants of Concern (VOC) displayed in **Table 1**. VOCs pose a significant challenge as they exhibit increased transmissibility, greater virulence, and reduced susceptibility to neutralization by antibodies acquired through natural infections or vaccination, leading to decreased effectiveness of treatment and vaccines.

Table 1: List of five variants of concerns (VOCs) and their descriptions

Name of Variants	Pango Lineage	Place of Isolation for the First Time	Mutated Amino Acid Residue in Spike RBD
Alpha	B.1.1.7 and Q lineage	September 2020, United Kingdom	N501Y
Beta	B.1.351 and descendent lineages	October 2020, South Africa	K417N, E484K, N501Y

Gamma	P.1 and descendent lineages	December 2020, Brazil	K417T, E484K, N501Y
Delta	B.1.167.2 and AY lineages	December 2020, India	L452R, T478K
Omicron	B1.1.529	November 2021, South Africa	S375F, S373P, S371L, G339D, K417N, N440K, G446S, S477N, T478K, E484A, Q493R, G496S, Q498R, N501Y, Y505H

Compared to other VOCs, some caused a greater impact. The alpha variant was found to be 43% - 82% more transmissible and also increased severity of disease was found in people infected with this variant (Davies *et al*., 2021). Delta variant is thought to have been the most prevalent type in many nations at the time of the lethal second wave of COVID-19, which spread fast over the world. The omicron variant, which contained more than 30 mutations in the spike protein and studies suggesting it is likely 2.8 times more fatal than the delta variant, is the most recent VOC announced by the WHO (Davies *et al*., 2021). People who have been infected with different variants display symptoms, and the timing of infection and/or the manifestation of symptoms varies according to the variants and this makes difficult to find the appropriate medication.

Though COVID-19 is no longer a global health pandemic there is significant evidence to suggest that new and potentially deadly coronaviruses may emerge in the future. Coronaviruses often originate in animals and can transmit to humans, as demonstrated by SARS-CoV-2, SARS-CoV, and MERS-CoV (Cui *et al*., 2019). Coronaviruses can rapidly evolve, giving rise to new variants with altered properties, including increased transmissibility or virulence (Markov *et al*., 2023). While it's impossible to predict exactly when and where the next pandemic will originate it is necessary to identify the inhibitor of SARS-CoV-2 and its emerging variants is to investigate the therapeutic properties of secondary metabolites and to aid the finding of potent metabolites against SARS-CoV-2.

1.2 Natural Products

Nature is a rich supply of medicines that need to be discovered and purified to be used as necessary biologicals, either separately or in combination, in the field of modern drug discovery. Numerous bioactive compounds make up natural products (NPs). Plants have produced a large number of secondary metabolites with a variety of structural and pharmacological characteristics (Gad *et al*., 2013). The traditional medical system's knowledge has set the path for continuous research into medicinal plants for use in creating pharmaceutical products (Mushtaq *et al*., 2018).

Low-molecular-weight NPs derived from plants via metabolism are effective therapeutic agents for a variety of ailments and have been aiding in the drug discovery process for decades. NPs and their structural analogs are used in wide therapeutic areas such as cancer (Chamberlin *et al*., 2019), cardiovascular diseases (Chang *et al*., 2020), viruses, and bacterial infections. NPs continue to be a promising source for the identification of scaffolds with a wide range of bioactivities and significant structural diversity that can be either directly developed or utilized as building blocks for the optimization of new medications (Atanosov *et al*., 2021). Thus, since the emergence of COVID-19, the usage of therapeutic plants and their products, as well as traditional herbal preparations, has risen substantially all across the world (Peng *et al*., 2020). *Tinospora cordifolia* is an important medicine in the Ayurvedic system of medication. Numerous chemical, pharmacological, pre-clinical, and clinical investigations have been conducted on this molecule, and several new therapeutic potential effects have been revealed. It is a plant often used in traditional medicine to boost memory and cognitive abilities (Osama M. Ahmed, 2021). Numerous compounds including polyphenols, terpenoids, lactones, aliphatic compounds, glycosides, alkaloids, etc. are present in *T. cordifolia*. The several pharmacological actions of *T. cordifolia* have been extensively researched over the past two decades. Owing to its therapeutic efficiency in immunological regulation, it may also be useful in treating viral and other illnesses (Abhishek Gupta et al., 2024). Thus, various *in silico* and *in vitro* approaches are employed to discover NPs against different diseases (Wasilewicz *et al*., 2023).

Phytochemicals are naturally existing bioactive substances that are found in plants and are ingested as fruits, vegetables, cereals, spices, drinks, and medications. Numerous phytochemicals serve as antioxidants, metal ion chelators, electron donors, hydrogen

donors, enzyme inhibitors, and singlet oxygen quenchers. Based on their metabolic function, phytochemicals are generally divided into primary and secondary (specialized) metabolites. The former includes proteins, carbohydrates, fat, and so on, while the latter includes flavonoids, alkaloids, saponins, terpenes, lignin, and glucosides (Saxena *et al*., 2013). The various and varied pharmacological activities of medicinal plants are mainly attributed to their phytochemical components.

1.2.1 Primary Metabolites

During the active growth phase (trophophase), plants produce several primary metabolites, such as carbohydrates, proteins, and lipids, and start when the necessary nutrients are present in the growth media (Zaynab *et al*., 2019). Primary metabolites impart their direct role in the reproduction, and growth of plants (Springob & Kutchan, 2009). Often found in seeds and other vegetative storage organs of plants, these metabolites are essential for fundamental cell metabolism and are therefore required for physiological growth.

1.2.2 Secondary Metabolites

Innumerable chemical compounds known as secondary metabolites are created by living cells via metabolic pathways that diverge from the primary metabolic pathways. Albrecht Kossel, who won the 1910 Nobel Prize in physiology or medicine, was the first to develop the term "secondary metabolite" (“The Imperial Agricultural Research Conference,” 1927). Secondary metabolites, the phytoconstituents exert a wide variety of effects on the plant itself and other living organisms. In addition, secondary metabolites originate from other mechanisms, such as the system of shikimic acid (A. Hussein & A. El-Anssary, 2019a). They become more competitive in their own environments as a result. Although secondary metabolites are not evident in a plant’s primary metabolism, they frequently play an important ecological role. For example, they can be used as chemical defences against microbes, insects, higher predators, can attract other pollinators, and even other plants (allelochemics). Secondary metabolites are the basis for the therapeutic effects of many modern medications and medicinal plants (Teoh, 2016).

Secondary metabolites play a significant role in the treatment of numerous ailments in traditional medicine and folk applications. In the framework of contemporary medicine, they supplied principal molecules for the discovery and synthesis of medications to treat

a range of disorders, from migraines to cancer (A. Hussein & A. El-Anssary, 2019b). According to reports, these compounds possess antibacterial, antifungal, and antiviral properties, which enable them to protect plants against diseases. Plant secondary metabolites also function as pheromones, attractants, stimulators, and antioxidants (Wink, 2018). The most bioactive constituents of secondary metabolites including alkaloids, flavonoids, terpenes, and phenolic compounds can be found in various plant parts (Nwokeji *et al*., 2016).

1.2.3 Types of Secondary Metabolites

There are differences in the chemical, structural, and functional characteristics of secondary metabolites. They are divided into the three main categories listed below:

- Phenolic compounds, e.g., flavonoids, tannins, coumarins, lignin, quinones
- Nitrogen-containing compounds, e.g., amino acids (non-protein), alkaloids, glycosides
- Terpenes or isoprenoids, e.g., terpenoids, essential oil rubber, triterpene, steroids

Below is a list of some significant secondary metabolites with therapeutic properties.

- **Flavonoids**

Flavonoids, which are secondary metabolites with a polyphenolic structure, form a substantial group of NPs commonly found in fruits, vegetables, and some beverages. Chemically flavonoids are based upon a fifteen-carbon skeleton consisting of two benzene rings linked via heterocyclic pyrane ring. They can be subdivided into different categories, including flavones, flavonols, and flavanones. **Figure 3** displays their general structures. Flavonoids exhibit diverse beneficial biochemical and antioxidant properties associated with various disorders, including cancer, Alzheimer's disease, atherosclerosis, etc., and are recognized for their potent antiviral effects (Panche *et al*., 2016). These biomolecules can influence viral infection at various stages, especially at the molecular level to prevent viral development (Lalani & Poh, 2020). Hesperidin common flavanone glycoside extracted from *Citrus* fruits has a lot of potential for heart diseases. An aglycone metabolite of hesperidin with high bioavailability is hesperetin. These two compounds have a better capacity to bind with transmembrane serine

protease 2 and ACE 2 confirmed by molecular docking and MD simulation (Cheng *et al*., 2021).

Pectolinarin isolated from plume thistles *(Cirsium spp*.), yellow toadflax (*Linaria vulgaris*), kaempferol extracted from the plant's Kale *(Brassica oleracea* var. *sabella*, beans (*Phaseolus vulgaris*), tea (*Camellia sinensis*), spinach (*Spinacia oleracea)*, herbacetin from Golden root. (*Rhodiola spp)*, Gossypium (*Gossypium hirsutism*), rhoifolin extracted from *Rhus succedanea*, bitter orange (*Citrus aurantium*), epigallocatechin gallate isolated from Tea (*Camellia Sinensis*), the skin of apple (*Malus domestica*), etc. have shown inhibition against SARS-CoV and SARS-CoV-2 M^{pro}, S glycoprotein (Jo *et al*., 2020;Tallei *et al*., 2020).

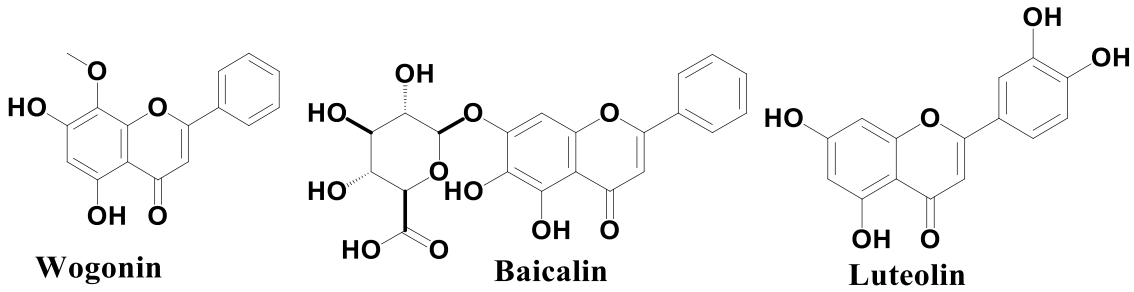

Figure 3: Structures of some flavonoids

- **Alkaloids**

Alkaloids, which typically consist of nitrogen atoms (**Figure 4**), are tiny organic compounds originating from plants, and present in around 20% of plant species (Ain *et al*., 2016). Alkaloids are primarily distinguished by the existence of one or more nitrogen atoms in a state of negative oxidation within their structures, leading to their alkaline properties and associated therapeutic advantages. There are about 12,000 alkaloids known for their biological activities.

Alkaloids have exhibited promising anti-SARS-CoV action by obstructing pathogenesis linked with the Target of the *Coronaviridae* family essential for the viral life cycle (Majnooni *et al*., 2021a) Fangchinoline, a compound derived from a species of *Menispermaceae* plant related to *Stephania tetrandra*, has anti-inflammatory and anticancer properties and prevents and treats HCoV-OC43 (Kim *et al*., 2019) Neferine, a bis benzylisoquinoline alkaloid, is mostly found in the *N. nucifera* seed embryos works for the treatment of obesity, arrhythmia, platelet, aggregation, hypomania, etc. Neferine exhibits a wide range of beneficial therapeutic effects, encompassing anti-

inflammatory, antiplatelet, anti-amnesic, antioxidant, anti-thrombotic, antihypertensive, and anti-cancer properties (Bharathi Priya *et al*., 2021a). The M^{pro} of SARS-CoV-2 was suppressed by the alkaloid compound 10- hydroxyusambarensine, which was found in African medicinal plants (Haq *et al*., 2023).

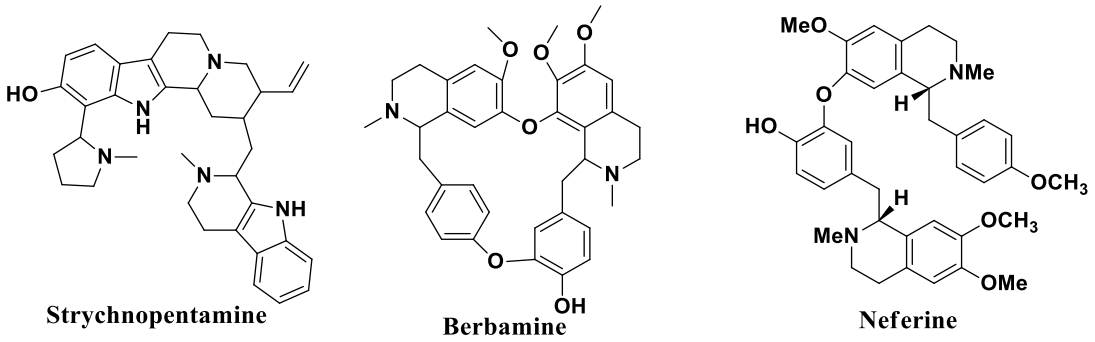

Figure 4: Some structures of alkaloids.

- **Triterpenoids**

Triterpenoids, crucial secondary metabolites in plants, consist of six isoprene units in their core structure (**Figure 5**). These compounds are prevalent in higher plants and are currently under investigation due to their diverse structure and broad range of antiviral properties against viruses such as Human Immunodeficiency Virus (HIV), influenza virus, hepatitis virus, and others (Liu *et al*., 2022). The bark of *Tripterygium regelii*, a member of the Celastraceae family, yielded quinones-methide triterpenes, including celastrol, pristimerin, tingenone, and iguesterin, which are then assessed for their potential to inhibit SARS-CoV M^{pro} (Ryu *et al*., 2010). Park *et al* found the diterpenoids isolated using an ethanolic extract of *S. miltiorrhiza* (a plant from the *Lamiaceae* family that is frequently employed as a remedy for a heart condition, particularly myocardial and angina pectoris, in China, Japan, korea, and other Asian nations) showed Inhibition against SARS-CoV $3CL^{pro}$ activity by 60% (Park *et al*., 2012).

It has been proven that the derivatives of quinones like tanshinones I, tanshinones II, methyl tanshinones, cryptotanshinone, dihydrotanshinone, and rosmariquinones which have been extracted from the roots of Asian medicinal plants *salvia miltiorrhiza*, a member of the *Lamiaceae* family were used to treat coronary heart diseases as well as thus diterpene quinones family (tanshinones) can stop the SARS-COV-2 virus from attacking its viral agents (Park *et al*., 2012). Quinone methide triterpenes extracted from the *Triterygium regelii* bark plant in the *Celastraceae* family utilized as traditional

Chinese medicine to cure inflammatory and autoimmune illnesses can also possess active action against $3CL^{pro}$ (Ryu *et al*., 2010).

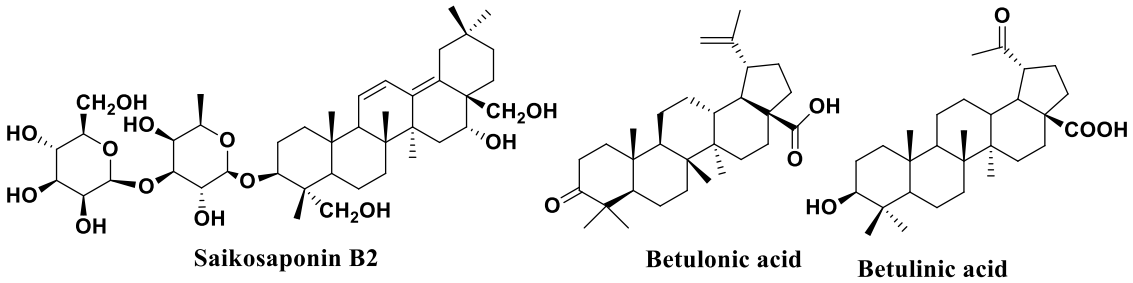

Figure 5: Structures of some triterpenoids.

- **Coumarins**

Coumarins are originally derived from the plant Dipteryx odorata Willd, are polyphenolic chemicals that are part of a series of colorless and crystalline oxygenated heterocyclic compounds (Küpeli Akkol *et al*., 2020) (**Figure 6**). It is common to find coumarin (1,2-benzopyrone or 2H-1-benzopyran-2-one) and coumarin derivatives in plants in heteroside form. To date, 800 naturally occurring coumarin derivative chemicals have been identified in roughly 600 genera across 100 families (Lacy, 2004). Rutamarin and kellerin have been identified as anti-herpes simplex virus (HSV) agents which are naturally occurring furanocoumarin and sesquiterpene coumarin, respectively (Xu *et al*., 2012). The inophyllum derivatives, (inophyllum-A, B, C, D, E, and soulattrolide), extracted from the leaves and twigs of the *Calophyllum inophyllum* plant were reported to have promising anti-HIV activity. Cordatolide A, a natural coumarin isolated from the leaves of the *Calophyllum cordate-oblongum* plant, was found to inhibit HIV-1 reverse transcriptase (Dharmaratne *et al*., 1998). Similarly, (+)-Calanolide C, a *pyranocoumarin* extracted from the fruits and twigs of the *Calophyllum lanigerum* plant has been shown to inhibit HIV replication (Kashman *et al*., 1992). Furthermore, wedelolactone, a naturally occurring coumarin in the *Wedelia Calendulacea* plant, was reported to be actively combating the Hepatitis C virus (Kaushik-Basu *et al*., 2008).

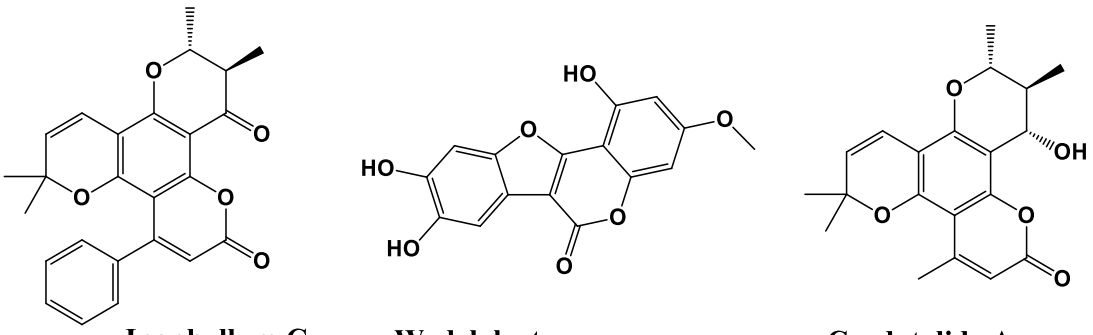

Figure 6: Structures of some coumarins.

- **Quinones**

Quinones, a class of organic compounds, originate from aromatic compounds like benzene or naphthalene. This process involves converting an even number of –CH= groups into –C(=O)- groups, with potential rearrangement of double bonds, leading to the formation of a cyclic dione structure with complete conjugation (Gold, 2019). The term is derived from quinic acid because it is one of the chemicals produced when quinic acid is oxidized. Quinones (**Figure 7**) are produced through oxidation of aromatic compounds and are commonly derived from reactive aromatic compounds containing electron-donating substituents such as phenols and catechols. These substituents enhance the ring's nucleophilicity and contribute to the generation of a significant redox potential needed to disrupt the aromaticity.

Anthraquinones like aloe-emodin and aloe-emodin acetate isolated from the leaves of the *Cassia roxburghii,* an herb used for its laxative and purgative properties that belong to the *Fabaceae/Leguminosae* family showed that these compounds have inhibitory activity against influenza virus A/WSN/33(H1N1) with inhibitory concentration 50 (IC_{50}) value of 2.00 and 10.23 g/ml respectively (Mohammed *et al*., 2013). Different quinones like purpurquinones B, purpurquinones C, and purpurester of anti-fungus extract isolated from the local red soil used to make purple pottery in Jianshui, Yunnan province, china showed high antiviral activity against H1N1 (Kim *et al*., 2012).

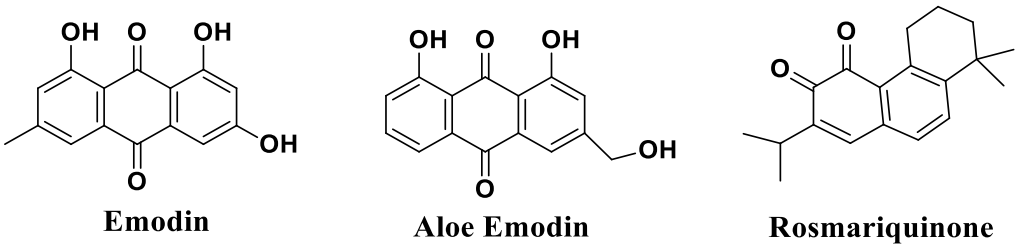

Figure 7: Structures of some quinones.

1.3 Computational Chemistry

A wide range of computational techniques are used in the field of computer-aided drug design (CADD) to find and create new therapeutic agents. CADD is essential for developing more effective ligands, finding new medications, and comprehending biological processes on a molecular scale (Prieto-Martínez *et al*., 2019). CADD boosts the drug discovery process by eliminating unfavorable candidates and helps scientists focus on a limited number of compounds preventing a lot of resources from hit and trial measures. CADD plays an even more significant role in case of epidemics like COVID-19 where immediate vaccines or drugs are required to combat a virus. With the help of CADD, a large number of potential phytochemicals from a natural library can be filtered, and then through further *in vivo, in vitro,* and clinical trials, a new drug could be discovered CADD encompasses two main approaches; one is Structure-Based Drug Designing (SBDD) and another is Ligand-Based Drug Designing (LBDD). SBDD mainly focuses on 3-dimensional structural analyses of macromolecules to locate binding sites and interactions significant for their biological function whereas LBDD focuses on correlating ligands with a target in terms of their physicochemical properties and biological activities (Sass, 2023). This information is then used to design drugs with greater efficiency. Common methods used in SBDD are molecular docking, structure-based virtual screening (SBVS), and molecular dynamic solutions (Gurung *et al*., 2021).

1.3.1 Pharmacokinetic Studies

A pharmacokinetic study of plant-based secondary metabolites involves the investigation of how these compounds are absorbed, distributed, metabolized, excreted, and potential toxicity to the body. According to (Hodgson, 2001), a chemical cannot be a drug unless it is properly absorbed into the body (absorption), distributed to the appropriate parts of the body (distribution), and metabolized in a way that does not immediately affect its activity, and eliminated suitably, a drug must get in, move around, hang out, and then get out. So, the five steps in pharmacokinetics are absorption, distribution, bioavailability, metabolism, and elimination. Traditionally, these parameters were studied at the final stages of drug discovery, but different software programs have made it possible to predict them at the initial stages. These parameters are responsible for maximum drug failure cases so understanding those beforehand saves a lot of time and effort (Tian *et al*., 2015) Many parameters affect the

absorption, distribution, metabolism, excretion, and toxicity (ADMET) properties of a biomolecule such as the molecular mass of the molecule, the surface charge of the molecule, glycosylation of protein, and the mechanism of target binding (Tibbitts *et al*., 2016). The parameters can be studied in detail.

- Absorption: This refers to the process by which the secondary metabolites are taken up into the bloodstream from the site of administration. The study may examine different routes of administration, such as oral, intravenous, topical, or inhalation, to determine the absorption rates and bioavailability of the metabolites.
- Distribution: Once absorbed, secondary metabolites are distributed throughout the body via the bloodstream. The study investigates the extent to which these compounds reach various tissues and organs, as well as their binding to plasma proteins or accumulation in specific sites.
- Metabolism: Secondary metabolites are often extensively metabolized in the body. The study aims to identify the metabolic pathways involved and the specific enzymes responsible for metabolite transformation. Metabolism can occur in the liver, but also in other tissues. Enzymes such as cytochrome P450 and glucuronosyltransferases play crucial roles in metabolizing secondary metabolites. It can lead to the formation of active or inactive metabolites, which may further contribute to the overall pharmacological effects.
- Excretion: The study assesses the elimination of secondary metabolites from the body, primarily through renal excretion (urine) and biliary excretion (feces), and in some cases, exhalation (breath) or sweating. The rate of elimination is influenced by factors such as the compound's molecular size, polarity, and stability of chemical compounds.
- Toxicity: Toxicity assessment is an essential aspect of drug development. It involves evaluating the potential adverse effects of a drug on various organs and systems in the body. Toxicity studies help determine safe and effective doses for human use.

By considering the ADMET properties of a drug candidate early in the drug discovery process, researchers can assess its viability, predict its pharmacokinetic and toxicological profiles, and optimize its structure for improved therapeutic outcomes.

1.3.2 Molecular Docking

A wide range of computational techniques are used in the field of CADD to find and create new therapeutic agents. CADD is essential for developing more effective ligands, finding new medications, and comprehending biological processes on a molecular scale (Prieto-Martínez *et al*., 2019). The binding mechanism and affinity between ligands and targets are generated using the structure-based computational technique known as molecular docking by foreseeing their interaction (**Figure 8**). The effectiveness of docking applications is largely dependent on the utilization of search algorithms and scoring mechanisms. The search methodology assesses the roto-translational and internal degrees of freedom of the ligand, subsequently generating a ligand pose within the binding site of a given target (McNutt *et al*., 2021). This can be accomplished by using a variety of docking technologies. Among the widely used programs are AutoDock Vina, Genetic Optimization for Ligand Docking (GOLD), Glide, Molecular Operating Environment (MOE), Internal Coordinate Mechanics Software (ICM), and Flex, (Muhammed *et al*., 2022).

- **AutoDock Vina:** It is a freely available software package that boasts user-friendly functionality. In contrast, the Vina interface exhibits a high degree of specialization and optimization, characterized by its unique ability to accomplish docking with minimal user input requirements (Eberhardt *et al*., 2021). To model the ligand flexibility while maintaining the rigidity of the receptor, AutoDock uses Monte Carlo simulated evolutionary, genetic, annealing, and Lamarckian genetic algorithm methods (Meng *et al*., 2011).
- **GOLD**: GOLD is a docking program that is based on the genetic algorithm described by Jones et al (Jones *et al*., 1997a). It is an automated tool for ligand docking that satisfies the essential criterion that the ligand must displace loosely bound water upon binding. It does this by using a genetic algorithm to explore the complete range of ligand conformational flexibility with partial flexibility of the protein.
- **MOE**: MOE is drug discovery software that is applied for structure-based design (Merz *et al*., 2010), ligand-based design (Erlanson *et al*., 2004), pharmacophore discovery, molecular modeling, virtual screening, simulations, and visualization all into one package. MOE virtual screening protocol, triangle matcher docking algorithm, and London dG scoring function were utilized in

conjunction with the MOE docking suit for virtual screening (Halim *et al*., 2021).

Two connected steps are involved in docking: first, the conformations of the ligand in the protein's active site are sampled, and then those conformations are raned using the scoring function. The scoring function aims to specify the correct poses from incorrect poses. The scoring function attempts to differentiate between correct and wrong poses, or active from inactive compounds in a fair of computation time. The binding affinity between the protein and ligand is estimated using scoring functions rather than calculated, and these functions make several assumptions and simplify complex situations. The extended force-field-based scoring function from AutoDock is given below:

$$V = W_{vdw} \sum_{i,j} \left(\frac{A_{ij}}{r_{ij}^{12}} - \frac{B_{ij}}{r_{ij}^{6}} \right) + W_{hbond} \sum_{i,j} E(t) \left(\frac{C_{ij}}{r_{ij}^{12}} - \frac{D_{ij}}{r_{ij}^{6}} \right) + W_{elec}$$

$$\sum_{i,j} \frac{q_i q_j}{e(r_{ij}) r_{ij}} + W_{sol} \sum_{i,j} \left(S_i V_j + S_j V_i \right) e^{\left({}^{-r_{ij}^2} / _{2\sigma^2} \right)}$$

Here, the pair-wise atomic energy of two atoms i and j are calculated by adding the energies of van der Waals, hydrogen bonds, coulomb bonds, and desolvation. W stands for weighted factors used to calibrate the empirical free energy. Molecular docking software, such as GOLD (Verdonk *et al*., 2003), AutoDock (Morris *et al*., 1998), and DOCK (Kuntz *et al*., 1982) present such scoring functions to users.

A technique called molecular docking is used to predict how planned chemicals fit into the target cavities and interact with the residue. In the computational drug development process, docking typically occurs between tiny compounds and macromolecules i.e. protein-ligand and protein-protein docking. In the process of developing new drugs, molecular docking has a significant role. Its early applications focused on analyzing the molecular interaction between ligands and targets. It now supports a wider range of drug discovery. There are a variety of uses in target fishing, polypharmacology, drug repurposing, virtual screening, and drug side effect prediction. The use of cutting-edge computer techniques, such as artificial intelligence, has improved docking methods (Dar & Mir, 2017). Depending upon the goals of the docking simulations, there are different types of molecular procedures, such as flexible ligand rigid receptor docking

(semi-flexible docking), rigid ligand and rigid receptor docking (rigid docking), flexible ligand and flexible receptor docking (flexible docking) (Gschwend *et al*., 1996).

Rigid docking: The protein as well as the ligand are both viewed as rigid entities in this method. The rigid docking is mostly performed for the catalytic protein where the catalytic binding sites are already fixed, and the ligands are flexible. The early version of DOCK (Kuntz *et al*., 1982), FTDOCK (Gabb *et al*., 1997), and FLOG (M. D. Miller *et al*., 1994) adopted the rigid docking.

Semi-flexible docking: The common approach, that compromises accuracy and computing speed, treats the flexible nature of ligand while maintaining the rigidity of the receptor during docking. Most of the docking programs adopted this methodology, such as AutoDock (Morris *et al*., 1998), FlexX (Rarey *et al*., 1996)

Flexible docking: It regards both the ligand and the protein as flexible counterparts. It refers to the simplest method, known as "soft-docking," (Jiang & Kim, 1991) reduces the van der Waals repulsion energy term in the scoring function to permit some degree of atom-atom overlap between the receptor and ligand. Some docking programs like GOLD (Knegtel *et al*., 1997), and FlexE (Claußen *et al*., 2001) adopted this methodology.

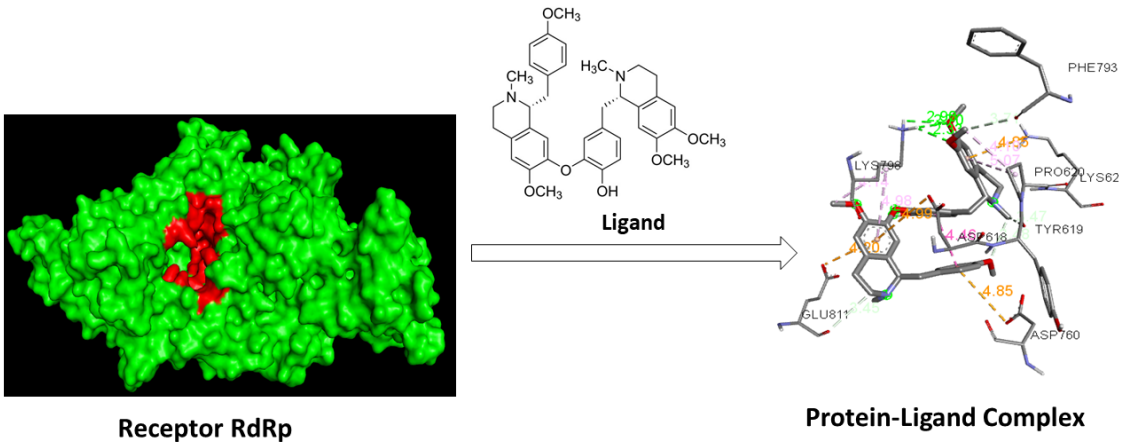

Figure 8: Demonstration of molecular docking program.

1.3.3 Molecular Dynamics (MD) Simulation

MD simulation is a computer-based method for simulating the physical motions of atoms and molecules. By permitting atoms and molecules to interact for a specific

duration, MD simulation has undergone significant advancements and has now reached a level of ability that enables its effective application in comprehending the complex relationship between macromolecular structure and function (Hospital *et al*., 2015). The prevalent form of MD simulation in GROMACS software involves computationally resolving Newton's law of motion for a particle system in interaction like proteins in water (Ode *et al*., 2012). It uses the classical equations of motion to describe the behavior of a system of atoms over time. The basic equation for MD simulations is the Newton's law of motion:

$$F = ma$$

Where 'F' represents the force exerted on every atom, 'm' stands for mass, and 'a' stands for acceleration.

In the context of MD simulations, the forces on each particle are typically derived from the force field, which contains mathematical functions and parameters representing the interatomic interactions. These interactions include bond interactions (bonds, angles, dihedrals) and non-covalent interactions (van der Waals forces and electrostatic interactions).

For non-covalent interactions, the two most common potentials used in MD simulations are:

Lennard-Jones potential:

$$V_{LJ}(r) = 4\varepsilon[\left(\frac{\sigma}{r}\right)^{12} - \left(\frac{\sigma}{r}\right)^{6}]$$

Where:

ε is the depth of the potential well, determining the strength of the attractive interactions

σ is the finite distance at which the potential is zero, related to the size of the particles, and

r is the interacting particle distance.

Coloumb potential:

$$V_{Coul}(r) = (\frac{1}{4\pi\varepsilon_0}\ \frac{q_i q_j}{\varepsilon r})$$

Where:

$\mathbf{q_i}$ and $\mathbf{q_j}$ are the charges of the interacting particles,

$\boldsymbol{\varepsilon_0}$ is the vacuum permittivity,

$\boldsymbol{\varepsilon r}$ is the dielectric constant of the medium (often set to 1 for simulations in a vacuum)

r is the distance between charged particles

These potentials play a crucial role in determining the behavior and properties of molecular systems during MD simulations. The force field parameters, including ε, σ, and charges are typically derived from experimental data and are used to calculate forces acting on each particle during the simulation.

During the simulation procedure, distinct force fields, namely AMBER, GROMOS, and CHARMM, are employed to amplify the motion of atoms and molecules, with each forcefield being parameterized uniquely (Durrant & McCammon, 2011). Force fields utilized in the fields of chemistry and biology are predominantly founded on molecular mechanics. These force fields incorporate a classical mechanic's approach to the interactions between particles, which can accurately replicate both structural and conformational alterations (van der Spoel, 2021). Simulation software, including CHARMM, AMBER, NAMD, and GROMACS, is currently utilized in drug discovery research. These software programs are designed to be compatible with the messaging passing interface, which results in decreased computation time (Hospital *et al*., 2015). GROMACS has played a crucial role in advancing computational investigations by providing a powerful and versatile tool for MD simulations. Its efficiency, accuracy, flexibility, and versatility have made it an indispensable asset for researchers across various scientific disciplines. It is renowned for its speed and efficiency making it suitable for large-scale simulations involving thousands or millions of atoms. It employs sophisticated force fields to accurately describe the interactions between atoms, providing reliable results for a wide range of systems. GROMACS offers a high degree of flexibility, allowing researchers to customize simulations to their specific needs. It supports various simulation techniques, such as constant volume, constant pressure, and temperature coupling, enabling the study of different thermodynamic conditions. It can be applied to a diverse range of systems, including proteins, nucleic

acids, lipids, and small molecules. It has been used to investigate a wide range of phenomena, such as protein folding, ligand binding, enzyme catalysis, membrane dynamics, and materials properties.

Key concepts in MD simulation:

- Force fields: To simulate the behavior of atoms and molecules, MD simulation uses force fields that describe the interactions between atoms, including bonded interactions (bonds, angles, dihedrals) and non-bonded interactions (van der Waals forces and electrostatic interactions).
- Equations of Motion: MD simulations numerically integrate the equations of motion, such as Newton's second law of motion, to determine the trajectories of atoms over time. Calculating the forces exerted on each atom is necessary for this and updating their positions and velocities accordingly.
- Time step: The MD simulation time is divided into discrete steps, known as the time step. A smaller time step provides more accurate results but requires more computational resources.
- Ensemble: In MD simulations, researchers typically specify an ensemble, which defines the conditions under which the system is simulated. Common ensembles include the microcanonical (NVE), canonical (NVT), and isothermal-isobaric (NPT) ensembles.
- Thermostats and Barostats: To control the temperature and pressure of the system during simulation, thermostats and barostats are used, respectively. These techniques help maintain a stable environment for the simulated system.
- Boundary Conditions: MD simulations typically use periodic boundary conditions to simulate an effectively infinite system by replicating the simulation box periodically in all directions.

GROMACS is used to investigate the mechanisms of biological processes, such as enzyme catalysis, dynamics of biological molecules in atomic levels, and protein-protein interactions. It is also used to study protein-ligand interactions, aiding in the design of new drugs. The stability of a protein-ligand complex during a simulation period can be assessed by computing various parameters such as Root Mean Square

Deviations (RMSD), Root Mean Square Fluctuations (RMSF), Radius of Gyration (Rg), Solvent accessible surface area (SASA) and hydrogen (H)-bond. These parameters are crucial in evaluating the functional reliability of the complex in a living system, which ultimately determines the efficacy of the drug. The RMSD analysis is utilized to assess the stability of a protein, whereas the RMSF analysis is employed to evaluate the flexibility of residues within the protein (Borjian Boroujeni *et al*., 2021). In the context of drug discovery, the residues located at the active site are of particular interest. Rg addresses the compactness of the complex, while H-bond analysis investigates the degree of interaction between the protein and the ligand (Hubbard & Kamran Haider, 2010). The capacity of the complex to retain the H-bond relationship exhibited in docking throughout the MD simulation is indicative of stability, as is the role of solvation in maintaining the H-bond interaction. More stable H-bonds between the ligand and its target protein during the ligand-protein dynamics simulation indicate greater interaction between the ligand and its target (Dandekar *et al*., 2021)). Similarly, SASA, which is the accessible region of protein that can interact with the neighboring solvent molecules, determines the protein stability and its folding study (Chothia, 1974; S. Miller *et al*., 1987)

It is important to note that while MD simulations offer valuable insights, they are not a replacement for experiments. Instead, they complement experimental data and provide atomistic details that are often challenging or impossible to obtain through direct experimentation. Additionally, MD simulations require significant computational resources, and the accuracy of the outcomes relies on the force field's quality and simulation parameters.

1.3.4 Binding Free Energy using MM/GBSA

The molecular mechanics' energy in conjunction with the generalized Born surface area (MM/GBSA) has become a widely accepted methodology for the computation of the free energy associated with the binding of the small ligands to biological receptors (Genheden & Ryde, 2015). The receptor-ligand complex has been subjected to molecular dynamics simulations, which have revealed that these simulations encompass an intermediate position in terms of accuracy and computational effort, between empirical scoring and strict alchemical perturbation approaches (Pattar *et al*., 2020). Moreover, The Prime MM-GBSA methodology is utilized to determine the

energy of optimized free receptors, free ligands, and the complex formed by the ligand and receptor (Mulakala & Viswanadhan, 2013a). MM/GBSA analysis is based on the formula:

The binding free energy (ΔG_{BFE}) can be decomposed into several components, with MM/GBSA commonly expressing it as follows:

$$\Delta G_{BFE} = \Delta E_{MM} + \Delta G_{Solv} + \Delta G_{SA}$$

Where,

- ΔE_{MM} is the molecular mechanics' energy difference between the complex and the individual components (e.g., protein and ligand) in the vacuum.
- ΔG_{Solv} is the solvation free energy term, calculated using a generalized Born or another implicit solvent model. It accounts for the desolvation or solvation of the complex in the solvent.
- ΔG_{SA} is the surface area term that corrects for the loss of configurational entropy upon complex formation. It estimates the changes in surface area between the complex and individual components.

1.3.5 Density Functional Theory (DFT) Analysis

Gaussview is a powerful graphical user interface (GUI) that significantly enhances the efficiency and accessibility of DFT investigations, an extensively utilized computational approach in chemistry and material science. It is employed to investigate the electronic structure and properties of molecules, visualizing results, and analyzing data, making the process of DFT calculations more intuitive and productive. It has proven to be particularly useful in analyzing the structural and electronic properties of secondary metabolites, which are bioactive compounds produced by plants. Here are some specific aspects that can be explored using DFT analysis:

- Structure determination: DFT calculations can be used to predict or refine the molecular structure of plant secondary metabolites. This is particularly useful when experimental techniques are unable to provide a complete or accurate structure. DFT can predict bond lengths, angles, and dihedral angles, which aid in understanding the three-dimensional arrangement of atoms.

- Electronic properties: DFT can reveal information about the electronic structure of plant metabolites, such as ionization potentials, electron affinities, and electron density distribution. These properties influence the compound's reactivity, stability, and interactions with other molecules.
- Frontier molecular orbitals: DFT permits the identification of frontier molecular orbitals, comprising the highest occupied molecular orbital (HOMO) and lowest unoccupied molecular orbital (LUMO). These orbitals are relevant to understanding the reactivity and chemical behavior of plant secondary metabolites, such as their ability to act as electron donors or acceptors in biochemical processes.
- Reactivity and chemical reactions: DFT calculations can predict reaction energies, transition states, and reaction pathways for plant metabolites. This information is valuable for understanding their chemical reactivity, identifying potential reaction sites, and investigating enzymatic or chemical transformations.
- Binding interactions: DFT can analyze the binding interactions between plant secondary metabolites and their target biomolecules, such as enzymes or receptors. Understanding the binding modes and binding energies can provide insights into the compound's mechanism of action and potential application in drug discovery.

By employing GaussView software for DFT calculations, researchers can gain a deeper understanding of the structure, reactivity, electronic properties, and binding interactions of plant secondary metabolites. This knowledge can contribute to the exploration of their biological activities, identification of new lead compounds, and optimization of their properties for various applications.

In drug modeling research, using GaussView, DFT calculation is used to analyze the specific electronic features of integrated pharmaceutical compounds as well as medication delivery mechanisms. DFT is therefore useful for describing both the characteristics of drugs and their inhibitory effect on pharmacological targets (Ye *et al*., 2022). Frontier molecular orbital (FMO) calculations are a significant characteristic that the DFT can be used to examine. The HOMO electrons' sensitivity to transferring to the LUMO can be accurately determined by using Frontier Molecular Orbitals (FMO). Additionally, HOMO and LUMO are critical quantum chemical parameters for

determining the reactivity of molecules and are utilized to derive several significant characteristics, including the chemical reactivity descriptors (Hagar *et al*., 2020). Some chemical reactivity descriptors, including electronegativity, electrophilicity, and global hardness and softness, can be computed using FMO, which controls the molecule's reactivity (Bagheri Novir & Aram, 2020).

1.4 Protein Assays using ELISA

The enzyme-linked immunosorbent assay (ELISA) is a powerful method for detecting and quantifying a specific protein in a complex mixture. This technique that was first presented by Engvall and Perlmann in 1971, allows for the use of certain antibodies to analyse protein samples that have been immobilized in microplate wells. ELISA are typically performed in 96-well or 384-well polystyrene plates, which passively bind antibodies and proteins. ELISAs are simple to create and execute because of the reagents' binding and immobilization. During the experiment, it will be easy to distinguish between bound and non-bound material because the ELISA reactants have been immobilized on the microplate surface. The use of high-affinity antibodies and the removal of non-specific bound materials make ELISA an effective technique for quantifying certain analytes in a crude sample. Commercially, a wide range of substrates for ELISA using horseradish peroxidase (HRP) are accessible. The desired assay sensitivity and the equipment available for signal detection determine which substrate is best.

Performing a spike protein assay using a 96-well plated ELISA kit with precoated spike protein ease the process as compared to traditional ELISA kits where manual coating of the plates is required. With a pre-coated kit, the spike protein is already immobilized onto the surface of the wells, saving time and reducing variability in the assay. The spike protein plays a critical role in the SARS-CoV-2 virus by enabling viral entry into host cells.

A general outline of the steps involved in performing a spike protein assay using a 96-well plated ELISA kit:

- **Sample preparation**: Prepare the compounds or crude extract of parts of medicinal plants that can interact with the spike protein.

- **Kit Equilibration**: Allow the pre-coated ELISA plate to reach room temperature, as specified in the kit instructions. This is essential to ensure proper binding of the target proteins during the assay.
- **Sample Incubation**: Add prepared samples and appropriate controls (e.g., positive and negative controls) to the designated wells of the pre-coated 96-well ELISA plate. The spike protein that is already coated on the plate will capture the target compounds present in the samples.
- **Incubation**: Incubate the plate to allow the interaction between the spike protein on the plate and the target proteins in the samples. This incubation step promotes specific binding and ensures that all potential interactions have a chance to occur.
- **Washing:** Wash the plate thoroughly with a wash buffer to remove any unbound components, including any unbound proteins and the samples.
- **Detection antibody addition**: Add a detection antibody that specifically recognizes the target proteins in the samples. This detection antibody should be labeled with an enzyme, such as horseradish peroxidase (HRP) for signal amplification.
- **Secondary antibody incubation**: Incubate the plate again to allow the detection antibody to bind to. The capture target proteins. This creates a "sandwich" complex with the spike protein acting as the capture antibody, the target proteins from samples, and the detection antibody.
- **Signal development**: Add a substrate solution containing a chromogenic or chemiluminescent substrate to the wells. If the detection antibody is conjugated to an enzyme, it will catalyze a reaction with the substrate, resulting in a detectable signal (color change or light emission).
- **Stop reaction**: After a specific incubation time, stop the enzymatic reaction to prevent further signal development.
- **Signal measurement**: Measure the absorbance in each well using a microplate reader. The signal intensity is proportional to the concentration of samples interacted with the target protein.

- **Data analysis**: Use a standard curve generated from known concentrations of the samples to quantify the amount of samples (compounds or crude extract).

Always carefully follow the specific instructions provided with the pre-coated ELISA kit to ensure accurate and reliable results. Additionally, appropriate controls and replicates should be included to validate the assay's results.

1.5 Research Objectives

1.5.1 General objective

To identify potent antiviral drug candidates for the treatment of COVID-19 by analyzing secondary metabolites through pharmacokinetics study, molecular docking, MD simulation, DFT analysis, and protein assays.

1.5.2 Specific objectives

- Selection of drug candidates from a large database of secondary metabolites using computational chemistry and correlating them with literature.
- Screening secondary metabolites through pharmacokinetics study
- Molecular docking of secondary metabolites with therapeutic target proteins: spike protein (PDB ID: 6M0J, 7NX8, and 7QNW), and RdRp (PDB ID: 6M71)
- MD simulations of potent drug candidates with targeted protein to identify the stability of complexes.
- Evaluation of reactivity of some selected secondary metabolites through DFT analysis
- Spike protein assays of potent drug candidate(s).

1.6 Research Gaps

Despite the availability of preventive vaccinations, effective antiviral medication for the treatment and prevention of COVID-19 is a matter of great concern. Although COVID-19 is no longer a pandemic, research for the discovery of therapeutic medicines to combat potentially fatal CoVs should be continued, as new and deadly CoVs can emerge at any time and pose a threat of spreading like earlier CoV pandemics. However, the research should first undergo an *in silico* analysis, followed by immunological protein assays, to make it more time and cost-efficient. This research includes the remedies belonging to secondary metabolites through protein-ligand complex's

molecular docking, MD simulations, and protein assay and aims to collect a maximum number of natural therapeutic agents that might be recommended against COVID-19.

1.7 Conceptual Framework

Selected secondary metabolites having antiviral properties were taken and were studied through a different web server such as PubChem (Hähnke *et al*., 2018) and ChemSpider (Pence & Williams, 2010). The metabolites were screened using Lipinski's rule of five and different servers (pkCSM, swissADME, ProTox II) to analyze their drug-likeness properties. Now, the target protein of SARS-CoV-2 and selected metabolites were docked to analyze the binding interactions of metabolites at the active pocket of a target protein using MOE, GOLD, and also AutoDock vina. And the suitable complexes of protein-ligand obtained from molecular docking were taken for MD simulations. The metabolite(s) identified as a potent drug by the *in silico* analysis were now further investigated through *in vitro* analysis.

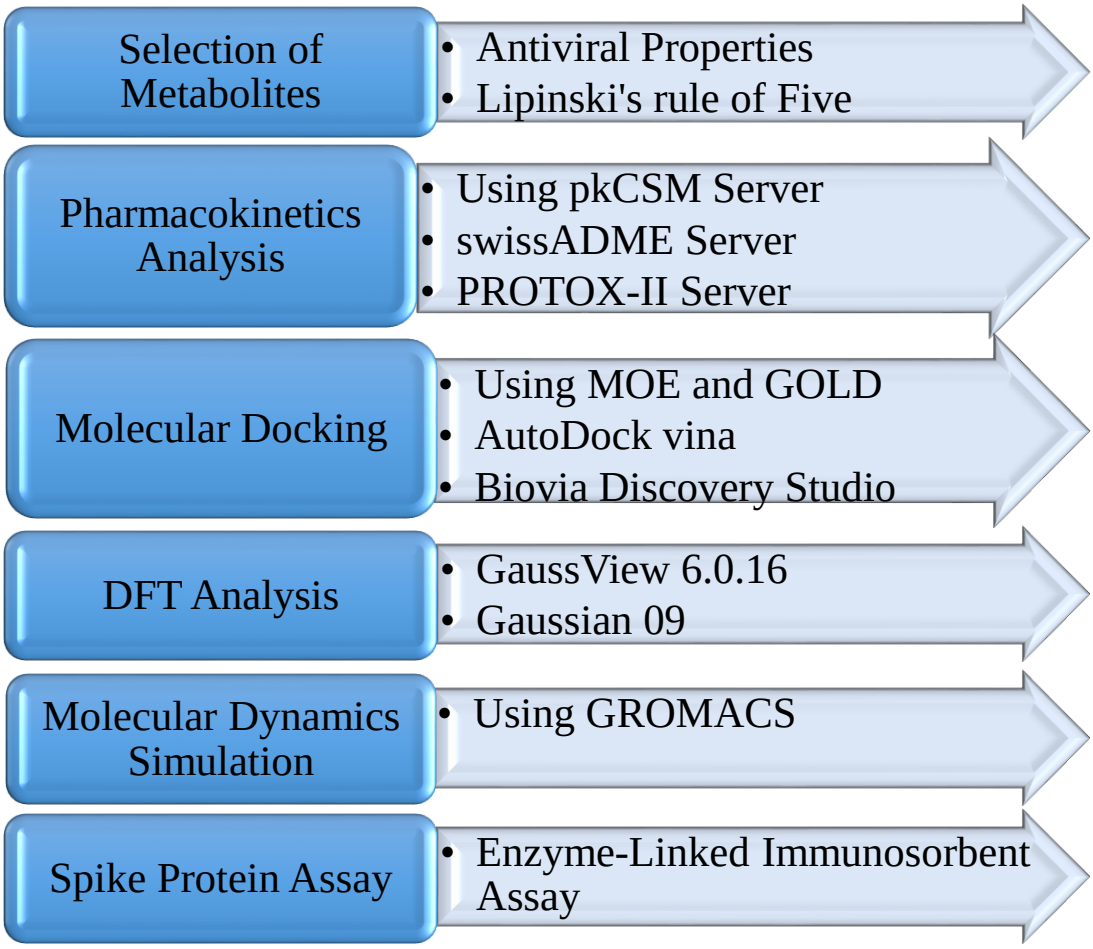

1.8 Hypothesis

Natural products extracted from medicinal plants, which show promising inhibitory action against viruses such as SARS-CoV, MERS-CoV, Influenza-parainfluenza, respiratory syncytial virus, chikungunya virus, might also be potent metabolites against SARS-CoV-2. However, screening big datasets of natural metabolites *in vitro* and *in vivo* has proven to be a time-consuming operation. Hence, investigations should be conducted using computational techniques followed by *in vitro* analysis is necessary for furnished shreds of evidence. This research will proceed by selecting a diverse library of 191 metabolites with antiviral characteristics which could hopefully be a promising sector of investigation in computational chemistry.

1.9 Rationale of the Study

The traditional way of drug development is a lengthy process, expensive and risky. In recent years, CADD has assisted in reducing the time scale, and expense faced by traditional methods. In this study, *in silico* approaches were used where possible pharmacological targets were computationally identified and massive groups of compounds were virtually screened for promising drug candidates. Thus, the quickest method of finding novel viral-entry inhibitors from natural sources could be used *in silico* methods. The finest resources for further investigation and inquiry are natural compounds, particularly those with known antiviral properties. Therefore, the extensive virtual screening and identification of secondary metabolites using *in silico* computational techniques, along with their safety and toxicity profiles, could be a turning point for academics and mankind in the fight against the pandemic.

CHAPTER 2

2. LITERATURE REVIEW

Although COVID-19 is no longer pandemic, there is still a need for specific antiviral therapeutics as new variant of coronavirus could reappear in any time. Researchers have turned towards natural resources, concentrating notably on plant metabolites, to find potential lead compounds to combat human diseases because pathogens are becoming more resistant to allopathic medications (Xu *et al*., 2020). Secondary metabolites are a source of naturally occurring antiviral substances that may be a viable alternative to current pharmaceuticals.

2.1 Computational Investigation

Tinospora cordifolia extract's chemical components, which belong to several classes including lignans, terpenoids, alkaloids, and steroids, have been investigated as possible COVID-19 alternatives for treatment based on their therapeutic potential. By altering the chemical structures and using computational geometry optimization and docking techniques, the list of components from *T. cordifolia* was reduced, which made it possible to modify their capacity to inhibit SARS-CoV-2 (Jena *et al*., 2021). The native Indian medicinal plant *T. cordifolia's* secondary metabolies have a high binding efficacy and are capable of inhibiting the SARS-CoV-2 main protease (Thakkar *et al*., 2021). Berberine extracted from *T. cordifolia* has been suggested as a strong metabolite to inhibit 3CLpro protein under the *in silico* investigation (Chowdhury, 2021). The compound tinosponone from *T. cordifolia* was found to be effective inhibitor of $3CL^{pro}$ of SARS-CoV-2, as demonstrated by the computer-aided drug design technique (Krupanidhi *et al*., 2021). Additionally, it was discovered that *T. cordifolia*, which has strong antiviral activity, is a promising dengue therapeutic (Paul *et al*., 2021). In addition berberine, isocolumbin, magnoflorine, and tinocordiside showed high binding efficacy against RBD, surface glycoprotein, RdRp, and main protease of SARS-CoV-2 (Sagar & Kumar, 2020). *T.crispa* methanolic extract shows potential as pyrexia reducers and sources of olites from the *Tinospora sps* should be investigated further against SARS-CoV-2 and employed for COVID-19 therapy.

A broad class of phytochemicals known as flavonoids is frequently present in a variety of foods and vegetables that are consumed by humans. Flavonoids have multiple

beneficial pharmacological effects, including the ability to combat viruses. It has been shown that these substances can prevent the spread of viruses by affecting crucial phases of the virus life cycle (Sadati *et al*., 2018). The flavonoids, hesperidin, naringin, and epigallocatechin-3-gallate (ECGC) were found to be potent inhibitors of SARS-CoV-2 S-RBD through computational studies (Bhowmik *et al*., 2021). Similarly, naringin was found to be a suitable drug candidate for the inhibition of spike protein (Jain *et al*., 2021). Amentoflavone, Bilobetin, and Silibinin showed inhibitory effects on the S1-RBD and $3CL^{pro}$ proteins of SARS-CoV-2 (Hadni *et al*., 2022). An analysis shows that luteolin and mundulinol have promising anti-COVID-19 properties by blocking the spike protein and M^{pro} of SARS-CoV-2 (El-Mageed *et al*., 2021).

The alkaloids, which belong to the most significant class of secondary metabolites found in plants, are heterocyclic compounds that are often produced from amino acids and contain one or more nitrogen atoms in their structure. They make up 15-20 % of all known natural substances and have an estimated 12,000 molecules in them (Rosales *et al*., 2020). Alkaloids are distinguished by their nitrogen atoms, which give rise to their alkaline characteristics and therapeutic effects. A molecular docking and MD simulation-based in silico analysis revealed ajamalicine, aranotin, and piperine exhibited potent interactions with the SARS-CoV-2 Nsp-15 protein (S. Kumar *et al*., 2021). According to a study, quinolone alkaloid have the ability to impede and even block the interaction between th S protein and the ACE 2 receptor, which makes them useful in managing SARS-CoV-2 infection (Mamkulathil Devasia *et al*., 2021).

Terpenes are naturally occurring isoprene-based molecules that exhibit chemical diversity and a multitude of medicinal actions (Bergman *et al*., 2019). This class of natural compounds extracted from a variety of medicinal plants has been established to possess curing properties for diverse ailments, such as malaria, cancer, and neurological disorders (Ricotta & Kwan, 2019) (Zhu & Chen, 2019) (Turner *et al*., 2017). Besides, terpenes have shown wide ranges of antiviral, anti-inflammatory, anti-microbial, and analgesic properties against SARS-CoV (Wen *et al*., 2007), herpes simplex virus, West Nile virus, Human Immunodeficiency Syndrome virus (Chatow *et al*., 2021), and therefore, could be used as novel medications or prototypes for developing effective pharmacotherapeutic agents. According to previous *in silico* analysis, terpenes, such as methyl tanshinoate, sugiol, and α-cadinol have been predicted to inhibit M^{pro} of SARS-CoV-2 (Diniz *et al*., 2021). Terpenes function as inhibitors, impeding the interaction

between the ACE-2 receptor and SARS-Cov-2 S-RBD, therefore reducing the virus's ability to infect host cells (Muhseen *et al*., 2020). Similarly, stachyflin, a terpenoid is the lead drug candidate for SARS-CoV-2–RdRp as it demonstrates a comparatively higher docking score than referral drugs remdesivir and favipiravir (Sahoo *et al.*, 2021). Plant-derived terpenoids, including 24-methylene cycloartenol and isoiguesterin have been identified as potential inhibitors of coronavirus cell entrance proteins using a virtual screening approach (Gyebi *et al*., 2021). The viral cysteine proteases, M^{pro} and PL^{pro}, of the SARS-CoV were discovered to be specifically and selectively inhibited by tanshinones (tanshinone IIB, methyl tanshinoate, dihydrotanshinone I, cryptotanshinone, and tanshinone I) extracted from *Salvia miltiorrhiza* (Park *et al*., 2012).

2.2 *In Vitro* Investigation

The ethanol extract of *T. cordifolia*, crude extract, and presence of distinct bioactive compound classes in the bioactive fraction have demonstrated effective and inhibitory antiviral activity against DENV-2, potentially impeding the virus's ability to infect the host cell (Paul *et al*., 2021). *T. cordifolia* stem extract possesses anti-viral, anti-fungal, and anti-bacterial properties. In the Vero cell line, its stem extract effectively suppresses the herpes simplex virus by 61.43% (S.M. Gopinatha, 2018). Analyzing the efficacy of natural compounds from *T. cordifolia*, tinocordiside and isocolumbin showed less than 1 μM IC_{50} value against surface glycoprotein and main protease.

Flavones derived from *Torreya nucifera*, such as amentoflavone, quercetin, luteolin, and apigenin, have also been shown to inhibit $3CL^{pro}$ (Jeong *et al*., 2010). Amentoflavone was highly effective at inhibiting the SARS-CoV $3CL^{pro}$ when tested *in vitro*, with an IC_{50} value of 8.3 μM (Ryu *et al*., 2010). Polyphenols, broussochalcone A, broussochalcone B, papyriflavonol A, broussoflavan A, kazinol A, B, F, and J, 4,7-trihydroxyflavane, 30-(3-methylbut-2-enyl)-30, and 4-hydroxyisolonchocarpin, isolated from *Broussonetia papyrifera* displayed promising activity against SARS-CoV (Park *et al*., 2017). Hypericin, cyanidin 3-glucoside, baicalin, glabridin, can inhibit M^{pro} of SARS-CoV-2 (Islam *et al*., 2020). The active (pure) compounds isolated from *Garcinia celebica L., Tripterygium regelii* (Sprague &Takeda), *Ecklonia cava, Utrica dioica, Allium sativum L., Scutellaria baicalensis* (Baikal skullcap), in different countries, have shown effective inhibitory activity against SARS-CoV and SARS-CoV-

2 (Kumaki *et al*., 2011); (Muchtaridi *et al*., 2020); (Park *et al*., 2013); (Ryu *et al*., 2010); (Jo *et al*., 2019).

Alkaloids and alkaloid-based compounds have significant repressive effects against SARS-CoV-2, according to an *in vitro* screening of alkaloid compounds (mainly antimalarial inhibitors). The antiviral activity of medicines based on pyronaridine alkaloids, hydroxyl-chloroquine, and chloroquine was found to be significant against SARS-CoV-2, with EC_{50} values of 1.8, 1.5, and 2.1 μM (Gendrot *et al*., 2020). With an *in vitro* study of the alkaloid, berberine was found to suppress influenza A virus (IAV) infections in RAW-264.7 cells at concentrations more than 1 μM; however, its IC_{50} was only 0.01 μM (Cecil *et al*., 2011). Berberine exhibited a direct repressive impact on IAV infection both *in vitro* and *in vivo*, and it significantly reduced the degenerative alterations in the mice's lungs (Wu *et al*., 2011). A study conducted in vitro investigated the effectiveness of several antiviral medications and alkaloids against SARS-CoV-2 in Vero E6 cells. The results showed that homorringtonine and emetine alkaloids were able to inhibit the virus with EC_{50} values of 2.55 μM and 0.46 μM, respectively (Choy *et al*., 2020).

In preclinical animal models, many terpenoids have been shown to possess cytotoxic effects against a range of cancer cells (J. Huang *et al*., 2008). With half maximal effective concentration of 365 μM against SARS-CoV-2, glycyrrhizin, a triterpenoid saponin, has been shown to inhibit replication of SARS-associated virus in several SARS patients (Van De Sand *et al*., 2021). Some *in vitro* studies also reveal that terpenes could be investigated as anti-SARS-CoV-2 drugs, with the possibility of using them as treatment or adjuvants to current COVID-19 therapies (Santos *et al*., 2022). Hence, different medicinal plants extract like saponin, flavonoids, alkaloids, terpenes, polyphenols, monoterpenoids, triterpenoids, have exhibited diverse antiviral activities (**Table 2**).

Secondary metabolites offer a promising avenue for the development of therapeutic agents against COVID-19. Their natural diversity, biological activities, and potential for drug repurposing make them attractive candidates. However, challenges related to chemical complexity, variability in production, toxicity, and the risk of drug resistance need to be carefully addressed. Further research and development are necessary to fully realize the potential of secondary metabolites as medication to combat COVID-19.

Table 2: Some secondary metabolites as antiviral agents.

Secondary metabolites	Activity Value (IC_{50} and EC_{50})	Inhibited Virus	reference
Glycyrrhizin	365 μM	SARS-CoV	(Cinatl *et al*., 2003)
Scutellarein	5.8 μM 0.86 μM (Nsp13)	SARS-CoV	(Yu *et al*., 2012); (Keum & Jeong, 2012)
Cyanidin	65.1 ± 14.6 μM	SARS-CoV, SARS-CoV-2	(Pitsillou *et al*., 2020)
Baicalin	7.4 μM	SARS-CoV, SARS-CoV-2	(H. Su, Yao, Zhao, Li, Liu, Shang, Xie, Ke, Gao, *et al*., 2020)
Luteolin	20.2 μM	SARS-CoV, SARS-CoV-2	(Boozari & Hosseinzadeh, 2021); (Ryu, Park, *et al*., 2010); (Jo *et al*., 2019)
Mimulone	14.4 μM	SARS-CoV	(Cho *et al*., 2013)
Amentoflavone	8.3 μM	SARS-CoV, SARS-CoV-2	(Boozari & Hosseinzadeh, 2021) (Goris *et al*., 2021; Jo *et al*., 2020)
Epigallocatechin Gallate	73 μM 2.47 µg/mL	SARS-CoV SARS-CoV-2	(Henss *et al*., 2021) (Nguyen *et al*., 2012)
Berberine	—	SARS-CoV-2	(Chowdhury, 2021)
Savinin	25 μg/ml	SARS- CoV-2 $3CL^{pro}$	(Wen *et al*., 2007)
Celastrol	10.3 μmol/l	SARS- CoV-2 $3CL^{pro}$	(Ryu, Park, *et al*., 2010)
Pristimerin	5.5 μmol/L	SARS- CoV-2 $3CL^{pro}$	(Ryu, Park, *et al*., 2010)
Tingenone	9.94 μmol/L	SARS- CoV-2 $3CL^{pro}$	(Ryu, Park, *et al*., 2010)
Iguesterin	2.64 μmol/L	SARS- CoV-2 $3CL^{pro}$	(Wen *et al*., 2007)
Aloe emodin	132.00 μM	SARS-CoV $3CL^{pro}$	(Lin *et al*., 2005)
Emodin	200 μM	Spike protein-pseudotyped to vero E6cell	(Ho *et a*l., 2007)
Herbacetin	33.17 μM	SARS-CoV $3CL^{pro}$	(Jo *et al*., 2020)
Rhoifolin	27.45 μM	SARS-CoV $3CL^{pro}$	(Jo *et al*., 2020)
Pectolinarin	37.78 μM	SARS- CoV $3CL^{pro}$	(Jo *et al*., 2020)
Baicalein	0.94 μM	SARS-CoV-2 $3CL^{pro}$ inhibitor	(H. Su, Yao, Zhao, Li, Liu, Shang, Xie, Ke, Hu, *et al*., 2020)
Cryptotanshinone	0.80 μM/226.70 μM	SARS-CoV PL^{pro} Inhibitor/SARS-CoV-2 $3CL^{pro}$	(Park *et al*., 2012)

Tomentin B	6.10 μM	SARS-CoV PL^{pro} Inhibitor	(Cho *et al*., 2013)
Tomentin E	5.00 μM	SARS CoV PL^{pro} Inhibitor	(Cho *et al*., 2013)
Inophyllum P	0.130 μM	HIV-1 reverse Transcriptase $3CL^{pro}$ SARS-CoV-2	(Abdizadeh *et al*., 2022)
Wedelolactone	36.1 μM	Hepatitis C virus (HCV) HCV, NS5B polymerase $3CL^{pro}$ of MERS CoV and SARS CoV	(Abdizadeh *et al*., 2022)
(+)- calanolide A	20 μM	HIV, SARS Coronavirus $3CL^{pro}$	(Chidambaram *et al*., 2021) (Kashman *et al*., 1992)
Polyflavonol A	3.7 μM	$3CL^{pro}$ and propane-like coronavirus protease	(Park *et al*., 2017)
7- phloroeckol	18.6±2.3 μM /42.1± .2 μM	Porcine epidemic diarrhea CoV (Blockage and binding of viral cell $3CL^{pro}$ SARS-CoV)	(Park *et al*., 2013)
Phlorofucofuroeckol	10.8±1.4 μM/16.7±3.3 μM	Porcine epidemic diarrhea CoV (Blockage and binding of viral cell $3CL^{pro}$ SARS-CoV)	(Kwon *et al*., 2013) (Park *et al*., 2013)
Daidzein	351±2.9 μM	Inhibitory against $3CL^{pro}$	(Nguyen *et al*., 2012)

CHAPTER 3

3. MATERIALS AND METHODS

3.1 Computational Chemistry

3.1.1 Computational Working Station

The computational investigations were conducted using GNU/Linux workstation equipped with an Intel Core-i7 processor, 8 GB RAM of system memory, and an Nvidia GeForce RTX 2060 64 GB GPU. The DFT was carried out through GaussView 6.0.16 software (Accessed on March 2023). MOE 2020.09 (Accessed on August 12, 2021) (Wolber & Langer, 2005) was utilized to prepare proteins, and ligands, analyze binding sites, and GOLD software version 4.0.1 (Accessed on November 20, 2020) was used in determining ligands binding to the target proteins (Jones *et al*., 1997b). AutoDock Vina 1.5.7 (Accessed on April 14, 2021) https://vina.scripps.edu/ (Trott & Olson, 2009) was utilized for the molecular docking of ligand and protein molecules, while the MD simulations for the complexes were conducted using GROMACS 5.1.1 (Accessed on September 21, 2021) https://manual.gromacs.org/5.1.1/download.html.

3.1.2 Selection of Plant-based Secondary Metabolites

After an extensive literature review, 191 metabolites with reported IC_{50} and/or EC_{50} values against different kinds of viruses such as SARS, MERS, HIV, HSV, DENV, HCV, and SARS-CoV-2 itself (**Appendix A1**) are selected.

3.1.3 Pharmacokinetic Study

Identification of drug-resembling properties of these selected metabolites was performed through the available bioinformatic tool swissADME http://www.swissadme.ch/ (Daina *et al*., 2017). Furthermore, ADMET analysis and forecasting of the toxicity of the selected metabolites were done via pkCSM https://biosig.lab.uq.edu.au/pkcsm/ and ProTox II web servers https://tox-new.charite.de/ (Pires *et al*., 2015) (Banerjee *et al*., 2018).

3.1.4 Preparation of Protein

- **Preparation of protein using MOE:** Crystal structure of the SARS-CoV-2 spike RBD [PDB ID: 6M0J (Lan *et al*., 2020)], RBD of spike glycoprotein (PDB

ID: 7NX8); and RdRp protein sequence of SARS-CoV-2 (PDB ID: 6M71 and 7B3C) were retrieved from research collaboratory for structural bioinformatic protein data bank (RCSB PDB) https://www.rcsb.org/ (Berman *et al*., 2000) and used for computational docking. MOE protein preparation wizard is utilized to eliminate water molecules, adding atomic charges and hydrogen atoms for every protein atom, the resulting structures were optimized. Moreover, energy minimization was done using parameters (Force Field: AMBER10: EHT; R-Field 1:80, cutoff [8,10], gradient:0.1, and Constraints: Rigid water molecule). Furtermore, a mutation was introduced into the resulting protein (7NX8) at position 417 by substituting asparagine (N) for threonine (T) using a sequence editor of MOE software's protein builder.

- **Preparation of protein using AutoDock tools:** Crystal structure of S1-RBD of SARS-CoV-2 Omicron variant (PDB ID: 7QNW) was uploaded from RCSB protein data bank, and each amino acid was examined individually, analyzed, confirmed, and using BIOVIA Discovery Studio, the protein was cleaned by removing unwanted chains, heteroatoms, and water molecules. The protein was then prepared using the AutoDock tool 1.5.6 by adding polar hydrogen atoms and Kollmann charges and it was ultimately saved in the .pdbqt format.

3.1.5 Preparation of Ligands

191 antiviral metabolites were reviewed, and ChemDraw files were generated (**Figure 9 and Appendix F1**), and accessed from the PubChem database using (Hähnke *et al*., 2018) ChemSpider (Pence & Williams, 2010) and processed into a different format (.sdf, .mol2, .pdb) using MOE-Molecule Builder, Pymol, and Discovery Studio. Ligands were prepared by using appropriate parameters of ligand preparation module such as optimization, ring conformation, 2D to 3D conversion, and protomers, tautomers, and ionization states at pH 7.0 as well as partial atomic charges using the OPLS3e force field were determined (Roos *et al*., 2019). The metabolites were then converted into the .mol2 and the .pdb file formats, and the MOE and AutoDock vina were used to minimize their energy for further process of molecular docking (Chen & Foloppe, 2010). To perform docking with AutoDock software, ligands were saved in the .pdbqt format and polar hydrogens were added for docking reasons.

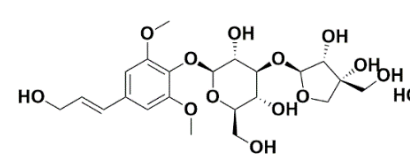

Cordifolioside A

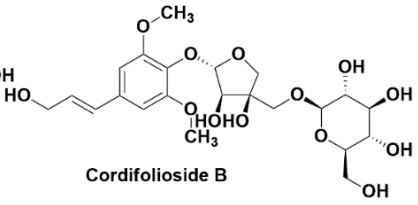

Cordifolioside B

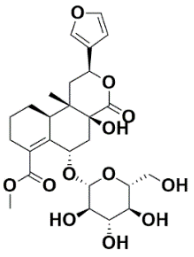

Cordioside

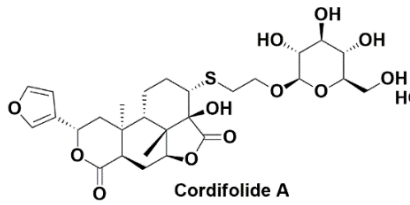

Cordifolide A

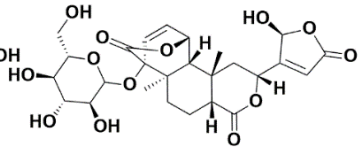

Cordifolide B

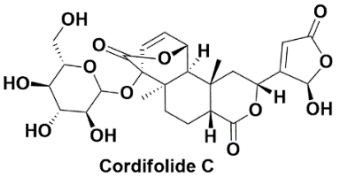

Cordifolide C

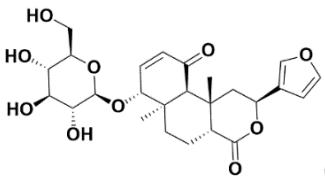

Tinosporaside

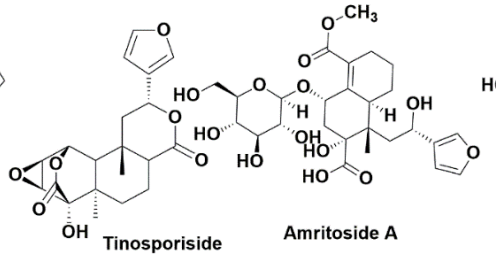

Tinosporiside

Amritoside A

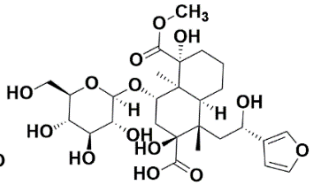

Amritoside B

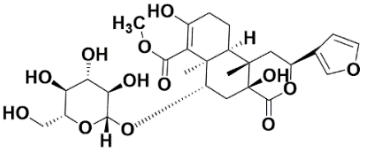

Amritoside C

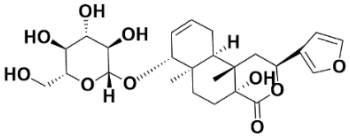

Amritoside D

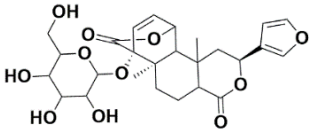

Palmitoside F

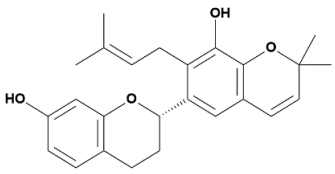

Kazinol B

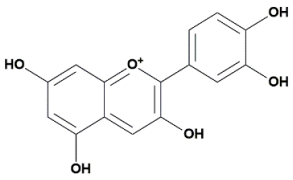

Cyanidin

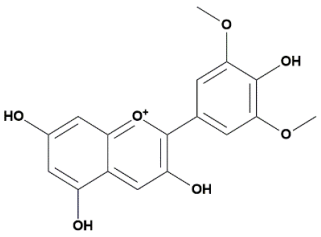

Malvidin

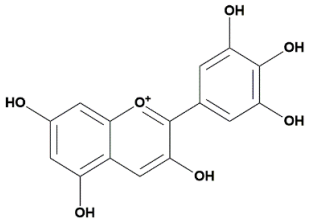

Delphinidin

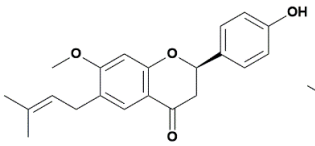

Bavachinin

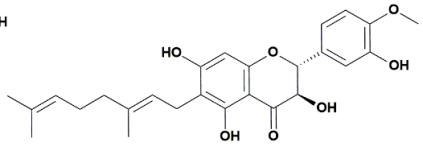

4'-O-Methyldiplacol

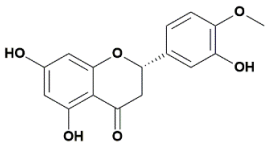

Hesperetin

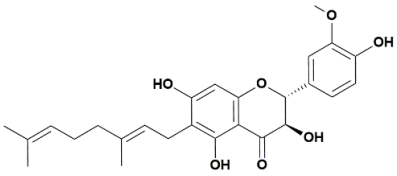

3'-O-Methyldiplacol

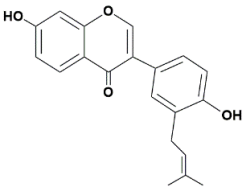

Neobavaisoflavone

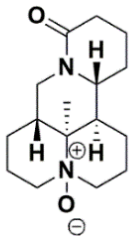

Oxysophoridine

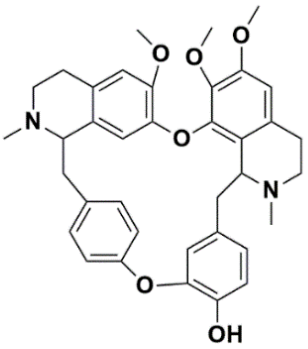

Berbamine

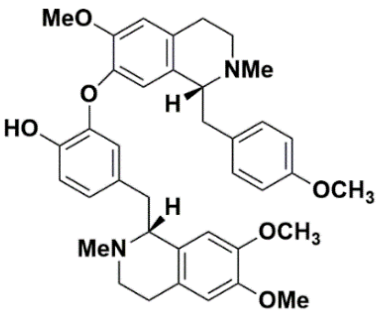

Neferine

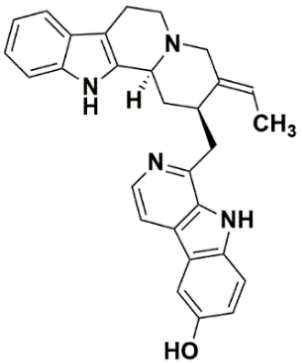

10'-hydroxyusambarensine

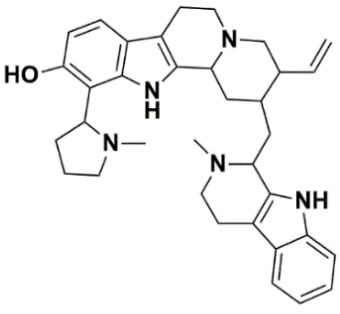

Strychnopentamine

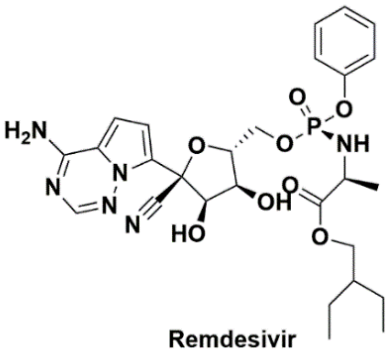

Remdesivir

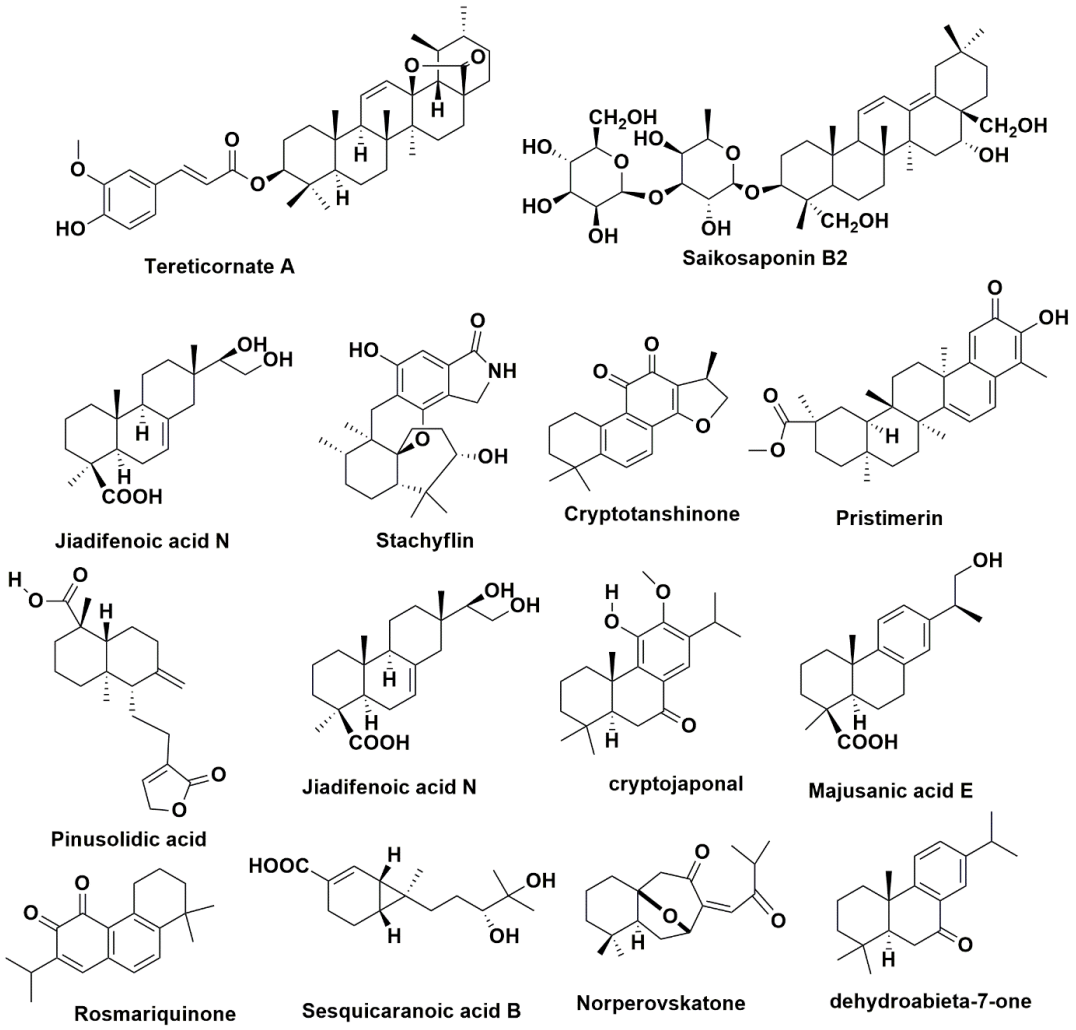

Figure 9: Some structures of selected secondary metabolites reported as antiviral agents from plants.

3.1.6 Binding Site Prediction

MOE Site Finder, employing the theory of alpha spheres, amino acid residues were identified within the binding site of the target protein, taking into account the receptor atoms' accessibility and relative positions (He *et al*., 2011). Additionally, the site finder predicted the number and names of the residues comprising the active site. **Figure 10** depicts the binding cavity of the spike protein, presenting a surface map and active site. The binding sites of target proteins can be analyzed and predicted through an extensive literature review (Bhowmik *et al*., 2021; Ortega *et al*., 2021) and also the binding pocket of the co-crystallized ligand with the target protein (Jin *et al*., 2020).

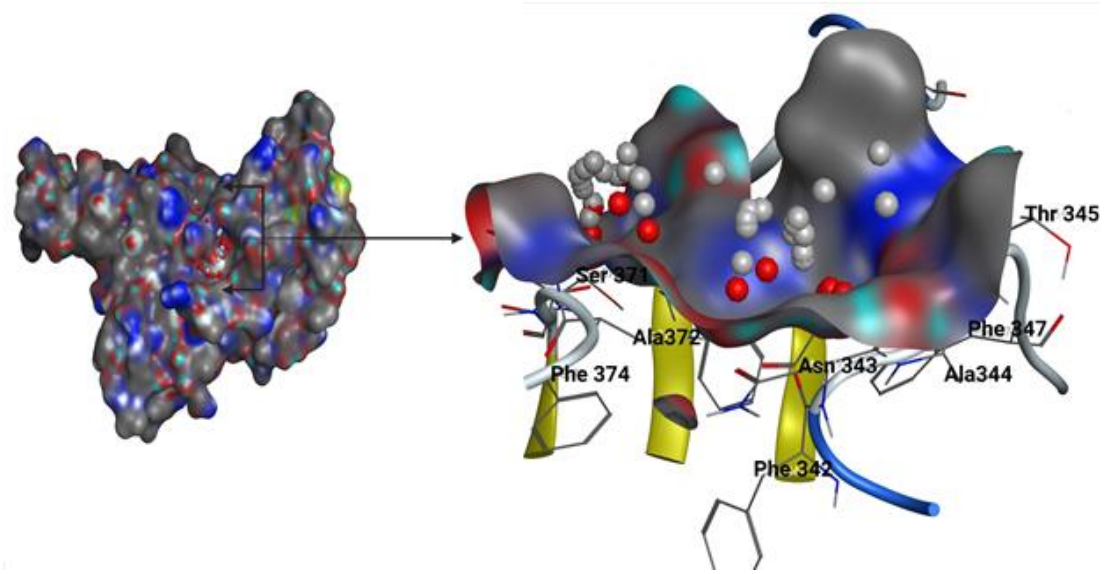

Figure 10: Surface map (left) and binding pocket (right) of the spike protein.

3.1.7 Molecular Docking and Validation

- **Molecular docking using MOE and GOLD**

  All the molecular docking investigations were performed on a Microsoft Windows workstation (Intel Core i5-9400 CPU processor and system memory 4GB RAM). MOE version 3.12 (Wolber & Langer, 2005) and GOLD software version 4.0.1 was used in determining ligands binding to the target proteins (Jones *et al*., 1997b) and applied to the GOLD software which were conducted for atoms within 10 Å of the submitted binding residues within the binding pocket. The complex stability for the selection of compounds from the docking poses was checked through computational analysis. To validate the docking results, using the GOLD default docking procedures, the top-scored compounds and the commercial medication were removed from their original binding site and then redocked into the same place (Onodera *et al*., 2007; Warren *et al*., 2006). Further, when the previous docking orientations of compound were placed over the lowest energy pose found during redocking, the RMSD was computed.

- **Molecular Docking using AutoDock Tools and BIOVIA Discovery Studio**

  The structures were improved by adding polar hydrogen atoms and Kollmann charges before being saved in the .pdbqt format by the AutoDock tools (https://vina.scripps.edu/) (Morris *et al*., 2009). With the dimensions 60 × 60 × 60 Å, a grid box was created and centered on the key residues where potent

compounds would preferably bind. Grid box centering plays a crucial role in molecular docking, significantly impacting the accuracy of predicted binding poses. The docking approach was tested if the co-crystallized ligand was present, and the binding pocket was considered to be acceptable if the RMSD was less than 2 Å between the co-crystallized and docked ligand (Elekofehinti *et al*., 2018) (Saliu *et al*., 2021).

3.1.8 DFT Analysis

The reactivity and effectiveness of the potent metabolites against SARS-CoV-2 spike protein were investigated employing a DFT analysis using the highest occupied molecular orbital (HOMO) and lowest unoccupied molecular orbital (LUMO) energy utilizing the 3-parameter, Becke, Lee-Yang-Parr (B3LYP) correlation function (Gill *et al*., 1992). The following equation estimates the band energy gap (ΔE):

$$\Delta E = E_{LUMO} - E_{HOMO} \quad (1)$$

The ionization potential (IP) and electron affinity (EA) of the molecules were calculated using the given equation (Vektariene *et al*., 2009):

$$IP = - E_{HOMO} \quad (2)$$

$$EA = - E_{LUMO} \quad (3)$$

The following equations were used to determine global softness (S), global hardness (η), electronegativity (χ), and chemical potential (μ) (Anigboro *et al*., 2021):

$$S = 1/\eta \quad (4)$$

$$\eta = \Delta E/2 \quad (5)$$

$$\chi = (I + A) / 2 \approx - \mu \quad (6)$$

$$\omega = \mu^2/2\eta \quad (7)$$

3.1.9 Molecular Dynamic Simulation

MD simulations were performed in GROMACS 5.1.1 using CHARMM36, CHARMM27, and GROMOS 43a1 force fields for protein-ligand systems to clarify the facts behind the efficiency of these drugs in protein inhibition (Mark & Nilsson, 2001); (Okimoto *et al*., 2009). The GROMACS tool was used to produce the protein topology file, and the SwissParam http://www.swissparam.ch/ and PRODRG and automated

topology builder (ATB) server were used to parameterize the ligand topology of natural metabolites and pick hits (Bugnon *et al*., 2023) (Schüttelkopf & van Aalten, 2004). By the addition of Na^+ (sodium ion) and Cl^- (chloride ion) with a 0.1 M ionic strength water environment, the solvated system was neutralized. Equilibration of systems (using NVT and NPT) at 1 bar pressure for 1ns was connected using a Parrinello-Rahman Barostat in this simulation (Mazumder *et al*., 2018). Using trajectories obtained from the simulation, calculation of root mean square deviation (RMSD), root mean square fluctuation (RMSF), the radius of gyration (Rg), binding free energy (BFE), solvent accessible surface area (SASA), and several hydrogen bonding analyses were performed. Additionally, using Lennard-Jones potential, short-range protein-ligand interaction energy was calculated.

All the MD runs were executed on an AMD processor (32 cores/64 thread) with 128 GB RAM, running an Ubuntu v14.041 Linux operating system on an HP Z230 workstation, Computational Laboratory, Central Department of Chemistry, Tribhuvan University, Kathmandu, Nepal.

3.1.10 Calculation of Binding-Free Energy

Prime Molecular Mechanics Generalized Born Surface Area (MM-GBSA) module of the Schrodinger suite with OPLS force field was used to analyze the binding free energies of protein-ligand complexes (Mulakala & Viswanadhan, 2013b). The docking complex determines the prime MM-GBSA approach and it helps to calculate the binding free energy of the protein-ligand system using the following formula;

$$\Delta G_{BFE} = \Delta E_{MM} + \Delta G_{Solv} + \Delta G_{SA}$$

The BFE acquired from prime MM/GBSA calculations, coupled with the docking score, was used to enhance the metabolites and choose the top compounds. The MM/GBSA method was adopted to calculate the ΔG_{BFE} in this research work.

3.2 *In Vitro* Study

3.2.1 Preparation of Crude Extract

About 40 g shade-dried ground powder of *Tinospora cordifolia* (stems, location: Bajhang; 2907 m) (Voucher Specimen TUCH-210052) and *vitis vinifera* (fruits collected from Kalimati market on June 2022) (Variety number: 22608; Origin of Variety: Australia; and Cultivar name: Malian) was extracted in methanol. It was left

for 72 hours in solvent and decanted, filtered, and concentrated using a rotatory evaporator to eliminate all traces of methanol. For yield calculations, the weight of the concentrated dry extract was noted and stored in the refrigerator at 4 °C.

3.2.2 Spike Protein Assay Using ELISA Kit

In vitro Spike S1-RBD and ACE2 Inhibitory Activity of SARS-CoV-2 by Enzyme-Linked Immunosorbent Assay (ELISA)

For testing, the potent metabolites, identified through computational investigations, suppress the interaction between ACE2 and SARS-CoV-2 S1-RBD, spike protein assays were performed with crude extracts as well as with pure potent compounds. *In vitro* S1-RBD assay was performed following the protocol of literature (Gangadevi *et al*., 2021) with few modifications. For each extract and pure compounds, the experiment was performed in triplicate, and the percentage of inhibition was reported as the mean ± standard error of the mean (SEM). Initially, to a 96-well plate coated with S1-RBD of the SARS-CoV-2 Omicron variant (ACROBiosystems; Catalog No. RP-13), varying concentrations of 100 µL crude extract of *T. cordifolia* and red grapes (*Vitis vinifera*), and pure compounds cryptotanshinone (Sigma-Aldrich: C5624-5mg, ≥ 98% (HPLC)), neferine (Sigma-Aldrich: SML0349-5mg, ≥ 98% (HPLC)), and molnupiravir (EIDD-2801) (Sigma-Aldrich: SML2873-5mg, ≥ 98% (HPLC)) were added, succeeded by preincubation at 37 ℃ for 4 hours. Then PBS buffer was used to wash the plates for three times and a blocking solution (1 % BSA and 0.05% Tween-20 in phosphate buffered saline (PBS)) was added to the well plate and again incubated for 1 hr at 37 °C. After three washes, 100 µL of hACE2 receptor protein (Novatein Biosciences Inc. Woburn, MA, USA; Catalog no.: PR-nCoV-4) (0.1 – 0.2 µg/mL) and binding buffer (0.1 % bovine serum albumin (BSA) in PBS, pH 7.2) were added and again incubated for 1 hr. The plates were washed and, 100 µL of 1:15000 dilution of goat anti-human IgG-Fc, HRP (NOVATEINBIO; Catalog no.: NB-A0101) was added to each well of 96 well plates and incubated at 37 ℃ for 30 minutes. Finally, the stop solution was added to end the reaction and at 450 nm absorbance was measured following three washes. The following formula was employed to evaluate the inhibitory activity:

$$\% \text{ Inhibition} = \left(\frac{A_{control} - A_{sample}}{A_{control}}\right) \times 100$$

Where, A is the absorbance of the sample and the control.

And to find the standard error of the mean following equation was utilized:

$$SE = \frac{\sigma}{\sqrt{n}}$$

where, SE is standard error of the mean; σ is standard deviation; and n is sample size.

The pictorial demonstration of the protein assay procedure is displayed in **Figure 11**.

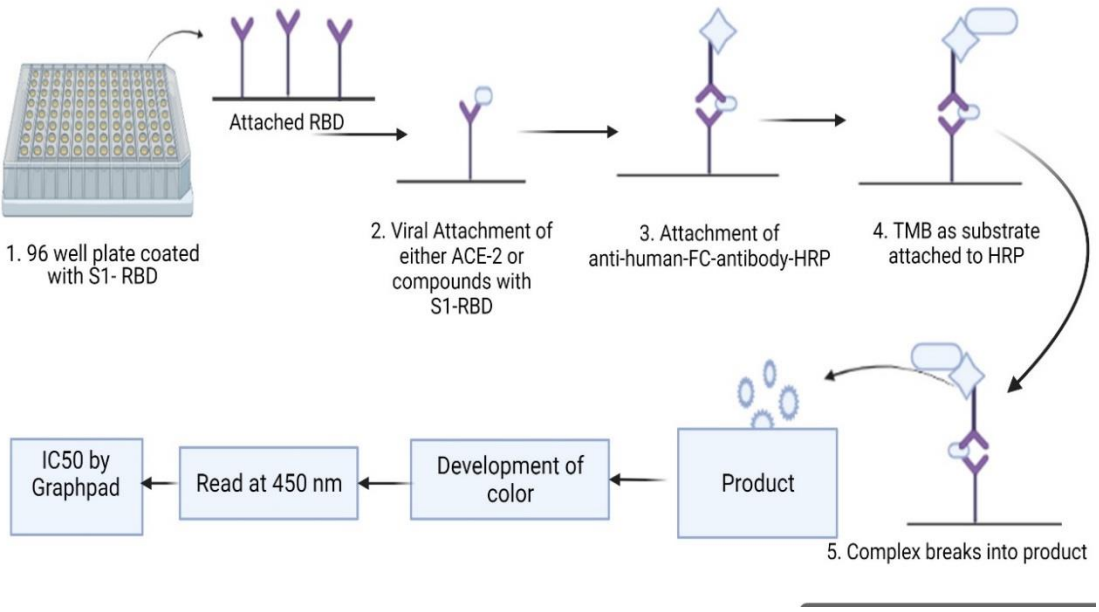

Figure 11: Showing *in vitro* process using ELISA technique.

CHAPTER 4

4. RESULTS AND DISCUSSION

4.1 Investigation of Secondary Metabolites from *Tinospora* species

4.1.1 Molecular Docking Analysis

The library of 26 secondary metabolites from *Tinospora sps*. being based on their antiviral properties were chosen for molecular docking which is promised to be a robust method for the selection of compounds in a short period (Fan *et al*., 2019). Molecular docking, which involves introducing small 3D structures of ligands into the binding pocket of receptors, can help to obtain insight into molecular recognition, drug discovery, and medicinal chemistry. The docking poses and ligand-protein interactions were used to analyze the results (Li *et al*., 2019). From this investigations, it was observed that cordifolioside A binds significantly into the binding pockets of S1-RBD with a GOLD Fitness Score of 58.27 (**Table 3**) which manifest the excellent binding affinity of protein-ligand complex. Likewise, tinosinenoside A with a GOLD Fitness Score of 54.86 interacts with the binding site residues. Besides, borapetoside C, borapetoside B, palmitoside G, and rhumphioside A have also demonstrated acceptable binding interaction with GOLD Fitness Scores of 54.52, 53.68, 50.80, and 50.77, respectively (Sharov *et al*., 2022).

Cordifolioside A has interacted through Thr 430, Phe 515, and Leu 517 residues of S1-RBD in the distance between 2.36 – 2.83 Å. These residues are predicted as key residues of S1-RBD of SARS-CoV-2 for the fusion to host cell. The protein-ligand interaction reveals four hydrogen bond interactions at the Thr 430, Phe 515, and Leu 517 **(Figure 12 b).** Similarly, remdesivir interacts with Ser 349, Asn 354, Ala 348, and Phe 347 (**Figure 12 a**) which have an interaction length of 1.92 – 2.94 Å. Besides, tinosinenoside A interacts with hydrogen bonds to Glu 516 and Lys 462 with the S1-RBD protein region **(Figure 12 c),** likewise, borapetoside C shows interactions (**Figure 12 d**) with Thr 430, Val 382, Leu 390, Leu 518. **Appendix F2** and **F3** display the 2D and 3D structures of the remaining compounds representing interactions with S1-RBD. Additionally, this study further investigated and clarified the interactions between target protein and ligands. Binding energies, proper poses, and docking accuracy prediction were measured by GOLD Fitness Scores values. Appendix B1 illustrates the

GOLD Fitness Scores in detail as well as interactions of ligands with residues and binding energies with bond length.

Table 3: The binding energies and docking score of natural compounds against S1-RBD by molecular docking assay

Compound	GOLD Fitness Score	Binding Free Energy MM/GBSA (ΔGbind) (kcal/mol)	Interacting Residues	Interaction Length (Å)
Remdesivir	28.53	-18.40	Ser 349 Asn 354 Ala 348 Phe 347	1.92 2.77 2.76/2.94 2.59
Cordiofolioside A	58.27	-25.09	Thr430 Phe515 Leu517	2.36 2.40/2.83 2.65
Tinosinenoside A	54.86	-22.75	Glu 516 Lys 462 Glu 465	1.69/2.77 2.42 4.96
Borapetoside C	54.52	-11.66	Thr 430 Val 382 Leu 390 Leu 518	2.29 4.76 5.48 4.82

a)

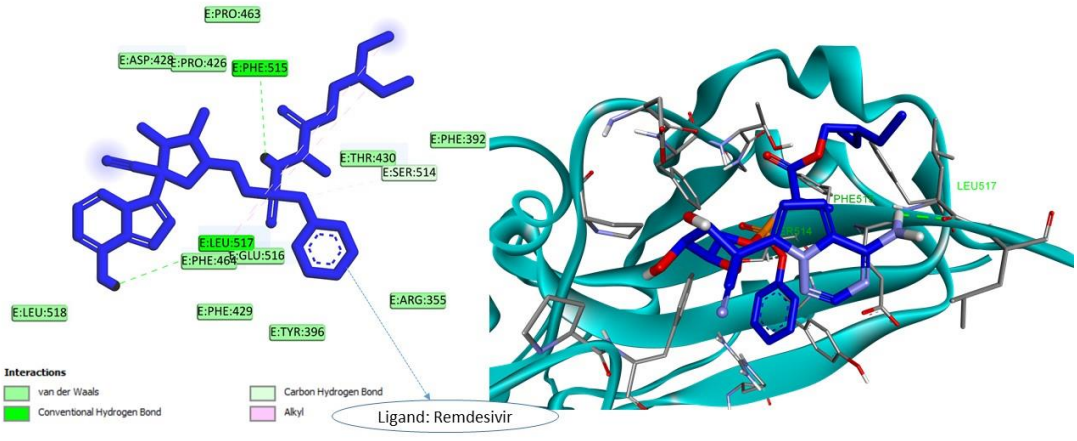

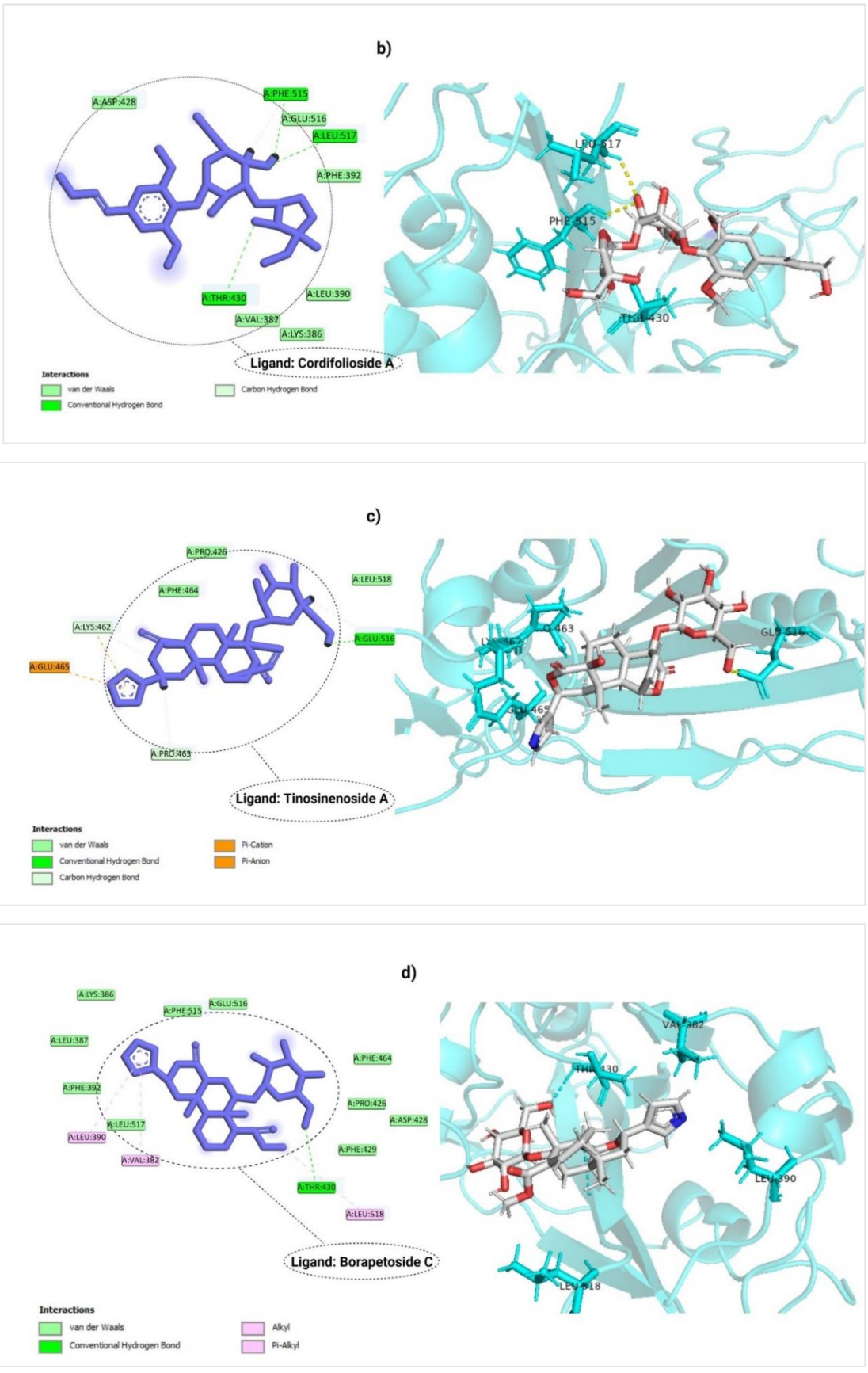

Figure 12: a), b), c), and d) displayed the interacted residues and the type of interactions of SARS-CoV-2 S1-RBD with remdesivir, cordifolioside A, tinosinenoside A, and borapetoside C respectively.

4.1.2 Molecular Dynamics Simulation Analysis

Three of the *Tinospora sps*, cordifolioside A, tinosinenoside A, and borapetoside C have demonstrated significant binding energies with S1-RBD. These three top-scored docked complexes in comparison to the remdesivir complex and apoprotein underwent 150 ns MD simulations to better explore the ligand-protein interactions.

RMSD is a crucial parameter to analyse the trajectories obtained from MD simulations. The RMSD of a protein-ligand complex system facilitates the calculation of the average distance resulting from the disclocation of a selected atom over a certain time interval (Bouback *et al*., 2021). The stability of the amino acids is examined by considering their C-alpha atoms throughout simulation.

The stability of the MD trajectories was determined using the backbone RMSD values of the atoms that pertain to the S1-RBD comlex. RMSD of cordifolioside A-S1-RBD, tinosinenoside A-S1-RBD, and borapetoside C-S1-RBD complexes were compared with remdesivir-S1-RBD along with apoprotein is shown in **Figure 13**. For the cordifolioside A-S1-RBD complex, the average RMSD value is less than 2 Å similar to apoprotein RMSD, reaching equilibrium after 10 ns suggesting.

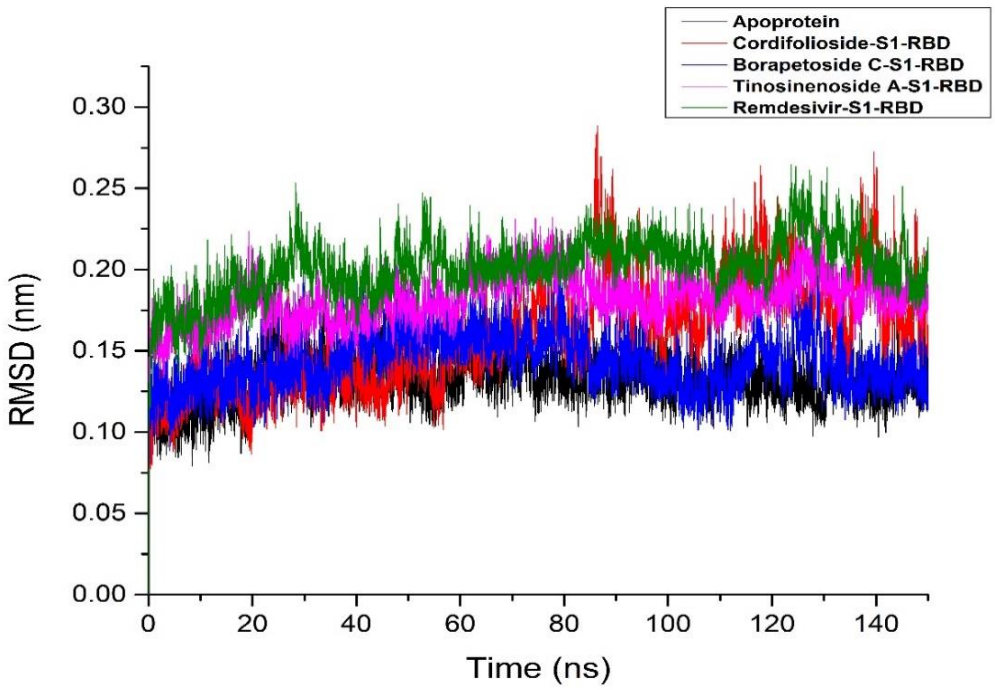

Figure 13: RMSD plots of apoprotein (apoprotein), cordifolioside A (red), tinosinenoside A (pink), borapetoside C (blue), and remdesivir (green) complexes.

It is as stable and the best compound in the dynamic environment. Similarly, for the S1-RBD-tinosinenoside A and S1-RBD-borapetoside C complexes, the protein and ligand are quite stable after 20 ns, and the average RMSD for protein and ligand are <2 Å, respectively. The RMSD of S1-RBD concerning remdesivir is below 2.5 Å. When specific ligands are bound, the fluctuations in the backbone of the S1-RBD can be explained by the discrepancies between the highest and lowest RMSD values.

The RMSF provides information about the flexibility between amino acid residues and how much the residues moves and fluctuates over a simulation period (Ahammad *et al*., 2021). Using VMD software, the RMSF of every amino acid around the ligand at 1 nm was computed in order to investigate the conformational flexibility of the leading active site during the simulation process. The RMSF values of the complexes were computed after analyzing the last 10 ns trajectory of the MD simulations. **Figure 14** displays the residues surrounding the ligand and their RMSF values in relation to the initial structures. In all S1-RBD complexes, the RMSF for the majority of the residues surrounding the ligand is less than 0.3 nm, suggesting stability during the MD simulation. The higher degree of fluctuation is caused by the individual chains' increased flexibility, yet the ligand stays steady throughout the simulation, demonstrating the stability of the binding site.

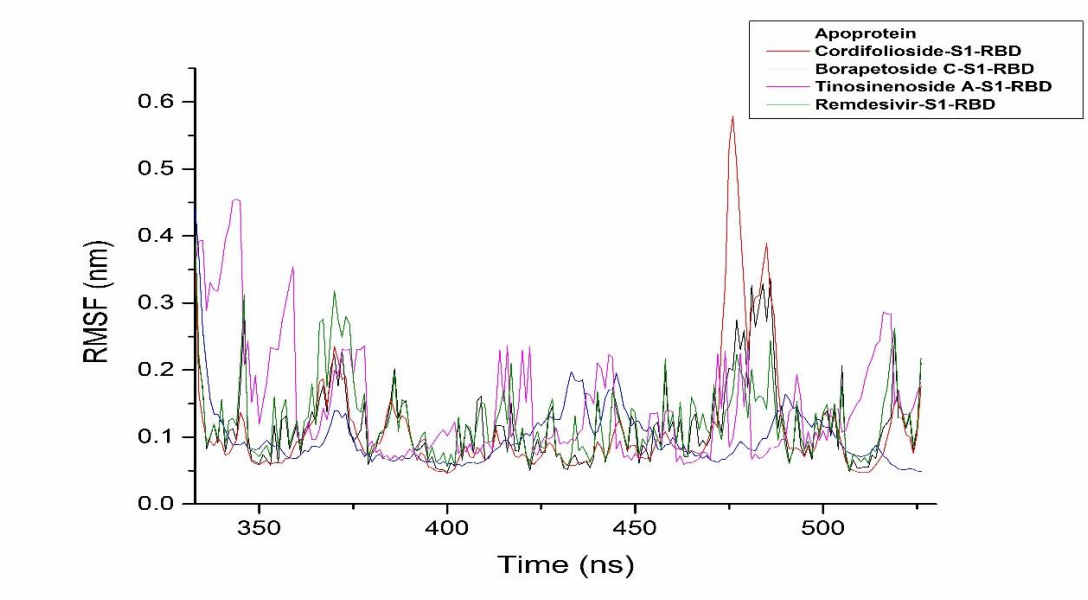

Figure 14: RMSF plots of apoprotein, cordifolioside A, tinosinenoside A, borapetoside C, and remdesivir complexes.

The fluctuation of both the N-terminal domain of remdesivir and cordifolioside A along with apoprotein were found to be almost similar. Conversely, in the case of cordifolioside A there was suppression in the loop region 360 to 380. The residues are highly flexible in cordifolioside A in the loop region 460 to 480, compared to remdesivir. The allosteric mechanism could be the cause of it. In the case of the tinosinenoside A, and borapetoside C, almost similar flexibility was observed compared to remdesivir except in the 360-380 region where remdesivir was more flexible.

The stability and compactness of the protei-ligand complexes and the apoprotein are determined by R_g. Apoprotein, cordifolioside A, tinosinenoside A, borapetoside C, and remdesivir complexes have average R_g values of 1.82, 1.85, 1.84, 1.845, and 1.83 nm, respectively. Together with the apoprotein, all protein-ligand complexes showed rather constant and steady R_g values. The R_g value shows that all complexes have good stability and perfectly overlaid structures (**Figure 15**).

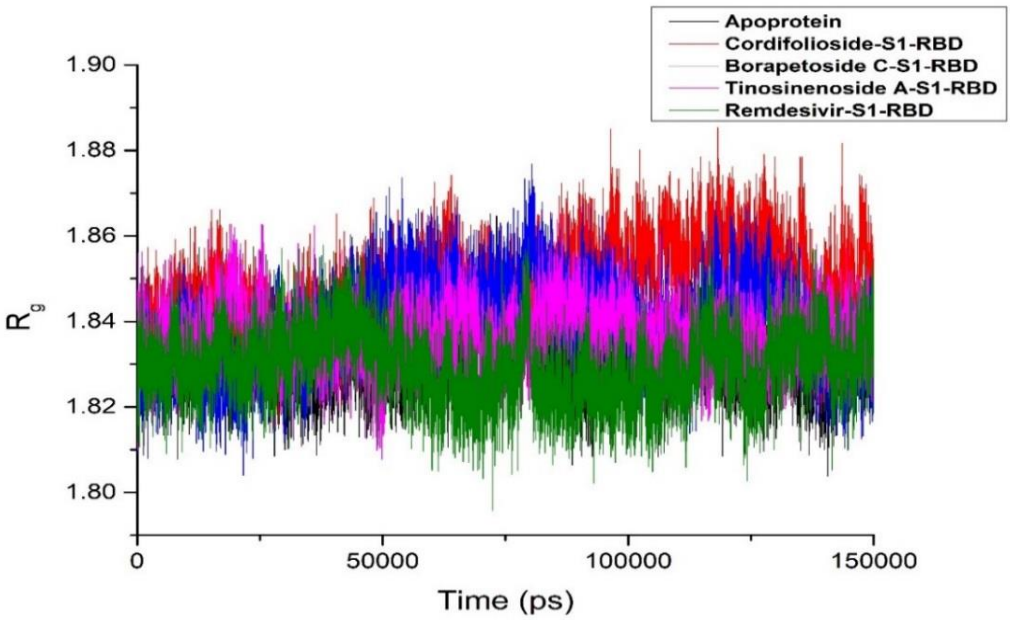

Figure 15: Rg plots of apoprotein, cordifolioside A, tinosinenoside A, borapetoside C, and remdesivir complexes.

4.1.3 Binding Free Energy (BFE) Analysis

The prime MM/GBSA method was utilized to ascertain the complex's strength by the computation of the absolute BFE (ΔG_{bind}) (Wang *et al*., 2019). On account of affinity and BFE, S1-RBD analysis shows that the compound cordifolioside A and tinosinenoside A, was preferred with significantly lower binding free energy (ΔG_{bind} -

25.09 and -22.75), respectively than remdevisir (-18.40 kcal/mol) suggesting strong binding affinity of cordifolioside A to spike protein.

Accordingly, steady interaction of cordifolioside A with S1-RBD is suggested by conformational dynamics analysis, BFE analysis, and molecular docking.

4.1.4 Analysis of ADMET Profiles

The pkCSM web server was used to analyze the ADMET characteristics of antiviral compounds enlisted in **Appendix C1**. Human intestinal absorption (HIA), skin permeability, and colon cancer cells (Caco-2) are all factors in drug absorption. In ADMET profiles, intestinal absorption values above 30% indicate good absorption in the human gut. Higher HIA indicates easier absorption of the compounds in the intestinal tract. Greater HIA denotes that the compounds are absorbed in the intestine with ease. Except for rumphioside C, all the remaining compounds showed better absorption values. The *in vivo* distribution of different medications in tissues is characterized by the volume of distribution (VDss), central nervous system (CNS) permeability, and blood-brain barrier (BBB) permeability. All of the metabolites were unable to easily penetrate the BBB. Based on the Cytochrome P450 (CYP) models for substrate and inhibitors, drug metabolism is best anticipated. CYP3A4 was suppressed by amritoside C, palmitoside F, lignan, and rumphioside B. Low renal clearance values were reported for all 26 metabolites. Cordifolioside A, cordifolioside B, and lignin were all classified as having toxicity class V by ProTox II, which also placed them in the hazardous group. Similarly, amritoside C, cordifolide B, cordifolide C, palmitoside F, borapetoside C, and rumphioside C were found to be harmful if swallowed and were categorized under toxicity class IV. Besides, rumphioside A and rumphioside B were fatal and classified under toxicity class II. Moreover, **Appendix D1** shows the confidence scores of active targets along with their predicted LD_{50} values.

4.1.5 DFT Analysis-based Band Gap Results

The band energy gap (E_{LUMO}-E_{HOMO}), LUMO, and HOMO are regarded as important quantum characteristics because they show how a molecule interacts with other species through ligand-ligand or protein-ligand interaction. In general, molecules with a low band energy gap are more polarizable, highly reactive, and have limited kinetic stability (Huang *et al*., 2017). According to Pearson's maximum hardness principle, the most reactive compound is the one with the lowest chemical hardness (Kumar *et al*., 2021).

Comparably, compounds with higher electronegativity will have more chemical reactivity with the target protein, since it reflects the electrophilic nature of the substance (Xu *et al*., 2020).

Table 4: Displays DFT results in terms of the following chemical reactivity descriptors.

Tested Compounds	E_{LUMO} (Hartree)	E_{HOMO} (Hartree)	Band energy gap (ΔE) (Hartree)	Ionization potential (I) (Hartree)	Electron affinity (A) (Hartree)	Global hardness (η)	Global softness (S)	Electronegativity (X)	Chemical potential (μ)	Electrophilicity index (ω)
Cordifolioside A	-0.03020	-0.20888	0.17868	0.20888	0.03020	0.08934	11.19319	0.11954	-0.11954	0.07998
Remdesivir	-0.03812	-0.21813	0.18001	0.21813	0.03812	0.07095	14.09543	0.12812	-0.12812	0.11572

In the present study, cordifolioside A and remdesivir (standard compound) were analyzed using DFT. Compared to remdesivir, cordifolioside A has a lower band gap energy of 0.17868 Hartree, indicating its higher binding affinity and significant reactivity (**Figure 16**).

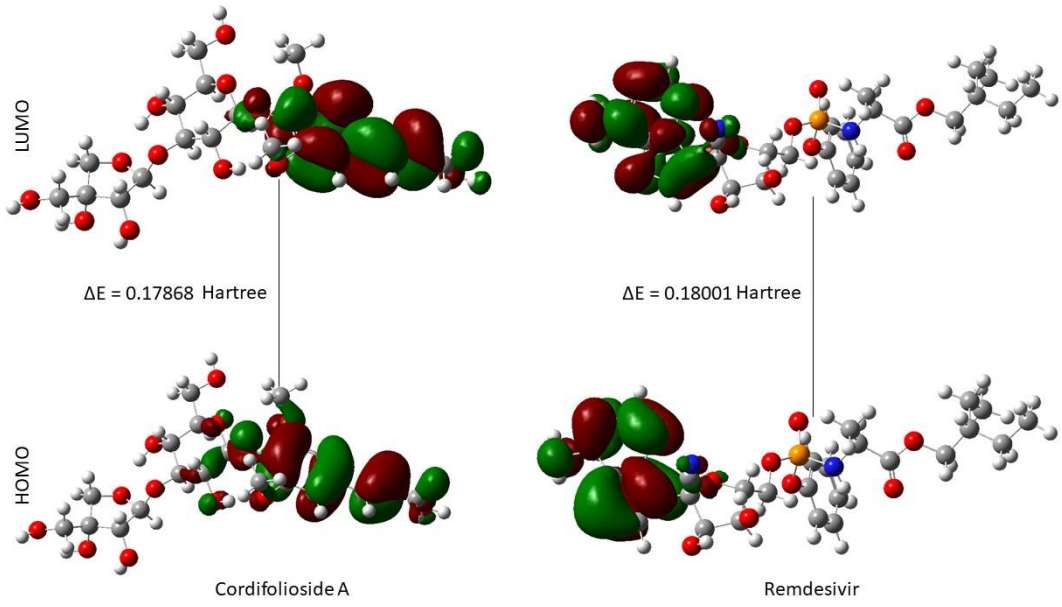

Figure 16: The band gap energies between HOMO and LUMO of cordifolioside A and remdesivir.

Furthermore, the reactivity measurements of chemical potential, electrophilicity index, global hardness, softness, and electrophilic nature show that cordifolioside A has a considerable affinity for S1-RBD of SARS-CoV-2 (**Table 4**).

4.1.6 Spike Protein Assay

Following encouraging *in silico* results that suggested metabolites from *Tinospora species* potentially stop hACE2 from interacting with SARS-CoV-2 S1-RBD protein, *in vitro* study of *Tinospora cordifolia* (Voucher Code: TUCH-210052) was performed against the S1-RBD of SARS-CoV-2.

$$\% \text{ inhibition} = \frac{\text{Abs(NC)} - \text{Abs(test)}}{\text{Abs(NC)}} \times 100\ \%$$

The methanolic extract of *Tinospora cordifolia* (5 mg/mL) demonstrated a significant % inhibition.

Table 5: Absorbance measurements with successive concentration range of crude extracts from T. cordifolia and determination of % of hACE 2 bound to the S1-RBD, as detected by an anti-human HRP antibody and TMB.

S. N.	*Tinospora cordifolia* methanolic extract (mg/mL)	Absorbance	% of hACE 2 bound to the S1-RBD (mean)
1	0	0.643	100
2	0.039063	0.539	83.8258
3	0.078125	0.519	80.7154
4	0.15625	0.489	76.0498
5	0.3125	0.437	67.9627
6	0.625	0.376	58.4759
7	1.25	0.323	50.2333
8	2.5	0.275	42.7683
9	5	0.212	32.9705

Thus, a wide concentration range of crude extracts from *T. cordifolia* was subsequently treated with hACE2 in S1-RBD 96-well-coated plates and a signal was discovered by employing an HRP-linked secondary antibody as shown in **Table 5**.

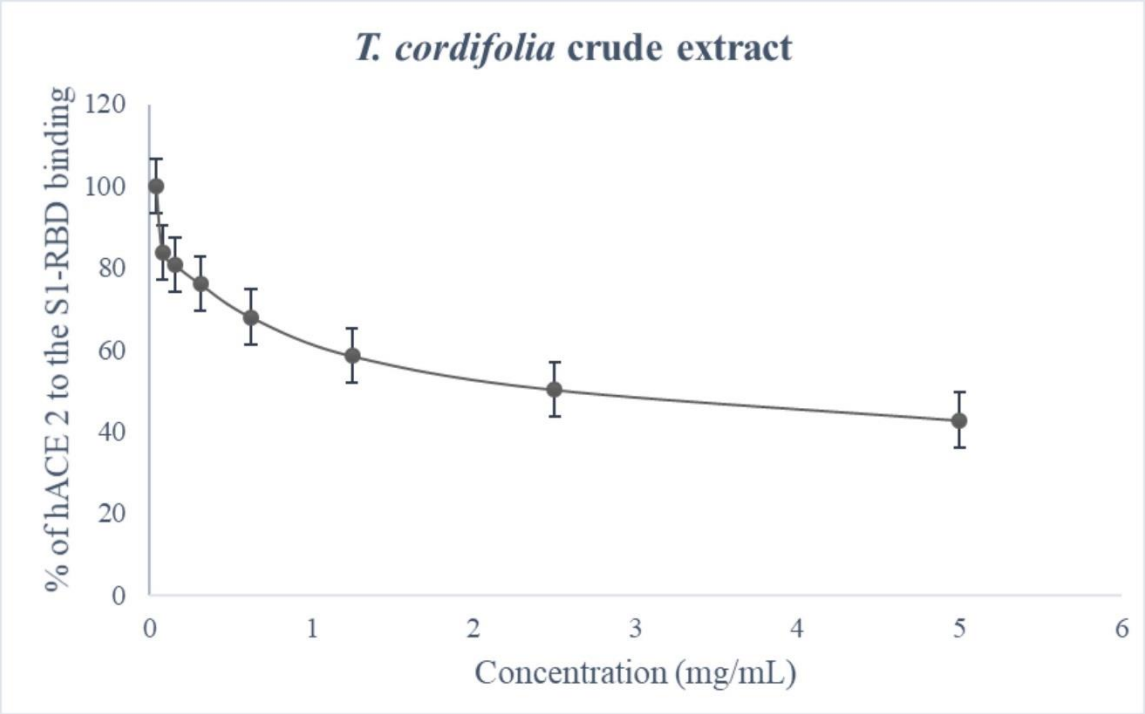

Figure 17: The graph showing the hACE 2 receptor binding with S1-RBD in successive concentrations of crude extract of *T. cordifolia*. From n =3 samples, the data represents mean ± SEM.

T. cordifolia crude extract was found to be effective at inhibiting the interaction between hACE2 and the S1-RBD protein. At a concentration of about 1.25 mg/mL, *T. cordifolia* extract reduced the binding of hACE2 with S1-RBD by 50% (**Figure 17**).

4.2 Investigation of Flavonoids

4.2.1 Pharmacokinetics Analysis of Flavonoids

The selected 36 flavonoids based on antiviral properties have good absorption rates. Further, since they are so important in regulating drug distribution, their skin permeability, the volume of distribution at steady-state (VDss), CNS permeability, and BBB permeability were analyzed. This research primarily focused on the human CYP3A4 among other CYPs enzymes and the flavonoids scutellarein, wogonin, luteolin, apigenin, fisetin, galangin, tomentin B, mimulone, bavachinin, corylifol A, neobavaisoflavone, kazinol A, kazinol B, and cyanidin inhibited it, suggesting that they may be metabolized in the liver. The majority of the flavonoids in this study passed Lipinski 's criteria, proving that they are suitable for use as medicines. The ADME chemical descriptors of the chosen flavonoids were determined by the swissADME webserver to suppress SARS-CoV-2. To test Lipinski's rule of five for determining drug-likeness, the five major physiochemical properties of the top hits six flavonoids

are shown in **Table 6** and their ADMET profiles are shown in **Table 7.** ADMET properties and drug-like properties of all selected flavonoids are listed in **Appendix C2 and E1**. Using ProTox II, which gives median lethal dosage (LD_{50}) values and toxicity classes, the toxicity of the chosen flavonoids was predicted. Flavonoids, scutellarein, wogonin, baicalin, luteolin, pectolinanin, apigenin, amentoflavone, rutin, rhoifolin, galangin, herbacetin, morin, daidzein, corylifol A, neobavaisoflavone, broussoflavon, kazinol A, cyanidin, malvidin, and delphinidin are discovered to come within toxicity class V ($2000 < LD_{50} \leq 5000$), and tomentin E includes in toxicity class VI ($LD_{50} > 5000$) in terms of acute oral toxicity (**Appendix D2**). The flavonoids fisetin and myricetin fall in toxicity class III ($50 < LD_{50} \leq 300$), and the remaining flavonoids belong to toxicity class IV ($300 < LD_{50} \leq 2000$).

Table 6: Prediction of drug-likeness properties of six flavonoids using swissADME.

Flavonoids	**Molecular Mass (<500)**	**Hydrogen bond donor (<5)**	**Hydrogen bond acceptor (<10)**	**LogP (<5)**
Cyanidin	287.24	5	6	0.56
4'-O-Methyldiplacol	454.51	4	7	4.32
Mimulone	408.49	3	5	4.80
Malvidin	331.30	4	7	0.71
Tomentin E	472.53	4	8	3.24
Neobavaisoflavone	322.35	2	4	3.74

Table 7: Prediction of pharmacokinetics profiles of six flavonoids using pkCSM and ProTox II.

Parameters	**Blood-Brain Barrier (BBB)**	**Human Intestinal Absorption (HIA)**	**CYP3A4 inhibitor**	**AMES toxicity**	**Hepato toxicity**	**LD_{50}**	**Toxicity class**
Cyanidin	-1.357	80.203	YES	YES	NO	5000	V
4'-O-Methyl Diplacol	-1.311	76.952	NO	NO	NO	2000	IV
Mimulone	-1.056	90.287	YES	NO	NO	2000	IV
Malvidin	-1.560	71.558	YES	NO	NO	5000	V
Tomentin E	-1.396	77.239	NO	YES	NO	10000	VI
Neobavaisoflavone	-0.09	94.31	YES	NO	NO	2500	V

4.2.2 Molecular Docking Analysis

Selected flavonoids with the K417N mutation in the SARS-CoV-2 S-RBD were then subjected to molecular docking studies. **Table 8** lists the top-scoring flavonoids' IC_{50} values, GOLD fitness scores, interacting distances, and S-RBD interacting residues. Cyanidin was previously investigated in vitro for SARS-CoV-2, and the current study demonstrates that it has a suitable GOLD fitness score of 51.91, showing its potency as an S-RBD inhibitor. Likewise, with GOLD fitness scores of 63.83, 61.60, 53.90, 52.01, 51.78, and 50.91, respectively, 4'-O-methyldiplacol, mimulone, neobavaisoflavone, malvidin, and tomentin E also interact precisely with the binding sites of S-RBD. Figure 3 illustrates how cyanidin interacts with the S-RBD through the amino acids Asn 343, Ser 371, and Ser 373 through hydrogen bonds and hydrophobic interactions, changing the protein conformation. Likewise, 4'-O-methyldiplacol interacted through Ser 349, Ser 399, Arg 346, and Ala 348; mimulone through Arg 346, Ala 348, Ser 349, Ser 399, and Asn 450; neobavaisoflavone through Ser 469, and Gln 474; malvidin through Arg 346, Phe 347, Ser 349, Asp 442, and Lys 444; and tomentin E through Glu 340, Lys 356, and Ser 399. **Appendix B2** presents in detail the GOLD fitness score, interacted residues, and interacting distances of all other selected flavonoids. The 2D and 3D structures of cyanidin, 4'-O-methyldiplacol, and mimulone are displayed in **Figure 18** while other potent compounds are displayed in **Appendix F4.**

Table 8: Binding free energies, GOLD fitness score, interacting residues of proteins, and IC50 values.

Compounds	**Binding free energies (kcal/mol)**	**GOLD fitness score**	**Interacting residues of S-RBD**	**Interaction distances (Å)**	**IC_{50} value (μM)**
Cyanidin	-25.09	51.91	Asn 343 Ser 371 Ser 373 Asn 437 Asn 440	2.26 2.37 1.96 2.97 2.2	65.1 ± 14.6 µM (SARS-CoV-2) (Pitsillou *et al*., 2020)
4′-O-Methyldiplacol	-18.40	63.83	Arg 346 Ala 348 Ser 349 Ser 399	4.07 3.57 2.35 2.43	9.2 µM (SARS-CoV) (Cho *et al*., 2013)

Mimulone	-21.23	61.60	Arg 346 Ala 348 Ser 349 Ser 399 Asn 450	2.40 3.59 2.24 2.26 2.54	14.4 µM (SARS-CoV) (Cho *et al*., 2013)
Malvidin	-22.03	52.01	Arg 346 Phe 347 Ser 349 Asp 442 Lys 444	2.72 1.83 2.24 2.68 2.20	0.04573 µM (SARS-CoV-2) (Wu *et al*., 2021)
Tomentin E	-25.02	50.91	Glu 340 Lys 356 Ser 399	2.30 2.37 2.07	5.0 µM (SARS-CoV) (Cho *et al*., 2013)
Neobavaisoflavone	-19.49	53.90	Ser 469 Gln 474	2.72 2.54	18.3 µM (SARS-CoV) (Kim *et al*., 2014)

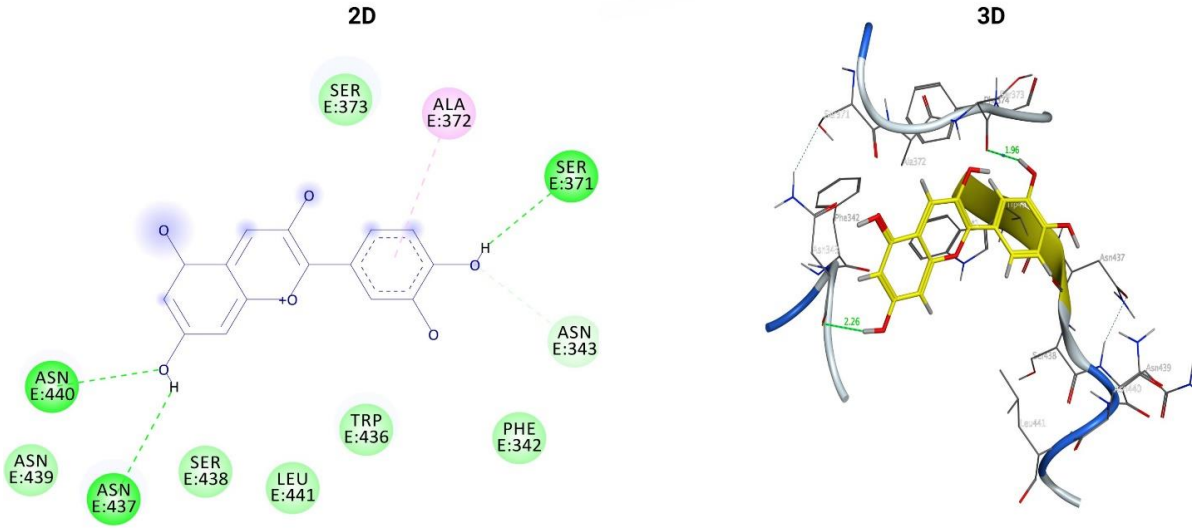

S-RBD Cyanidin Complex

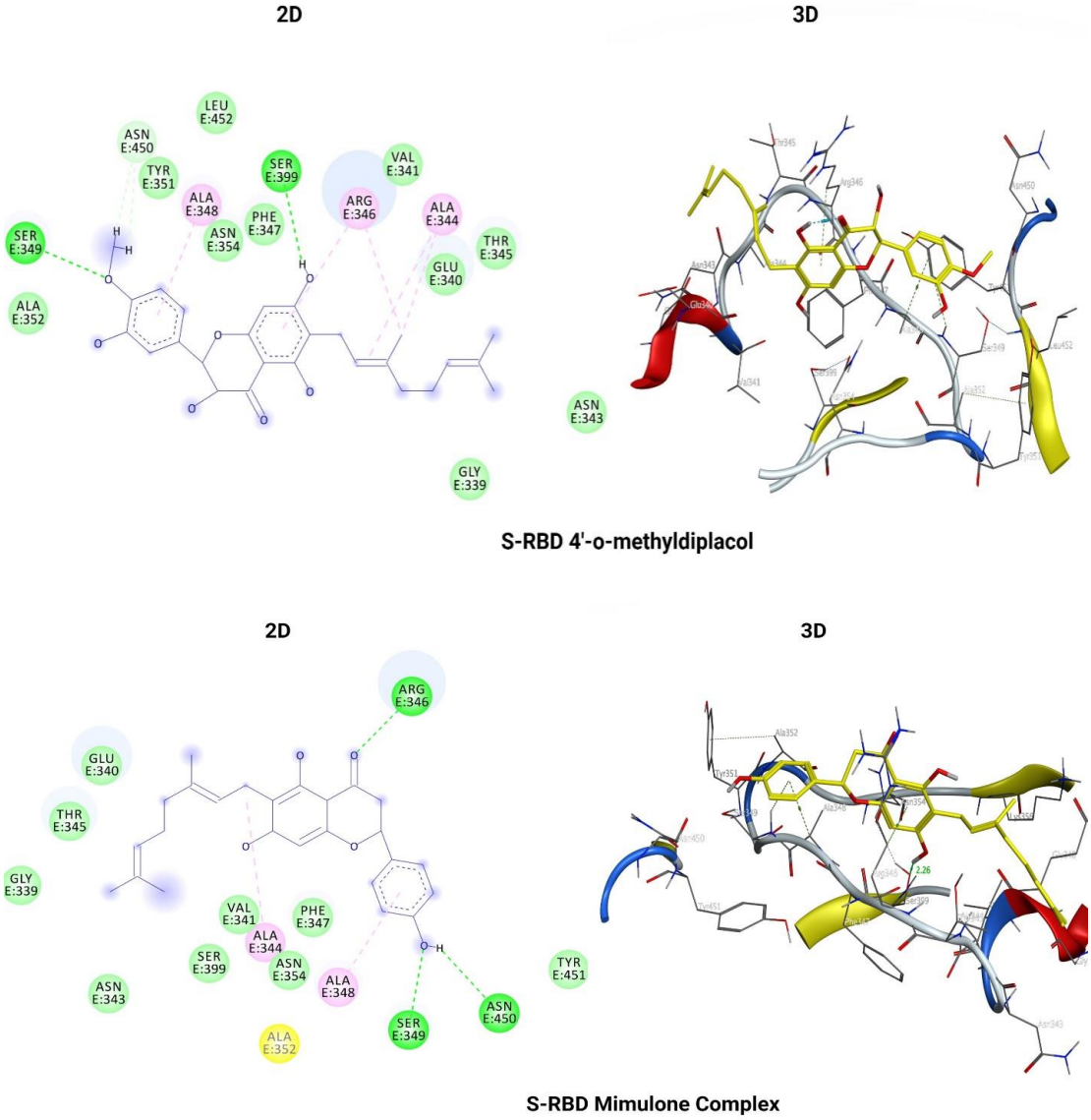

Figure 18: The 2D and 3D interaction display of cyanidin, 4'-O-methyldiplacol, and mimulone complexed with SARS-CoV-2 S-RBD.

4.2.3 Molecular Dynamics Simulation Analysis

Our study shows that cyanidin exhibits a stronger binding affinity with the S protein along with appropriate pharmacokinetics properties. Although docking analysis can yield an acceptable binding mode, solvent effects, and protein flexibility were not adequately explored. To understand the interactions between the ligand and the protein, MD simulations were performed on the docked complexes. **Figure 19 (A)** displays the RMSD values for the human serum albumin (HSA)-cyanidin complex and S-RBD-cyanidin complex. The S-RBD-cyanidin complex had an average RMSD of 0.39 nm reaching equilibrium in 80 ns. The RMSD of cyanidin cation was discovered to be stable initially from 36 nm to 60 ns and then from 80 ns to 100 ns. Comparatively,

substantial RMSD were seen for the HSA-cyanidin complex, pointing to the unstable complex nature. This finding provides credence to the hypothesis that cyanidin binds to S-RBD rather than HSA. To further compute the residual flexibility over 100 ns the RMSF was performed and displayed in **Figure 19 (B)**. For each residue around the ligand-protein complex, the RMSF is less than 0.36 nm. To calculate the conformational stability of the protein-ligand, the time evolution plot of Rg was computed. The ligand is successfully fitted at the active site of the S protein, as shown by the Rg trajectory of the cyanidin-S-RBD complex, which reaches equilibrium at approximately 35 ns and remains stable for 35 ns-100 ns **[Figure 19 (C)]**. Whereas, the HSA-cyanidin Rg trajectory optimizes equilibrium for about 60 to 80 ns. The structural compactness of the protein-ligand complexes of the S-RBD-cyanidin shown to be stable by Rg plots, with an average Rg value of 1.6 nm, whereas the HSA-cyanidin cation complex has an average Rg value of 3.5 nm, demonstrating its instability in comparison. In conclusion, protein-ligand compactness increases with decreasing Rg value, and this results in greater affinity between them (Bhowmik *et al*., 2020a).

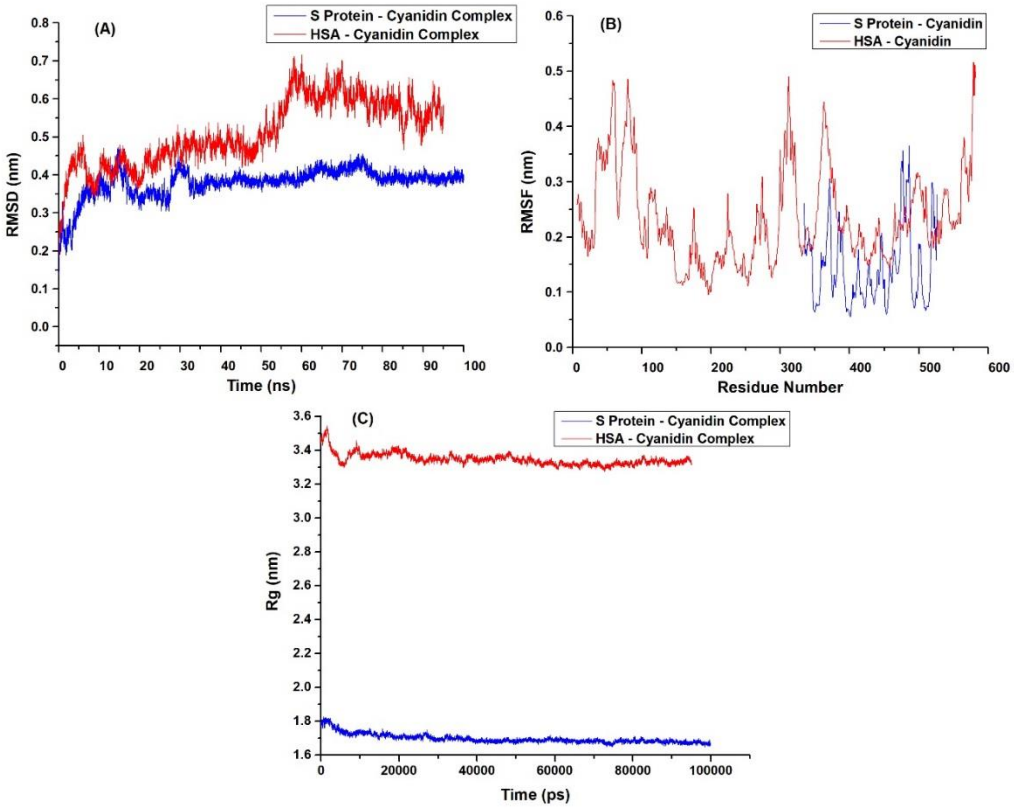

Figure 19: The plots of (A) RMSD, (B) RMSF, and (C) Rg during 100 ns MD simulation of S protein-cyanidin complex and HSA-cyanidin complex.

4.2.4 Binding-Free Energies (BFE) Analysis

The primary MM/GBSA approach was performed to calculate the absolute BFE that ascertains the degree of the protein-ligand interactions and assesses the reaction of active residues to ligands. The flavonoids, cyanidin, 4'-O-methyldiplacol, and mimulone have noticeably low BFE (ΔG_{bind} -25.09, -21.23, and -18.40 kcal/mol, respectively) which indicates they have high affinity with protein. As a result, the molecular docking and conformational dynamics analyses are supported by BFE, which demonstrated the stable binding of cyanidin with S-RBD. These findings may aid in a better understanding of COVID-19 medication design based on structure.

4.2.5 DFT Analysis-based Band Gap Results

Based on the findings of pharmacokinetics properties, molecular docking and MD simulations, DFT analysis was carried out to find out the reactivity of cyanidin in comparison to standard drug remdesivir. **Table 9** represents DFT results with chemical reactivity descriptors. Cyanidin was interestingly discovered to be more reactive with band gap energy of 0.1243 Hartree (**Figure 20**) lower than the standard drug, remdesivir (0.18001 Hartree).

Table 9: Displays DFT results in terms of the following chemical reactivity descriptors.

Tested Compounds	E_{LUMO} (Hartree)	E_{HOMO} (Hartree)	Band energy gap (ΔE) (Hartree)	Ionization potential (I) (Hartree)	Electron affinity (A) (Hartree)	Global hardness (η)	Global softness (S)	Electronegativity (X)	Chemical potential (μ)	Electrophilicity index (ω)
Cyanidin	-0.01535	-0.13965	0.1243	0.13965	0.001535	0.06215	16.09010	0.0705925	-0.0705925	0.04009
Remdesivir	-0.03812	-0.21813	0.18001	0.21813	0.03812	0.07095	14.09543	0.12812	-0.12812	0.11572

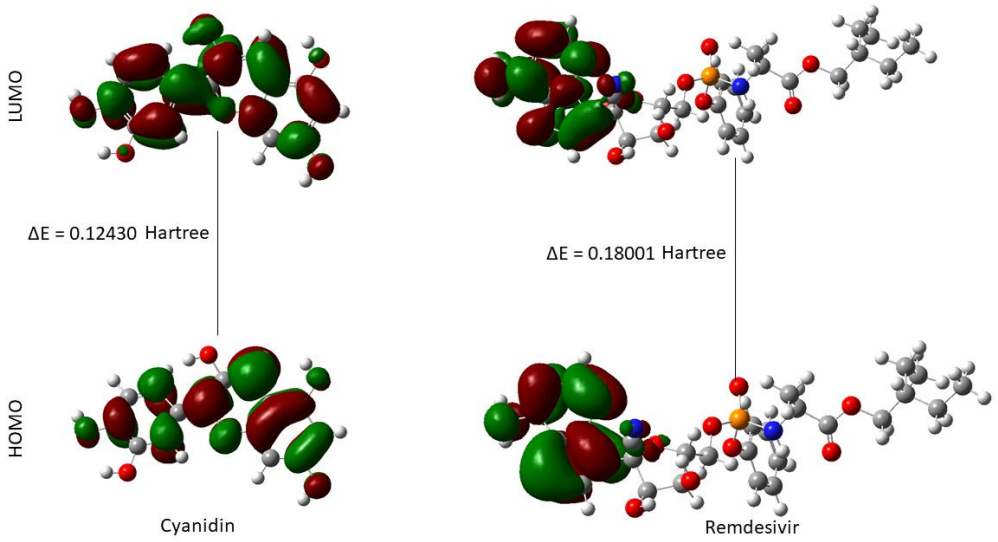

Figure 20: The band gap energies between HOMO and LUMO of cyanidin and remdesivir.

4.2.6 Spike Protein Assay

After receiving encouraging *in silico* results showing that cyanidin might inhibit the interaction between hACE2 and SARS-CoV-2 S1-RBD, the crude red grapes (*Vitis vinifera*) (Variety number: 22608; Origin of Variety: Australia; and Cultivar name: Malian) extract containing cyanidin (Kallithraka *et al*., 2009) (Rienth *et al*., 2021) was subjected to a test *in vitro* using an ELISA.

Table 10: Absorbance measurements with successive concentration range of crude extracts from red grapes and determination of % of hACE 2 bound to the S1-RBD, as detected by an anti-human HRP antibody and TMB.

S.N.	Concentration (mg/mL)	Absorbance (mean)	% of hACE2 bound to the S1-RBD (mean)
1.	0.000	0.614	100.0000
2.	0.078125	0.423	68.8925
3.	0.15625	0.361	58.7948
4.	0.3125	0.356	57.9805
5.	0.625	0.321	52.2801
6.	1.25	0.316	51.4658
7.	2.5	0.282	45.9283
8.	5	0.269	43.8111
9.	10	0.223	36.3192

On 96-well plates coated with S1-RBD, hACE2 was incubated with various amounts of extract, and the signal was produced using HRP-linked secondary antibody. Notably, this study found that red grape extract might prevent hACE2 from interacting with the S1-RBD protein (**Figure 21**). At a concentration of approximately 1.25 mg/mL, red grapes crude extract reduced the binding of hACE2 with S1-RBD by almost 50% (**Table 10)**. Overall, this method offers substantial mediation evidence that cyanidin, a key flavonoid in red grapes (*Vitis vinifera*), may prevent hACE2 and SARS-CoV-2 S1-RBD from binding to each other.

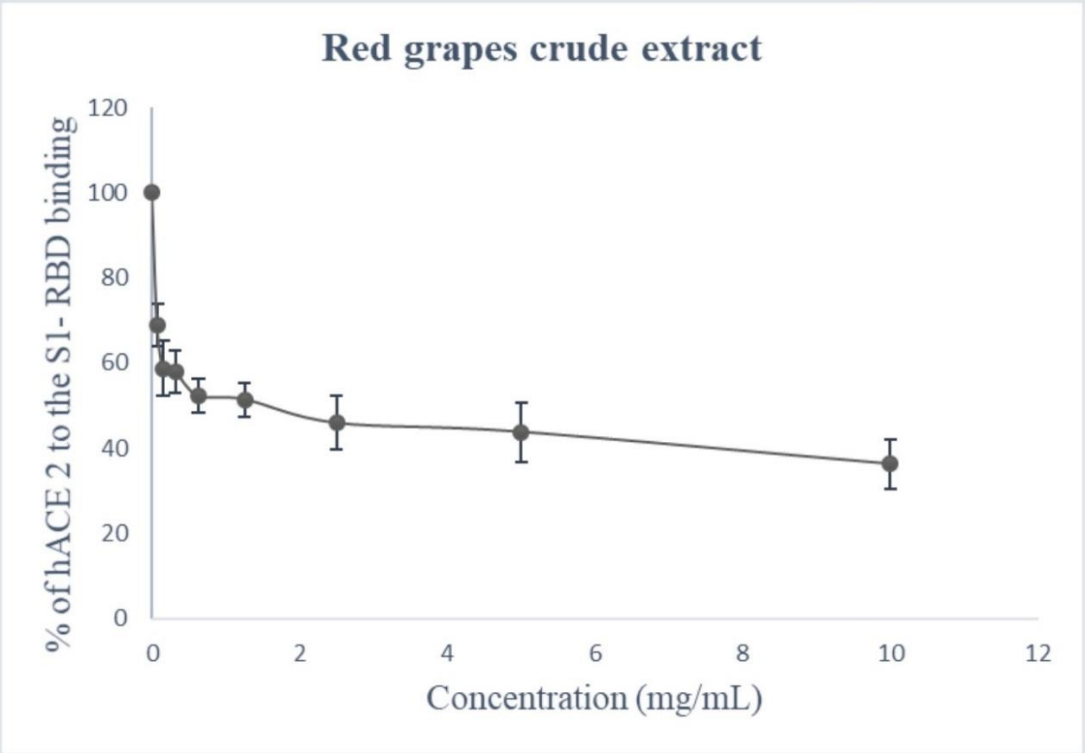

Figure 21: ELISA analysis of the hACE2 receptor's S1-RBD protein binding curve in the presence of successive concentrations of red grapes (*Vitis vinifera*) crude extracts. From n =3 samples, the data represents mean ± SEM.

4.3 Investigation of Alkaloids

4.3.1 Prediction of Activity Spectra for Substances (PASS) Analysis of Alkaloids

Based on molecular characteristics, the PASS analysis predicts the biological activities. **Figure 22** represents the findings from the PASS analysis of selected 79 alkaloids revealing that oxysophoridine along with remdesivir have broad antiviral effects. Likewise, the substances strychnopentamine, berbamine, and neferine showed anti-viral entry activity, anti-hepatitis B, C, and anti-HIV-1 integrase. The threshold Pa values of < 3 for these alkaloids indicated limited anti-viral activity (Filimonov *et al*.,

2020). Despite the low threshold Pa values for neferine and berbamine, the in vitro research on these alkaloids' ability to combat SARS-CoV-2 is promising, thus molecular docking and MD simulation studies were carried out.

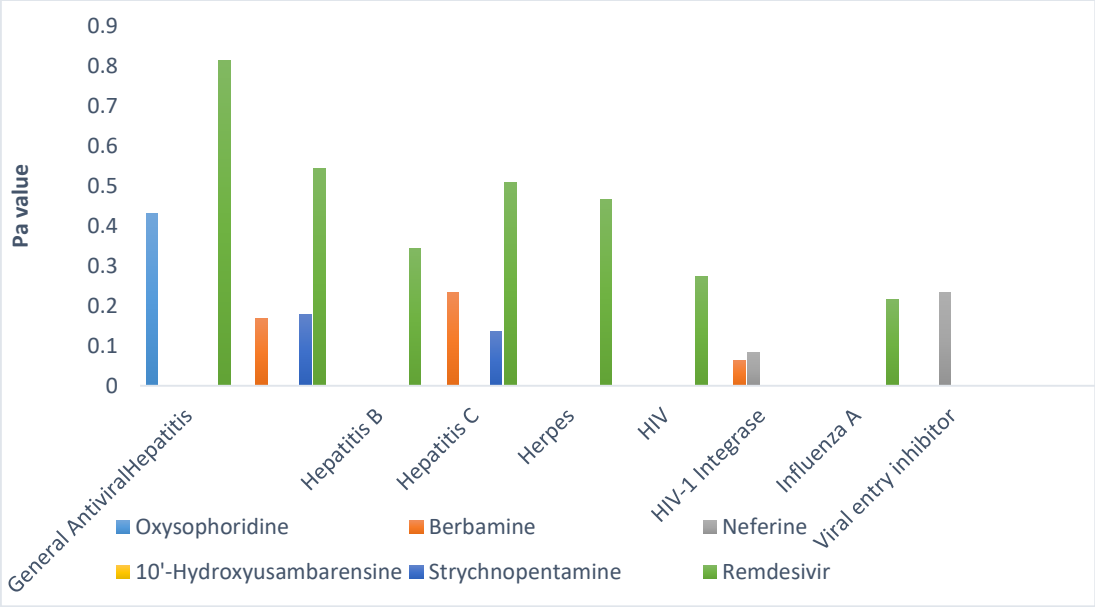

Figure 22: The anticipated antiviral activity of alkaloids utilizing PASS server.

4.3.2 Pharmacokinetics Analysis of Alkaloids

Pharmacokinetic analysis yields significant parameters useful in drug research and development programmes and these characteristics of natural alkaloids were calculated using the pkCSM web server. Water solubility, Caco-2 permeability, and VDss determine how well the compound is absorbed. **Table 11** displayed oxysophorodine, berbamine, neferine, 10'-hydroxyusambarensine, strychnopentamine, and remdesivir were all discovered to be only moderately soluble in water. The Caco-2 permeability and HIA parameters of drugs also influence their bioavailability. Here, seven alkaloids are permeable since their permeability values are larger than 0.9 (Sinha *et al*., 2022). All medications enter the body through the gastrointestinal tract, and the compounds with HIA levels of more than 30% are regarded as being easily absorbed in the human intestine (Yan *et al*., 2008). Neferine exhibits a 100% HIA value, as do all of the most popular alkaloids. Contrarily, a number of variables, including VDss are used to calculate the extent of drug dispersion throughout the body. VDss values are the most useful for determining the total dose of a medication needed to achieve a constant blood plasma concentration. A greater log VDss value denotes drug distribution in tissues instead of plasma. If this value is > 0.45, the VDss is greater while lower if < -0.15

(Bhowmik *et al*., 2020b). As indicated in **Table 11**, all of the chosen alkaloids have fraction unbound values ranging from 0.0995 to 0.455. All of the selected alkaloids mentioned are not cytochrome P450 inhibitors, with the exception of neferine and strychnopentamine.

Table 11: The pharmacokinetic prediction (Absorption, Distribution, and Metabolism) of Oxysophorodine, Berbamine, Neferine, 10′-Hydroxyusambarensine, Strychnopentamine, and Remdesivir (Standard ligand).

Alkaloids	**Oxysophorodine**	**Berbamine**	**Neferine**	**10′-Hydroxyusambarensine**	**Strychnopentamine**	**Remdesivir**
Water solubility log mol/L	-3.921	-2.983	-3.056	-2.995	-2.945	-3.07
Caco-2 permeability log 10^-6 cm/s	1.304	1.165	0.986	0.519	0.821	0.635
Human Intestinal Absorption (%)	96.293	92.311	90.324	89.792	89.516	71.109
VDss (log L/kg)	0.409	-0.63	-0.286	0.114	2.03	0.307
CYP3A4	NO	NO	YES	NO	NO	NO
CYP2D6	NO	NO	NO	NO	YES	NO

Analysis of toxicity is essential for determining if a medication candidate will be useful. Here, it is discovered that berbamine and 10'-hydroxyusambarensine exhibits AMES toxicity, indicating that they might be mutagenic and carcinogenic compounds. According to our investigation, remdesivir, strychnopentamine, and 10'-hydroxyusambarensine are all hepatotoxic compounds. Additionally, the lethal dosage (LD_{50}) number reveals the concentration of a drug that kills 50 % of test animals (Sinha et al., 2022). The compound is more toxic if the LD_{50} value is low. All of the examined alkaloids have higher LD_{50} values, which indicate fewer fatal effects. As indicated in **Table 12**, the ProTox II study further manifested that the selected alkaloids showed toxicity class of IV. The outcomes of the swissADME analysis of those alkaloids are also shown in **Table 13**.

Table 12: The pharmacokinetic prediction (Excretion and Toxicity) of Oxysophorodine, Berbamine, Neferine, 10′-Hydroxyusambarensine, Strychnopentamine, and Remdesivir (Standard ligand).

Alkaloids	Oxysophoridine	Berbamine	Neferine	10′-Hydroxyusambarensine	Strychnopentamine	Remdesivir
Total Clearance (log ml/min/kg)	1.066	0.724	1.007	1.109	0.947	0.198
AMES toxicity	NO	YES	NO	YES	NO	NO
Oral rat toxicity (LD_{50}(mg/kg))	2.653	2.494	2.304	2.363	2.148	2.043
Hepatotoxicity	NO	NO	NO	YES	YES	YES
Toxicity class	IV	IV	IV	IV	IV	IV

Table 13: M The prediction of drug-like properties of Oxysophorodine, Berbamine, Neferine, 10′-Hydroxyusambarensine, Strychnopentamine, and Remdesivir utilizing swissADME web server.

S. Table 1:	Alkaloids	PubChem ID	Molecular Mass	Hydrogen bond donor (HBD < 5)	Hydrogen bond acceptor (HBA < 10)	LogP <5	Molar refractivity (40-130)	Drug likeness >0
1.	**Oxysophoridine**	114850	278.39	0	2	1.22	87.80	0.55
2.	**Berbamine**	275182	608.72	1	8	5.15	181.60	0.55
3.	**Neferine**	159654	624.77	1	8	5.47	188.02	0.55
4.	**10′-Hydroxyusambarensine**	10433813	448.56	3	3	4.40	142.46	0.55
5.	**Strychnopentamine**	6712640	549.75	3	4	4.68	180.14	0.55
6.	**Remdesivir**	121304016	602.58	4	12	1.50	150.43	0.17

4.3.3 Molecular Docking Analysis

The results of chosen alkaloids' molecular docking with RdRp are summarized in **Table 14** together with their S-score, RMSD refines values, interacting residues, and bond lengths. Having a lower S-score value means the protein and ligand are interacting well. The present study discovered that berbamine interacts with Asp 618 and Asp 761, two of the catalytic residues of RdRp (Aranda *et al*., 2022) with an interacting distance of 4.37 nm and a good S-score of -2.61. Furthermore, binding affinity obtained utilizing

AutoDock tools demonstrated berbamine with lowest binding energy of -9.8 kcal/mol, while remdesivir displayed binding energy of -8.1 kcal/mol. Recent research revealed that berbamine exhibits anti-SARS-CoV-2 action in Vero-E6 cells with an EC_{50} of roughly 2.4 µM (Huang *et al*., 2021). Additionally, it has been noted that this compound exhibits antiviral activity against SARS-CoV-2 (Xia *et al*., 2021), indicating the possibility of it becoming a possible therapeutic candidate for COVID-19. Neferine also displays a good interaction with the RdRp of SARS-CoV-2, as evidenced by its favorable S-score, -5.083. Neferine exhibits significant interaction with Asp 618 and Asp 760 with suitable binding energy of -9.1 kcal/mol, which suggests that it inhibits RdRp activity and it has also demonstrated a good EC_{50} of less than 10 µM (Majnooni *et al*., 2021b). **Table 14** lists the interaction residues of RdRp and binding of the leading alkaloids with RdRp. Neferine is said to prevent SARS-CoV-2 and other coronaviruses from entering the body by obstructing host calcium channels, which then prevents the Ca^{2+}-dependent membrane fusion process. Neferine demonstrates its potent antiviral action against many coronaviruses by inhibiting Ca^{2+}-dependent membrane fusion (Yang *et al*., 2021). Ground on in silico and wet-lab tests, neferine may be a strong therapeutic candidate against SAR-CoV-2. Neferine also exhibits anti-cancer efficacy via inducing apoptosis, cell cycle arrest, and a number of other routes. Compared to currently available anticancer medications like taxol, cisplatin, and doxorubicin, it offers a wide range of therapeutic uses, including anti-cancerous, anti-inflammatory, and anti-anxiety (Bharathi Priya *et al*., 2021b). Neferine's potential as a cancer treatmentwas furthersupported by earlier molecular docking research that revealed its ability to bind with drug-binding pockets in an efficient manner (Kadioglu *et al*., 2017).

Multiple alkaloids have shown promising results when docked against the binding sites of therapeutic target proteins of SARS-CoV-2 (spike, PL^{pro}, RdRp, and M^{pro}) (Pandeya *et al*., 2020). Present studies discovered that neferine and berbamine had the ability to bind in the palm region's catalytic sites of RdRp. This interaction might decrease RdRp actions and obstruct viral transcription and replication. To determine if the ligand interacts with HSA or RdRp protein, research was also done on how neferine and berbamine interact with the protein HSA (PDB ID: 1A06). The interactions between neferine-HSA and berbamine-HSA complexes, however, were incredibly weak, showing that neferine and berbamine strongly attach to the RdRp of SARS-CoV-2 instead HSA protein. To learn more about protei-ligand stability, 90 ns of MD

simulation was performed for neferine complex in light of its robust protein-ligand binding. Additionally, their promising *in vitro* experimental results and possible medical uses. **Figures 23, 24, and 25** displays 2D structures of neferine, berbamine, and remdesivir complexes with RdRp, prepared utilizing MOE.

Table 14: A summary of the chosen naturally occurring alkaloids′ molecular docking investigations with RdRp.

Compounds	**S-score**	**RMSD Refine**	**Interaction**	**Bond length (Å)**	**Target Site/ Virus**
Oxysophoridine	-3.304	1.312	Cys 622	3.17	SARS-CoV-2
Berbamine	-2.6064	1.34	Asp 618 Asp761	2.76 4.37	SARS-CoV-2
Neferine	-5.083	1.32	Asp 760 Tyr 619	2.88 4.34	SARS-CoV-2
10'-hydroxyusambarensine	-4.66	1.47	Asp 761 Glu 811	3.2 4.25	SARS-CoV-2
Strychnopentamine	-3.64	1.067	Asp 761 Arg 555	SARS-CoV-2	SARS-CoV-2
Remdesivir	-5.581	1.57	Asp 618 Asp 760 Tyr 619	3.14 2.92/3.13 3.26	

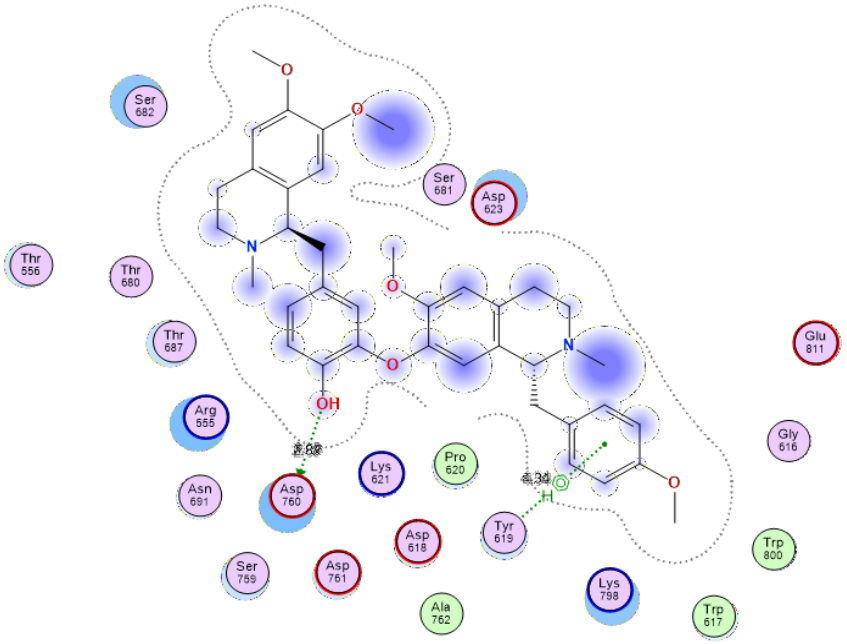

Figure 23: 2D structures showing interactions between neferine and residues of RdRp obtained using MOE..

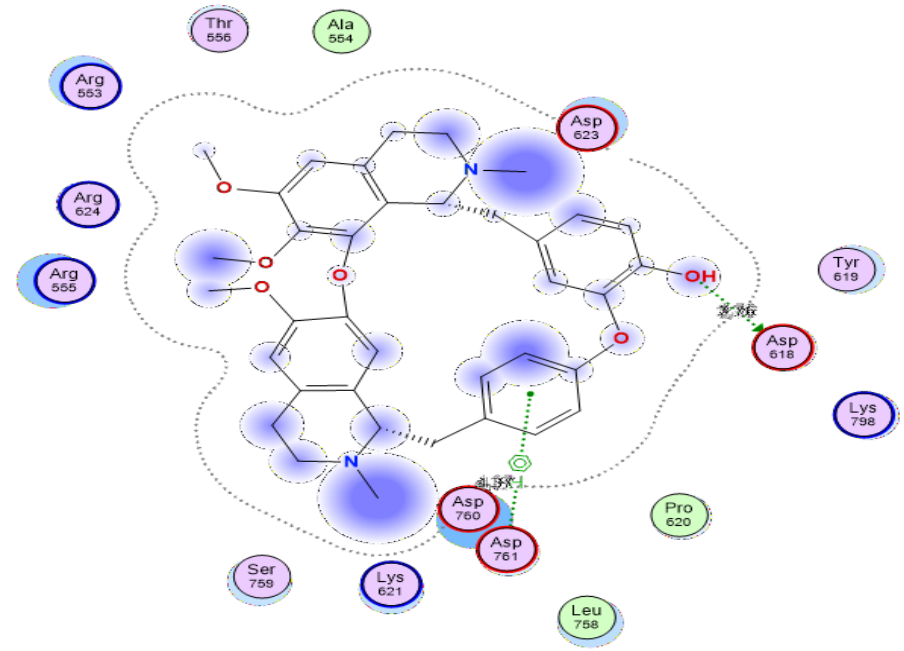

Figure 24: 2D structures showing interactions between berbamine and residues of RdRp obtained using MOE.

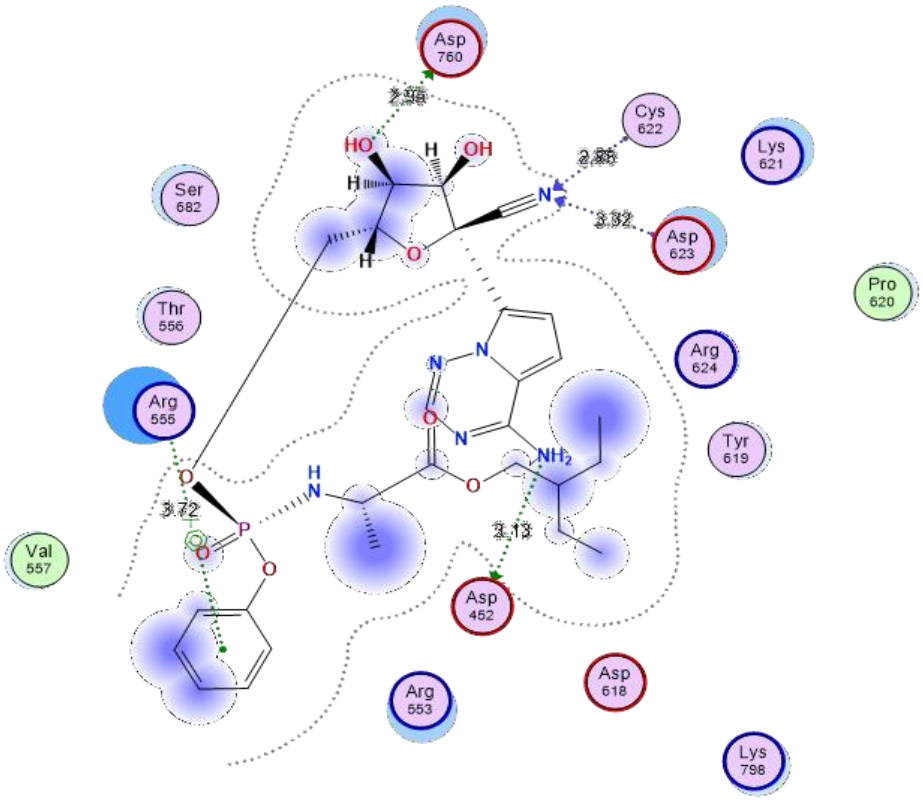

Figure 25: 2D structures showing interactions between remdesivir and residues of RdRp obtained using MOE.

4.3.4 Binding Energies Analysis

Using AutoDock Vina, the semi-empirical binding energies of potent alkaloids were calculated. **Table 15** summarises the interacting residues with binding energies of alkaloids with RdRp. With a binding energy of -9.8 kcal/mol, berbamine has the lowest binding energies and interacts with Cys 622, Asp 623, Ser 682, Asp 760, and Asp 761. Asp 618, Tyr 619, Lys 621, Asp 618, Asp 760, and Lys 798 are interacting residues with a binding energy of -9.1 kcal/mol. The interacting amino acid residues in remdesivir are Trp 617, Asp 618, Cys 622, Asp 760, Asp 761, Cys 813, and Ser 814, with a binding energy of -8.1 kcal/mol. **Figures 26, 27, and 28** displayed 2D and 3D structures of complexes.

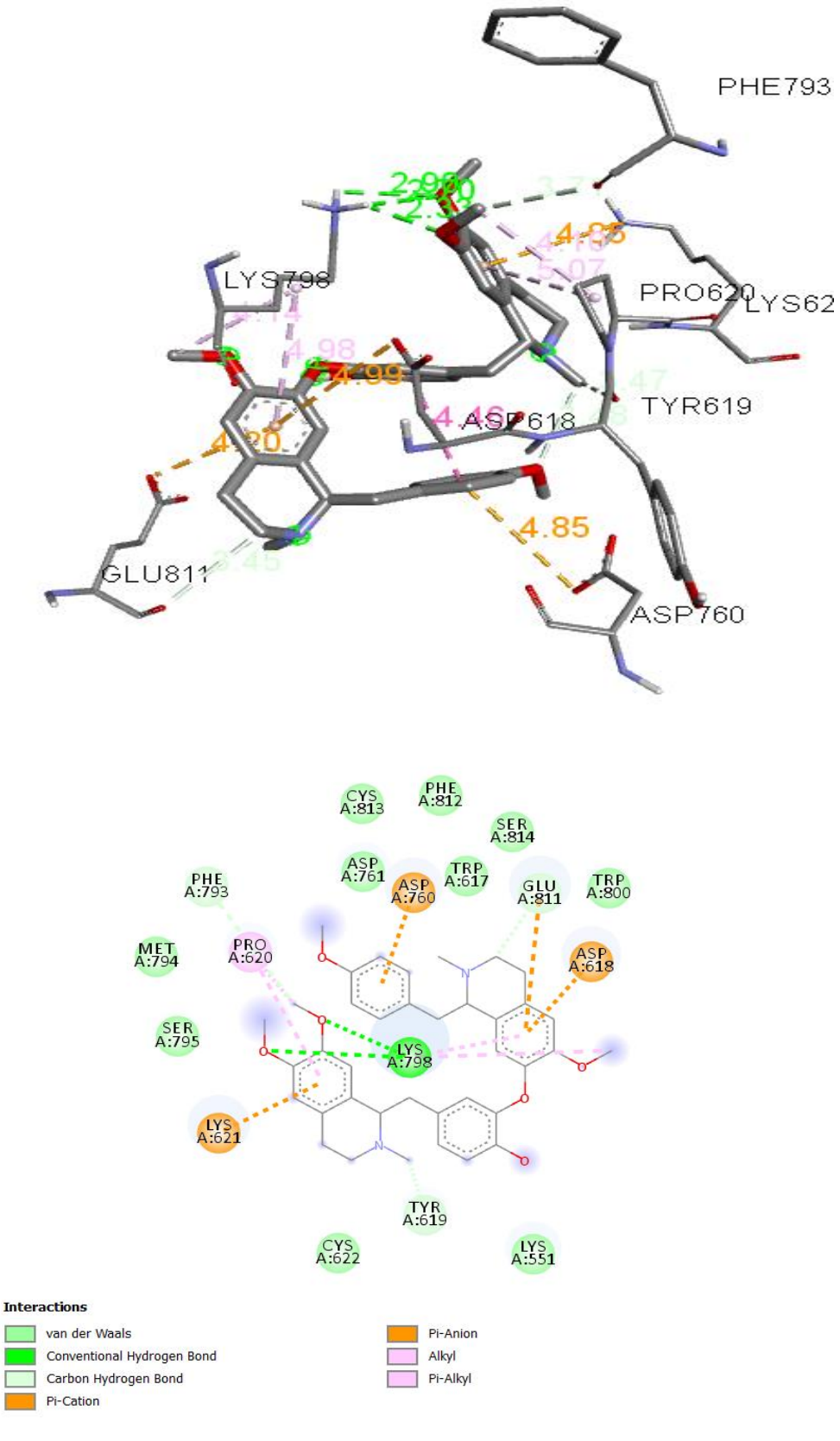

Figure 26: 3D and 2D structures showing interactions between neferine and residues of RdRp.

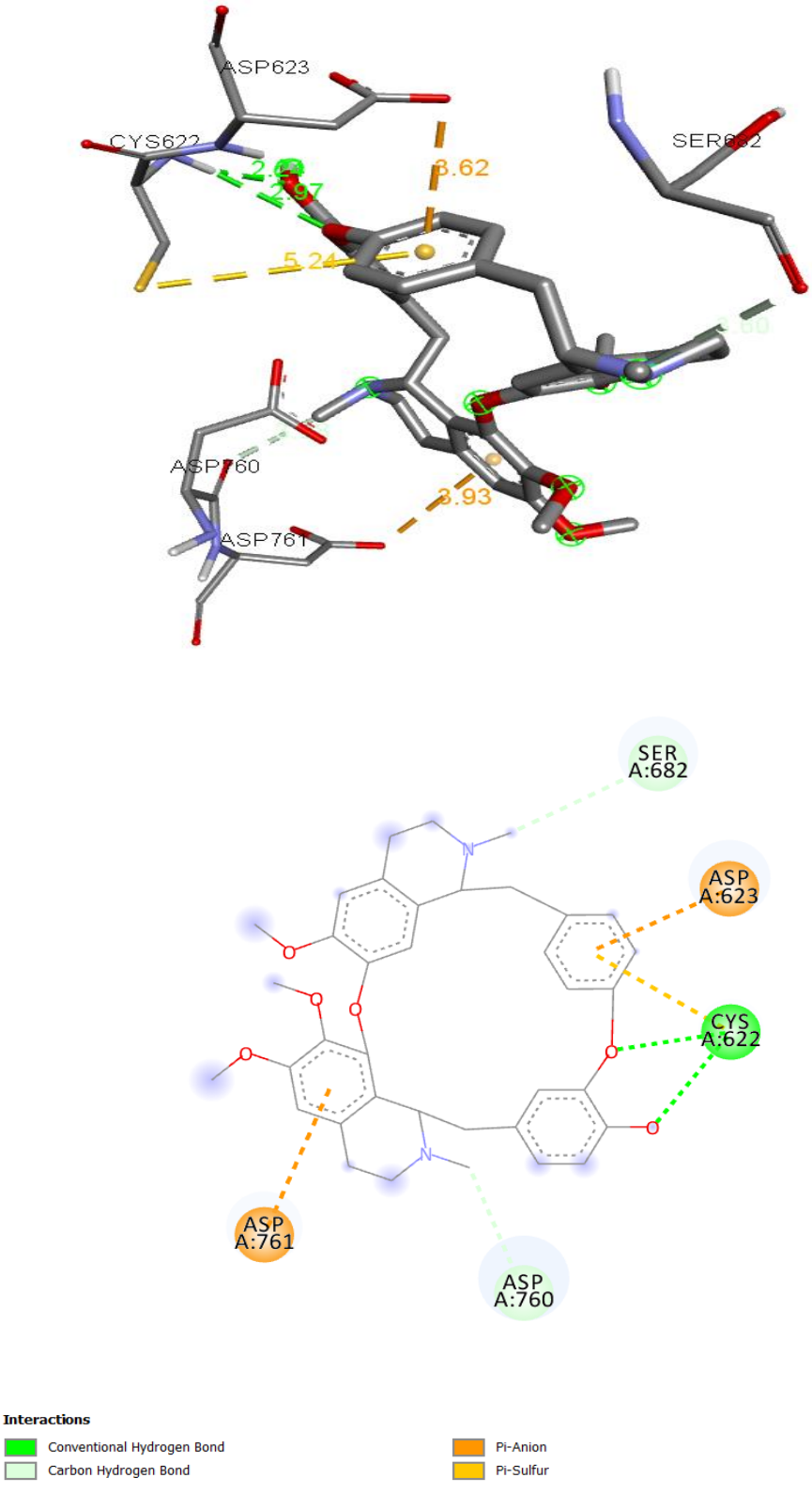

Figure 27: 3D and 2D structures showing interaction between berbamine and residues of RdRp.

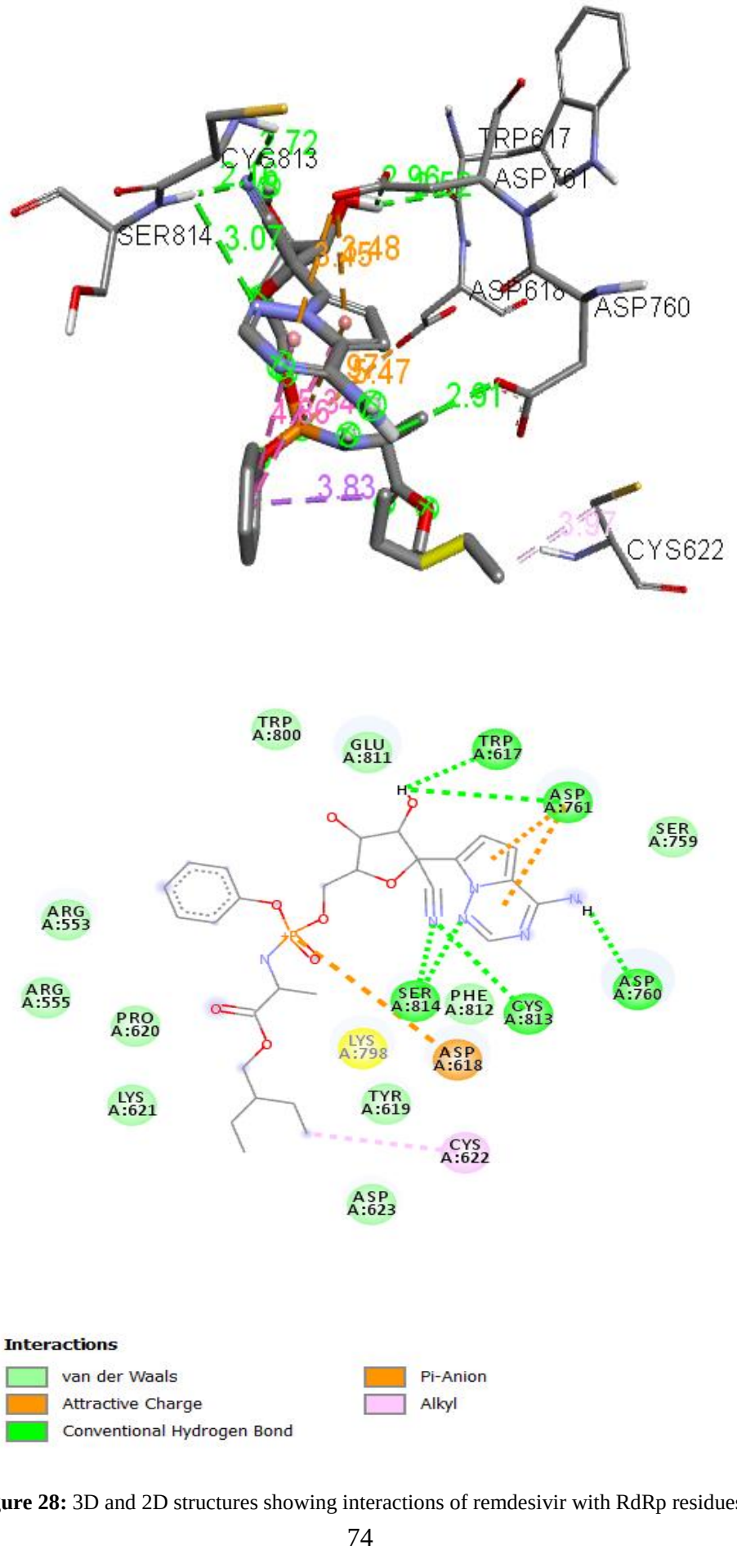

Figure 28: 3D and 2D structures showing interactions of remdesivir with RdRp residues.

Table 15: Summary of the binding free energies of potent alkaloids of RdRp along with interacting residues.

Compounds	Binding energy (kcal/mol)	Interacting residues
Oxysophoridine	-6.8	Ser 784, Lys 780
Berbamine	-9.8	Asp 761, Asp 760, Cys 622, Ser 682, Asp 623
Neferine	-9.1	Asp 760, Asp 618, Lys 621, Lys 798, Tyr 619
10'-hydroxyusambarensine	-8.9	Pro 323, Glu 350, Arg 349, Val 315, Pro 461
Strychnopentamine	-9.2	Tyr 619, Asp 623, Ser 682, Asp 760, Asp 761
Remdesivir	-8.1	Trp 617, Asp 618, Cys 622, Asp 760,Asp 761, Cys 813, Ser 814

4.3.5 MD Simulations Analysis

Neferine, one of the chosen alkaloids, was discovered to exhibit favorable interactions with RdRp. The neferine-RdRp complex was subjected to 90 ns MD simulations in order to better understand the interaction between ligands and receptors. **Figure 29(A)** displays the RMSD values for the neferine-RdRp complexes. The study finds the average RMSD fluctuations is 0.26 nm of protein-ligand complex that suggests the less deviation and high stability of neferine-RdRp complex throughout the simulations. And from the plot it can be illustrated that the complex undergoes equilibrium after 40 ns. **Figure 29 (B)** displays a plot of the RMSF values against the amount of amino acid residues when compared with starting structures. In the neferine-RdRp complex, the RMSF is smaller than 0.19 nm for each surrounding residue which depicts the stability of protein during the simulation period.

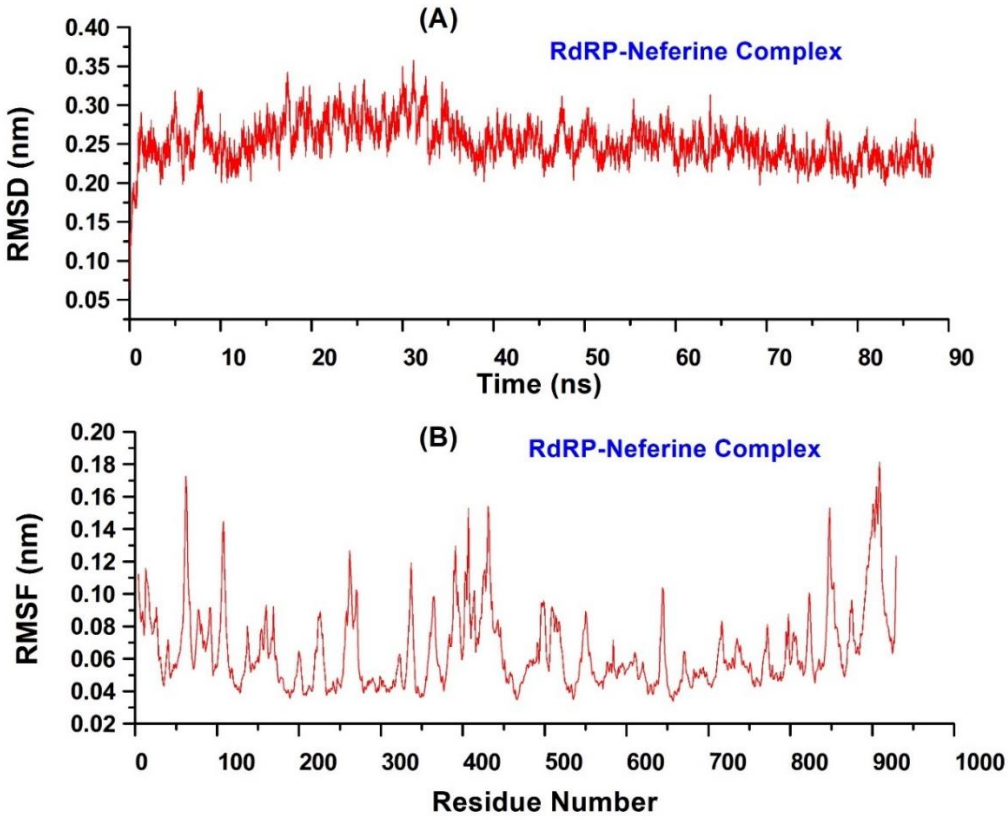

Figure 29: The plots of (A) RMSD and (B) RMSF plots for the neferine-RdRp complex.

4.3.6 DFT Analysis-based Band Gap Results

To determine the reactivity of neferine relative to the standard medication remdesivir, DFT analysis was performed based on the results of pharmacokinetics properties, molecular docking, and MD simulations. Interestingly, band gap energy (**Figure 30**) of neferine (0.19874 Hartree) was found to be similar to the standard drug which corroborate its reactivity to the target protein. **Table 16** represents the DFT results of neferine and remdesivir.

Table 16: Displays DFT results in terms of the following chemical reactivity descriptors.

Tested Compounds	E_{LUMO} (Hartree)	E_{HOMO} (Hartree)	Band energy gap (ΔE) (Hartree)	Ionization potential (I) (Hartree)	Electron affinity (A) (Hartree)	Global hardness (η)	Global softness (S)	Electronegativity (X)	Chemical potential (μ)	Electrophilicity index (ω)
Neferine	0.00344	-0.19530	0.19874	0.19530	-0.00344	0.09937	10.06339	0.09593		0.04630
Remdesivir	-0.03812	-0.21813	0.18001	0.21813	0.03812	0.07095	14.09543	0.12812	-0.12812	0.11572

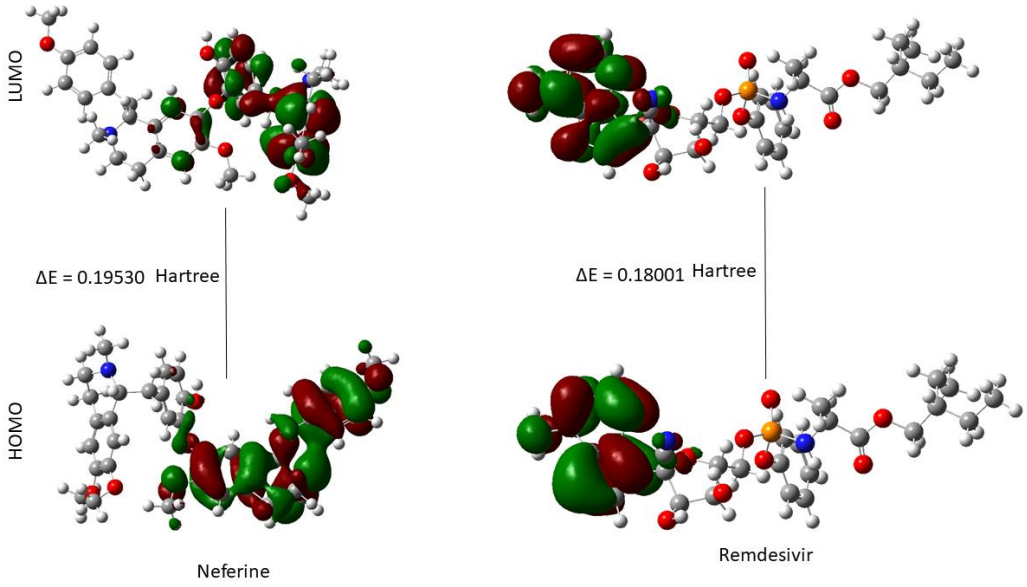

Figure 30: The band gap energies between HOMO and LUMO of neferine and remdesivir.

4.3.7 Molecular Docking of Neferine with S1-RBD of SARS-CoV-2 Omicron Variant

Neferine shows acceptable binding energy (-7.6 kcal/mol) with significant binding interactions with key residues of S1-RBD of SARS-CoV-2 Omicron variant. Neferine interacted with Arg 493 and Leu 452 residues that are responsible for interacting of S1-

RBD with human ACE-2 (Han *et al*., 2022; Z. Liu *et al*., 2021). **Figures 31** and **32** display 2D and 3D interactions of neferine complexed with S1-RBD of SARS-CoV-2 Omicron variant.

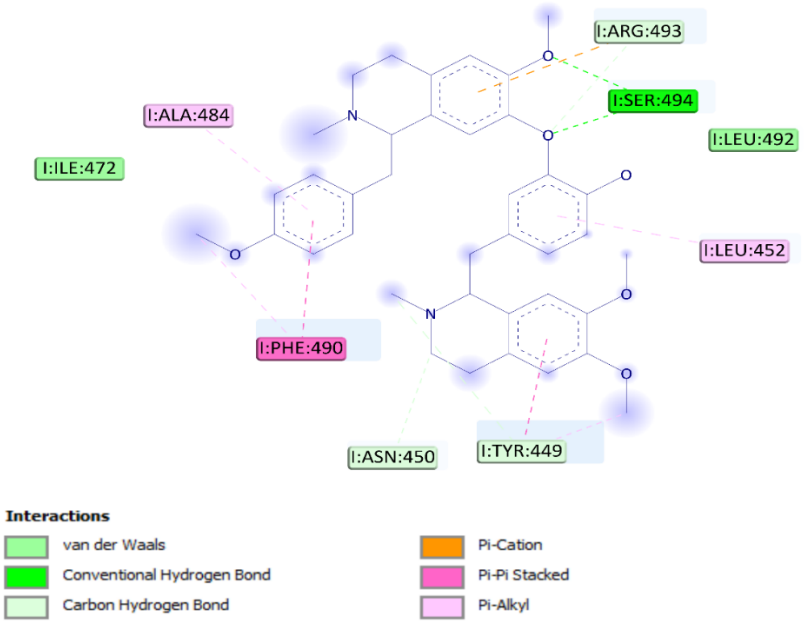

Figure 31: 2D structure of neferine-S1-RBD complex showing interactions with key residues.

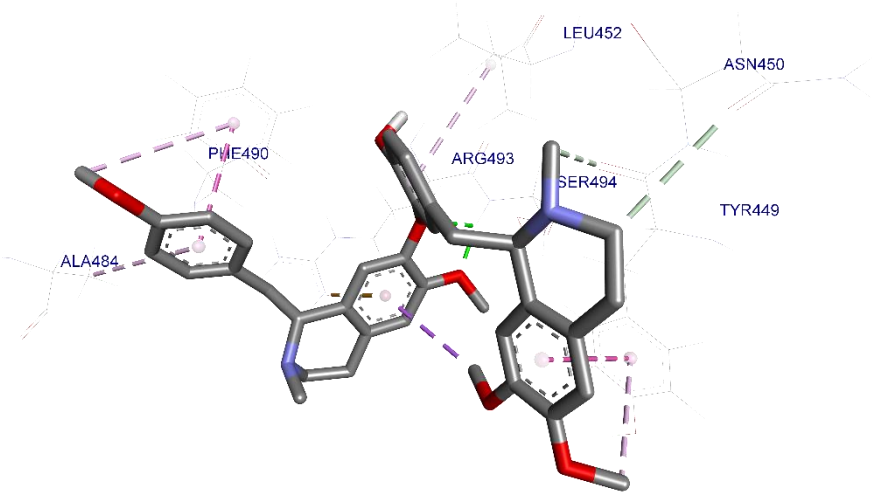

Figure 32: 3D structure of neferine complexed with S1-RBD.

4.3.8 Spike Protein Assay Analysis

Using enzyme-linked immunosorbent assay, neferine was evaluated *in vitro* in response to promising *in silico* findings that suggested it might hinder the interaction between S1-RBD of SARS-CoV-2 Omicron and hACE2. Varying concentration of neferine was

incubated in 96-well plates coated with S1-RBD along with hACE2. An HRP-linked secondary antibody was used to produce the signal. **Table 17** displays absorbance and % inhibition at 450 nm. Neferine inhibits the interaction between hACE2 and S1-RBD protein, according to *in vitro* studies. IC_{50} of 99.60 ± 0.328 µg/mL of neferine is responsible for the 50 % inhibition of the binding of hACE2 with S1-RBD of spike protein (**Figure 33**).

Table 17: Absorbance measurements with successive concentration range of neferine and determination of % of hACE 2 bound to the S1-RBD of SARS-CoV-2 Omicron, as detected by an anti-human HRP antibody and TMB.

S.N.	Neferine (µg/mL)	Absorbance	% of hACE 2 bound to the S1-RBD (mean)
1	0	2.252	100
2	15.125	2.255	85.2062
3	31.25	2.087	78.0931
4	62.50	1.850	69.2017
5	125	1.275	47.6731
6	250	1.071	41.1464

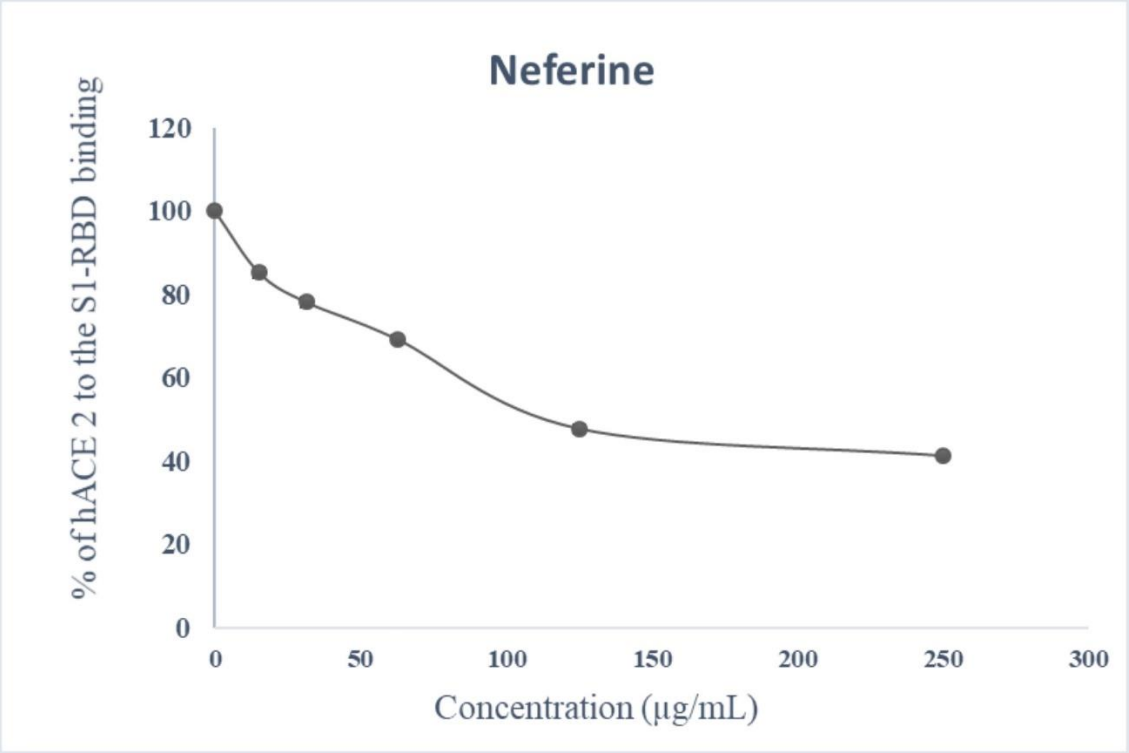

Figure 33: The binding curve of hACE2 receptor to S1-RBD Omicron variant in the presence of successive concentration of neferine. The data represent mean ± SEM from n = 3 samples.

4.4 Investigation of Terpenes

4.4.1 Molecular Docking Analysis

A total of 50 terpenes selected, based on their antiviral properties, were docked through AutoDock tools with S1-RBD of the SARS-CoV-2 Omicron variant. The energies of binding for docked compounds are shown in **Appendix B3**. The docking studies along with considering toxicity class revealed that saikosaponin B2 and cryptotanshinone are the potent inhibitors of the target protein used. Utilizing the docked positions for each of these terpenes, Discovery Studio was used to create images of the molecular interaction network of ligands with the target protein, **Figures 34 (a, b, and c)** represent the 2D and 3D interaction and images of saikosaponin B2, cryptotanshinone, and molnupiravir with target protein. **Appendix F5** represents 2D and 3D structures of some compounds depicting interactions with S1-RBD.

One conformation for each ligand with the least RMSD was chosen from all the conformations formed during docking. Since the key residues make up the majority of the interacting residues of target proteins, these compounds exhibit acceptable binding affinities with good binding interactions. Oxane ring hydroxyl groups of saikosaponin B2 were shown to form hydrogen bonds with Phe 374, Thr 376, Asn 437, and Tyr 508. Additionally, Pro 373, Phe 374, and Lys 440 of spike proteinformed H-bond with the hydroxymethyl group of the oxane ring, with binding energy of -9.3 kcal/mol. One of the several amino acid residues of spike implicated in immune evasion is Lys 440 (Guo *et al*., 2022) (**Figure 34 d**) and is in charge of ensuring that ACE2 and S1-RBD Omicron have a good association. Cryptotanshinone interacts through pi-alkyl with Trp 436 of S1-RBD Omicron and pi-pi T-stacked with Phe 374 and Phe 375. A prior work by Ong et al. suggested that Trp 436 possibly played a role in the inactivation of human coronaviruses following UVC wavelength absorption at Trp 436 (Ong *et al*., 2022). With a binding energy of -7.6 kcal/mol, the keto group of cyclohex-dien-dione of cryptotanshinone establishes a hydrogen bond interaction with the amine group of Lys 440. One of the several amino acid residues of S1-RBD, Lys 440 is implicated in immune escape (Guo *et al*., 2022) and is in charge of creating an effective interaction between S1-RBD and ACE2 (Da Costa *et al*., 2022). Notably, an H-bond interaction is exhibited by Lys 440 in saikosaponin B2 and cryptotanshinone. Molnupiravir did not exhibit any interactions with the important residues of S1-RBD and exhibited -6.6

kcal/mol binding energy. The binding energies and H-bond along with other interactions of these compounds with the S1-RBD are summarized in **Table 18.** Furthermore, an explanatory theory concerning the mode of action of metabolites can be developed through the use of these computational methods and theoretical molecular docking procedures.

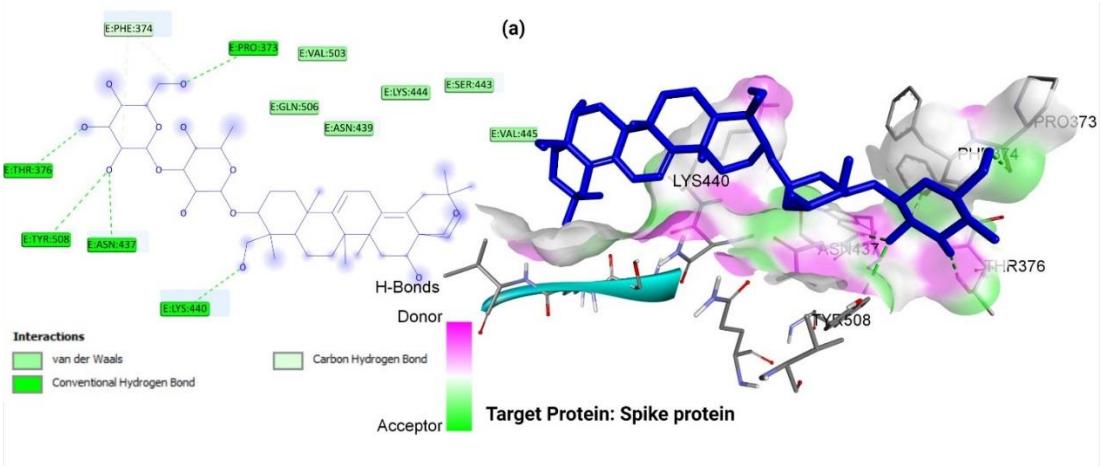

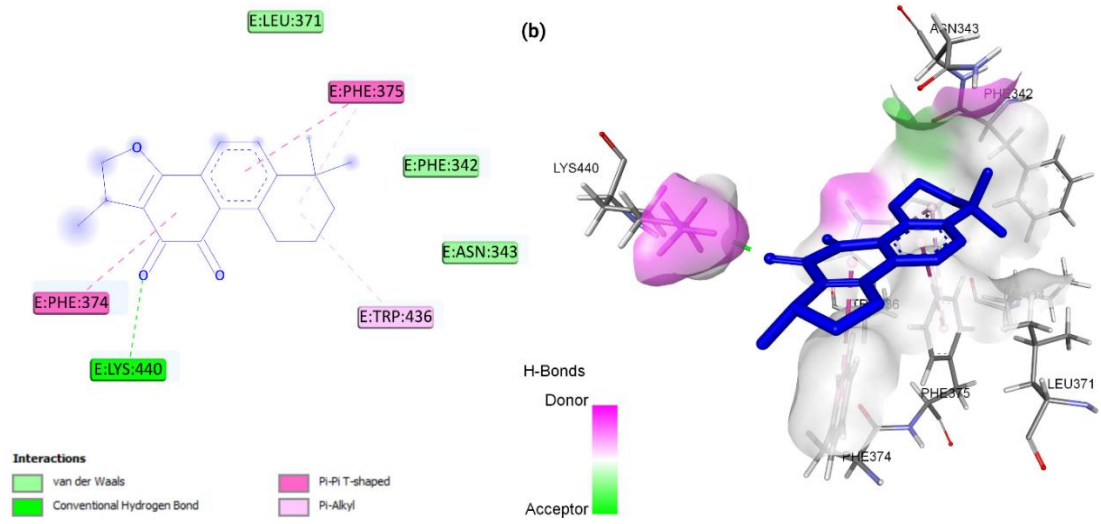

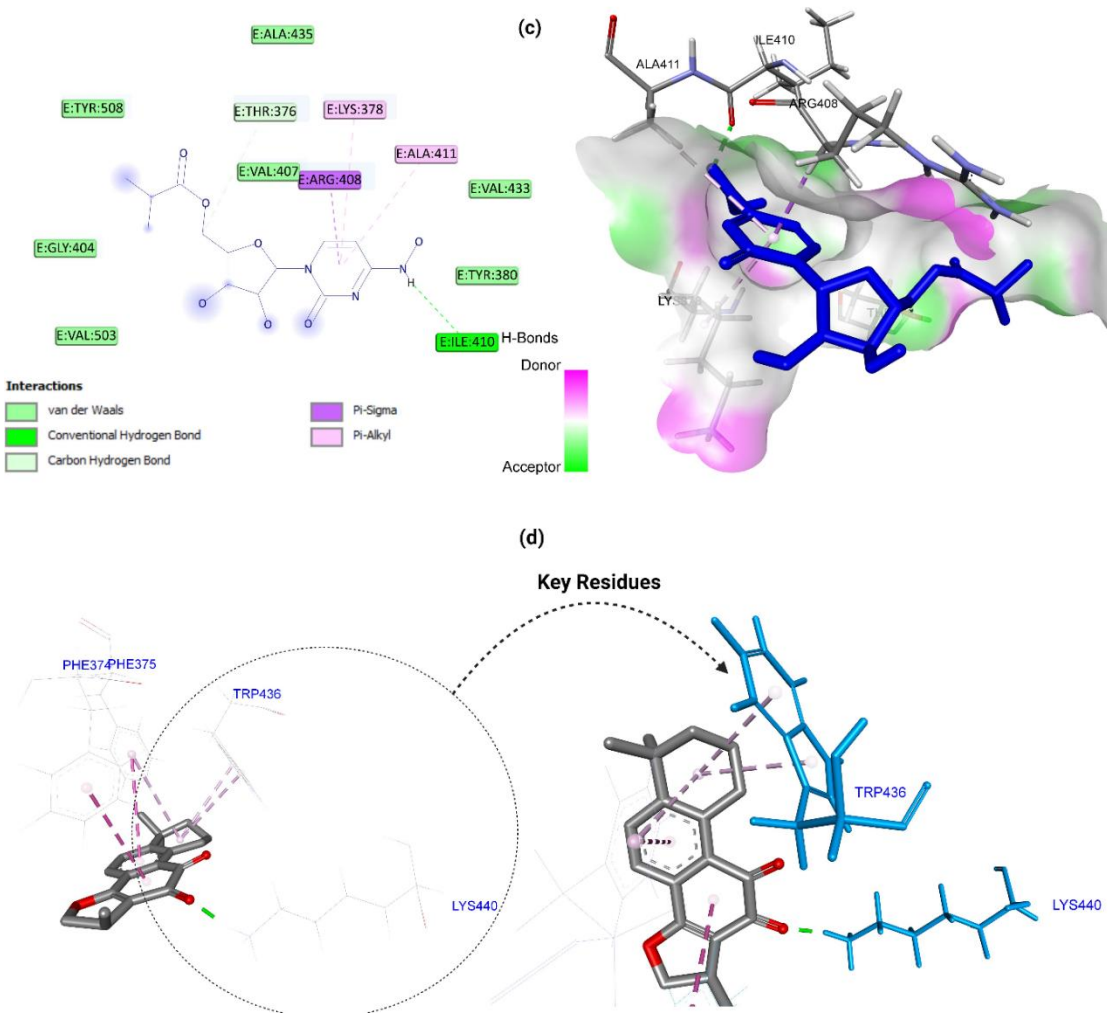

Figure 34: (a), (b), and (c) shows 2D and 3D representations of the docking complex of saikosaponin B2, cryptotanshinone, and molnupiravir with the S1-RBD; (d) represents the key residue of S1-RBD.

Table 18: PubChem ID of potent terpenes and reference compound; binding affinity; the interacting amino acid residues of the S1-RBD of SARS-CoV-2 Omicron variant.

Tested Compounds	PubChem ID	Binding Affinity (kcal/mol)	Interacting Amino Acid Residues
Saikosaponin B2	21637642	–9.3	Pro 373, Phe 374, Thr 376, Asn 437, Lys 440, Tyr 508
Cryptotanshinone	160254	–7.6	Lys 440, Phe 374, Phe 375, Trp 436
Molnupiravir	145996610	-6.6	Ile 410, Thr 376, Arg 408, Ala 411, Lys 378

4.4.2 DFT Analysis-based Band Gap Results

In the current study, two terpenes (saikosaponin B2 and cryptotanshinone), based on molecular docking results along with reference compound molnupiravir, were chosen for the DFT analysis. The results demonstrated that both cryptotanshinone and saikosaponin B2 have effective reactivity due to the low band gap of HOMO and LUMO i.e., 0.11842 and 0.18415 Hartree, respectively, compared to the reference drug (ΔE = 0.4491 Hartree) demonstrated in **Figure 35**. This shows both inhibitors have a high binding affinity for their target proteins. Furthermore, electrophilic nature, global hardness, softness, chemical potential, and electrophilicity index that is concerned with the reactivity (**Table 19**) suggest the high potency of these five compounds towards respective SARS-CoV-2 proteins.

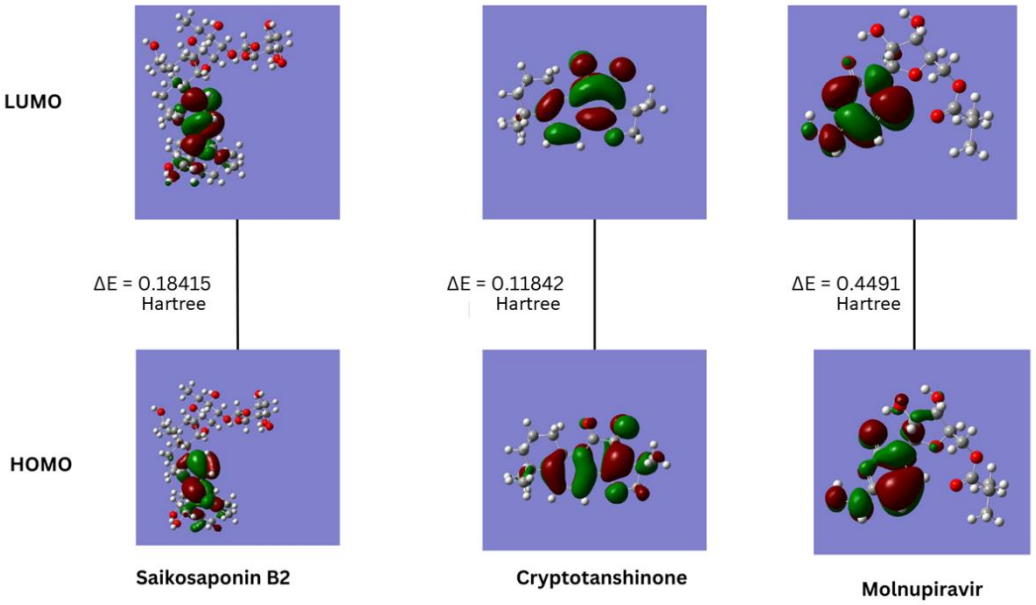

Figure 35: The band gap energies between HOMO and LUMO of saikosaponin B2, cryptotanshinone, and molnupiravir.

Table 19: Displays DFT results in terms of the following chemical reactivity descriptors.

Tested Compounds	E_{LUMO} (Hartree)	E_{HOMO} (Hartree)	Band energy gap (ΔE) (Hartree)	Ionization potential (I) (Hartree)	Electron affinity (A) (Hartree)	Global hardness (η)	Global softness (S)	Electronegativity (X)	Chemical potential (μ)	Electrophilicity index (ω)
Saikosaponin B2	-0.01839	-0.20254	0.18415	0.20254	0.01839	0.092075	10.8607	0.110465	-0.110465	0.06626
Cryptotanshinone	-0.10747	-0.22589	0.11842	0.22589	0.10747	0.05921	16.8890	0.16668	-0.16668	0.23461
Molnupiravir	0.09951	-0.34959	0.4491	0.34959	-0.09951	0.22455	4.45335	0.12503	-0.12503	0.03481

4.4.3 MD Simulation Analysis

The dynamic behaviour and stability of the protein-ligand complexes and apoprotein were determined via MD simulations. Cryptotanshinone and saikosaponin B2 complexed with S1-RBD having high binding affinity were selected for the MD simulations, and the structural changes and dynamic behavior that occurred within the complexes were analyzed in terms of RMSD, RMSF, R_g, SASA, and number of hydrogen bonding.

- **Root-mean-square-deviation (RMSD):** RMSD is a crucial metric used to assess the structural stability of a system over time in molecular dynamics simulations. GROMACS provides the *gmx rms* tool to perform this analysis. The dynamic behavior, and structural and conformational shifts within the backbone of apoprotein and protein-ligand complexes were accessed via RMSD analysis (Muralidharan *et al*., 2021). The RMSD plot of apoprotein and protein-

ligand complexes within 100 ns simulation trajectory is displayed in **Figure 36**. The RMSD plot showed both cryptotanshinone-protein complex and apoprotein reached stability after 40 ns though after 78 ns, a small fluctuation was seen in the backbone of the apoprotein, whereas molnupiravir-protein complex gained stability after 20 ns up to 80 ns after which slight fluctuation was observed. On the other hand, the saikosaponin B2-protein complex does not demonstrate acceptable stability with a 100 ns simulation trajectory. The simulation result reveals that cryptotanshinone-protein complex with an average RMSD of 0.3474 nm (**Table 20**), is more stabilized with 100 ns simulation compared to apoprotein, saikosaponin B2-protein complex, and molnupiravir-protein complex.

Table 20: The average values of RMSD, RMSF, Rg, and SASA

Complex	**Cryptotanshinone-protein complex**	**Saikosaponin B2-protein complex**	**Molnupiravir-protein complex**	**Apoprotein**
Average RMSD (nm)	0.3474	0.5433	0.39197	0.4101
Average RMSF (nm)	0.1465	0.1708	0.1763	0.1734
Average R_g (nm)	1.1301	1.1352	1.1443	1.1311
Average SASA (nm^2)	95.1708	98.0475	94.4377	96.006

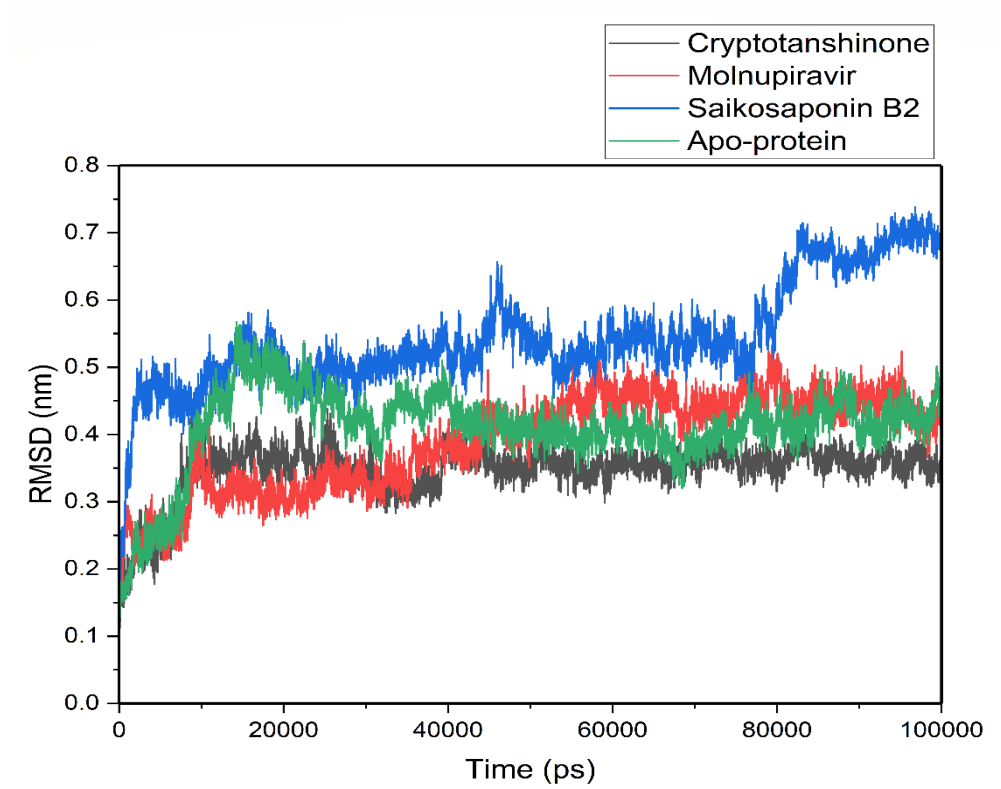

Figure 36: RMSD plot of cryptotanshinone, saikosaponin B2, and molnupiravir complexes and apoprotein.

- **Root-mean-square-fluctuations (RMSF):** The fluctuating behaviour of each amino acids of the backbone of apoprotein and protein-ligand complexes was assessed via RMSF analysis. The greater RMSF values disclose information about the loop and protease-labile regions of the protein by indicating more flexibility and mobility in certain protein regions (Ilyas *et al*., 2022). Similarly, the lower RMSF value represents the protein's secondary structure like helices and sheets. Protein secondary structures like helices and sheets are also indicated by a lower RMSF value. During the 100 ns simulation, the apoprotein and complexes possessed similar fluctuations in the same residues (**Figure 37)**. Apoprotein, cryptotanshinone-protein complex, and saikosaponin B2-protein complex have average RMSF values of 0.1734 nm, 0.1465 nm, and 0.1708 nm respectively (**Table 20).**

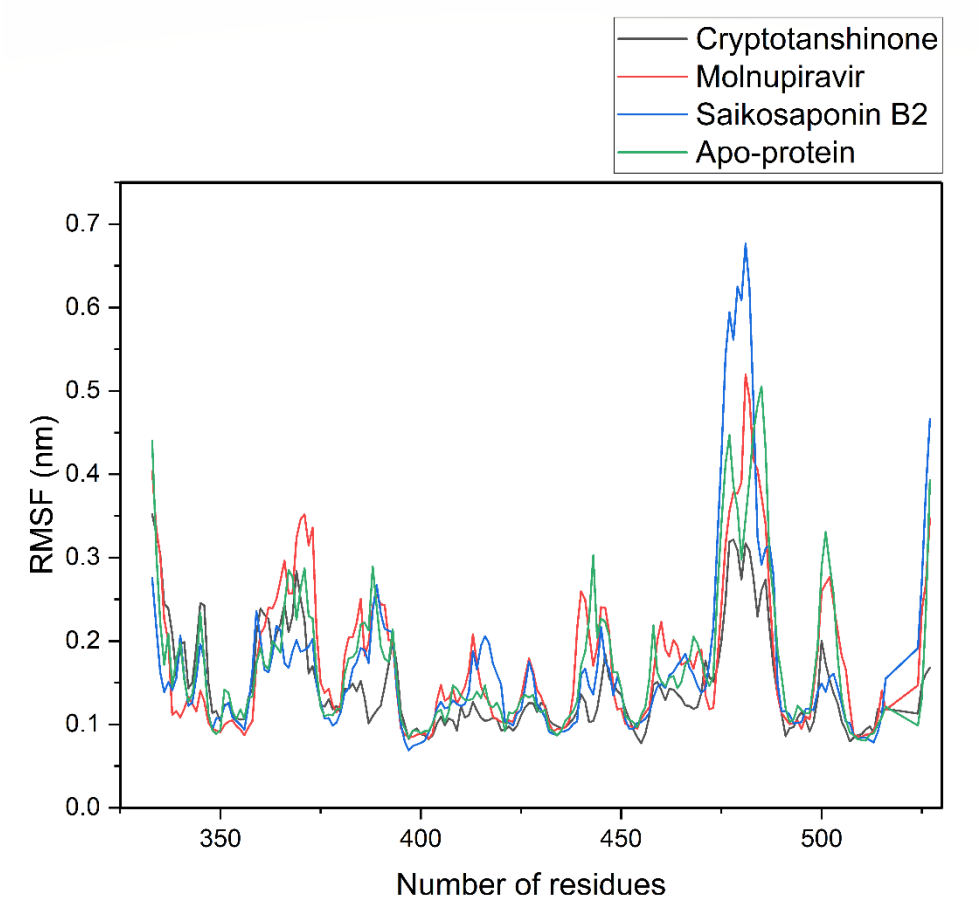

Figure 37: RMSF plot of cryptotanshinone, saikosaponin B2, and molnupiravir complexes and apoprotein.

- **Radius of gyration (R_g):** The stability and compactnesss of ligand-protein complexes and apoprotein were evaluated employing R_g values. The folded and unfolded conformation of the apoprotein and protein-ligand complexes can also be ascertained by utilizing the R_g value. MD simulation trajectory was utilized to estimate the structural compactness of apoprotein and protein-ligand complexes for computing R_g values (**Figure 38**).

  Average R_g values of apoprotein, cryptotanshinone-S1-RBD, saikosaponin B2-S1-RBD, and molnupiravir-S1-RBD were 1.1311, 1.1301, 1.1352, and 1.1443 nm respectively (**Table 20**). Together with the apoprotein, all protein-ligand complexes showed in fact stable and steady R_g values. The R_g value shows that all complexes have good stability and properly formed overlaid structures. The R_g results show that throughout the 100 ns simulation trajectory, the apoprotein and all three protein-ligand complexes attained folded form and compact structure.

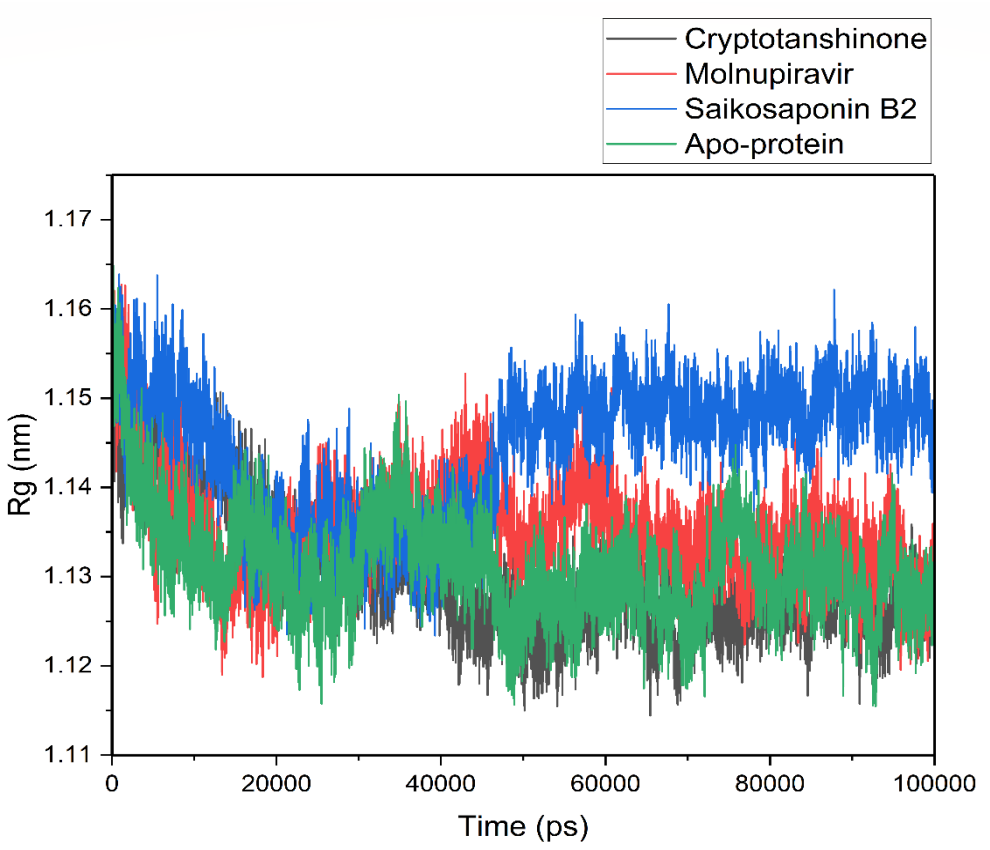

Figure 38: Rg plot of cryptotanshinone, saikosaponin B2, and molnupiravir complexes and apoprotein.

- **Solvent accessible surface area (SASA):** The accessible section of protein to water and organic solvent is determined by the SASA parameter. To assess the degree of conformational changes that occurs on interaction, the SASA parameter is essential. Less surface area is accessible for interaction with solvent molecules due to the complex forming a compact structure, as indicated by the lower SASA value. It was reported that the average SASA for the complexes of apoprotein, cryptotanshinone-protein, saikosaponin B2-protein, and molnupiravir-protein were 96.006, 95.1708, 98.0475, and 94.4377 nm^2, respectively (**Table 20)**. The SASA plot reveals that the cryptotanshinone and molnupiravir (reference) bind effectively to the binding site of the protein and form a more compact structure compared to saikosaponin B2. Due to this cryptotanshinone-protein and molnupiravir-protein complexes have the lowest surface area for interaction with the solvent molecules. The SASA plot of all three complexes along with apo-protein is displayed in **Figure 39.**

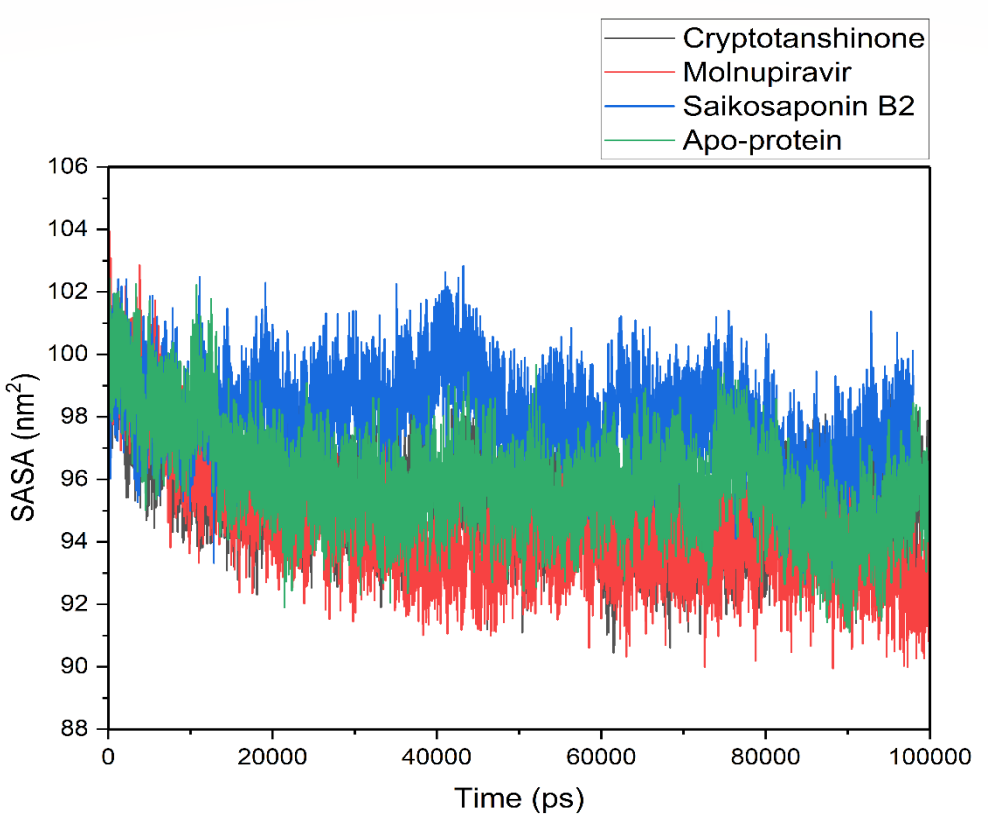

Figure 39: A SASA plot of cryptotanshinone, saikosaponin B2, and molnupiravir complexes and apoprotein.

- **Hydrogen bond analysis:** Hydrogen bonds play a crucial role in substrate binding to proteins and impact various biological processes such as drug affinity, metabolism, adsorption, and specificity. For this reason, it's important to identify hydrogen bonding patterns by monitoring the dynamic fluctuations of each protein-ligand complex. It was noted that both cryptotanshinone-protein, saikosaponin B2-protein, and reference (molnupiravir)-protein complexes maintain hydrogen bonding throughout the 100 ns simulation trajectory. Cryptotanshinone-protein complex exhibited up to three hydrogen bonds whereas saikosaponin B2-protein complex exhibited a maximum of four hydrogen bonds and the molnupiravir complex exhibited up to seven hydrogen bonds displayed in **Figure 40**.

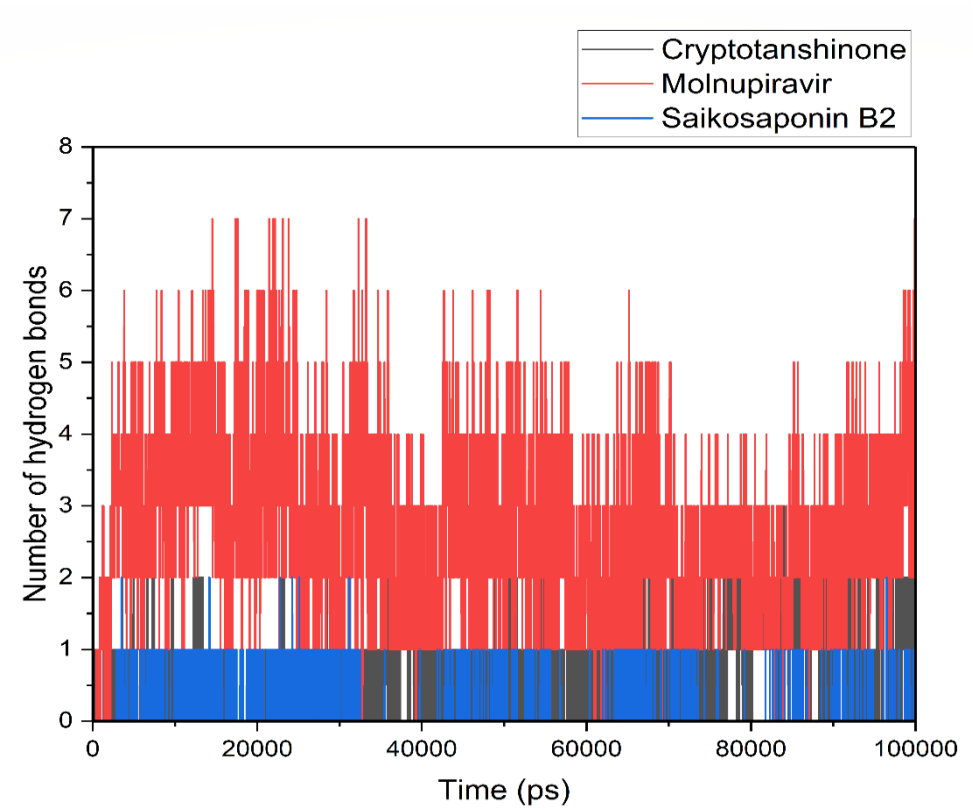

Figure 40: H-bonding plot of cryptotanshinone, saikosaponin B2, and molnupiravir complexes and apoprotein.

4.4.4 Pharmacokinetic Analysis

A medication must enter the target organ in an appropriate quantity and remain there in a physiologically active condition long enough for the biochemical reactions to take place in order for it to be effective (Daina *et al*., 2017). This research work used the swissADME, ProTox II, and pkCSM server among the several prediction models that were available to investigate the pharmacological effects of molnupiravir and cryptotanshinone. Drug lipophilicity is measured by octanol/water partition coefficients (log P values). Lipinski states that compounds moving on to Phase II clinical trials should have a lipophilicity range of log P < 5 (Waring, 2010) (Lipinski *et al*., 2001). The drug-like properties and the rule of five, which describes the possibility of a compound functioning as an oral medication, were both exhibited by cryptotanshinone and molnupiravir. The TPSA is a parameter to evaluate the ability of drug to permeate cells: TPSA >140 $Å^2$ denotes poor permeability of drugs, while TPSA ≤ 60 $Å^2$ denotes high intestinal permeability (Fernandes & Gattass, 2009) (Van de Waterbeemd, 2007). Cryptotanshinone has a TPSA of less than 60 $Å^2$ whereas molnupiravir has more than

140 $Å^2$ TPSA revealing its lower intestinal permeability. **Table 21** lists the drug-like properties of cryptotanshinone and molnupiravir.

Furthermore, the pkCSM server facilitates the assessment of the potency of compound, pharmacological characteristics, and related safety concerns (Pires *et al*., 2015). The intestine is the principal site of oral medication absorption; drug absorption within the intestines that is less than 30% is deemed insufficient. Because of their high rates of intestinal absorption, molnupiravir and cryptotanshinone have appropriate intestinal absorption and they also showed suitable water solubility level to be appropriate drug candidate. The absorption and bioavailability of oral drugs is evaluated by measuring the permeability of the Caco-2; an apparent permeability coefficient (Papp) value > 8 × 10^{-6} cm/s is considered as a favourable permeability value (Lagorce *et al*., 2017). ADMET analysis (**Table 22**) revealed cryptotanshinone is moderately water soluble and has low Caco-2 permeability with no AMES toxicity and hepatotoxicity while molnupiravir shows hepatotoxicity. To prevent neurotoxicity, it is preferable for drugs with an action site that is not relate to the brain in order to pass through the blood-brain barrier (BBB) (Muehlbacher *et al*., 2011), and remarkably, cryptotanshinone is unable to cross the BBB because compounds having log BB ≤ 0.3 do not reach the brain sufficiently. ADMET scans CYP parameters to display drug metabolism (Wu *et al*., 2012). In human liver microsomes, the metabolic enzymes CYP1A2, CYP2A6, and CYP3A4 may be responsible for the metabolism of cryptotanshinone (Zeng *et al*., 2018).

Additionally, the ProTox II server is useful for analysing the toxicities and has categorized toxicity into six main classes: Class I and II (deadly if ingested), Class III (poisonous if ingested), Class IV (harmful if ingested), Class V (may be harmful if ingested) and Class VI (non-toxic) (Banerjee *et al*., 2018). Cryptotanshinone was found in toxicity class VI and molnupiravir in toxicity class IV. To further validate the drug-like, ADMET and MD simulation of cryptotanshinone, the S1-RBD assay was performed.

Table 21: Potent compounds showing drug-likeness properties.

S.N.	Compounds	Number of rotatable bonds	TPSA	LogP	Molar refractivity	Lipinski Rule of Five
1	Saikosaponin B2	7	218.99	1.86	201.50	No; 3 violations
2	Cryptotanshinone	0	43.37	3.43	85.13	Yes; 0 violation
3	Molnupiravir	6	143.14	0.17	76.02	Yes; 0 violation

Table 22: ADMET profiles of saikosaponin B2, cryptotanshinone, and molnupiravir.

S.N.	Compounds	Caco-2 Permeability (log Papp 10-6 cm/s)	Intestinal absorption (%absorbed)	BBB Permeation	CYP Inhibition	Ames Toxicity	Hepatotoxicity	LD_{50} in Rat(mol/kg)	Toxicity class
1	Saikosaponin B2	-0.708	34.463	-1.504	No	No	No	2.946	V
2	Cryptotanshinone	1.327	97.189	0.284	Yes(CYP 1A2, CYP2C19 , YP3A4)	No	No	1.976	VI
3	Molnupiravir	0.531	53.464	-1.057	No	0.203	No	Yes	IV

4.4.5 Spike Protein Assay

Using an enzyme-linked immunosorbent assay, cryptotanshinone was evaluated through *in vitro* in response to promising *in silico* findings that suggested it might block the interaction between SARS-CoV-2 S1-RBD Omicron variant and hACE2. The *in vitro* results of cryptotanshinone were compared with molnupiravir. **Tables 23** display determination of the % of hACE2 bound to the S1-RBD. Varying concentration of cryptotanshinone and molnupiravir was incubated in 96-well plates coated with S1-RBD along with hACE2. An HRP-linked secondary antibody was used to produce the signal. The results obtained from in vitro suggest that the interaction of hACE2 with S1-RBD protein was inhibited by cryptotanshinone. With IC_{50} of 25.5 ± 0.463 μg/mL of cryptotanshinone is responsible for the 50 % inhibition of the binding of hACE2 with S1-RBD of spike protein, which is slightly lower than the concentration (29.73 ± 1.248

µg/mL) of the reference drug (**Figure 41**). Thus, the *in vitro* experiment also supports cryptotanshinone as a more potent inhibitor S1-RBD compared to molnupiravir.

Table 23: Absorbance measurements with successive concentration range of cryptotanshinone and reference compound (molnupiravir) and determination of % of hACE 2 bound to the S1-RBD of SARS-CoV-2 Omicron, as detected by an anti-human HRP antibody and TMB.

Concentration (µg/mL)	**Absorbance (mean)**		**% of hACE2 bound to the S1-RBD (mean)**	
	Cryptotanshinone	**Molnupiravir**	**Cryptotanshinone**	**Molnupiravir**
0.000	2.022	2.643	100.0000	100.0000
15.125	1.394	1.903	67.9337	73.2312
31.25	1.033	1.388	50.3168	51.2675
62.50	0.802	0.985	39.0838	36.8331
125	0.602	0.51	29.3372	19.6368
250	0.412	0.284	20.0780	10.6129

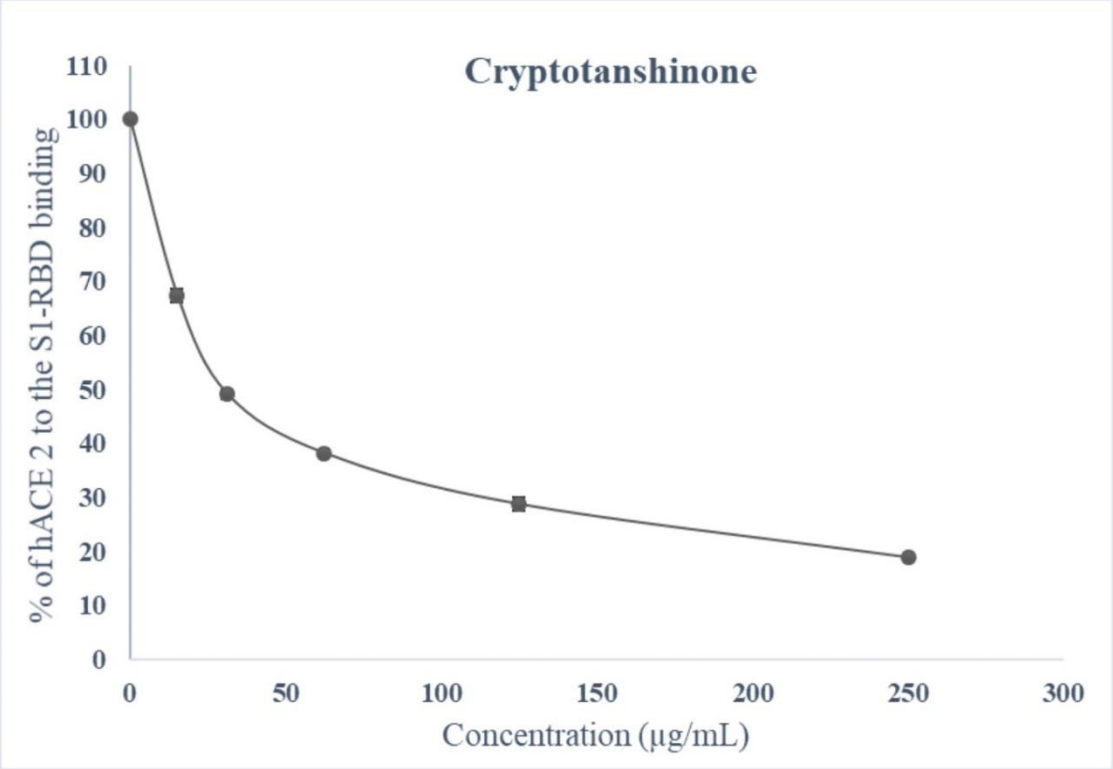

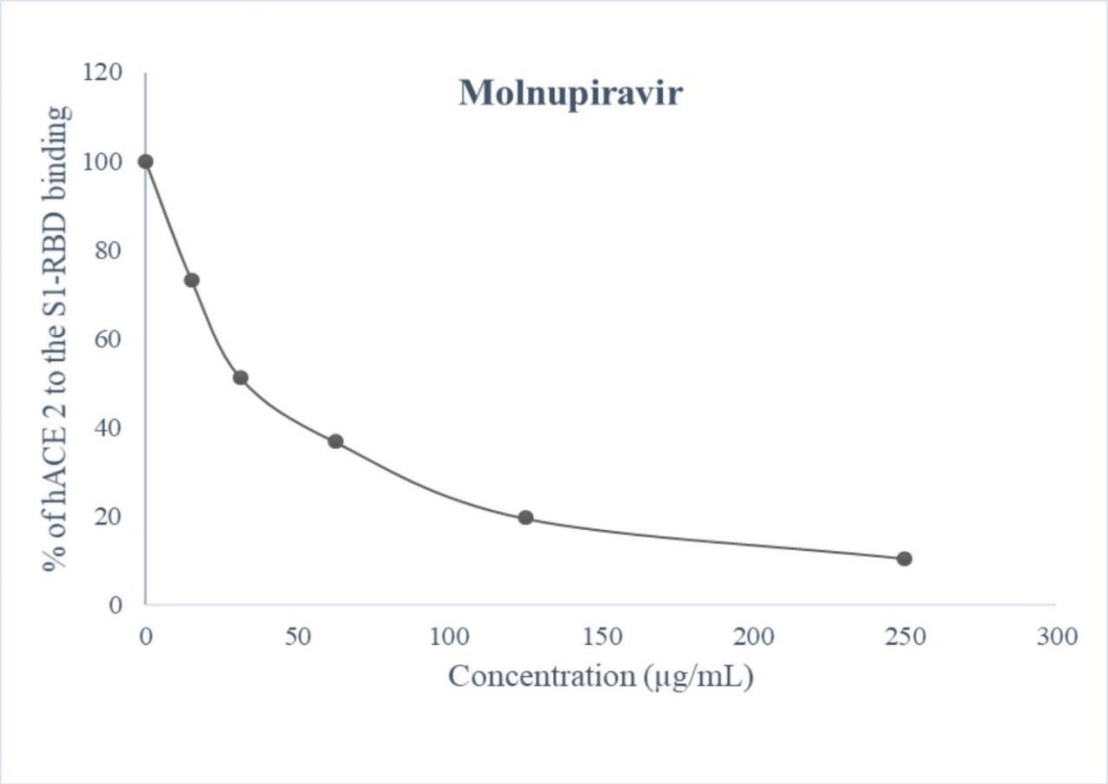

Figure 41: The binding curve of % of hACE2 receptor to S1-RBD Omicron variant in the presence of successive concentration of cryptotanshinone and molnupiravir. The data represent mean ± SEM from n = 3 samples.

CHAPTER 5

5. CONCLUSIONS AND RECOMMENDATION

Although there are various COVID-19 vaccines available, there is a need to produce medications that are effective against SARS-CoV-2. Drug repurposing is one of the most practical methods for creating medications to combat this infection. To find the most effective drugs for inhibiting SARS-CoV-2, 191 compounds were evaluated in this research utilizing computational techniques followed by *in vitro* assays. After conducting an extensive investigation into potent compounds for the inhibition of SARS-CoV-2, this research work has identified cordifolioside A, cyanidin, neferine, and cryptotanshinone as promising candidates with strong inhibitory effects against the SARS-CoV-2. The research was motivated by the urgent need for effective treatments against the COVID-19 pandemic caused by SARS-CoV-2.

The findings of this research provide substantial evidence for the efficacy and potential of identified compounds as promising antiviral agents against SARS-CoV-2. These compounds exhibit potent inhibitory effects, which makes them attractive candidates for further preclinical and clinical studies. Moreover, the elucidation of these compounds' mechanisms through various computational techniques serves as a solid foundation for drug development efforts.

However, it is essential to acknowledge that drug development is a complex and time-consuming process. Therefore, while the results are encouraging, further research and validation are necessary before these compounds can be translated into clinically approved treatments for COVID-19. Nonetheless, the discoveries made in this thesis open new avenues for antiviral drug design, not only for SARS-CoV-2 but also for other related viruses and emerging pathogens. It is hoped that this research will contribute significantly to the ongoing global efforts to combat viral outbreaks and public health emergencies.

CHAPTER 6

6. SUMMARY

The global pandemic caused by different variants of SARS-CoV-2 has affected millions of people, therefore, necessitates the exploration of explicit SARS-CoV-2 inhibitors. The secondary metabolites present in medicinal plants attributed for their antiviral properties presents significant avenue to control COVID-19 infections. This study aimed to investigate a library of secondary metabolites ascribed for the antiviral properties and screened the potential SARS-CoV-2 variants inhibitors via comprehensive *in silico* study including molecular docking, molecular dynamics simulation, pharmacokinetics analysis, DFT study, and MM/GBSA calculation, further, well supported by *in vitro* assay.

Among 26 active metabolites present in *Tinospora* species, cordifolioside A demonstrated S1-RBD of SARS-CoV-2 wild variants inhibition displaying considerable hydrogen bonding interaction with active site of protein and prominent binding energy. Further analyses incorporating protein-ligand stability spanning 150 ns MD simulation, strong reactivity in the substrate binding domain, favorable pharmacokinetics, and *in vitro* assay further strengthened the validity of cordifolioside A as potent compounds.

Analysis of 36 flavonoids through *in silico* investigations validated by spike protein assay reveals cyanidin as an effective inhibitors of S protein of SARS-CoV-2 with the K417N mutation.

Neferine as RdRp SARS-CoV-2 inhibitors identified by computational analysis of a library of alkaloids metabolites, on further study in spike protein, found to be explicit inhibitors.

Out of 50 screened antiviral-based terpenes metabolites, cryptotanshinone was found to inhibit omicron's spike protein ascribing their H-bond interaction with binding site, prominent binding energy, favorable reactivity, stable protein-ligand complex, acceptable pharmacokinetic properties and spike protein assay.

Conclusively, screening of various library of secondary metabolites through *in silico* and *in vitro* studies revealed cordifolioside A, cyanidin, neferine, and cryptotanshinone as potential inhibitors of spike protein of SARS-CoV-2.

REFERENCES

A. Hussein, R., & A. El-Anssary, A. (2019a). Plants Secondary Metabolites: The Key Drivers of the Pharmacological Actions of Medicinal Plants. In P. F. Builders (Ed.), *Herbal Medicine*. IntechOpen. https://doi.org/10.5772/intechopen.76139

A. Hussein, R., & A. El-Anssary, A. (2019b). Plants Secondary Metabolites: The Key Drivers of the Pharmacological Actions of Medicinal Plants. In P. F. Builders (Ed.), *Herbal Medicine*. IntechOpen. https://doi.org/10.5772/intechopen.76139

Abdizadeh, R., Hadizadeh, F., & Abdizadeh, T. (2022). *In Silico* Analysis and Identification of Antiviral Coumarin Derivatives against 3-chymotrypsin-like Main Protease of the Novel Coronavirus SARS-CoV-2. *Molecular Diversity*, **26**(2): 1053–1076. https://doi.org/10.1007/s11030-021-10230-6

Abhishek Gupta, Priyanka Gupta, & Abhisek Gupta, Priyanka Gupta, Gunjan Bajpai. (2024). *Tinospora cordifolia* (Giloy): An Insight on the Multifarious Pharmacological Paradigms of a Most Promising Medicinal Ayurvedic Herb. *Heliyon*, **10**(4). https://doi.org/10.1016/j.heliyon.2024.e26125

Ahammad, F., Alam, R., Mahmud, R., Akhter, S., Talukder, E. K., Tonmoy, A. M., Fahim, S., Al-Ghamdi, K., Samad, A., & Qadri, I. (2021). Pharmacoinformatics and Molecular Dynamics Simulation-based Phytochemical Screening of Neem Plant (*Azadiractha indica*) against Human Cancer by Targeting MCM7 Protein. *Briefings in Bioinformatics*, *bbab098*. https://doi.org/10.1093/bib/bbab098

Ahmad, W., Jantan, I., & Bukhari, S. N. A. (2016). Tinospora crispa (L.) Hook. f. & Thomson: A Review of Its Ethnobotanical, Phytochemical, and Pharmacological Aspects. *Frontiers in Pharmacology*, **7**. https://doi.org/10.3389/fphar.2016.00059

Ain, Q.-U.-, Khan, H., Mubarak, M. S., & Pervaiz, A. (2016). Plant Alkaloids as Antiplatelet Agent: Drugs of the Future in the Light of Recent Developments. *Frontiers in Pharmacology*, **7**. https://www.frontiersin.org/articles/10.3389/fphar.2016.00292

Akram, M., Tahir, I. M., Shah, S. M. A., Mahmood, Z., Altaf, A., Ahmad, K., Munir, N., Daniyal, M., Nasir, S., & Mehboob, H. (2018). Antiviral Potential of Medicinal Plants against HIV, HSV, Influenza, Hepatitis, and Coxsackievirus: A Systematic Review. *Phytotherapy Research*, **32**(5): 811–822. https://doi.org/10.1002/ptr.6024

Anigboro, A. A., Avwioroko, O. J., Akeghware, O., & Tonukari, N. J. (2021). Anti-obesity, Antioxidant and *In Silico* Evaluation of *Justicia carnea* Bioactive Compounds as Potential Inhibitors of an Enzyme Linked with Obesity: Insights from Kinetics, Semi-empirical Quantum Mechanics and Molecular Docking Analysis. *Biophysical Chemistry*, **274**, 106607. https://doi.org/10.1016/j.bpc.2021.106607

Aranda, J., Wieczór, M., Terrazas, M., Brun-Heath, I., & Orozco, M. (2022). Mechanism of Reaction of RNA-dependent RNA Polymerase from SARS-CoV-2. *Chem Catalysis*, **2**(5): 1084–1099. https://doi.org/10.1016/j.checat.2022.03.019

Bagheri Novir, S., & Aram, M. R. (2020). Quantum Mechanical Simulation of Chloroquine Drug Interaction with C_{60} Fullerene for Treatment of COVID-19. *Chemical Physics Letters*, **757**, 137869. https://doi.org/10.1016/j.cplett.2020.137869

Banerjee, P., Eckert, A. O., Schrey, A. K., & Preissner, R. (2018). ProTox-II: A Webserver for the Prediction of Toxicity of Chemicals. *Nucleic Acids Research*, **46**(W1): W257–W263. https://doi.org/10.1093/nar/gky318

Bergman, M. E., Davis, B., & Phillips, M. A. (2019). Medically Useful Plant Terpenoids: Biosynthesis, Occurrence, and Mechanism of Action. *Molecules*, **24**(21): 3961. https://doi.org/10.3390/molecules24213961

Berman, H. M., Westbrook. J., Feng. Z., Gilliland. G., Bhat, T. N., Weissig. H., Shindyalov, I. N, & Bourne, P. E. (2000). The Protein Data Bank. *Nucleic Acids Research*, **28**(1): 235–242. https://doi.org/10.1093/nar/28.1.235

Bertram, S., Dijkman, R., Habjan, M., Heurich, A., Gierer, S., Glowacka, I., Welsch, K., Winkler, M., Schneider, H., Hofmann-Winkler, H., Thiel, V., & Pöhlmann, S. (2013). TMPRSS2 Activates the Human Coronavirus 229E for Cathepsin-Independent Host Cell Entry and Is Expressed in Viral Target Cells in the Respiratory Epithelium. *Journal of Virology*, **87**(11): 6150–6160. https://doi.org/10.1128/JVI.03372-12

Bharathi Priya, L., Huang, C., Hu, R., Balasubramanian, B., & Baskaran, R. (2021a). An Updated Review on Pharmacological Properties of Neferine—A Bisbenzylisoquinoline Alkaloid from *Nelumbo nucifera*. *Journal of Food Biochemistry*, **45**(12). https://doi.org/10.1111/jfbc.13986

Bharathi Priya, L., Huang, C.-Y., Hu, R.-M., Balasubramanian, B., & Baskaran, R. (2021b). An Updated Review on Pharmacological Properties of Neferine—A Bisbenzylisoquinoline Alkaloid from *Nelumbo nucifera*. *Journal of Food Biochemistry*, **45**(12): e13986. https://doi.org/10.1111/jfbc.13986

Bhowmik, D., Nandi, R., Jagadeesan, R., Kumar, N., Prakash, A., & Kumar, D. (2020a). Identification of Potential Inhibitors against SARS-CoV-2 by

Targeting Proteins Responsible for Envelope Formation and Virion Assembly using Docking Based Virtual Screening, and Pharmacokinetics Approaches. *Infection, Genetics and Evolution*, **84**, 104451. https://doi.org/10.1016/j.meegid.2020.104451

Bhowmik, D., Nandi, R., Jagadeesan, R., Kumar, N., Prakash, A., & Kumar, D. (2020b). Identification of Potential Inhibitors against SARS-CoV-2 by Targeting Proteins Responsible for Envelope Formation and Virion Assembly using Docking Based Virtual Screening, and Pharmacokinetics Approaches. *Infection, Genetics and Evolution*, **84,** 104451. https://doi.org/10.1016/j.meegid.2020.104451

Bhowmik, D., Nandi, R., Prakash, A., & Kumar, D. (2021). Evaluation of Flavonoids as 2019-nCoV Cell Entry Inhibitor through Molecular Docking and Pharmacological Analysis. *Heliyon*, **7**(3): e06515. https://doi.org/10.1016/j.heliyon.2021.e06515

Boozari, M., & Hosseinzadeh, H. (2021). Natural Products for COVID -19 Prevention and Treatment Regarding to Previous Coronavirus Infections and Novel Studies. *Phytotherapy Research*, **35**(2): 864–876. https://doi.org/10.1002/ptr.6873

Borjian Boroujeni, M., Shahbazi Dastjerdeh, M., Shokrgozar, M., Rahimi, H., & Omidinia, E. (2021). Computational Driven Molecular Dynamics Simulation of Keratinocyte Growth Factor Behavior at Different pH Conditions. *Informatics in Medicine Unlocked*, **23**, 100514. https://doi.org/10.1016/j.imu.2021.100514

Bosch, B. J., Van Der Zee, R., De Haan, C. A. M., & Rottier, P. J. M. (2003). The Coronavirus Spike Protein Is a Class I Virus Fusion Protein: Structural and

Functional Characterization of the Fusion Core Complex. *Journal of Virology*, **77**(16): 8801–8811. https://doi.org/10.1128/JVI.77.16.8801-8811.2003

Bouback, T. A., Pokhrel, S., Albeshri, A., Aljohani, A. M., Samad, A., Alam, R., Hossen, M. S., Al-Ghamdi, K., Talukder, M. E. K., Ahammad, F., Qadri, I., & Simal-Gandara, J. (2021). Pharmacophore-Based Virtual Screening, Quantum Mechanics Calculations, and Molecular Dynamics Simulation Approaches Identified Potential Natural Antiviral Drug Candidates against MERS-CoV S1-NTD. *Molecules*, **26**(16): Article 16. https://doi.org/10.3390/molecules26164961

Bugnon, M., Goullieux, M., Röhrig, U. F., Perez, M. A. S., Daina, A., Michielin, O., & Zoete, V. (2023). SwissParam 2023: A Modern Web-Based Tool for Efficient Small Molecule Parametrization. *Journal of Chemical Information and Modeling*, **63**(21): 6469–6475. https://doi.org/10.1021/acs.jcim.3c01053

Cecil, C. E., Davis, J. M., Cech, N. B., & Laster, S. M. (2011). Inhibition of H1N1 Influenza A Virus Growth and Induction of Inflammatory Mediators by the Isoquinoline Alkaloid Berberine and Extracts of Goldenseal (*Hydrastis canadensis*). *International Immunopharmacology*, **11**(11): 1706–1714. https://doi.org/10.1016/j.intimp.2011.06.002

Chamberlin, S. R., Blucher, A., Wu, G., Shinto, L., Choonoo, G., Kulesz-Martin, M., & McWeeney, S. (2019). Natural Product Target Network Reveals Potential for Cancer Combination Therapies. *Frontiers in Pharmacology*, **10**, 557. https://doi.org/10.3389/fphar.2019.00557

Chan, J. F. W., Lau, S. K. P., To, K. K. W., Cheng, V. C. C., Woo, P. C. Y., & Yuen, K.-Y. (2015). Middle East Respiratory Syndrome Coronavirus: Another

Zoonotic Betacoronavirus Causing SARS-Like Disease. *Clinical Microbiology Reviews*, **28**(2): 465–522. https://doi.org/10.1128/CMR.00102-14

Chang, X., Zhang, T., Zhang, W., Zhao, Z., & Sun, J. (2020). Natural Drugs as a Treatment Strategy for Cardiovascular Disease through the Regulation of Oxidative Stress. *Oxidative Medicine and Cellular Longevity*, **2020**, 1–20. https://doi.org/10.1155/2020/5430407

Chatow, L., Nudel, A., Nesher, I., Hayo Hemo, D., Rozenberg, P., Voropaev, H., Winkler, I., Levy, R., Kerem, Z., Yaniv, Z., & Eyal, N. (2021). *In Vitro* Evaluation of the Activity of Terpenes and Cannabidiol against Human Coronavirus E229. *Life*, **11**(4): 290. https://doi.org/10.3390/life11040290

Chen, I.-J., & Foloppe, N. (2010). Drug-like Bioactive Structures and Conformational Coverage with the LigPrep/ConfGen Suite: Comparison to Programs MOE and Catalyst. *Journal of Chemical Information and Modeling*, **50**(5): 822–839. https://doi.org/10.1021/ci100026x

Cheng, F.-J., Huynh, T.-K., Yang, C.-S., Hu, D.-W., Shen, Y.-C., Tu, C.-Y., Wu, Y.-C., Tang, C.-H., Huang, W.-C., Chen, Y., & Ho, C.-Y. (2021). Hesperidin is a Potential Inhibitor against SARS-CoV-2 Infection. *Nutrients*, **13**(8): 2800. https://doi.org/10.3390/nu13082800

Chidambaram, S., El-Sheikh, M. A., Alfarhan, A. H., Radhakrishnan, S., & Akbar, I. (2021). Synthesis of Novel Coumarin Analogues: Investigation of Molecular Docking Interaction of SARS-CoV-2 Proteins with Natural and Synthetic Coumarin Analogues and their Pharmacokinetics Studies. *Saudi Journal of Biological Sciences*, **28**(1): 1100–1108. https://doi.org/10.1016/j.sjbs.2020.11.038

Cho, J. K., Curtis-Long, M. J., Lee, K. H., Kim, D. W., Ryu, H. W., Yuk, H. J., & Park, K. H. (2013). Geranylated Flavonoids Displaying SARS-CoV Papain-like Protease Inhibition from the Fruits of *Paulownia tomentosa*. *Bioorganic & Medicinal Chemistry*, **21**(11): 3051–3057. https://doi.org/10.1016/j.bmc.2013.03.027

Chothia, C. (1974). Hydrophobic Bonding and Accessible Surface Area in Proteins. *Nature*, **248**(5446): Article 5446. https://doi.org/10.1038/248338a0

Choudhary, S., Malik, Y. S., & Tomar, S. (2020). Identification of SARS-CoV-2 Cell Entry Inhibitors by Drug Repurposing Using in silico Structure-Based Virtual Screening Approach. *Frontiers in Immunology*, **11**, 1664. https://doi.org/10.3389/fimmu.2020.01664

Chowdhury, P. (2021). In Silico Investigation of Phytoconstituents from Indian Medicinal Herb '*Tinospora cordifolia* (giloy)' against SARS-CoV-2 (COVID-19) by Molecular Dynamics Approach. *Journal of Biomolecular Structure and Dynamics*, **39**(17): 6792–6809. https://doi.org/10.1080/07391102.2020.1803968

Choy, K.-T., Wong, A. Y.-L., Kaewpreedee, P., Sia, S. F., Chen, D., Hui, K. P. Y., Chu, D. K. W., Chan, M. C. W., Cheung, P. P.-H., Huang, X., Peiris, M., & Yen, H.-L. (2020). Remdesivir, Lopinavir, Emetine, and Homoharringtonine Inhibit SARS-CoV-2 Replication *In Vitro*. *Antiviral Research*, **178**, 104786. https://doi.org/10.1016/j.antiviral.2020.104786

Cinatl, J., Morgenstern, B., Bauer, G., Chandra, P., Rabenau, H., & Doerr, H. (2003). Glycyrrhizin, an Active Component of Liquorice Roots, and Replication of SARS-associated Coronavirus. *The Lancet*, **361**(9374): 2045–2046. https://doi.org/10.1016/S0140-6736(03)13615-X

Claußen, H., Buning, C., Rarey, M., & Lengauer, T. (2001). FlexE: Efficient Molecular Docking Considering Protein Structure Variations. *Journal of Molecular Biology*, **308**(2): 377–395. https://doi.org/10.1006/jmbi.2001.4551

Costanzi, E., Kuzikov, M., Esposito, F., Albani, S., Demitri, N., Giabbai, B., Camasta, M., Tramontano, E., Rossetti, G., & Zaliani, A. (2021). Structural and Biochemical Analysis of the Dual Inhibition of MG-132 against SARS-CoV-2 Main Protease (Mpro/3CLpro) and Human Cathepsin-L. *International Journal of Molecular Sciences*, **22**(21): 11779.

Cui, J., Li, F., & Shi, Z.-L. (2019). Origin and Evolution of Pathogenic Coronaviruses. *Nature Reviews Microbiology*, **17**(3): 181–192. https://doi.org/10.1038/s41579-018-0118-9

Da Costa, C. H. S., De Freitas, C. A. B., Alves, C. N., & Lameira, J. (2022). Assessment of Mutations on RBD in the Spike Protein of SARS-CoV-2 Alpha, Delta and Omicron Variants. *Scientific Reports*, **12**(1): 8540. https://doi.org/10.1038/s41598-022-12479-9

Daina, A., Michielin, O., & Zoete, V. (2017). SwissADME: A Free Web Tool to Evaluate Pharmacokinetics, Drug-likeness and Medicinal Chemistry Friendliness of Small Molecules. *Scientific Reports*, **7**(1): 42717. https://doi.org/10.1038/srep42717

Dandekar, P. D., Kotmale, A. S., Chavan, S. R., Kadlag, P. P., Sawant, S. V., Dhavale, D. D., & RaviKumar, A. (2021). Insights into the Inhibition Mechanism of Human Pancreatic α-Amylase, a Type 2 Diabetes Target, by Dehydrodieugenol B Isolated from *Ocimum tenuiflorum*. *ACS Omega*, **6**(3): 1780–1786. https://doi.org/10.1021/acsomega.0c00617

Dar, A. M., & Mir, S. (2017). Molecular Docking: Approaches, Types, Applications and Basic Challenges. *Journal of Analytical & Bioanalytical Techniques*, **08**(02). https://doi.org/10.4172/2155-9872.1000356

Davies, N. G., Abbott, S., Barnard, R. C., Jarvis, C. I., Kucharski, A. J., Munday, J. D., Pearson, C. A. B., Russell, T. W., Tully, D. C., Washburne, A. D., Wenseleers, T., Gimma, A., Waites, W., Wong, K. L. M., Van Zandvoort, K., Silverman, J. D., CMMID COVID-19 Working Group, COVID-19 Genomics UK (COG-UK) Consortium, Diaz-Ordaz, K., Keogh, R., Eggo, R. M., Funk, S., Jit, M., Atkins, K. E., Edmunds, W. J. (2021). Estimated Transmissibility and Impact of SARS-CoV-2 Lineage B.1.1.7 in England. *Science*, **372**(6538): eabg3055. https://doi.org/10.1126/science.abg3055

Dharmaratne, H., Wanigasekera, W., Mata-Greenwood, E., & Pezzuto, J. (1998). Inhibition of Human Immunodeficiency Virus Type 1 Reverse Transcriptase Activity by Cordatolides Isolated from *Calophyllum cordato-oblongum*. *Planta Medica*, **64**(05): 460–461. https://doi.org/10.1055/s-2006-957483

Diniz, L. R. L., Perez-Castillo, Y., Elshabrawy, H. A., Filho, C. da S. M. B., & de Sousa, D. P. (2021). Bioactive Terpenes and Their Derivatives as Potential SARS-CoV-2 Proteases Inhibitors from Molecular Modeling Studies. *Biomolecules*, **11**(1): 74. https://doi.org/10.3390/biom11010074

Durrant, J. D., & McCammon, J. A. (2011). Molecular dynamics simulations and drug discovery. *BMC Biology*, **9**(1): 71. https://doi.org/10.1186/1741-7007-9-71

Eberhardt, J., Santos-Martins, D., Tillack, A. F., & Forli, S. (2021). AutoDock Vina 1.2.0: New Docking Methods, Expanded Force Field, and Python Bindings. *Journal of Chemical Information and Modeling*, **61**(8): 3891–3898. https://doi.org/10.1021/acs.jcim.1c00203

Elekofehinti, O. O., Ejelonu, O. C., Kamdem, J. P., Akinlosotu, O. B., Famuti, A., Adebowale, D. D., Iwaloye, O., Bulu, Y. I., Kade, I. J., & Rocha, J. B. T. (2018). Discovery of Potential Visfatin Activators using *In Silico* Docking and ADME Predictions as Therapy for Type 2 Diabetes. *Beni-Suef University Journal of Basic and Applied Sciences*, **7**(2): 241–249. https://doi.org/10.1016/j.bjbas.2018.02.007

El-Mageed, H. R. A., Abdelrheem, D. A., Rafi, Md. O., Sarker, Md. T., Al-Khafaji, K., Hossain, Md. J., Capasso, R., & Emran, T. B. (2021). *In Silico* Evaluation of Different Flavonoids from Medicinal Plants for Their Potency against SARS-CoV-2. *Biologics*, **1**(3): 416–434. https://doi.org/10.3390/biologics1030024

Erlanson, D. A., McDowell, R. S., & O'Brien, T. (2004). Fragment-Based Drug Discovery. *Journal of Medicinal Chemistry*, **47**(14): 3463–3482. https://doi.org/10.1021/jm040031v

Estari, M., Venkanna, L., & Reddy, A. S. (2012). *In Vitro* Anti-HIV Activity of Crude Extracts from *Tinospora cordifolia*. *BMC Infectious Diseases*, **12**(S1): P10, 1471-2334-12-S1-P10. https://doi.org/10.1186/1471-2334-12-S1-P10

Fan, J., Fu, A., & Zhang, L. (2019). Progress in Molecular Docking. *Quantitative Biology*, **7**(2): 83–89. https://doi.org/10.1007/s40484-019-0172-y

Fernandes, J., & Gattass, C. R. (2009). Topological Polar Surface Area Defines Substrate Transport by Multidrug Resistance Associated Protein 1 (MRP1/ABCC1). *Journal of Medicinal Chemistry*, **52**(4): 1214–1218. https://doi.org/10.1021/jm801389m

Filimonov, D. A., Rudik, A. V., Dmitriev, A. V., & Poroikov, V. V. (2020). Computer-Aided Estimation of Biological Activity Profiles of Drug-Like Compounds

Taking into Account Their Metabolism in Human Body. *International Journal of Molecular Sciences*, **21**(20): Article 20. https://doi.org/10.3390/ijms21207492

Fouchier, R. A. M., Kuiken, T., Schutten, M., Van Amerongen, G., Van Doornum, G. J. J., Van Den Hoogen, B. G., Peiris, M., Lim, W., Stöhr, K., & Osterhaus, A. D. M. E. (2003). Koch's Postulates Fulfilled for SARS Virus. *Nature*, **423**(6937): 240–240. https://doi.org/10.1038/423240a

Gabb, H. A., Jackson, R. M., & Sternberg, M. J. E. (1997). Modelling Protein Docking Using Shape Complementarity, Electrostatics and Biochemical Information 1 1Edited by J. Thornton. *Journal of Molecular Biology*, **272**(1): 106–120. https://doi.org/10.1006/jmbi.1997.1203

Gad, H. A., El-Ahmady, S. H., Abou-Shoer, M. I., & Al-Azizi, M. M. (2013). Application of Chemometrics in Authentication of Herbal Medicines: A Review: Chemometry and Herbal Medicines. *Phytochemical Analysis*, **24**(1): 1–24. https://doi.org/10.1002/pca.2378

Gangadevi, S., Badavath, V. N., Thakur, A., Yin, N., De Jonghe, S., Acevedo, O., Jochmans, D., Leyssen, P., Wang, K., Neyts, J., Yujie, T., & Blum, G. (2021). Kobophenol A Inhibits Binding of Host ACE2 Receptor with Spike RBD Domain of SARS-CoV-2, a Lead Compound for Blocking COVID-19. *The Journal of Physical Chemistry Letters*, **12**(7): 1793–1802. https://doi.org/10.1021/acs.jpclett.0c03119

Gendrot, M., Andreani, J., Boxberger, M., Jardot, P., Fonta, I., Le Bideau, M., Duflot, I., Mosnier, J., Rolland, C., Bogreau, H., Hutter, S., La Scola, B., & Pradines, B. (2020). Antimalarial drugs inhibit the replication of SARS-CoV-2: An *In Vitro* Evaluation. *Travel Medicine and Infectious Disease*, **37**, 101873.

https://doi.org/10.1016/j.tmaid.2020.101873

Genheden, S., & Ryde, U. (2015). The MM/PBSA and MM/GBSA Methods to Estimate Ligand-binding Affinities. *Expert Opinion on Drug Discovery*, **10**(5): 449–461. https://doi.org/10.1517/17460441.2015.1032936

Gill, P. M. W., Johnson, B. G., Pople, J. A., & Frisch, M. J. (1992). The Performance of the Becke—Lee—Yang—Parr (B—LYP) Density Functional Theory with Various Basis Sets. *Chemical Physics Letters*, **197**(4–5): 499–505. https://doi.org/10.1016/0009-2614(92)85807-M

Gold, V. (Ed.). (2019). *The IUPAC Compendium of Chemical Terminology: The Gold Book* (4th ed.). International Union of Pure and Applied Chemistry (IUPAC). https://doi.org/10.1351/goldbook

Goris, T., Pérez-Valero, Á., Martínez, I., Yi, D., Fernández-Calleja, L., San León, D., Bornscheuer, U. T., Magadán-Corpas, P., Lombó, F., & Nogales, J. (2021). Repositioning Microbial Biotechnology Against COVID-19: The Case of Microbial Production of Flavonoids. *Microbial Biotechnology*, **14**(1): 94–110. https://doi.org/10.1111/1751-7915.13675

Gschwend, D. A., Good, A. C., & Kuntz, I. D. (1996). Molecular Docking Towards Drug Discovery. *Journal of Molecular Recognition*, **9**(2): 175–186. https://doi.org/10.1002/(SICI)1099-1352(199603)9:2<175::AID-JMR260>3.0.CO;2-D

Guo, Y., Han, J., Zhang, Y., He, J., Yu, W., Zhang, X., Wu, J., Zhang, S., Kong, Y., Guo, Y., Lin, Y., & Zhang, J. (2022). SARS-CoV-2 Omicron Variant: Epidemiological Features, Biological Characteristics, and Clinical Significance. *Frontiers in Immunology*, **13**, 877101. https://doi.org/10.3389/fimmu.2022.877101

Gurung, A. B., Ali, M. A., Lee, J., Farah, M. A., & Al-Anazi, K. M. (2021). An Updated Review of Computer-Aided Drug Design and Its Application to COVID-19. *BioMed Research International*, **2021**, 1–18. https://doi.org/10.1155/2021/8853056

Gyebi, G. A., Ogunyemi, O. M., Ibrahim, I. M., Ogunro, O. B., Adegunloye, A. P., & Afolabi, S. O. (2021). SARS-CoV-2 Host Cell Entry: An *In Silico* Investigation of Potential Inhibitory Roles of Terpenoids. *Journal of Genetic Engineering and Biotechnology*, **19**(1): 113. https://doi.org/10.1186/s43141-021-00209-z

Habibzadeh, P., & Stoneman, E. K. (2020). The Novel Coronavirus: A Bird's Eye View. *The International Journal of Occupational and Environmental Medicine*, **11**(2): 65–71. https://doi.org/10.15171/ijoem.2020.1921

Hadni, H., Fitri, A., Benjelloun, A. T., Benzakour, M., & Mcharfi, M. (2022). Evaluation of Flavonoids as Potential Inhibitors of the SARS-CoV-2 Main Protease and Spike RBD: Molecular Docking, ADMET Evaluation and Molecular Dynamics Simulations. *Journal of the Indian Chemical Society*, **99**(10): 100697. https://doi.org/10.1016/j.jics.2022.100697

Hagar, M., Ahmed, H. A., Aljohani, G., & Alhaddad, O. A. (2020). Investigation of Some Antiviral N-Heterocycles as COVID 19 Drug: Molecular Docking and DFT Calculations. *International Journal of Molecular Sciences*, **21**(11): 3922. https://doi.org/10.3390/ijms21113922

Hähnke, V. D., Kim, S., & Bolton, E. E. (2018). PubChem Chemical Structure Standardization. *Journal of Cheminformatics*, **10**(1): 36. https://doi.org/10.1186/s13321-018-0293-8

Halim, S. A., Sikandari, A. G., Khan, A., Wadood, A., Fatmi, M. Q., Csuk, R., & Al-Harrasi, A. (2021). Structure-Based Virtual Screening of Tumor Necrosis

Factor-α Inhibitors by Cheminformatics Approaches and Bio-Molecular Simulation. *Biomolecules*, **11**(2): 329. https://doi.org/10.3390/biom11020329

Han, P., Li, L., Liu, S., Wang, Q., Zhang, D., Xu, Z., Han, P., Li, X., Peng, Q., Su, C., Huang, B., Li, D., Zhang, R., Tian, M., Fu, L., Gao, Y., Zhao, X., Liu, K., Qi, J., Gao, G. F., Wang, P. (2022). Receptor Binding and Complex Structures of Human ACE2 to Spike RBD from Omicron and Delta SARS-CoV-2. *Cell*, **185**(4): 630-640.e10. https://doi.org/10.1016/j.cell.2022.01.001

Haq, I. U., Fayyaz, F., Shafqat, A., Basit, A., Hussain, F., Aziz, I., Khan, Z. I., Aqib, A. I., Siddique, F., Younas, U., & Rahim, K. (2023). Natural Products and SARS-CoV-2. *Application of Natural Products in SARS-CoV-2*, **2023**, (pp. 1–24). https://doi.org/10.1016/B978-0-323-95047-3.00021-6

Haque, Md. A., Jantan, I., & Abbas Bukhari, S. N. (2017). *Tinospora species*: An Overview of their Modulating Effects on the Immune System. *Journal of Ethnopharmacology*, **207**, 67–85. https://doi.org/10.1016/j.jep.2017.06.013

He, J., Wei, D.-Q., Wang, J.-F., & Chou, K.-C. (2011). Predicting Protein-Ligand Binding Sites Based on an Improved Geometric Algorithm. *Protein & Peptide Letters*, **18**(10): 997–1001. https://doi.org/10.2174/092986611796378756

Henss, L., Auste, A., Schürmann, C., Schmidt, C., Von Rhein, C., Mühlebach, M. D., & Schnierle, B. S. (2021). The Green Tea Catechin Epigallocatechin Gallate Inhibits SARS-CoV-2 Infection. *Journal of General Virology*, **102**(4). https://doi.org/10.1099/jgv.0.001574

Ho, T., Wu, S., Chen, J., Li, C., & Hsiang, C. (2007). Emodin Blocks the SARS Coronavirus Spike Protein and Angiotensin-Converting Enzyme 2 Interaction. *Antiviral Research*, **74**(2): 92–101. https://doi.org/10.1016/j.antiviral.2006.04.014

Hodgson, J. (2001). ADMET—turning Chemicals into Drugs. *Nature Biotechnology*, **19**(8): 722–726. https://doi.org/10.1038/90761

Hoffmann, M., Kleine-Weber, H., Schroeder, S., Krüger, N., Herrler, T., Erichsen, S., Schiergens, T. S., Herrler, G., Wu, N.-H., Nitsche, A., Müller, M. A., Drosten, C., & Pöhlmann, S. (2020). SARS-CoV-2 Cell Entry Depends on ACE2 and TMPRSS2 and is Blocked by a Clinically Proven Protease Inhibitor. *Cell*, **181**(2): 271-280.e8. https://doi.org/10.1016/j.cell.2020.02.052

Hospital, A., Goñi, J. R., Orozco, M., & Gelpi, J. L. (2015). Molecular Dynamics Simulations: Advances and Applications. *Advances and Applications in Bioinformatics and Chemistry*, **8**, 37–47. https://doi.org/10.2147/AABC.S70333

Huang, J., Wu, L., Tashiro, S., Onodera, S., & Ikejima, T. (2008). Reactive Oxygen Species Mediate Oridonin-Induced HepG2 Apoptosis Through p53, MAPK, and Mitochondrial Signaling Pathways. *Journal of Pharmacological Sciences*, **107**(4): 370–379. https://doi.org/10.1254/jphs.08044FP

Huang, L., Yuen, T. T.-T., Ye, Z., Liu, S., Zhang, G., Chu, H., & Yue, J. (2021). Berbamine Inhibits SARS-CoV-2 Infection by Compromising TRPMLs-Mediated Endolysosomal Trafficking of ACE2. *Signal Transduction and Targeted Therapy*, **6**(1): 168. https://doi.org/10.1038/s41392-021-00584-6

Huang, Y., Rong, C., Zhang, R., & Liu, S. (2017). Evaluating Frontier Orbital Energy and HOMO/LUMO Gap with Descriptors from Density Functional Reactivity Theory. *Journal of Molecular Modeling*, **23**(1): 3. https://doi.org/10.1007/s00894-016-3175-x

Huang, Y., Yang, C., Xu, X., Xu, W., & Liu, S. (2020). Structural and Functional Properties of SARS-CoV-2 Spike Protein: Potential Antivirus Drug

Development for COVID-19. *Acta Pharmacologica Sinica*, **41**(9): 1141–1149. https://doi.org/10.1038/s41401-020-0485-4

Hubbard, R. E., & Kamran Haider, M. (2010). Hydrogen Bonds in Proteins: Role and Strength. *Encyclopedia of Life Sciences*, *John Wiley & Sons, Ltd.* https://doi.org/10.1002/9780470015902.a0003011.pub2

Ilyas, U., Nazir, B., Altaf, R., Muhammad, S. A., Zafar, H., Paiva-Santos, A. C., Abbas, M., & Duan, Y. (2022). Investigation of Anti-Diabetic Potential and Molecular Simulation Studies of Dihydropyrimidinone Derivatives. *Frontiers in Endocrinology*, **13**, 1022623. https://doi.org/10.3389/fendo.2022.1022623

Imbert, I., Guillemot, J.-C., Bourhis, J.-M., Bussetta, C., Coutard, B., Egloff, M.-P., Ferron, F., Gorbalenya, A. E., & Canard, B. (2006). A Second, Non-Canonical RNA-dependent RNA Polymerase in SARS Coronavirus. *The EMBO Journal*, **25**(20): 4933–4942. https://doi.org/10.1038/sj.emboj.7601368

Islam, M. T., Sarkar, C., El-Kersh, D. M., Jamaddar, S., Uddin, S. J., Shilpi, J. A., & Mubarak, M. S. (2020). Natural Products and Their Derivatives against Coronavirus: A Review of the Non-Clinical and Pre-Clinical Data. *Phytotherapy Research*, **34**(10): 2471–2492. https://doi.org/10.1002/ptr.6700

Jain, A. S., Sushma, P., Dharmashekar, C., Beelagi, M. S., Prasad, S. K., Shivamallu, C., Prasad, A., Syed, A., Marraiki, N., & Prasad, K. S. (2021). *In Silico* Evaluation of Flavonoids as Effective Antiviral Agents on the Spike Glycoprotein of SARS-CoV-2. *Saudi Journal of Biological Sciences*, **28**(1): 1040–1051. https://doi.org/10.1016/j.sjbs.2020.11.049

Jena, S., Munusami, P., Mm, B., & Chanda, K. (2021). Computationally Approached Inhibition Potential of *Tinospora cordifolia* towards COVID-19 Targets. *VirusDisease*, **32**(1): 65–77. https://doi.org/10.1007/s13337-021-00666-7

Jeong, H. J., Kim, J. H., Kim, Y. M., Park, J.-Y., Kim, D., Nguyen, T. T. H., Park, S.-J., Chang, J. S., Park, K. H., Rho, M.-C., & Lee, W. S. (2010). Biflavonoids from *Torreya nucifera* Displaying SARS-CoV 3CL(pro) Inhibition. *Bioorganic & Medicinal Chemistry*, **18**(22): 7940–7947. https://doi.org/10.1016/j.bmc.2010.09.035

Jiang, F., & Kim, S.-H. (1991). "Soft Docking": Matching of Molecular Surface Cubes. *Journal of Molecular Biology*, **219**(1): 79–102. https://doi.org/10.1016/0022-2836(91)90859-5

Jin, Z., Du, X., Xu, Y., Deng, Y., Liu, M., Zhao, Y., Zhang, B., Li, X., Zhang, L., Peng, C., Duan, Y., Yu, J., Wang, L., Yang, K., Liu, F., Jiang, R., Yang, X., You, T., Liu, X., … Yang, H. (2020). Structure of M^{pro} from SARS-CoV-2 and Discovery of its Inhibitors. *Nature*, **582**(7811): 289–293. https://doi.org/10.1038/s41586-020-2223-y

Jiraungkoorskul, W. (2019). Efficiency of *Tinospora crispa* against *Culex quinquefasciatus* larva. *Environmental Science and Pollution Research*, **26**(15): 14712–14716. https://doi.org/10.1007/s11356-018-2429-9

Jo, S., Kim, H., Kim, S., Shin, D. H., & Kim, M. (2019). Characteristics of Flavonoids as Potent MERS-CoV 3C-Like Protease Inhibitors. *Chemical Biology & Drug Design*, **94**(6): 2023–2030. https://doi.org/10.1111/cbdd.13604

Jo, S., Kim, S., Shin, D. H., & Kim, M.-S. (2020). Inhibition of SARS-CoV 3CL Protease by Flavonoids. *Journal of Enzyme Inhibition and Medicinal Chemistry*, **35**(1): 145–151. https://doi.org/10.1080/14756366.2019.1690480

Jones, G., Willett, P., Glen, R. C., Leach, A. R., & Taylor, R. (1997a). Development and Validation of a Genetic Algorithm for Flexible Docking 1 1Edited by F. E. Cohen. *Journal of Molecular Biology*, **267**(3): 727–748.

https://doi.org/10.1006/jmbi.1996.0897

Jones, G., Willett, P., Glen, R. C., Leach, A. R., & Taylor, R. (1997b). Development and Validation of a Genetic Algorithm for Flexible Docking11Edited by F. E. Cohen. *Journal of Molecular Biology*, **267**(3): 727–748. https://doi.org/10.1006/jmbi.1996.0897

Kadioglu, O., Law, B. Y. K., Mok, S. W. F., Xu, S.-W., Efferth, T., & Wong, V. K. W. (2017). Mode of Action Analyses of Neferine, a Bisbenzylisoquinoline Alkaloid of Lotus (*Nelumbo nucifera*) against Multidrug-Resistant Tumor Cells. *Frontiers in Pharmacology*, **8**, 238. https://doi.org/10.3389/fphar.2017.00238

Kallithraka, S., Aliaj, L., Makris, D. P., & Kefalas, P. (2009). Anthocyanin Profiles of Major Red Grape (*Vitis vinifera* L.) Varieties Cultivated in Greece and Their Relationship with *In Vitro* Antioxidant Characteristics. *International Journal of Food Science & Technology*, **44**(12): 2385–2393. https://doi.org/10.1111/j.1365-2621.2008.01869.x

Kashman, Y., Gustafson, K. R., Fuller, R. W., Cardellina, J. H., McMahon, J. B., Currens, M. J., Buckheit, R. W., Hughes, S. H., Cragg, G. M., & Boyd, M. R. (1992). HIV Inhibitory Natural Products. Part 7. The Calanolides, a Novel HIV-Inhibitory Class of Coumarin Derivatives from the Tropical Rainforest Tree, *Calophyllum lanigerum*. *Journal of Medicinal Chemistry*, **35**(15): 2735–2743. https://doi.org/10.1021/jm00093a004

Kaushik, N. K., Bagavan, A., Rahuman, A. A., Zahir, A. A., Kamaraj, C., Elango, G., Jayaseelan, C., Kirthi, A. V., Santhoshkumar, T., Marimuthu, S., Rajakumar, G., Tiwari, S. K., & Sahal, D. (2015). Evaluation of Antiplasmodial Activity of

Medicinal Plants from North Indian Buchpora and South Indian Eastern Ghats. *Malaria Journal*, **14**(1): 65. https://doi.org/10.1186/s12936-015-0564-z

Kaushik-Basu, N., Bopda-Waffo, A., Talele, T. T., Basu, A., Costa, P. R. R., Da Silva, A. J. M., Sarafianos, S. G., & Noel, F. (2008). Identification and Characterization of Coumestans as Novel HCV NS5B Polymerase Inhibitors. *Nucleic Acids Research*, **36**(5): 1482–1496. https://doi.org/10.1093/nar/gkm1178

Keum, Y.-S., & Jeong, Y.-J. (2012). Development of Chemical Inhibitors of the SARS coronavirus: Viral Helicase as a Potential Target. *Biochemical Pharmacology*, **84**(10): 1351–1358. https://doi.org/10.1016/j.bcp.2012.08.012

Khater, I., & Nassar, A. (2021). *In Silico* Molecular Docking Analysis for Repurposing Approved Antiviral Drugs against SARS-CoV-2 Main Protease. *Biochemistry and Biophysics Reports*, **27**, 101032. https://doi.org/10.1016/j.bbrep.2021.101032

Kim, D., Min, J., Jang, M., Lee, J., Shin, Y., Park, C., Song, J., Kim, H., Kim, S., Jin, Y.-H., & Kwon, S. (2019). Natural Bis-Benzylisoquinoline Alkaloids-Tetrandrine, Fangchinoline, and Cepharanthine, Inhibit Human Coronavirus OC43 Infection of MRC-5 Human Lung Cells. *Biomolecules*, **9**(11): 696. https://doi.org/10.3390/biom9110696

Kim, D. W., Seo, K. H., Curtis-Long, M. J., Oh, K. Y., Oh, J.-W., Cho, J. K., Lee, K. H., & Park, K. H. (2014). Phenolic Phytochemical Displaying SARS-CoV Papain-Like Protease Inhibition from the Seeds of *Psoralea corylifolia*. *Journal of Enzyme Inhibition and Medicinal Chemistry*, **29**(1): 59–63. https://doi.org/10.3109/14756366.2012.753591

Kim, J. Y., Jeong, H. J., Park, J.-Y., Kim, Y. M., Park, S.-J., Cho, J. K., Park, K. H., Ryu, Y. B., & Lee, W. S. (2012). Selective and Slow-Binding Inhibition of Shikonin Derivatives Isolated from *Lithospermum erythrorhizon* on Glycosyl Hydrolase 33 and 34 Sialidases. *Bioorganic & Medicinal Chemistry*, **20**(5): 1740–1748. https://doi.org/10.1016/j.bmc.2012.01.011

Knegtel, R. M. A., Kuntz, I. D., & Oshiro, C. M. (1997). Molecular Docking to Ensembles of Protein Structures 1 1Edited by B. Honig. *Journal of Molecular Biology*, **266**(2): 424–440. https://doi.org/10.1006/jmbi.1996.0776

Krupanidhi, S., Abraham Peele, K., Venkateswarulu, T. C., Ayyagari, V. S., Nazneen Bobby, Md., John Babu, D., Venkata Narayana, A., & Aishwarya, G. (2021). Screening of Phytochemical Compounds of *Tinospora cordifolia* for Their Inhibitory Activity on SARS-CoV-2: An *In Silico* Study. *Journal of Biomolecular Structure and Dynamics*, **39**(15): 5799–5803. https://doi.org/10.1080/07391102.2020.1787226

Kumaki, Y., Wandersee, M. K., Smith, A. J., Zhou, Y., Simmons, G., Nelson, N. M., Bailey, K. W., Vest, Z. G., Li, J. K.-K., Chan, P. K.-S., Smee, D. F., & Barnard, D. L. (2011). Inhibition of Severe Acute Respiratory Syndrome Coronavirus Replication in a Lethal SARS-CoV BALB/c Mouse Model by Stinging Nettle Lectin, *Urtica dioica* Agglutinin. *Antiviral Research*, **90**(1): 22–32. https://doi.org/10.1016/j.antiviral.2011.02.003

Kumar, C. B. P., Raghu, M. S., Prasad, K. N. N., Chandrasekhar, S., Jayanna, B. K., Alharthi, F. A., Prashanth, M. K., & Kumar, K. Y. (2021). Investigation of Biological Activity of 2,3-Disubstituted Quinazolin-4(1 *H*)-ones against *Mycobacterium tuberculosis* and DNA *via* Docking, Spectroscopy and DFT Studies. *New Journal of Chemistry*, **45**(1): 403–414.

https://doi.org/10.1039/D0NJ03800H

Kumar, S., Kashyap, P., Chowdhury, S., Kumar, S., Panwar, A., & Kumar, A. (2021). Identification of Phytochemicals as Potential Therapeutic Agents that Binds to Nsp15 Protein Target of Coronavirus (SARS-CoV-2) that are Capable of Inhibiting Virus Replication. *Phytomedicine*, **85**, 153317. https://doi.org/10.1016/j.phymed.2020.153317

Kuntz, I. D., Blaney, J. M., Oatley, S. J., Langridge, R., & Ferrin, T. E. (1982). A Geometric Approach to Macromolecule-Ligand Interactions. *Journal of Molecular Biology*, **161**(2): 269–288. https://doi.org/10.1016/0022-2836(82)90153-X

Küpeli Akkol, E., Genç, Y., Karpuz, B., Sobarzo-Sánchez, E., & Capasso, R. (2020). Coumarins and Coumarin-Related Compounds in Pharmacotherapy of Cancer. *Cancers*, **12**(7): 1959. https://doi.org/10.3390/cancers12071959

Kwon, H.-J., Ryu, Y. B., Kim, Y.-M., Song, N., Kim, C. Y., Rho, M.-C., Jeong, J.-H., Cho, K.-O., Lee, W. S., & Park, S.-J. (2013). *In Vitro* Antiviral Activity of Phlorotannins Isolated from *Ecklonia cava* against Porcine Epidemic Diarrhea Coronavirus Infection and Hemagglutination. *Bioorganic & Medicinal Chemistry*, **21**(15): 4706–4713. https://doi.org/10.1016/j.bmc.2013.04.085

Lacy, A. (2004). Studies on Coumarins and Coumarin-Related Compounds to Determine their Therapeutic Role in the Treatment of Cancer. *Current Pharmaceutical Design*, **10**(30): 3797–3811. https://doi.org/10.2174/1381612043382693

Lagorce, D., Douguet, D., Miteva, M. A., & Villoutreix, B. O. (2017). Computational Analysis of Calculated Physicochemical and ADMET Properties of Protein-

Protein Interaction Inhibitors. *Scientific Reports*, **7**(1): 46277. https://doi.org/10.1038/srep46277

Lagunin, A., Stepanchikova, A., Filimonov, D., & Poroikov, V. (2000). PASS: Prediction of Activity Spectra for Biologically Active Substances. *Bioinformatics*, **16**(8): 747–748. https://doi.org/10.1093/bioinformatics/16.8.747

Lalani, S., & Poh, C. L. (2020). Flavonoids as Antiviral Agents for Enterovirus A71 (EV-A71). *Viruses*, **12**(2): 184. https://doi.org/10.3390/v12020184

Lan, J., Ge, J., Yu, J., Shan, S., Zhou, H., Fan, S., Zhang, Q., Shi, X., Wang, Q., Zhang, L., & Wang, X. (2020). Structure of the SARS-CoV-2 Spike Receptor-Binding Domain Bound to the ACE2 Receptor. *Nature*, **581**(7807): 215–220. https://doi.org/10.1038/s41586-020-2180-5

Letko, M., Marzi, A., & Munster, V. (2020). Functional Assessment of Cell Entry and Receptor Usage for SARS-CoV-2 and Other Lineage B Betacoronaviruses. *Nature Microbiology*, **5**(4): 562–569. https://doi.org/10.1038/s41564-020-0688-y

Li, G., Fan, Y., Lai, Y., Han, T., Li, Z., Zhou, P., Pan, P., Wang, W., Hu, D., Liu, X., Zhang, Q., & Wu, J. (2020). Coronavirus Infections and Immune Responses. *Journal of Medical Virology*, **92**(4): 424–432. https://doi.org/10.1002/jmv.25685

Li, L., Koh, C. C., Reker, D., Brown, J. B., Wang, H., Lee, N. K., Liow, H., Dai, H., Fan, H.-M., Chen, L., & Wei, D.-Q. (2019). Predicting Protein-Ligand Interactions Based on Bow-Pharmacological Space and Bayesian Additive Regression Trees. *Scientific Reports*, **9**(1): 7703. https://doi.org/10.1038/s41598-019-43125-6

Li, R. W., David Lin, G., Myers, S. P., & Leach, D. N. (2003). Anti-inflammatory Activity of Chinese Medicinal Vine Plants. *Journal of Ethnopharmacology*, **85**(1): 61–67. https://doi.org/10.1016/S0378-8741(02)00339-2

Li, W., Moore, M. J., Vasilieva, N., Sui, J., Wong, S. K., Berne, M. A., Somasundaran, M., Sullivan, J. L., Luzuriaga, K., Greenough, T. C., Choe, H., & Farzan, M. (2003). Angiotensin-Converting Enzyme 2 is a Functional Receptor for the SARS Coronavirus. *Nature*, **426**(6965): 450–454. https://doi.org/10.1038/nature02145

Lin, C.-W., Tsai, F.-J., Tsai, C.-H., Lai, C.-C., Wan, L., Ho, T.-Y., Hsieh, C.-C., & Chao, P.-D. L. (2005). Anti-SARS Coronavirus 3C-Like Protease Effects of *Isatis indigotica* Root and Plant-Derived Phenolic Compounds. *Antiviral Research*, **68**(1): 36–42. https://doi.org/10.1016/j.antiviral.2005.07.002

Lipinski, C. A., Lombardo, F., Dominy, B. W., & Feeney, P. J. (2001). Experimental and Computational Approaches to Estimate Solubility and Permeability in Drug Discovery and Development Settings 1PII of Original Article: S0169-409X(96)00423-1. The Article was Originally Published in Advanced Drug Delivery Reviews 23 (1997) 3–25. *Advanced Drug Delivery Reviews*, **46**(1–3): 3–26. https://doi.org/10.1016/S0169-409X(00)00129-0

Liu, Y., Yang, L., Wang, H., & Xiong, Y. (2022). Recent Advances in Antiviral Activities of Triterpenoids. *Pharmaceuticals*, **15**(10): 1169. https://doi.org/10.3390/ph15101169

Liu, Z., VanBlargan, L. A., Bloyet, L.-M., Rothlauf, P. W., Chen, R. E., Stumpf, S., Zhao, H., Errico, J. M., Theel, E. S., Liebeskind, M. J., Alford, B., Buchser, W. J., Ellebedy, A. H., Fremont, D. H., Diamond, M. S., & Whelan, S. P. J. (2021). Identification of SARS-CoV-2 Spike Mutations that Attenuate Monoclonal and

Serum Antibody Neutralization. *Cell Host & Microbe*, **29**(3): 477-488.e4. https://doi.org/10.1016/j.chom.2021.01.014

Lvov, D. K., Alkhovsky, S. V., Kolobukhina, L. V., & Burtseva, E. I. (2020). Etiology of epidemic outbreaks COVID-19 in Wuhan, Hubei province, Chinese People Republic Associated with 2019-nCoV (*Nidovirales, Coronaviridae, Coronavirinae, Betacoronavirus*, Subgenus *Sarbecovirus*): Lessons of SARS-CoV Outbreak. *Problems of Virology*, **65**(1): 6–15. https://doi.org/10.36233/0507-4088-2020-65-1-6-15

Majnooni, M. B., Fakhri, S., Bahrami, G., Naseri, M., Farzaei, M. H., & Echeverría, J. (2021a). Alkaloids as Potential Phytochemicals against SARS-CoV-2: Approaches to the Associated Pivotal Mechanisms. *Evidence-Based Complementary and Alternative Medicine*, **2021**, 1–21. https://doi.org/10.1155/2021/6632623

Majnooni, M. B., Fakhri, S., Bahrami, G., Naseri, M., Farzaei, M. H., & Echeverría, J. (2021b). Alkaloids as Potential Phytochemicals against SARS-CoV-2: Approaches to the Associated Pivotal Mechanisms. *Evidence-Based Complementary and Alternative Medicine*, **2021**, e6632623. https://doi.org/10.1155/2021/6632623

Mamkulathil Devasia, R., Altaf, M., Fahad Alrefaei, A., & Manoharadas, S. (2021). Enhanced Production of Camptothecin by Immobilized Callus of *Ophiorrhiza mungos* and a Bioinformatic Insight into its Potential Antiviral Effect against SARS-CoV-2. *Journal of King Saud University - Science*, **33**(2): 101344. https://doi.org/10.1016/j.jksus.2021.101344

Manjrekar, P. N., Jolly, C. I., & Narayanan, S. (2000). Comparative Studies of the Immunomodulatory Activity of *Tinospora cordifolia* and *Tinospora sinensis*. *Fitoterapia*, **71**(3): 254–257. https://doi.org/10.1016/S0367-326X(99)00167-7

Manne, M., Goudar, G., Varikasuvu, S. R., Khetagoudar, M. C., Kanipakam, H., Natarajan, P., Ummiti, M. D., Yenagi, V. A., Chinthakindi, S., Dharani, P., Thota, D. S. S., Patil, S., & Patil, V. (2021). Cordifolioside: Potent Inhibitor against M^{pro} of SARS-CoV-2 and Immunomodulatory through Human TGF-β and TNF-α. *3 Biotech*, **11**(3): 136. https://doi.org/10.1007/s13205-021-02685-z

Mark, P., & Nilsson, L. (2001). Structure and Dynamics of the TIP3P, SPC, and SPC/E Water Models at 298 K. *The Journal of Physical Chemistry A*, **105**(43): 9954–9960. https://doi.org/10.1021/jp003020w

Markov, P. V., Ghafari, M., Beer, M., Lythgoe, K., Simmonds, P., Stilianakis, N. I., & Katzourakis, A. (2023). The Evolution of SARS-CoV-2. *Nature Reviews Microbiology*, **21**(6): 361–379. https://doi.org/10.1038/s41579-023-00878-2

Mazumder, S., Dahal, S. R., Chaudhary, B. P., & Mohanty, S. (2018). Structure and Function Studies of Asian Corn Borer *Ostrinia furnacalis* Pheromone Binding Protein2. *Scientific Reports*, **8**(1): 17105. https://doi.org/10.1038/s41598-018-35509-x

McNutt, A. T., Francoeur, P., Aggarwal, R., Masuda, T., Meli, R., Ragoza, M., Sunseri, J., & Koes, D. R. (2021). GNINA 1.0: Molecular Docking with Deep Learning. *Journal of Cheminformatics*, **13**(1): Article 1. https://doi.org/10.1186/s13321-021-00522-2

Meng, X.-Y., Zhang, H.-X., Mezei, M., & Cui, M. (2011). Molecular Docking: A Powerful Approach for Structure-Based Drug Discovery. *Current Computer Aided-Drug Design*, **7**(2): 146–157.

https://doi.org/10.2174/157340911795677602

Merz, K. M., Ringe, D., & Reynolds, C. H. (Eds.). (2010). *Drug design: Structure- and ligand-based approaches*. Cambridge University Press.

Miller, M. D., Kearsley, S. K., Underwood, D. J., & Sheridan, R. P. (1994). FLOG: A System to Select 'Quasi-Flexible' Ligands Complementary to a Receptor of known Three-Dimensional Structure. *Journal of Computer-Aided Molecular Design*, **8**(2): 153–174. https://doi.org/10.1007/BF00119865

Miller, S., Lesk, A. M., Janin, J., & Chothia, C. (1987). The Accessible Surface Area and Stability of Oligomeric Proteins. *Nature*, **328**(6133): Article 6133. https://doi.org/10.1038/328834a0

Mintah, S. O., Asafo-Agyei, T., Archer, M.-A., Junior, P. A.-A., Boamah, D., Kumadoh, D., Appiah, A., Ocloo, A., Boakye, Y. D., & Agyare, C. (2019). Medicinal Plants for Treatment of Prevalent Diseases. *Pharmacognosy - Medicinal Plants*. https://doi.org/10.5772/intechopen.82049

Mohammed, M. M. D., El-Souda, S. S., El-Hallouty, S. M., & Kobayashi, N. (2013). Antiviral and Cytotoxic Activities of Anthraquinones Isolated from *Cassia roxburghii* linn. Leaves. *Herba Polonica*, **59**(4): 33–44. https://doi.org/10.2478/hepo-2013-0022

Morris, G. M., Goodsell, D. S., Halliday, R. S., Huey, R., Hart, W. E., Belew, R. K., & Olson, A. J. (1998). Automated Docking using a Lamarckian Genetic Algorithm and an Empirical Binding Free Energy Function. *Journal of Computational Chemistry*, **19**(14): 1639–1662. https://doi.org/10.1002/(SICI)1096-987X(19981115)19:14<1639::AID-JCC10>3.0.CO;2-B

Morris, G. M., Huey, R., Lindstrom, W., Sanner, M. F., Belew, R. K., Goodsell, D. S., & Olson, A. J. (2009). AutoDock4 and AutoDockTools4: Automated docking with Selective Receptor Flexibility. *Journal of Computational Chemistry*, **30**(16): 2785–2791. https://doi.org/10.1002/jcc.21256

Muchtaridi, M., Sugijanto, M., Mohd Gazzali, A., & Wahab, H. A. (2020). Anti-Neuraminidase Bioactives from Manggis Hutan (*Garcinia celebica* L.) Leaves: Partial Purification and Molecular Characterization. *Molecules*, **25**(4): 821. https://doi.org/10.3390/molecules25040821

Muehlbacher, M., Spitzer, G. M., Liedl, K. R., & Kornhuber, J. (2011). Qualitative Prediction of Blood–Brain Barrier Permeability on a Large and Refined Dataset. *Journal of Computer-Aided Molecular Design*, **25**(12): 1095–1106. https://doi.org/10.1007/s10822-011-9478-1

Muhammed, M. T., Kuyucuklu, G., Kaynak-Onurdag, F., & Aki-Yalcin, E. (2022). Synthesis, Antimicrobial Activity, and Molecular Modeling Studies of Some Benzoxazole Derivatives. *Letters in Drug Design & Discovery*, **19**(8): 757–768. https://doi.org/10.2174/1570180819666220408133643

Muhseen, Z. T., Hameed, A. R., Al-Hasani, H. M. H., Tahir ul Qamar, M., & Li, G. (2020). Promising Terpenes as SARS-CoV-2 Spike Receptor-Binding Domain (RBD) Attachment Inhibitors to the Human ACE2 Receptor: Integrated Computational Approach. *Journal of Molecular Liquids*, **320**, 114493. https://doi.org/10.1016/j.molliq.2020.114493

Mulakala, C., & Viswanadhan, V. N. (2013a). Could MM-GBSA be Accurate Enough for Calculation of Absolute Protein/Ligand Binding Free Energies? *Journal of Molecular Graphics and Modelling*, **46**, 41–51. https://doi.org/10.1016/j.jmgm.2013.09.005

Mulakala, C., & Viswanadhan, V. N. (2013b). Could MM-GBSA be Accurate Enough for Calculation of Absolute Protein/Ligand Binding Free Energies? *Journal of Molecular Graphics and Modelling*, **46**, 41–51. https://doi.org/10.1016/j.jmgm.2013.09.005

Muralidharan, N., Sakthivel, R., Velmurugan, D., & Gromiha, M. M. (2021). Computational Studies of Drug Repurposing and Synergism of Lopinavir, Oseltamivir and Ritonavir Binding with SARS-CoV-2 Protease against COVID-19. *Journal of Biomolecular Structure and Dynamics*, **39**(7): 2673–2678. https://doi.org/10.1080/07391102.2020.1752802

Mushtaq, S., Abbasi, B. H., Uzair, B., & Abbasi, R. (2018). Natural Products as Reservoirs of Novel Therapeutic Agents. *EXCLI Journal;* **17**, 420-451*; ISSN* 1611-2156. https://doi.org/10.17179/EXCLI2018-1174

Nguyen, T. T. H., Woo, H.-J., Kang, H.-K., Nguyen, V. D., Kim, Y.-M., Kim, D.-W., Ahn, S.-A., Xia, Y., & Kim, D. (2012). Flavonoid-Mediated Inhibition of SARS Coronavirus 3C-Like Protease Expressed in *Pichia pastoris*. *Biotechnology Letters*, **34**(5): 831–838. https://doi.org/10.1007/s10529-011-0845-8

Nwokeji, P., Enodiana, O. I., Ezenweani, R., Osasere, O.-I., Akatah, H., & Abiola. (2016). *The Chemistry of Natural Product: Plant Secondary Metabolites*.

Ode, H., Nakashima, M., Kitamura, S., Sugiura, W., & Sato, H. (2012). Molecular Dynamics Simulation in Virus Research. *Frontiers in Microbiology*, **3**. https://www.frontiersin.org/articles/10.3389/fmicb.2012.00258

Okimoto, N., Futatsugi, N., Fuji, H., Suenaga, A., Morimoto, G., Yanai, R., Ohno, Y., Narumi, T., & Taiji, M. (2009). High-Performance Drug Discovery: Computational Screening by Combining Docking and Molecular Dynamics Simulations. *PLoS Computational Biology*, **5**(10): e1000528.

https://doi.org/10.1371/journal.pcbi.1000528

Ong, Q., Ronnie Teo, J. W., Dela Cruz, J., Wee, E., Wee, W., & Han, W. (2022). Irradiation of UVC LED at 277 nm Inactivates Coronaviruses in Association to Photodegradation of Spike Protein. *Heliyon*, **8**(10): e11132. https://doi.org/10.1016/j.heliyon.2022.e11132

Onodera, K., Satou, K., & Hirota, H. (2007). Evaluations of Molecular Docking Programs for Virtual Screening. *Journal of Chemical Information and Modeling*, **47**(4): 1609–1618. https://doi.org/10.1021/ci7000378

Ortega, J. T., Jastrzebska, B., & Rangel, H. R. (2021). Omicron SARS-CoV-2 Variant Spike Protein Shows an Increased Affinity to the Human ACE2 Receptor: An *In Silico* Analysis. *Pathogens*, **11**(1): 45. https://doi.org/10.3390/pathogens11010045

Osama M. Ahmed. Chapter 3.2.13—*Tinospora cordifolia*. *Naturally Occurring Chemicals Against Alzheimer's Disease*, **2021**, 351-358. https://doi.org/10.1016/B978-0-12-819212-2.00029-3

Panche, A. N., Diwan, A. D., & Chandra, S. R. (2016). Flavonoids: An overview. *Journal of Nutritional Science*, **5**, e47. https://doi.org/10.1017/jns.2016.41

Pandeya, K. B., Ganeshpurkar, A., & Mishra, M. K. (2020). Natural RNA Dependent RNA Polymerase Inhibitors: Molecular Docking Studies of Some Biologically Active Alkaloids of *Argemone mexicana*. *Medical Hypotheses*, **144**, 109905. https://doi.org/10.1016/j.mehy.2020.109905

Paraiso, I. L., Revel, J. S., & Stevens, J. F. (2020). Potential Use of Polyphenols in the Battle against COVID-19. *Current Opinion in Food Science*, **32**, 149–155. https://doi.org/10.1016/j.cofs.2020.08.004

Park, J.-Y., Kim, J. H., Kim, Y. M., Jeong, H. J., Kim, D. W., Park, K. H., Kwon, H.-J., Park, S.-J., Lee, W. S., & Ryu, Y. B. (2012). Tanshinones as Selective and Slow-Binding Inhibitors for SARS-CoV Cysteine Proteases. *Bioorganic & Medicinal Chemistry*, **20**(19): 5928–5935. https://doi.org/10.1016/j.bmc.2012.07.038

Park, J.-Y., Kim, J. H., Kwon, J. M., Kwon, H.-J., Jeong, H. J., Kim, Y. M., Kim, D., Lee, W. S., & Ryu, Y. B. (2013). Dieckol, a SARS-CoV $3CL^{pro}$ Inhibitor, Isolated from the Edible Brown Algae *Ecklonia cava*. *Bioorganic & Medicinal Chemistry*, **21**(13): 3730–3737. https://doi.org/10.1016/j.bmc.2013.04.026

Park, J.-Y., Yuk, H. J., Ryu, H. W., Lim, S. H., Kim, K. S., Park, K. H., Ryu, Y. B., & Lee, W. S. (2017). Evaluation of Polyphenols from *Broussonetia papyrifera* as Coronavirus Protease Inhibitors. *Journal of Enzyme Inhibition and Medicinal Chemistry*, **32**(1): 504–512. https://doi.org/10.1080/14756366.2016.1265519

Pattar, S. V., Adhoni, S. A., Kamanavalli, C. M., & Kumbar, S. S. (2020). *In Silico* Molecular Docking Studies and MM/GBSA Analysis of Coumarin-Carbonodithioate Hybrid Derivatives Divulge the Anticancer Potential against Breast Cancer. *Beni-Suef University Journal of Basic and Applied Sciences*, **9**(1): 36. https://doi.org/10.1186/s43088-020-00059-7

Paul, A., Vibhuti, A., & Raj, V. S. (2021). Evaluation of antiviral activity of Andrographis paniculata and Tinospora cordifolia using in silico and in vitro assay against DENV-2. *Journal of Pharmacognosy and Phytochemistry*, **10**(2): 486–496. https://doi.org/10.22271/phyto.2021.v10.i2f.13847

Pence, H. E., & Williams, A. (2010). ChemSpider: An Online Chemical Information Resource. *Journal of Chemical Education*, **87**(11): 1123–1124. https://doi.org/10.1021/ed100697w

Peng, F., Tu, L., Yang, Y., Hu, P., Wang, R., Hu, Q., Cao, F., Jiang, T., Sun, J., Xu, G., & Chang, C. (2020). Management and Treatment of COVID-19: The Chinese Experience. *Canadian Journal of Cardiology*, **36**(6): 915–930. https://doi.org/10.1016/j.cjca.2020.04.010

Pires, D. E. V., Blundell, T. L., & Ascher, D. B. (2015). pkCSM: Predicting Small-Molecule Pharmacokinetic and Toxicity Properties Using Graph-Based Signatures. *Journal of Medicinal Chemistry*, **58**(9): 4066–4072. https://doi.org/10.1021/acs.jmedchem.5b00104

Pitsillou, E., Liang, J., Karagiannis, C., Ververis, K., Darmawan, K. K., Ng, K., Hung, A., & Karagiannis, T. C. (2020). Interaction of Small Molecules with the SARS-CoV-2 Main Protease *In Silico* and *In Vitro* Validation of Potential Lead Compounds Using an Enzyme-Linked Immunosorbent Assay. *Computational Biology and Chemistry*, **89**, 107408. https://doi.org/10.1016/j.compbiolchem.2020.107408

Praiwala, B., Priyanka, S., Raghu, N., Gopenath, N., Gnanasekaran, A., Karthikeyan, M., Indumathi, R., Ebrahim, N. K., Pugazhandhi, B., Pradeep, P., Ranjith, M. S., Balasubramanian, S., & Basalingappa, K. M. (2019). *In Vitro* Anti-Bacterial Activity of *Tinospora cordifolia* Leaf Extract and its Phytochemical Screening. *Journal of Biomedical Sciences*, **5**(2): 10–17. https://doi.org/10.3126/jbs.v5i2.23633

Prieto-Martínez, F. D., López-López, E., Eurídice Juárez-Mercado, K., & Medina-Franco, J. L. (2019). Computational Drug Design Methods—Current and Future Perspectives. *In Silico Drug Design*, **2019**, 19–44. https://doi.org/10.1016/B978-0-12-816125-8.00002-X

Rahimi, A., Mirzazadeh, A., & Tavakolpour, S. (2021). Genetics and Genomics of SARS-CoV-2: A Review of the Literature with the Special Focus on Genetic Diversity and SARS-CoV-2 Genome Detection. *Genomics*, **113**(1): 1221–1232. https://doi.org/10.1016/j.ygeno.2020.09.059

Rajasekaran, D., Palombo, E. A., Chia Yeo, T., Lim Siok Ley, D., Lee Tu, C., Malherbe, F., & Grollo, L. (2013). Identification of Traditional Medicinal Plant Extracts with Novel Anti-Influenza Activity. *PLoS ONE*, **8**(11): e79293. https://doi.org/10.1371/journal.pone.0079293

Rakib, A., Ahmed, S., Islam, Md. A., Haye, A., Uddin, S. M. N., Uddin, M. M. N., Hossain, M. K., Paul, A., & Emran, T. B. (2020). Antipyretic and Hepatoprotective Potential of *Tinospora crispa* and Investigation of Possible Lead Compounds through *In Silico* Approaches. *Food Science & Nutrition*, **8**(1): 547–556. https://doi.org/10.1002/fsn3.1339

Rakib, A., Paul, A., Chy, Md. N. U., Sami, S. A., Baral, S. K., Majumder, M., Tareq, A. M., Amin, M. N., Shahriar, A., Uddin, Md. Z., Dutta, M., Tallei, T. E., Emran, T. B., & Simal-Gandara, J. (2020). Biochemical and Computational Approach of Selected Phytocompounds from *Tinospora crispa* in the Management of COVID-19. *Molecules*, **25**(17): 3936. https://doi.org/10.3390/molecules25173936

Rarey, M., Kramer, B., Lengauer, T., & Klebe, G. (1996). A Fast Flexible Docking Method using an Incremental Construction Algorithm. *Journal of Molecular Biology*, **261**(3): 470–489. https://doi.org/10.1006/jmbi.1996.0477

Ricotta, E., & Kwan, J. (2019). Artemisinin-Resistant Malaria as a Global Catastrophic Biological Threat. In T. V. Inglesby & A. A. Adalja (Eds.), *Global Catastrophic Biological Risks*, **424**, 33–57. Springer International Publishing.

https://doi.org/10.1007/82_2019_163

Rienth, M., Vigneron, N., Darriet, P., Sweetman, C., Burbidge, C., Bonghi, C., Walker, R. P., Famiani, F., & Castellarin, S. D. (2021). Grape Berry Secondary Metabolites and Their Modulation by Abiotic Factors in a Climate Change Scenario–A Review. *Frontiers in Plant Science*, **12**, 643258. https://doi.org/10.3389/fpls.2021.643258

Roos, K., Wu, C., Damm, W., Reboul, M., Stevenson, J. M., Lu, C., Dahlgren, M. K., Mondal, S., Chen, W., Wang, L., Abel, R., Friesner, R. A., & Harder, E. D. (2019). OPLS3e: Extending Force Field Coverage for Drug-Like Small Molecules. *Journal of Chemical Theory and Computation*, **15**(3): 1863–1874. https://doi.org/10.1021/acs.jctc.8b01026

Rosales, P. F., Bordin, G. S., Gower, A. E., & Moura, S. (2020). Indole Alkaloids: 2012 Until Now, Highlighting the New Chemical Structures and Biological Activities. *Fitoterapia*, **143**, 104558. https://doi.org/10.1016/j.fitote.2020.104558

Ryu, Y. B., Jeong, H. J., Kim, J. H., Kim, Y. M., Park, J.-Y., Kim, D., Naguyen, T. T. H., Park, S.-J., Chang, J. S., & Park, K. H. (2010). Biflavonoids from *Torreya nucifera* Displaying SARS-CoV $3CL^{pro}$ Inhibition. *Bioorganic & Medicinal Chemistry*, **18**(22): 7940–7947. https://doi.org/10.1016/j.bmc.2010.09.035

Ryu, Y. B., Park, S.-J., Kim, Y. M., Lee, J.-Y., Seo, W. D., Chang, J. S., Park, K. H., Rho, M.-C., & Lee, W. S. (2010). SARS-CoV $3CL^{pro}$ Inhibitory Effects of Quinone-Methide Triterpenes from *Tripterygium regelii*. *Bioorganic & Medicinal Chemistry Letters*, **20**(6): 1873–1876. https://doi.org/10.1016/j.bmcl.2010.01.152

Sadati, S., Gheibi, N., Ranjbar, S., & Hashemzadeh, M. (2018). Docking Study of Flavonoid Derivatives as Potent Inhibitors of Influenza H1N1 Virus Neuraminidase. *Biomedical Reports*. https://doi.org/10.3892/br.2018.1173

Sagar, V., & Kumar, A. H. (2020). Efficacy of Natural Compounds from *Tinospora cordifolia* Against SARS-CoV-2 Protease, Surface Glycoprotein and RNA Polymerase. *Biology, Engineering, Medicine and Science Reports*, **6**(1): 6–8. https://doi.org/10.5530/bems.6.1.2

Sahoo, A., Fuloria, S., Swain, S. S., Panda, S. K., Sekar, M., Subramaniyan, V., Panda, M., Jena, A. K., Sathasivam, K. V., & Fuloria, N. K. (2021). Potential of Marine Terpenoids against SARS-CoV-2: An *In Silico* Drug Development Approach. *Biomedicines*, **9**(11): 1505. https://doi.org/10.3390/biomedicines9111505

Saliu, T. P., Umar, H. I., Ogunsile, O. J., Okpara, M. O., Yanaka, N., & Elekofehinti, O. O. (2021). Molecular Docking and Pharmacokinetic Studies of Phytocompounds from Nigerian Medicinal Plants as Promising Inhibitory Agents against SARS-CoV-2 Methyltransferase (nsp16). *Journal of Genetic Engineering and Biotechnology*, **19**(1): 172. https://doi.org/10.1186/s43141-021-00273-5

Santos, S., Barata, P., Charmier, A., Lehmann, I., Rodrigues, S., Melosini, M. M., Pais, P. J., Sousa, A. P., Teixeira, C., Santos, I., Rocha, A. C., Baylina, P., & Fernandes, R. (2022). Cannabidiol and Terpene Formulation Reducing SARS-CoV-2 Infectivity Tackling a Therapeutic Strategy. *Frontiers in Immunology*, **13**, 841459. https://doi.org/10.3389/fimmu.2022.841459

Sass, P. (Ed.). (2023). *Antibiotics: Methods and Protocols* (Vol. 2601). Springer US. https://doi.org/10.1007/978-1-0716-2855-3

Saxena, M., Saxena, J., Nema, R., Singh, D., & Gupta, A. (2013). *Journal of Pharmacognosy and Phytochemistry*. **1**(6): 15.

Schüttelkopf, A. W., & van Aalten, D. M. F. (2004). *PRODRG*: A Tool for High-Throughput Crystallography of Protein–Ligand Complexes. *Acta Crystallographica Section D Biological Crystallography*, **60**(8): 1355–1363. https://doi.org/10.1107/S0907444904011679

Shang, J., Ye, G., Shi, K., Wan, Y., Luo, C., Aihara, H., Geng, Q., Auerbach, A., & Li, F. (2020). Structural Basis of Receptor Recognition by SARS-CoV-2. *Nature*, **581**(7807): 221–224. https://doi.org/10.1038/s41586-020-2179-y

Sharov, A., Burkhanova, T., Taskın Tok, T., Babashkina, M., & Safin, D. (2022). Computational Analysis of Molnupiravir. *International Journal of Molecular Sciences*, **23**(3): 1508. https://doi.org/10.3390/ijms23031508

Singh, D., & Yi, S. V. (2021). On the Origin and Evolution of SARS-CoV-2. *Experimental & Molecular Medicine*, **53**(4): 537–547. https://doi.org/10.1038/s12276-021-00604-z

Singh, S., Srivastava, R., & Choudhary, S. (2011). Antifungal and High-Performance Liquid Chromatography Analysis of the Crude Extracts of *Acorus calamus, Tinospora cordifolia* and *Celestrus paniculatus*. *Archives of Phytopathology And Plant Protection*, **44**(9): 902–910. https://doi.org/10.1080/03235400903395369

Sinha, M., Jagadeesan, R., Kumar, N., Saha, S., Kothandan, G., & Kumar, D. (2022). In-Silico Studies on Myo Inositol-1-phosphate Synthase of *Leishmania donovani* in Search of Anti-leishmaniasis. *Journal of Biomolecular Structure and Dynamics*, **40**(8): 3371–3384. https://doi.org/10.1080/07391102.2020.1847194

S.M. Gopinatha, R. P. (2018). Antiviral Prospective of *Tinospora cordifolia* on HSV-1. *International Journal of Current Microbiology and Applied Sciences*, **7**(1): 3617–3624. https://doi.org/10.20546/ijcmas.2018.701.425

Springob, K., & Kutchan, T. M. (2009). Introduction to the Different Classes of Natural Products. In A. E. Osbourn & V. Lanzotti (Eds.), *Plant-derived Natural Products: Synthesis, Function, and Application* 3–50. https://doi.org/10.1007/978-0-387-85498-4_1

Su, H., Yao, S., Zhao, W., Li, M., Liu, J., Shang, W., Xie, H., Ke, C., Gao, M., Yu, K., Liu, H., Shen, J., Tang, W., Zhang, L., Zuo, J., Jiang, H., Bai, F., Wu, Y., Ye, Y., & Xu, Y. (2020). Discovery of Baicalin and Baicalein as Novel, Natural Product Inhibitors of SARS-CoV-2 3CL Protease *In Vitro* [Preprint]. *Molecular Biology*. https://doi.org/10.1101/2020.04.13.038687

Su, H., Yao, S., Zhao, W., Li, M., Liu, J., Shang, W., Xie, H., Ke, C., Hu, H., Gao, M., Yu, K., Liu, H., Shen, J., Tang, W., Zhang, L., Xiao, G., Ni, L., Wang, D., Zuo, J., Jiang, H. L., Bai, F., Wu, Y., Ye, Y., & Xu, Y. (2020). Anti-SARS-CoV-2 Activities *In Vitro* of Shuanghuanglian Preparations and Bioactive Ingredients. *Acta Pharmacologica Sinica*, **41**(9): 1167–1177. https://doi.org/10.1038/s41401-020-0483-6

Su, S., Wong, G., Shi, W., Liu, J., Lai, A. C. K., Zhou, J., Liu, W., Bi, Y., & Gao, G. F. (2016). Epidemiology, Genetic Recombination, and Pathogenesis of Coronaviruses. *Trends in Microbiology*, **24**(6): 490–502. https://doi.org/10.1016/j.tim.2016.03.003

Subissi, L., Imbert, I., Ferron, F., Collet, A., Coutard, B., Decroly, E., & Canard, B. (2014). SARS-CoV ORF1b-Encoded Nonstructural Proteins 12–16:

Replicative enzymes as antiviral targets. *Antiviral Research*, **101**, 122–130. https://doi.org/10.1016/j.antiviral.2013.11.006

Tallei, T. E., Tumilaar, S. G., Niode, N. J., Fatimawali, Kepel, B. J., Idroes, R., Effendi, Y., Sakib, S. A., & Emran, T. B. (2020). Potential of Plant Bioactive Compounds as SARS-CoV-2 Main Protease (Mpro) and Spike (S) Glycoprotein Inhibitors: A Molecular Docking Study. *Scientifica*, **2020**, e6307457. https://doi.org/10.1155/2020/6307457

Teoh, E. S. (2016). Secondary Metabolites of Plants. In E. S. Teoh (Ed.), *Medicinal Orchids of Asia*, 59–73. https://doi.org/10.1007/978-3-319-24274-3_5

Thakkar, S. S., Shelat, F., & Thakor, P. (2021). Magical Bullets from an Indigenous Indian Medicinal Plant *Tinospora cordifolia*: An *In Silico* Approach for the Antidote of SARS-CoV-2. *Egyptian Journal of Petroleum*, **30**(1): 53–66. https://doi.org/10.1016/j.ejpe.2021.02.005

The Imperial Agricultural Research Conference. (1927). *Science*, **66**(1709): 293–294. https://doi.org/10.1126/science.66.1709.293.b

the International Natural Product Sciences Taskforce, Atanasov, A. G., Zotchev, S. B., Dirsch, V. M., & Supuran, C. T. (2021). Natural Products in Drug Discovery: Advances and Opportunities. *Nature Reviews Drug Discovery*, **20**(3): 200–216. https://doi.org/10.1038/s41573-020-00114-z

Tian, S., Wang, J., Li, Y., Li, D., Xu, L., & Hou, T. (2015). The Application of *In Silico* Drug-Likeness Predictions in Pharmaceutical Research. *Advanced Drug Delivery Reviews*, **86**, 2–10. https://doi.org/10.1016/j.addr.2015.01.009

Tibbitts, J., Canter, D., Graff, R., Smith, A., & Khawli, L. A. (2016). Key Factors Influencing ADME Properties of Therapeutic Proteins: A Need for ADME

Characterization in Drug Discovery and Development. *mAbs*, **8**(2): 229–245. https://doi.org/10.1080/19420862.2015.1115937

Trott, O., & Olson, A. J. (2009). AutoDock Vina: Improving the Speed and Accuracy of Docking with a New Scoring Function, Efficient Optimization, and Multithreading. *Journal of Computational Chemistry*, **31**(2): 455-461. https://doi.org/10.1002/jcc.21334

Turner, S. E., Williams, C. M., Iversen, L., & Whalley, B. J. (2017). Molecular Pharmacology of Phytocannabinoids. In A. D. Kinghorn, H. Falk, S. Gibbons, & J. Kobayashi (Eds.), *Phytocannabinoids*, **103**, 61–101. https://doi.org/10.1007/978-3-319-45541-9_3

Vaheri, A., Strandin, T., Hepojoki, J., Sironen, T., Henttonen, H., Mäkelä, S., & Mustonen, J. (2013). Uncovering the Mysteries of Hantavirus Infections. *Nature Reviews Microbiology*, **11**(8): 539–550. https://doi.org/10.1038/nrmicro3066

Van De Sand, L., Bormann, M., Alt, M., Schipper, L., Heilingloh, C. S., Steinmann, E., Todt, D., Dittmer, U., Elsner, C., Witzke, O., & Krawczyk, A. (2021). Glycyrrhizin Effectively Inhibits SARS-CoV-2 Replication by Inhibiting the Viral Main Protease. *Viruses*, **13**(4): 609. https://doi.org/10.3390/v13040609

Van de Waterbeemd, H. (2007). *In Silico* Models to Predict Oral Absorption. In *Comprehensive Medicinal Chemistry II* 669–697. https://doi.org/10.1016/B0-08-045044-X/00145-0

van der Spoel, D. (2021). Systematic Design of Biomolecular Force Fields. *Current Opinion in Structural Biology*, **67**, 18–24. https://doi.org/10.1016/j.sbi.2020.08.006

Vektariene, A., Vektaris, G., & Svoboda, J. (2009). A Theoretical Approach to the Nucleophilic Behavior of Benzofused thieno[3,2-b]furans using DFT and HF Based Reactivity Descriptors. *Arkivoc*, **2009**(7): 311–329. https://doi.org/10.3998/ark.5550190.0010.730

Verdonk, M. L., Cole, J. C., Hartshorn, M. J., Murray, C. W., & Taylor, R. D. (2003). Improved Protein-Ligand Docking using GOLD. *Proteins: Structure, Function, and Bioinformatics*, **52**(4): 609–623. https://doi.org/10.1002/prot.10465

Walls, A. C., Park, Y.-J., Tortorici, M. A., Wall, A., McGuire, A. T., & Veesler, D. (2020). Structure, Function, and Antigenicity of the SARS-CoV-2 Spike Glycoprotein. *Cell*, **181**(2): 281-292.e6. https://doi.org/10.1016/j.cell.2020.02.058

Wang, E., Sun, H., Wang, J., Wang, Z., Liu, H., Zhang, J. Z. H., & Hou, T. (2019). End-Point Binding Free Energy Calculation with MM/PBSA and MM/GBSA: Strategies and Applications in Drug Design. *Chemical Reviews*, 119(16): 9478–9508. https://doi.org/10.1021/acs.chemrev.9b00055

Wang, H., Wang, Y., Wang, W., Fu, P., Liu, P., & Zhu, W. (2011). Anti-influenza Virus Polyketides from the Acid-Tolerant Fungus *Penicillium purpurogenum* JS03-21. *Journal of Natural Products*, **74**(9): 2014–2018. https://doi.org/10.1021/np2004769

Waring, M. J. (2010). Lipophilicity in Drug Discovery. *Expert Opinion on Drug Discovery*, **5**(3): 235–248. https://doi.org/10.1517/17460441003605098

Warren, G. L., Andrews, C. W., Capelli, A.-M., Clarke, B., LaLonde, J., Lambert, M. H., Lindvall, M., Nevins, N., Semus, S. F., Senger, S., Tedesco, G., Wall, I. D., Woolven, J. M., Peishoff, C. E., & Head, M. S. (2006). A Critical Assessment

of Docking Programs and Scoring Functions. *Journal of Medicinal Chemistry*, **49**(20): 5912–5931. https://doi.org/10.1021/jm050362n

Wasilewicz, A., Kirchweger, B., Bojkova, D., Abi Saad, M. J., Langeder, J., Bütikofer, M., Adelsberger, S., Grienke, U., Cinatl Jr., J., Petermann, O., Scapozza, L., Orts, J., Kirchmair, J., Rabenau, H. F., & Rollinger, J. M. (2023). Identification of Natural Products Inhibiting SARS-CoV-2 by Targeting Viral Proteases: A Combined *In Silico* and *In Vitro* Approach. *Journal of Natural Products*, **86**(2): 264–275. https://doi.org/10.1021/acs.jnatprod.2c00843

Wen, C.-C., Kuo, Y.-H., Jan, J.-T., Liang, P.-H., Wang, S.-Y., Liu, H.-G., Lee, C.-K., Chang, S.-T., Kuo, C.-J., Lee, S.-S., Hou, C.-C., Hsiao, P.-W., Chien, S.-C., Shyur, L.-F., & Yang, N.-S. (2007). Specific Plant Terpenoids and Lignoids Possess Potent Antiviral Activities against Severe Acute Respiratory Syndrome Coronavirus. *Journal of Medicinal Chemistry*, **50**(17): 4087–4095. https://doi.org/10.1021/jm070295s

Wink, M. (2018). Plant Secondary Metabolites Modulate Insect Behavior-Steps Toward Addiction. *Frontiers in Physiology*, **9**, 364. https://doi.org/10.3389/fphys.2018.00364

Wolber, G., & Langer, T. (2005). LigandScout: 3-D Pharmacophores Derived from Protein-Bound Ligands and Their Use as Virtual Screening Filters. *Journal of Chemical Information and Modeling*, **45**(1): 160–169. https://doi.org/10.1021/ci049885e

Woo, P. C. Y., Lau, S. K. P., Lam, C. S. F., Lau, C. C. Y., Tsang, A. K. L., Lau, J. H. N., Bai, R., Teng, J. L. L., Tsang, C. C. C., Wang, M., Zheng, B.-J., Chan, K.-H., & Yuen, K.-Y. (2012). Discovery of Seven Novel Mammalian and Avian Coronaviruses in the Genus Deltacoronavirus Supports Bat Coronaviruses as

the Gene Source of Alphacoronavirus and Betacoronavirus and Avian Coronaviruses as the Gene Source of Gammacoronavirus and Deltacoronavirus. *Journal of Virology*, **86**(7): 3995–4008. https://doi.org/10.1128/JVI.06540-11

Wrapp, D., Wang, N., Corbett, K. S., Goldsmith, J. A., Hsieh, C.-L., Abiona, O., Graham, B. S., & McLellan, J. S. (2020). Cryo-EM Structure of the 2019-nCoV Spike in the Prefusion Conformation. *Science*, **367**(6483): 1260–1263. https://doi.org/10.1126/science.abb2507

Wu, X., Wang, J., Tan, L., Bui, J., Gjerstad, E., McMillan, K., & Zhang, W. (2012). *In Vitro* ADME Profiling Using High-Throughput Rapid Fire Mass Spectrometry: Cytochrome P450 Inhibition and Metabolic Stability Assays. *SLAS Discovery*, **17**(6): 761–772. https://doi.org/10.1177/1087057112441013

Wu, Y., Li, J., Kim, Y., Wu, J., Wang, Q., & Hao, Y. (2011). *In Vivo* and *in Vitro* Antiviral Effects of Berberine on Influenza Virus. *Chinese Journal of Integrative Medicine*, **17**(6): 444–452. https://doi.org/10.1007/s11655-011-0640-3

Wu, Y., Pegan, S. D., Crich, D., Desrochers, E., Starling, E. B., Hansen, M. C., Booth, C., Nicole Mullininx, L., Lou, L., Chang, K. Y., & Xie, Z.-R. (2021). Polyphenols as Alternative Treatments of COVID-19. *Computational and Structural Biotechnology Journal*, **19**, 5371–5380. https://doi.org/10.1016/j.csbj.2021.09.022

Xia, B., Shen, X., He, Y., Pan, X., Liu, F.-L., Wang, Y., Yang, F., Fang, S., Wu, Y., Duan, Z., Zuo, X., Xie, Z., Jiang, X., Xu, L., Chi, H., Li, S., Meng, Q., Zhou, H., Zhou, Y., Cheng, X., Xin, X., Jin, L., Zhang, H. L., Yu, D. D., Li, M. H., Feng, X. L., Chen, J., Jiang, H., Xiao, G., Zheng, Y. T., Zhang, L. K., Shen, J., Li, J., & Gao, Z. (2021). SARS-CoV-2 Envelope Protein Causes Acute

Respiratory Distress Syndrome (ARDS)-Like Pathological Damages and Constitutes an Antiviral Target. *Cell Research*, **31**(8): Article 8. https://doi.org/10.1038/s41422-021-00519-4

Xia, S., Zhu, Y., Liu, M., Lan, Q., Xu, W., Wu, Y., Ying, T., Liu, S., Shi, Z., Jiang, S., & Lu, L. (2020). Fusion Mechanism of 2019-nCoV and Fusion Inhibitors Targeting HR1 Domain in Spike Protein. *Cellular & Molecular Immunology*, **17**(7): 765–767. https://doi.org/10.1038/s41423-020-0374-2

Xu, C., Cheng, F., Chen, L., Du, Z., Li, W., Liu, G., Lee, P. W., & Tang, Y. (2012). *In Silico* Prediction of Chemical Ames Mutagenicity. *Journal of Chemical Information and Modeling*, **52**(11): 2840–2847. https://doi.org/10.1021/ci300400a

Xu, H., Tu, X., Fan, G., Wang, Q., Wang, X., & Chu, X. (2020). Adsorption Properties Study of Boron Nitride Fullerene for the Application as Smart Drug Delivery Agent of Anti-Cancer Drug Hydroxyurea by Density Functional Theory. *Journal of Molecular Liquids*, **318**, 114315. https://doi.org/10.1016/j.molliq.2020.114315

Xu, J., Zhao, S., Teng, T., Abdalla, A. E., Zhu, W., Xie, L., Wang, Y., & Guo, X. (2020). Systematic Comparison of Two Animal-to-Human Transmitted Human Coronaviruses: SARS-CoV-2 and SARS-CoV. *Viruses*, **12**(2): 244. https://doi.org/10.3390/v12020244

Yan, A., Wang, Z., & Cai, Z. (2008). Prediction of Human Intestinal Absorption by GA Feature Selection and Support Vector Machine Regression. *International Journal of Molecular Sciences*, **9**(10): 1961–1976. https://doi.org/10.3390/ijms9101961

Yang, Y., Yang, P., Huang, C., Wu, Y., Zhou, Z., Wang, X., & Wang, S. (2021). Inhibitory Effect on SARS-CoV-2 Infection of Neferine by Blocking Ca^{2+} - Dependent Membrane Fusion. *Journal of Medical Virology*, **93**(10): 5825–5832. https://doi.org/10.1002/jmv.27117

Ye, N., Yang, Z., & Liu, Y. (2022). Applications of Density Functional Theory in COVID-19 Drug Modeling. *Drug Discovery Today*, **27**(5): 1411–1419. https://doi.org/10.1016/j.drudis.2021.12.017

Yu, M.-S., Lee, J., Lee, J. M., Kim, Y., Chin, Y.-W., Jee, J.-G., Keum, Y.-S., & Jeong, Y.-J. (2012). Identification of Myricetin and Scutellarein as Novel Chemical Inhibitors of the SARS Coronavirus Helicase, nsP13. *Bioorganic & Medicinal Chemistry Letters*, **22**(12): 4049–4054. https://doi.org/10.1016/j.bmcl.2012.04.081

Zaki, A. M., Van Boheemen, S., Bestebroer, T. M., Osterhaus, A. D. M. E., & Fouchier, R. A. M. (2012). Isolation of a Novel Coronavirus from a Man with Pneumonia in Saudi Arabia. *New England Journal of Medicine*, **367**(19): 1814–1820. https://doi.org/10.1056/NEJMoa1211721

Zaynab, M., Fatima, M., Sharif, Y., Zafar, M. H., Ali, H., & Khan, K. A. (2019). Role of Primary Metabolites in Plant Defense against Pathogens. *Microbial Pathogenesis*, **137**, 103728. https://doi.org/10.1016/j.micpath.2019.103728

Zeng, J., Fan, Y., Tan, B., Su, H., Li, Y., Zhang, L., Jiang, J., & Qiu, F. (2018). Charactering the Metabolism of Cryptotanshinone by Human P450 Enzymes and Uridine Diphosphate Glucuronosyltransferases *In Vitro*. *Acta Pharmacologica Sinica*, **39**(8), 1393–1404. https://doi.org/10.1038/aps.2017.144

Zhang, Y., & Tang, L. V. (2021). Overview of Targets and Potential Drugs of SARS-CoV-2 According to the Viral Replication. *Journal of Proteome Research*, **20**(1): 49–59. https://doi.org/10.1021/acs.jproteome.0c00526

Zhou, P., Fan, H., Lan, T., Yang, X.-L., Shi, W.-F., Zhang, W., Zhu, Y., Zhang, Y.-W., Xie, Q.-M., Mani, S., Zheng, X.-S., Li, B., Li, J.-M., Guo, H., Pei, G.-Q., An, X.-P., Chen, J.-W., Zhou, L., Mai, K.-J., Wu, Z. X., Li, D., Anderson, D. E., Zhang, L. B., Li, S. Y., Mi, Z. Q., He, T. T., Cong, F., Guo, P. J., Huang, r., Luo, Y., Liu, X. L., Chen, J., Huang, Y., Sun, Q., Zhang, X. L. L., Wang, Y. Y., Xing, S. Z., Chen, Y. S., Sun, Y., Li, J., Daszak, P., Wang, L.F., Shi, Z. L., Tong, Y. G., & Ma, J.-Y. (2018). Fatal Swine Acute Diarrhoea Syndrome Caused by an HKU2-Related Coronavirus of Bat Origin. *Nature*, **556**(7700): 255–258. https://doi.org/10.1038/s41586-018-0010-9

Zhu, L., & Chen, L. (2019). Progress in Research on Paclitaxel and Tumor Immunotherapy. *Cellular & Molecular Biology Letters*, **24**(1): 40. https://doi.org/10.1186/s11658-019-0164-y

APPENDICES

Appendix A1: List of major natural compounds of *Tinospora species* medicinal plants

SN	Tinospora species	Pharmacological properties	Major Natural compounds selected for the study
1.	*Tinospora cordifolia*	• 1. Anti-SARS *(Manne et al*., 2021) • 2. Anti-Influenza (Rajasekaran *et al*., 2013) • 3. Anti-Herpes (Akram *et al*., 2018) • 4. Anti-HIV (Estari *et al*., 2012) • 5. Anti-bacterial (Praiwala *et al*., 2019) • 6. Anti-fungal (Singh *et al*., 2011) 7. Anti-malarial (Kaushik *et al*., 2015) 8. Anti-inflammatory (Mintah *et al*., 2019)	Cordifolioside A(1) Cordifolioside B(2) Cordioside(3) Cordifolide A(4) Cordifolide B(5) Cordifolide C(6) Tinosporaside(7) Tinosporiside(8) Amritoside A(9) Amritoside B(10) Amritoside C(11) Amritoside D(12) Palmitoside F(13) Palmitoside G(14)
2.	*Tinospora sinensis*	Immunomodulatory (Haque *et al*., 2017; Manjrekar *et al*., 2000) Anti-inflammatory (Li *et al*., 2003)	Lignan(15) Tinosinenoside A(16) Tinosinenoside B(17) Tinosinenoside C(18) Tinosineside A(19) Tinosineside B(20)
3.	*Tinospora crispa*	Anti-SARS (Rakib *et al*., 2020) Treatment of diabetes, hypertension backache (Ahmad *et al*., 2016) Anti-pyretic (Rakib *et al*., 2020) Anti-malarial (Jiraungkoorskul, 2019)	Borapetoside A(21) Borapetoside B(22) Borapetoside C(23) Rumphioside A(24) Rumphioside B(25) Rumphioside C(26)

Appendix A2: Some selected secondary metabolites with antiviral properties

Potential Secondary Metabolites	IC_{50} value (in µM)	Target site/Virus	Citation
Scutellarein	5.8 µM 0.86 µM (nsp13)	SARS-CoV	https://doi.org/10.1016/j.bmcl.2012.04.081 https://doi.org/10.1016/j.bcp.2012.08.012
Wogonin	2.1 µM (137.6 µM) CMC, HEK293T cells, CK8 assay, SPR assay	SARS-CoV SARS-CoV-2 (binds to ACE-2)	https://doi.org/10.1080/14756366.2021.1873977 https://doi.org/10.1002/ptr.7030
Baicalin	7.4 µM	SARS-CoV-2	https://doi.org/10.1101/2020.04.13.038687
Luteolin	20.2 µM	SARS-CoV-2	https://doi.org/10.1002/ptr.6873 https://doi.org/10.1016/j.bmc.2010.09.035 https://doi.org/10.1080/14756366.2019.1690480
Pectolinarin	37.78 µM	SARS-CoV, SARS-CoV-2	https://doi.org/10.1080/14756366.2019.1690480 https://doi.org/10.1111/1751-7915.13675
Apigenin	280.8 µM	SARS-CoV-2 SARS-CoV	https://doi.org/10.1002/ptr.6873 https://doi.org/10.1016/j.bmc.2010.09.035 https://doi.org/10.1080/14756366.2019.1690480
Amentoflavone	8.3 µM	SARS-CoV, SARS-CoV-2	https://doi.org/10.1002/ptr.6873 https://doi.org/10.1111/1751-7915.13675 https://doi.org/10.1080/14756366.2019.1690480 https://doi.org/10.1016/j.bmc.2010.09.035
Rutin	110 µM	SARS-CoV-2	https://doi.org/10.1016/j.jviromet.2012.03.020

			https://doi.org/10.1177/1934578X21991723
Rhoifolin	27.45 µM	SARS-CoV	https://doi.org/10.1080/14756366.2019.1690480
Fisetin	85 µM	SARS-CoV-2	https://doi.org/10.1016/j.ejphar.2020.173759
Galangin	44.40 - 173.92 µM	Herpes	https://doi.org/10.26434/chemrxiv.12115359.v1 https://doi.org/10.1016/S0378-8741(97)01514-6
Herbacetin	40.50 µM (MERS-CoV) 33.17 µM (SARS-CoV-2)	MERS-CoV, SARS-CoV, SARS-CoV-2	https://doi.org/10.1080/14756366.2019.1690480 https://doi.org/10.1111/1751-7915.13675
Myricetin	2.7 µM	SARS-CoV	https://doi.org/10.1016/j.bmcl.2012.04.081
Morin	9.42 µg/mL	MERS-CoV, SARS-CoV, Dengue Virus	https://doi.org/10.1080/07391102.2021.1871863 http://dx.doi.org/10.31838/srp.2020.9.118
Tomentin A	6.2 ± 0.04 µM(FRET)	SARS-CoV	https://doi.org/10.1016/j.bmc.2013.03.027
Tomentin B	6.1 ± 0.02 µM	SARS-CoV	https://doi.org/10.1016/j.bmc.2013.03.027
Tomentin E	5.0 ± 0.06 µM	SARS-CoV	https://doi.org/10.1016/j.bmc.2013.03.027
Naringenin	150 µM (FRET assay)	HCoV229, HCoVOC43, SARS-CoV-2	https://doi.org/10.1155/2020/5630838
Mimulone	14.4 µM	SARS-CoV	https://doi.org/10.1016/j.bmc.2013.03.027
Diplacone	10.4 µM	SARS-CoV	https://doi.org/10.1016/j.bmc.2013.03.027
Hesperetin	8.3 µM(cb) 60 µM(cf)	SARS-CoV, SARS-CoV-2	https://doi.org/10.1016/j.antiviral.2005.07.002 https://doi.org/10.1002/ptr.6873 https://doi.org/10.1007/s11101-020 09720-6

			https://doi.org/10.1111/cbdd.13604
3'-o-methyldiplacol	9.5 ± 0.10 µM	SARS-CoV	https://doi.org/10.1016/j.bmc.2013.03.027
Bavachinin	38.4 µM	SARS-CoV	https://doi.org/10.1007/s11101-020-09720-6 https://doi.org/10.3109/14756366.2012.753591
4'-o- methyldiplacol	9.2 µM Cell-free assay (Fluorescence-based deubiquitination)	SARS-CoV	https://doi.org/10.1016/j.bmc.2013.03.027
Daidzein	105 µM 26.8 µM(cf); 56 µM	SARS-CoV, SARS-CoV-2	https://doi.org/10.1016/j.antiviral.2005.07.002 https://doi.org/10.1007/s11101-020-09720-6
Corylifol A	32.3µM	SARS-CoV	https://doi.org/10.1007/s11101-020-09720-6
Puerarin	381µM	SARS-CoV	https://doi.org/10.1007/s11101-020-09720-6
Neobavaisoflavone	18.3µM	SARS-CoV	https://doi.org/10.1007/s11101-020-09720-6
Epigallocatechin gallate	73 µM 2.47 µg/mL	SARS-CoV SARS-CoV-2	https://doi.org/10.1155/2020/5630838 https://doi.org/10.1099/jgv.0.001574 https://doi.org/10.1007/s10529-011-0845-8
Silymarin	15.2 ± 3.53 µg/mL	MERS-CoV, SARS-CoV-2, Enterovirus 71	https://doi.org/10.1002/ptr.7084 https://doi.org/10.3390/v12020184
Broussoflavan A	92.4µM(CLpro) 20.4µM(PLpro)	SARS-CoV, MERS-CoV	https://doi.org/10.1007/s11101-020-09720-6 https://doi.org/10.1080/14756366.2016.1265519
Kazinol A	92.4 µM(3CLpro) 66.2 µM (PLpro)	SARS-CoV	https://doi.org/10.1007/s11101-020-09720-6 https://doi.org/10.1080/14756366.2016.1265519

Kazinol B	233.3μM(3CLpro) 31.4 μM (PLpro)	SARS-CoV	https://doi.org/10.1007/s11101-020-09720-6 https://doi.org/10.1080/14756366.2016.1265519
Cyanidin cation	65.1 ± 14.6 μM	SARS-CoV SARS-CoV-2	https://doi.org/10.1016/j.compbiolchem.2020.107408 https://doi.org/10.1016/j.ejpe.2021.01.001
Malvidin	0.04573 μM (SARS-CoV-2)	SARS-CoV SARS-CoV-2	https://doi.org/10.1016/j.csbj.2021.09.022 https://doi.org/10.1016/j.ejpe.2021.01.001
Delphinidin	8.5 μM(DPPH)	SARS-CoV SARS-CoV-2	https://doi.org/10.1016/j.ejpe.2021.01.001
Stachybotrydial (Mer-NF5003F)	4.32 μg/ml	HSV-1	https://doi.org/10.1055/s-2004-832652
Stachyflin	0.003 μM 0.2–0.6 μM	A/WSN/33 virus H1 or H2 subtype influenza	https://doi.org/10.1007/s007050050552
α-Pinene β-myrcene	270μg/ml 200μg/ml	SARS-CoV HSV-1	https://doi.org/10.1002/cbdv.20089045
Limonene	5.9 μg/ml	HSV-1	https://doi.org/10.1016/j.heliyon.2020.e05703
Abietane	1.39μM ($3CL^{pro}$)	SARS-CoV	https://doi.org/10.1021/jm070295s
Norperovskatone Biperovskatone	0.11 mM(HBsAg)/0.18mM (HBeAg) 0.33mM(HBsAg)/0.12 mM (HBeAg)	Hepatitis B Virus	https://doi.org/10.1016/j.tet.2015.04.017
7-β-hydroxydeoxycryptojaponol cryptojaponol	1.15μM Yea >10μM	SARS-CoV	https://doi.org/10.1021/jm070295s
Ferruginol Pinusolidic acid Dehydroabieta-7-one α-cadinol 6,7-dehydroroyleanone	1.39μM 4.71μM 4.00μM 4.44μM	SARS-CoV	https://doi.org/10.1021/jm070295s

	5.55μM		
Jiadifenoic acid J Jiadifenoic acid K Jiadifenoic acid L Jiadifenoic acid M Jiadifenoic acid N Jiadifenoic acid O Jiadifenoic acid P Sesquicaranoic acid A Sesquicaranoic acid B	151.5±14.8μmol/mL 3.9±0.7μmol/mL 48.1±3.1μmol/mL 11.6±1.6μmol/mL 7.0±0.8μmol/mL 20.6±0.04μmol/mL 22.2±2.4μmol/mL 70.3±6.8μmol/mL >37.0μmol/mL	Coxsackievirus B3	https://doi.org/10.1016/j.tet.2014.05.006
Majusanic acid E Majusanic acid F	17.4μM/mL 12.8μM/mL	Coxsackievirus B3	https://doi.org/10.1021/np400638r
Cedrane-3β,1,2-diol 3β,12-diacetoxyabieta-6,8,11.13-tetraene	>10μM 1.57Mm	SARS-CoV	https://doi.org/10.1021/jm070295s
Tanshinone IIA	89.1 ± 5.2μM ($3CL^{pro}$) 1.6 ± 0.5μM(PL^{pro})	SARS-CoV-2 M^{pro} SARS-CoV-2 PL^{pro}	https://doi.org/10.1016/j.bmc.2012.07.038 https://doi.org/10.3390/biom11010074
Methyl tanshinonate	21.1 ± 0.8μM($3CL^{pro}$) 9.2 ± 2.8μM(PL^{pro})		
Tanshinone IIB	24.8 ± 0.8μM ($3CL^{pro}$) 10.7 ± 1.7μM(PL^{pro})		
Cryptotanshinone	226.7 ± 6.2μM ($3CL^{pro}$) 0.8 ± 0.2μM(PL^{pro})		
Rosmariquinone	21.1 ± 0.8μM ($3CL^{pro}$) 30.0 ± 5.5μM(PL^{pro})		
p-Cymene	16μg/ml	HSV-1	https://doi.org/10.1002/ptr.2955 https://doi.org/10.5897/AJB2015.15070
α-Terpinene γ-Terpinene	8.5μg/ml 7μg/ml	HSV-1	https://doi.org/10.1002/ptr.2955

			https://doi.org/10.1039/C6RA02683D
α-Terpineol	22µg/ml	HSV-1	https://doi.org/10.1002/ptr.2955
Saikosaponin A Saikosaponin B2 Saikosaponin D	8.6 ± 0.3 µmol/L 1.7 ± 0.1 µmol/L 13.2±0.3 µmol/L	HCoV-229E	https://doi.org/10.1111/j.1401681.2006.04415.x
Celastrol Pristimerin Tingenone Iguesterin	0.3 µM 5.5 µM 9.9 µM 2.6 µM	SARS-CoV ($3CL^{pro}$)	https://doi.org/10.1016/j.bmcl.2010.01.152
Tereticornate A	0.96 µg/mL	HSV-1	https://doi.org/10.3390/v10070360
β-Caryophyllene	8 ± 3.4 µM 11 ± 4.9 µM	HSV-1 DENV	https://doi.org/10.5530/pj.2018.1.11
Betulonic acid	0.63 µM	SARS-CoV	https://doi.org/10.1021/jm070295s
Betulinic acid	10µM($3CL^{pro}$)	SARS-CoV	https://doi.org/10.1021/jm070295s
Glycyrrhizin	365 µM	SARS-CoV	https://doi.org/10.1021/jm0493008
Lucialdehyde B	0.075µg/ml	HSV	https://doi.org/10.1021/np0501886

Appendix B: Binding energies and protein-ligand interactions residues

Appendix B1: GOLD Fitness Score, binding energies along with interacted residues of S1-RBD.

Compounds	**GOLD Fitness Score**	**Binding Energy (Kcal/mol)**	**Interacting Residues**	**Bond Length (Å)**
Cordifolioside-B (2)	43.06	-9.3	Thr 430 Phe 515	2.8 2.2
Cordioside (3)	40.64	-7.7	Thr 430 Glu 516 Leu 517	2.6/3.7 2.3 2.0/2.9
Cordifolide-A (4)	47.85	-8.9	Asp 428 Thr 430	2.2 2.9
Cordifolide-B (5)	44.45	-9.7	Asp 428 Thr 430	2.0 3.0
Cordifolide-C (6)	42.63	-9.8	Arg 355 Asp 428	3.1 2.1
Tinosporaside (7)	39.92	-9.3	Thr 430 Asp 428	3.5 2.2
Tinosporiside (8)	38.38	-8.4	Arg 355	2.9
Amritoside-A (9)	41.26	-6.8	Thr 430 Glu 516	2.9 2.2
Amritoside-B (10)	50.08	-6.9	Asp 428 Leu 517 Glu 516	2.4 3.5 2.2
Amritoside-C (11)	41.70	-7.2	Glu 516	2.2
Amritoside-D (12)	40.62	-7.3	Glu 516	1.9
Palmitoside-F (13)	46.82	-8.8	Arg 355	3.2
Palmitoside-G (14)	50.80	-	Asp 428	1.9/2.1
Lignan (15)	44.66	-7.7	Phe 464 Arg 355	2.0 3.1
Tinosinenoside-B (17)	48.58	-8.6	Glu 516	1.9
Tinosinenoside-C (18)	44.81	-8.4	Leu 517	2.0
Tinosineside-A (19)	46.20	-8.8	Arg 355 Thr 430 Glu 516	2.9 3.0 2.0
Tinosineside-B (20)	46.90	-8.5	Thr 430	3.9
Borapetoside-A (21)	40.09	-9.2	Thr 430	3.1/3.2

			Asp 428	1.9
Borapetoside-B (22)	53.68	-	Thr 430 Phe 515	3.1 2.2
Rhumphioside-B (25)	43.01	-8.3	Thr 430	2.9
Rhumphioside-C (26)	45.32	-8.3	Thr 430 Phe 515	3.3 2.4

Appendix B2: GOLD Fitness Score and interacted residues of S-RBD with ligands

Compounds	GOLD Fitness Score	Interacting residues	Bond length (Å)
Scutellarein	42.01	Glu 340 Arg 346 Ser 399	2.15 2.20 2.08
Wogonin	36.30	Asn 343	2.02
Luteolin	46.27	Glu 340 Thr 345 Arg 355	2.24 2.19 1.97
Apigenin	48.66	Thr 345 Arg 355	1.87 1.96
Fisetin	46.33	Glu 340 Val 341 Ser 399	4.24 4.55 2.30
Galangin	48.35	Asp 467 Tyr 473	1.79 4.38
Herbacetin	47.02	Ser 371 Trp 436 Asn 437	2.08 2.06 2.08
Morin	42.86	Glu340 Glu 340 Ser 399	2.37 3.15 2.22
Tomentin A	41.32	Phe 342 Thr 345	2.45 4.27
Tometin B	52.18	Gly 339	2.15

		Thr 345 Arg 355	2.41 2.12
Naringenin	42.82	Val 341 Thr 345 Ser 399	4.53 2.04 2.10
Diplacone	45.49	Asn 343 Arg 509	1.97 2.49
Hesperetin	42.78	Ser 371 Ser 373	2.13 2.31
3’-o-Methyldiplacol	45.26	Ser 373	2.13
Bavachinin	42.58	Ser 373 Asn 437	3.75 3.94
Daidzein	45.34	Asp 467 Ser 469 Gln 474	1.96 3.67 2.40
Puerarin	48.12	Ser 371 Asn 437 Asn 440 Leu 441 Leu 441 Arg 509	2.44 2.19 2.20 3.93 3.94 2.29
Silymarin	32.21	Phe 342 Asn 439 Asn 440	1.88 2.31 2.43
Broussoflavan A	47.03	Asn 370 Ser 371 Ser 373	1.97 2.20 4.86
Kazinol B	38.92	Ala 372 Ser 373	3.79 4.52

Appendix B3: PubChem ID and binding affinity of terpenes with spike of SARS CoV-2 omicron variant.

S.N	Compounds	PubChem ID	Binding Affinities (kcal/mol)
			S-RBD
1.	Stachybotrydial	3035835	-7.2
2	Stachyflin	493326	-8.0
3	α-Pinene	6654	-5.4
4	β-myrcene	31253	-5.4
5	Limonene	22311	-5.6
6	Abietane	6857485	-7.3
7	Norperovskatone	-	-6.8
8	Biperovskatone	-	-8.8
9	7-β-hydroxydeoxycryptojaponol	14827260	-7.1
10	cryptojaponol	11724205	-6.8
11	Ferruginol	442027	-7.2
12	Pinusolidic acid	25880646	-7.3
13	Dehydroabieta-7-one		-7.5
14	α-cadinol	6431302	-8.7
15	6,7-dehydroroyleanone	2751794	-7.3
16	Jiadifenoic acid J	102369038	-7.1
17	Jiadifenoic acid K	102369039	-7.8
18	Jiadifenoic acid L	102369040	-7.4
19	Jiadifenoic acid M	-	-7.3
20	Jiadifenoic acid N	90468202	-7.3
21	Jiadifenoic acid O	102369041	-7.1
22	Jiadifenoic acid P	90468203	-7.1
23	Sesquicaranoic acid A	102369042	-6.7
24	Sesquicaranoic acid B	102369043	-6.5
25	Majusanic acid E	72705062	-7.2
26	Majusanic acid F	72705063	-7.3
27	Cedrane-3β,1,2-diol	44427462	-6.7
28	3β,12-diacetoxyabieta-6,8,11.13-tetraene	-	-7.4
29	Tanshinone IIA	164676	-7.6
30	Methyl tanshinonate	14610613	-6.8
31	Tanshinone IIB	9926694	-7.4
32	Cryptotanshinone	160254	-7.6
33	Rosmariquinone	160142	-7.2

34	p-Cymene	7463	-5.6
35	α-Terpinene	7462	-5.6
36	γ-Terpinene	7461	-5.5
37	α-Terpineol	17100	-5.3
38	Saikosaponin A	167928	-8.7
39	Saikosaponin B2	21637642	-9.3
40	Saikosaponin D	107793	-9.1
41	Celastrol	122724	-7.5
42	Pristimerin	159516	-7.3
43	Tingenone	101520	-8.1
44	Iguesterin	46881919	-7.7
45	Tereticornate A	129316505	-9.2
46	β-caryophyllene	20831623	-5.9
47	Betulonic acid	122844	-7.4
48	Betulinic acid	64971	-7.2
49	Glycyrrhizin	14982	-9.1
50	Lucialdehyde B	10343868	-7.3

Appendix C: ADMET properties

Appendix C1: ADMET properties of *Tinospora* sps.

	Parameters	**1**	**2**	**3**	**4**	**5**	**6**	**7**	**8**	**9**	**10**	**11**	**12**	**13**	**14**
Absorption	Water solubility (log mol/L)	-1.965	-2.112	-2.88	-3.504	-3.393	-3.393	-3.079	-3.073	-4.633	-2.704	-3.823	-3.757	-4.819	-2.936
	Ca-co2 permeability (log Papp 10-6 cm/s)	-0.368	-0.613	-0.408	-0.307	0.591	0.591	-0.348	-0.386	1.077	-0.237	1.178	1.267	0.485	-0.404
	Intestinal absorption (% absorbed)	31.087	46.863	52.66	49.384	69.799	69.799	59.506	54.034	94.917	43.031	92.024	95.383	100	57.067
	Skin permeability (log Kp)	-2.735	-2.737	-2.743	-2.737	-2.735	-2.735	-2.919	-2.784	-3.485	-2.735	-3.38	-3.538	-3.203	-2.784
Distribution	VDss (Human, log L/Kg)	0.009	-0.293	-0.515	0.02	-0.003	-0.003	-1.01	-0.673	0.114	-0.73	0.008	0.151	-0.079	-0.611
	BBB Permeability (logBB)	-1.636	-1.884	-1.682	-1.836	-1.435	-1.435	-1.553	-1.348	-0.364	-1.467	-0.653	-0.233	-0.922	-1.384
	CNS Permeability (log PS)	-5.353	-4.946	-4.934	-4.925	-4.591	-4.591	-5.079	-4.194	-2.906	-3.564	-3.017	-2.966	-3.05	-4.273

Metabolism	CYP1A2	NO	NO	NO	NO	NO	NO	NO	NO	NO	NO	NO	NO	NO	NO
	CYP2C19	NO	NO	NO	NO	NO	NO	NO	NO	NO	NO	NO	NO	NO	NO
	CYP2C9	NO	NO	NO	NO	NO	NO	NO	NO	NO	NO	NO	NO	NO	NO
	CYP2D6	NO	NO	NO	NO	NO	NO	NO	NO	NO	NO	NO	NO	NO	NO
	CYP3A4	NO	NO	NO	NO	NO	NO	NO	NO	NO	NO	YES	NO	YES	NO
Excretion	Renal OCT2 substrate clearance	NO	NO	NO	NO	NO	NO	NO	NO	NO	NO	NO	NO	NO	NO
	Total Clearance (logml/min/kg)	0.846	0.768	0.857	0.541	0.574	0.574	0.637	0.605	1.247	0.978	1.058	1.021	0.878	0.755
Toxicity	Ames Toxicity	NO	NO	NO	NO	NO	NO	NO	NO	NO	NO	NO	NO	NO	NO
	Hepatotoxicity	NO	NO	NO	NO	NO	NO	NO	NO	NO	YE	YE	NO	NO	NO
	LD50	2.778	2.949	3.78	3.471	3.003	3.354	3.521	3.113	2.988	2.77	3.718	3.57	3.844	3.354

	Parameters	15	16	17	18	19	20	21	22	23	24	25	26
Absorption	Water solubility (log mol/L)	-5.67	-3.131	-2.763	-2.458	-2.485	-2.485	-2.478	-3.24	-3.252	-3.067	-3.399	-2.44
	Caco2 permeability (log Papp 10-6 cm/s)	1.283	-0.199	-0.285	-0.341	-0.369	-0.369	-0.348	-0.613	-0.568	-0.769	-0.788	-0.672
	Intestinal absorption (% absorbed)	100	60.315	50.062	35.534	43.643	43.643	58.162	61.003	65.794	56.616	62.835	12.633
	Skin permeability (log Kp)	-2.736	-2.736	-2.752	-2.736	-2.736	-2.736	-2.736	-2.759	-2.792	-2.743	-2.747	-2.735
Distribution	VDss (Human, log L/Kg)	-0.73	-0.082	-0.468	-0.192	-0.225	-0.225	-0.005	-0.658	-0.791	-0.401	-0.464	0.236
	BBB Permeability (logBB)	-1.17	-1.625	-1.509	-1.621	-1.705	-1.705	-1.468	-1.687	-1.644	-1.716	-1.934	-2.139
	CNS Permeability (log PS)	-3.273	-4.978	-4.916	-5.053	-5.072	-5.072	-4.859	-4.868	-4.774	-4.949	-4.89	-5.289
Metabolism	CYP1A2	NO	NO	NO	NO	NO	NO	NO	NO	NO	NO	NO	NO
	CYP2C19	YES	NO	NO	NO	NO	NO	NO	NO	NO	NO	NO	NO
	CYP2C9	YES	NO	NO	NO	NO	NO	NO	NO	NO	NO	NO	NO
	CYP2D6	NO	NO	NO	NO	NO	NO	NO	NO	NO	NO	NO	NO
	CYP3A4	YES	NO	NO	NO	NO	NO	NO	NO	NO	NO	YES	NO
Excretion	Renal OCT2 substrate clearance	NO	NO	NO	NO	NO	NO	NO	NO	NO	NO	NO	NO
	Total Clearance (logml/ min/kg)	0.341	0.616	0.755	0.865	0.863	0.863	0.511	0.635	0.646	0.765	0.787	0.923
Toxicity	Ames Toxicity	NO	NO	NO	NO	NO	NO	NO	NO	NO	NO	NO	NO
	Hepatotoxicity	NO	NO	NO	NO	NO	NO	NO	NO	NO	NO	NO	NO
	LD50		3.74	3.68	4.18	4.20	4.50	3.28	3.90	3.99	3.86	3.90	4.08

Appendix C2: ADMET properties of selected flavonoids.

	Parameters	1	2	3	4	5	6	7	8	9	10	11	12
Absor	Water solubility (log mol/L)	-3.168	-3.482	-2.896	-3.129	-3.012	-2.983	-2.893	-2.916	-3.149	-3.066	-3.216	-3.022

	Caco2 permeability (log Papp 10-6 cm/s)	0.213	0.92	-0.651	0.686	-0.115	0.886	0.166	-1.101	-0.167	0.125	0.776	0.217
	Intestinal absorption (% absorbed)	76.061	94.964	31.129	84.776	34.309	91.637	87.367	38.049	30.44	84.659	94.681	72.224
	Skin permeability (log Kp)	-2.735	-2.762	-2.735	-2.735	-2.735	-2.746	-2.735	-2.735	-2.735	-2.735	-2.736	-2.735
Distribution	VDss (Human, log L/Kg)	-0.376	-0.216	-0.736	-0.04	-0.209	-0.176	-1.009	-0.019	0.03	0.018	-0.172	0.075
	BBB Permeability (logBB)	-1.386	0.041	-1.91	-1.291	-2.513	-1.048	-2.206	-2.88	-2.327	-1.23	-1.115	-1.652
	CNS Permeability (log PS)	-2.598	-2.298	-4.637	-2.43	-5.48	-2.247	-3.477	-5.98	-5.327	-2.394	-2.257	-3.542
Metabolism	CYP1A2	Yes	Yes	No	Yes	No	Yes	No	No	No	Yes	Yes	Yes
	CYP2C19	No	Yes	No	No	No	Yes	No	No	No	No	Yes	No
	CYP2C9	Yes	Yes	No	Yes	No	Yes	No	No	No	Yes	Yes	No
	CYP2D6	No	No	No	No	No	No	No	No	No	No	No	No
	CYP3A4	Yes	Yes	No	Yes	No	Yes	No	No	No	Yes	Yes	No
Excretion	Renal OCT2 substrate clearance	No	No	No	No	No	No	No	No	No	No	No	No
	Total Clearance (logml/ min/kg)	0.5	0.4	0.2	0.6	0.5	0,6	0.6	0.1	0.4	0.4	0.3	0.5
Toxicity	Ames Toxicity	No	No	No	No	No	No	No	No	No	No	No	No
	Hepatotoxicity	No	No	No	No	No	No	No	No	No	No	No	No
	Rat Oral Toxicity(LD50)	2.505	2.953	2.452	2.537	2.805	2.406	2.474	2.526	2.897	2.598	2.402	2.343

	Parameters	**13**	**14**	**15**	**16**	**17**	**18**	**19**	**20**	**21**	**22**	**23**	**24**
Absorption	Water solubility (log mol/L)	-2.959	-3.119	-4.156	-4.746	-4.385	-3.338	-4.68	-4.191	-3.592	-3.94	-5.569	-4.186
	Caco2 permeability (log Papp 10-6 cm/s)	0.383	0.896	1.201	1.367	1.114	1.117	1.018	0.939	0.93	0.544	1.107	0.962

	Intestinal absorption (% absorbed)	62.597	70.913	84.425	89.016	77.239	89.969	90.287	84.205	72.766	76.904	94.657	76.952
	Skin permeability (log Kp)	-2.735	-2.735	-2.737	-2.755	-2.735	-2.813	-2.757	-2.736	-2.745	-2.735	-2.892	-2.735
Distribution	VDss (Human, log L/Kg)	0.469	0.299	0.613	0.517	0.851	-	0.159	0.139	-0.07	0.651	0.325	0.664
	BBB Permeability (logBB)	-1.717	-1.573	-1.415	-1.343	-1.396	-1.013	-1.056	-1.287	-1.121	-1.246	-0.145	-1.311
	CNS Permeability (log PS)	-3.726	-3.39	-3.13	-3.034	-3.269	-2.291	-1.995	-2.972	-3.099	-3.109	-1.858	-3.133
Metabolism	CYP1A2	Yes	Yes	No	No	No	Yes	No	No	Yes	No	Yes	No
	CYP2C19	Yes	No	No	No	No	Yes	Yes	Yes	Yes	No	Yes	No
	CYP2C9	No	No	No	Yes	No	No	Yes	Yes	No	No	Yes	No
	CYP2D6	No	No	No	No	No	No	No	No	No	No	No	No
	CYP3A4	No	No	No	Yes	No	No	Yes	No	No	No	Yes	No
Excretion	Renal OCT2 substrate clearance	No	No	No	No	No	No	No	No	No	No	No	No
	Total Clearance (logml/ min/kg)	0.612	0.681	0.117	0.205	0.163	0.08	0.683	0.389	0.141	0.422	0.148	0.467
Toxicity	Ames Toxicity	No	No	No	No	Ye	No	No	No	Ye	No	No	No
	Hepatotoxicity	No	No	No	No	xx	No	No	No	No	No	No	No
	Rat Oral Toxicity (LD50)	2.167	2.019	2.795	2.815	2.655	1.882	2.338	2.271	2.258	2.323	2.343	2.411

	Parameters	**25**	**26**	**27**	**28**	**29**	**30**	**31**	**32**	**33**	**34**	**35**	**36**
Absorption	Water solubility (log mol/L)	-3.325	-4.92	-3.494	-4.242	-2.935	-3.008	-4.134	-4.898	-5.418	-3.155	-3.402	-2.888
	Caco2 permeability (log Papp 10-6 cm/s)	1.027	0.542	-0.099	0.712	-0.758	0.456	1.3033	0.78	1.264	-0.067	0.338	-0.217
	Intestinal absorption (% absorbed)	92.844	93.342	55.931	94.31	45.948	61.337	79.885	89.342	90.849	80.203	71.558	72.936

	Skin permeability (log Kp)	-2.812	-2.752	-2.735	-2.778	-2.735	-2.735	-2.736	-2.798	-3.042	-2.735	-2.736	-2.735
Distribution	VDss (Human, log L/Kg)	-0.199	0.196	-0.176	0.167	0.071	0.273	0.494	0.232	0.745	-0.295	0.206	0.403
	BBB Permeability (logBB)	-0.154	-0.136	-1.762	-0.09	-2.361	-1.757	-0.964	-0.92	-0.034	-1.357	-1.56	-1.677
	CNS Permeability (log PS)	-1.974	-1.707	-4.072	-1.807	-4.304	-3.711	-2.781	-1.815	-1.534	-2.372	-3.255	-3.311
Metabolism	CYP1A2	Yes	Yes	No	Yes	Yes	No	No	Yes	No	Yes	Yes	Yes
	CYP2C19	Yes	Yes	No	Yes	No	No	Yes	Yes	Yes	Yes	No	No
	CYP2C9	Yes	Yes	No	Yes	No	No	Yes	Yes	Yes	Yes	Yes	Yes
	CYP2D6	No	No	No	No	No	No	No	No	No	No	No	No
	CYP3A4	No	Yes	No	Yes	No	No	No	Yes	Yes	Yes	Yes	No
Excretion	Renal OCT2 substrate clearance	No	No	No	No	No	No	No	No	No	No	No	No
	Total Clearance (logml/ min/kg)	0.20	0.30	0.14	0.24	0.45	0.05	0.37	0.54	0.38	0.65	0.81	0.65
Toxicity	Ames Toxicity	Yes	No	No	No	Yes	Yes	No	No	No	Yes	No	Yes
	Hepatotoxicity	No	No	Yes	No	No	No	Yes	No	No	No	No	No
	Rat Oral Toxicity (LD50)	1.933	1.926	3.047	2.077	2.823	2.631	2.641	2.028	2.273	2.662	2.393	2.792

Appendix C3: ADMET Profiles of terpenes.

Compounds	**Absorption**	**Distribution**	**Metabolism**	**Excretion**	**Toxicity**

Rat Oral Toxicity (LD 50)	2.3	2.455	1.738	1.643	1.848	2.104	1.904	2.822	2.22	2.191
Hepato Toxicity	NO	YES	NO	NO	NO	NO	No	Yes	No	No
Ames Toxicity	NO	NO	NO	NO	NO	No	No	No	No	No
Renal OCT2 substrate clearance	NO	NO	NO	NO	NO	No	No	No	No	No
Total clearance	0.409	0.196	0.043	0.438	0.213	0.625	0.979	-0.804	0.511	0.474
CYP3A4	NO	NO	NO	NO	NO	Yes	No	Yes	No	Yes
CYP2D6	NO	NO	NO	NO	NO	No	No	No	No	No
CYP2C9	NO	NO	NO	NO	NO	No	No	No	Yes	No
CYP2C19	NO	NO	NO	NO	NO	No	No	No	Yes	Yes
CYP1A2	NO	NO	NO	NO	NO	Yes	No	No	Yes	Yes
CNS permeability (log PS)	-1.978	-1.879	-2.181	-1.902	-2.37	-0.932	-2.635	-2.059	-1.517	-1.554
BBB permeability(log BB)	-0.175	-0.442	0.788	0.781	0.723	0.868	0.301	-0.304	-0.199	0.16
VDss(Human, log L/kg)	0.607	0.921	0.666	0.363	0.396	0.33	0.236	0.011	0.377	0.46
Skin permeability(log Kp)	-3.431	-3.077	-1.796	-1.043	-1.721	-2.626	-3.126	-2.739	-3.18	-2.891
Intestinal absorption(% absorbed)	91.986	92.85	95.123	94.696	95.89	95.997	97.93	96.904	91.69	91.86
Caco-2 Permeability(log Papp 10-	1.206	1.158	1.374	1.4	1.397	1.412	1.387	1.443	1.433	1.481
Water solubility(log mol/L)	-4.243	-3.617	-3.772	-4.497	-3.568	-6.636	-3.597	-4.084	-5.187	-5.391
Compounds	1.Stachybotrydial	2.Stachyflin	3.α-Pinene	4.β-myrcene	5.Limonene	6.Abietane	7.Norperovskatone	8.Biperovskatone	9.7-β-hydroxyde oxycryptojaponol	10.Cryptojaponol

2.491	2.209	2.175	1.631	1.809	3.01	2.529	2.387	1.952	2.127	2.257	1.869	1.727
No	No	No	No	No	No	No	No	No	No	No	No	No
No	NO	No	No	No	No	No	No	No	No	No	No	No
N0	No	No	No	YES	No	No	No	No	No	No	No	No
0.688	1.047	0.91	1.085	0.857	0.7	0.762	0.83	0.995	0.729	0.771	0.965	1.083
Yes	Yes	No	No	NO	No	No	No	No	No	No	No	No
No	No	NO	No	NO	No	No	No	No	No	No	No	No
No	NO	No	Yes	NO	No	No	No	No	No	No	No	No
YES	NO	Yes	Yes	No	No	No	No	No	No	No	No	No
YEs	No	Yes	No	No	No	No	No	No	No	No	No	No
-1.06	-1.988	-1.349	-2.299	-1.626	-2.351	-2.36	-1.956	-2.015	-2.33	-2.052	-2.166	-3.419
0.609	0.002	0.595	0.595	0.145	-0.566	0.002	-0.089	0.025	-0.595	-0.362	0.057	-0.758
0.675	-1.048	0.914	0.478	0.067	-1.168	-0.499	-1.577	-1.38	-1.286	-1.522	-1.074	-1.066
-2.732	-2.727	-2.144	-1.882	-3.523	-2.733	-2.721	-2.73	-2.735	-2.731	-2.735	-2.735	-2.73
92.88	100	94.912	92.89	93.442	99.14	97.488	100	99.446	97.80	100	98.886	93.141
1.274	0.739	1.257	1.496	1.384	0.934	1.419	0.995	0.9	0.806	1.006	0.842	0.941
-5.609	-3.346	-6.512	-4.347	-4.806	-3.297-	-3.918	-3.295	-2.583	-2.924	-3.023	-2.465	-2.334
11.Ferruginol	12.Pinusolidic acid	13.Dehydroabieta-7-one	14.α-cadinol	15.6,7-dehydroroyleanone	16.Jiadifenoic acid J	17.Jiadifenoic acid K	18.Jiadifenoic acid L	19.Jiadifenoic acid M	20.Jiadifenoic acid N	21.Jiadifenoic acid O	22.Jiadifenoic acid P	23.Sesquicaranoic acid A

1.727	2.739	2.739	1.651	2.195	2.488	2.536	2.476	1.976	2.071	1.704	1.766
No	No	No	No	No	YES	NO	YES	No	No	NO	No
No	No	No	No	No	NO	NO	YES	No	No	NO	No
No	No	No	No	No	NO	NO	NO	No	No	NO	No
1.083	0.825	0.825	0.913	0.66	0.822	0.962	0.181	0.85	0.98	O.239	0.223
No	No	No	No	No	NO	NO	NO	Yes	No	NO	No
No	No	No	No	No	NO	NO	NO	No	No	NO	NO
No	No	No	No	No	YES	YES	YES	No	No	NO	No
No	No	No	No	Yes	YES	YES	YES	Yes	Yes	NO	No
No	Yes	Yes	No	Yes	YES	YES	YES	Yes	Yes	YES	No
-3.419	-1.995	-1.995	-2.484	-1.241	-1.462	-1.754	-1.933	-1.894	-1.776	-1.349	-2.049
-0.758	-0.022	-0.022	0.112	0.713	0.31	-0.146	-0.07	0.284	0.145	0.471	0.754
-1.066	-0.894	-0.894	0.356	1.086	0.612	0.419	0.544	0.614	0.386	0.611	0.412
-2.73	-2.732	-2.732	-3.02	-2.184	-2.341	-2.524	-2.903	-2.728	-2.486	-1.03	-1.489
93.141	99.26	99.26	93.276	94.352	97.04	98.161	96.336	97.189	98.792	93.613	96.219
0.941	1.274	1.274	1.592	1.368	1.382	1.094	1.092	1.327	1.157	1.532	1.414
-2.334	-3.385	-3.385	-3.415	-6.711	-4.911	-4.7	-4.066	-4.559	-4.583	-4.073	-3.941
24.Sesquicaranoic acid B	25.Majusanic acid E	26.Majusanic acid F	27.Cedrane-3beta, 12-diol	28.3ß,12-diacetoxyabieta-6,8,11.13-tetraene	29.Tanshinone IIA	30.Methyl Tanshionate	31.Tanshinone IIB	32.Cryptotanshinone	33.Rosmariquinone	34.p-Cymene	35.α- Terpinene

1.766	1.923	3.099	2.946	3.099	2.617	2.501	2.259	2.084	2.416	1.678	2.236	2.185
NO	NO	NO	NO	NO	YES	No	No	YES	No	NO	NO	NO
NO	NO	NO	NO	NO	NO	No	No	NO	No	NO	NO	NO
NO	NO	NO	NO	NO	NO	No	No	NO	No	NO	NO	NO
0.217	1.219	0.06	0.18	0.06	-0.09	-0.03	0.064	0.106	-0.49	1.088	0.064	0.124
NO	NO	NO	NO	NO	NO	No	No	NO	No	NO	NO	NO
NO	NO	NO	NO	NO	NO	No	No	NO	No	NO	NO	NO
NO	NO	NO	NO	NO	NO	No	No	NO	No	NO	NO	NO
NO	NO	NO	NO	NO	NO	No	No	NO	No	NO	NO	NO
-2.049	-2.807	-4.102	-4.19	-4.102	-1.263	-1.183	-1.014	-2.06	-1.917	-2.182	-1.144	-1.624
0.754	0.305	-1.404	-1.504	-1.404	0.172	0.071	0.134	0.336	-0.301	0.74	-0.25	0.07
0.412	0.207	-0.668	-0.927	-0.668	-1.321	-0.33	0.002	0.365	-0.094	0.653	-1.395	-1.16
-1.489	-2.418	-2.735	-2.735	-2.735	-2.735	-2.999	-2.875	-3.067	-2.747	-1.596	-2.735	-2.735
96.219	94.183	44.601	34.463	44.60	99.871	94.962	95.636	94.247	95.381	95.304	100	99.229
1.414	1.489	0.386	-0.708	0.386	0.504	0.563	1.445	1.339	0.613	1.434	1.402	0.447
-3.941	-2.039	-3.818	-3.598	-3.818	-3.188	-6.152	-5.558	-6.609	-4.891	-5.534	-3.169	-3.276
36.γ- Terpinene	37.α- Terpineol	38.Saikosaponin A	39.Saikosaponin B2	40.Saikosaponin D	41.Celastrol	42.Pristimerin	43.Tingenone	44.Iguesterin	45.Tereticornate A	46.β- Caryophyllene	47.Betulonic acid	48.Betulinic acid

49.glycyrrhizin	-2.892	-0.774	0	-2.735	-0.648	-1.562	-3.822	NO	NO	NO	NO	NO	-0.288	NO	-2.479
50.Lucialdehyde B	-5.622	1.501	98.581	-2.65	-0.087	-0.311	-1.284	NO	NO	NO	NO	NO	0.352	NO	1.893

Appendix D: Prediction of toxicity using ProTox II

Appendix D1: Prediction of toxicity of secondary metabolites inhibiting metabolic enzymes using ProTox-II

Compound	LD50mg/Kg	Toxicity class	Probability
Cordifolioside-A (1)	4000	5	0.99
Cordifolioside-B (2)	4000	5	0.99
Cordioside (3)	274	3	0.96
			0.76
Cordifolide-A (4)	244	4	0.99
			0.71
			0.74
.Cordifolide-B (5)	500	4	0.99
			0.79
			0.76
			0.81
Cordifolide-C (6)	500	4	0.99
			0.79
			0.76
			0.81
Tinosporaside (7)	274	3	0.99
Tinosporiside (8)	280	3	0.96
Amritoside-A (9)	274	3	0.97
Amritoside-B (10)	244	3	-
Amritoside-C (11)	555	4	0.96
			0.79
			0.83
			0.72
Amritoside-D (12)	274	3	0.96
			0.75
			0.73
			0.77
Palmitoside-F (13)	310	3	0.99
Palmitoside-G (14)	274	3	0.98
Lignan (15)	4000	5	0.94
Tinosinenoside-A (16)	274	3	0.99
			0.73
			0.74

			0.75
Tinosinenoside-B (17)	274	3	0.98
			0.73
			0.74
			0.75
Tinosinenoside-C (18)	244	3	0.99
			0.73
			0.75
			0.74
			0.81
Tinosineside-A (19)	244	3	0.99
			0.73
			0.75
			0.74
			0.81
Tinosineside-B (20)	244	3	0.99
			0.70
			0.73
			0.80
Borapetoside-A (21)	244	3	0.99
			0.73
Borapetoside-B(22)	555	4	0.99
Borapetoside-C (23)	555	4	0.99
			0.78
Rumphioside-A (24)	50	2	0.99
			0.87
Rumphioside-B (25)	50	2	0.99
			0.87
Rumphioside-C (26)	2000	4	0.99
			0.87
Remdesivir (Commercial drug)	1000	4	-

Appendix D2: Prediction of toxicity of flavonoids inhibiting metabolic enzymes using ProTox-II.

Compound	**LD_{50} mg/Kg**	**Toxicity class**	**Probability**
Scutellarein(1)	3919	5	0.91 0.87 0.95 1.0
Wogonin(2)	3919	5	0.97 0.88 0.89 0.92
Baicalin(3)	5000	5	-
Luteolin(4)	3919	5	0.91 0.87 0.95
Pectolinarin(5)	5000	5	1.0 0.99
Apigenin(6)	2500	5	1.0 1.0
Amentoflavone(7)	3919	5	1.0 1.0
Rutin(8)	5000	5	1.0 1.0
Rhoifolin(9)	5000	5	0.96 0.83
Fistein (10)	159	3	0.78 0.77
Galangin(11)	3919	5	0.98 0.91
Herbacetin(12)	3919	5	0.71 0.84
Myricetin(13)	159	3	0.86 0.82
Morin(14)	3919	5	1.0 1.0
Tomentin A(15)	2000	4	0.95 1.0
Tomentin B(16)	2000	4	0.96 0.91

Tomentin E(17)	10000	6	0.87
			0.95
Naringenin(18)	2000	4	1.0
			0.91
Mimulone(19)	2000	4	0.87
			0.95
Diplacone (20)	2000	4	1.0
			1.0
Hesperetin(21)	2000	4	0.96
			1.0
3’-O-Methyl Diplacol (22)	2000	4	0.95
			1.0
Bavachinin(23)	2000	4	0.99
			0.99
4’-O-Methyl Diplacol (24)	2000	4	0.99
			0.74
Daidzein(25)	2430	5	0.74
			-
Corylifol A(26)	2500	5	0.76
			0.90
Puerarin(27)	382	4	0.94
			0.91
Neobavaisoflavone(28)	2500	5	0.94
			1.0
Epigallocatechin gallate (29)	1000	4	0.71
			1.0
Silymarin(30)	2000	4	1.0
			0.91
Broussoflavan A(31)	2500	5	1.0
			0.95
Kazinol A(32)	2500	5	0.70
			-
Kazinol B(33)	500	4	0.96
			0.76
Cyanidin (34)	5000	5	-
			0.97
Malvidin(35)	5000	5	0.99
			0.94
Delphinidin(36)	5000	5	0.87
			0.99

			0.79 0.92 0.82 0.83 0.79 0.92

Appendix D3: Prediction of toxicity class of terpenes using ProTox-II.

Compounds	LD50 mg/kg	Toxicity class	Probability
Stachybotrydial	1740	4	0.96
Stachyflin	4000	5	0.79
α-Pinene	3700	5	-
β-myrcene	5000	5	1.0 1.0
Limonene	4400	5	-
Abietane	15380	6	-
Norperovskatone	900	4	0.83
Biperovskatone	1100	4	0.99
7β-hydroxydeoxycryptojaponol	5010	6	0.78
Cryptojaponol	1180	4	-
Ferruginol	2000	4	0.72
Pinusolidic acid	34	2	-
Dehydroabieta-7-one	1190	4	-
α-cadinol	2830	5	-
6,7-dehydroroyleanone	900	4	-
Jiadifenoic acid J	1270	4	
Jiadifenoic acid K	2148	5	
Jiadifenoic acid L	570	4	
Jiadifenoic acid M	9000	6	
Jiadifenoic acid N	2000	4	
Jiadifenoic acid O	500	4	0.87
Jiadifenoic acid P	560	4	
Sesquicaranoic acid A	9000	6	
Sesquicaranoic acid B	9000	6	
Majusanic acid E	1200	4	

Majusanic acid F	1200	4	
Cedrane-3β,1,2-diol	2000	4	-
3β,12-diacetoxyabieta-6,8,11.13-tetraene	547	4	0.79
Tanshinone IIA	1230	4	-
Methyl tanshinonate	1230	4	-
Tanshinone IIB	1230	4	-
Cryptotanshinone	8000	6	0.96
Rosmariquinone	1400	4	-
p-Cymene	3	1	-
α-Terpinene	1680	4	-
γ-Terpinene	2500	5	-
α-Terpineol	2830	5	-
Saikosaponin A	2000	4	0.99
Saikosaponin B2	4000	5	0.99
Saikosaponin D	2000	4	0.99
Celastrol	2000	4	0.73
Pristimerin	8000	6	0.78
Tingenone	2000	4	0.88
Iguesterin	2000	4	0.97
Tereticornate A	3800	5	0.99
β-caryophyllene	1190	4	0.96 1.00 0.99 1.0
Betulonic acid	2610	5	-
Betulinic acid	2150	5	0.88
Glycyrrhizin	1190	4	0.99
Lucialdehyde B	2300	5	0.88 0.79 0.73

Appendix E: Drug-like properties

Appendix E1: Drug-like properties of selected flavonoids designed to inhibit SARS-CoV-2 by SwissADME server

S.N.	Compound	MW (g/mol)	Log p	HBA	HBD	TPSA (Å²)	RB	Molar refractivity	No. of heavy atoms
1.	Scutellarein	286.24	2.08	6	4	111.13	1	76.01	21
2.	Wogonin	284.26	2.55	5	2	79.90	2	78.46	21
3.	Baicalin	446.36	1.58	11	6	187.12	4	106.72	32
4	Luteolin	286.24	1.86	6	4	111.13	1	76.01	21
5.	Pectolinarin	622.57	3.41	15	7	227.20	8	148.29	44
6.	Apigenin	270.24	1.89	5	3	90.90	1	73.99	20
7.	Amentoflavone	538.46	3.06	10	6	181.80	3	146.97	40
8.	Rutin	610.52	0.46	16	10	269.43	6	141.38	43
9.	Rhoifolin	578.52	-0.64	14	8	228.97	6	137.33	41
10.	Fisetin	286.24	1.55	6	4	111.13	1	76.01	21
11.	Galangin	270.24	2.08	5	3	90.90	1	73.99	20
12.	Herbacetin	302.24	1.50	7	5	131.36	1	78.03	22
13.	Myricetin	318.24	0.79	8	6	151.59	1	80.06	23
14.	Morin	302.24	1.20	7	5	131.36	1	78.03	22
15.	Tomentin A	442.50	3.59	7	4	116.45	5	120.61	32
16.	Tomentin B	456.53	3.98	7	3	105.45	6	125.08	33
17.	Tomentin E	472.53	3.24	8	4	125.68	6	126.24	34
18.	Naringenin	272.25	1.84	5	3	86.99	1	71.57	20
19.	Mimulone	408.49	4.80	5	3	86.99	6	118.85	30
20.	Diplacone	424.49	4.42	6	4	107.22	6	120.87	31

21.	Hesperetin	302.28	1.91	6	3	96.22	2	78.06	22
22.	3’-o-methyldiplacol	454.51	4.07	7	4	116.45	7	126.51	33
23.	Bavachinin	338.40	3.92	4	1	55.76	4	97.74	25
24.	4’-o-methyldiplacol	454.51	4.32	7	4	116.45	7	126.51	33
25.	Daidzein	254.24	1.77	4	2	70.67	1	71.97	19
26.	Corylifol A	390.47	5.15	4	2	70.67	6	119.25	29
27.	Puerarin	416.38	0.23	9	6	160.82	3	104.59	30
28.	Neobavaisoflavone	322.35	3.74	4	2	70.67	3	95.69	24
29.	Epigallocatechin gallate	458.37	1.53	11	8	197.37	4	112.06	33
30.	Silymarin	482.44	1.59	10	5	155.14	4	120.55	57
31.	Broussoflavan A	426.50	3.42	6	4	99.38	3	118.97	31
32.	Kazinol A	394.50	5.09	4	3	69.92	5	118.59	59
33.	Kazinol B	392.49	4.93	4	2	58.92	3	116.97	57
34.	Cyanidin	287.24	0.56	6	5	114.29	1	76.17	32
35.	Malvidin	331.30	0.71	7	4	112.52	3	87.13	39
36.	Delphinidin	303.24	0.13	7	6	134.52	1	78.20	33

Appendix E2: Drug-Likeness properties of terpenes.

Compounds	No. of Rotatable Bonds	TPSA (Å^2)	Log p	Molar refractivity	Druglikeness(Lipinski)
Stachybotrydial	2	83.83	3.32	107.53	Yes; 0 violation
Stachyflin	0	78.79	3.24	111.71	Yes; 0 violation
α-Pinene	0	0.00	3.44	45.22	Yes; 1 violation
β-myrcene	4	0.00	3.43	48.76	Yes; 0 violation
Limonene	1	0.00	3.35	47.12	Yes; 0 violation
Abietane	1	0.00	6.14	91.39	Yes; 1 violation
Norperovskatone	2	43.37	3.10	83.09	Yes; 0 violation
Biperovskatone	2	85.22	6.88	181.70	No; 2 violations
7-β-hydroxydeoxycryptojaponol	2	49.69	4.37	99.29	Yes; 0 violation
Cryptojaponol	2	46.53	4.61	98.55	Yes; 0 violation
Ferruginol	1	20.23	5.26	91.64	Yes; 1 violation
Pinusolidic acid	4	63.60	3.76	93.50	Yes; 0 violation
Dehydroabieta-7-one	1	17.07	5.03	90.03	Yes; 1 violation
α-cadinol	1	20.23	3.43	70.72	Yes; 0 violation
6,7-dehydroroyleanone	1	54.37	3.64	91.94	Yes; 0 violation
Jiadifenoic acid J	3	77.76	2.80	93.59	Yes; 0 violation
Jiadifenoic acid K	2	46.53	4.18	93.06	Yes; 0 violation
Jiadifenoic acid L	4	142.88	4.87	174.84	Yes; 1 violation
Jiadifenoic acid M	2	74.60	3.00	93.32	Yes; 0 violation
Jiadifenoic acid N	3	77.76	2.97	94.75	Yes; 0 violation
Jiadifenoic acid O	2	66.76	2.75	84.46	Yes; 0 violation
Jiadifenoic acid P	1	74.60	2.41	79.63	Yes; 0 violation
Sesquicaranoic acid A	5	77.76	1.92	73.39	Yes; 0 violation
Sesquicaranoic acid B	5	77.7	1.91	73.39	Yes; 0 violation
Majusanic acid E	3	57.53	3.55	92.55	Yes; 0 violation
Majusanic acid F	3	57.53	3.57	92.55	Yes; 0 violation
Cedrane-3β,1,2-diol	1	40.46	2.73	69.72	Yes; 0 violation
3β,12-diacetoxyabieta-6,8,11.13-tetraene	5	52.60	4.90	112.33	Yes: 1 violation
Tanshinone IIA	0	47.28	3.80	84.70	Yes; 0 violation
Methyl tanshinonate	1	64.35	3.24	89.71	Yes; 0 violation
Tanshinone IIB	1	67.51	4.75	85.86	Yes; 0 violation

Cryptotanshinone	0	43.37	3.43	85.13	Yes;0 violation
Rosmariquinone	1	34.14	4.04	86.16	Yes;0 violation
p-Cymene	1	0.00	3.50	45.99	Yes; 1 violation
α-Terpinene	1	0.00	3.30	47.12	Yes;0 violation
γ-Terpinene	1	0.00	3.35	47.12	Yes;0 violation
α-Terpineol	1	20.23	2.58	48.80	Yes;0 violation
Saikosaponin A	6	207.99	1.78	199.82	No; 3 violations
Saikosaponin B2	7	218.99	1.86	201.50	No; 3 violations
Saikosaponin D	6	207.99	2.05	199.82	No; 3 violations
Celastrol	1	74.60	5.12	131.29	Yes; 1 violation
Pristimerin	2	63.60	5.58	135.61	Yes; 1 violation
Tingenone	0	54.37	5.07	125.18	Yes; 1 violation
Iguesterin	0	37.30	5.69	124.50	Yes; 1 violation
Tereticornate A	5	82.06	7.33	182.22	No; 2 violations
Beta-caryophyllene	0	0.00	4.24	68.78	Yes; 0 violation
Betulonic acid	2	54.37	6.17	135.95	Yes; 1 violation
Betulinic acid	2	74.60	5.13	132.78	Yes; 1 violation
Glycyrrhizin	7	267.04	1.49	202.84	No; 3 violations
Lucialdehyde B	5	51.21	5.98	136.48	Yes; 1 violation

Appendix F: Chemdraw structures and 2D and 3D structures of secondary metabolites

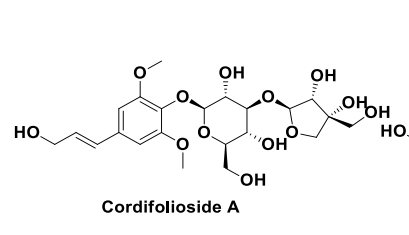
Cordifolioside A

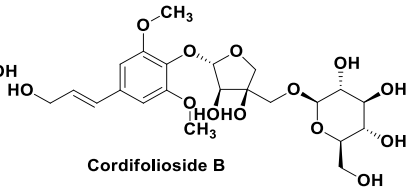
Cordifolioside B

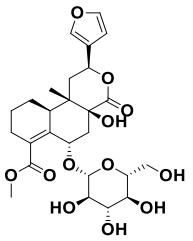
Cordioside

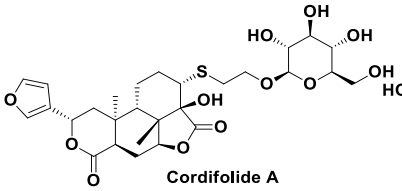
Cordifolide A

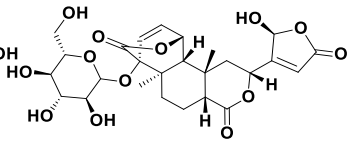
Cordifolide B

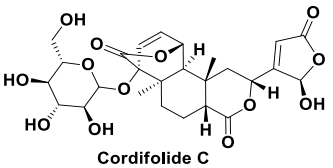
Cordifolide C

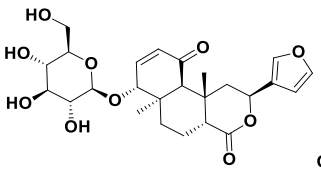
Tinosporaside

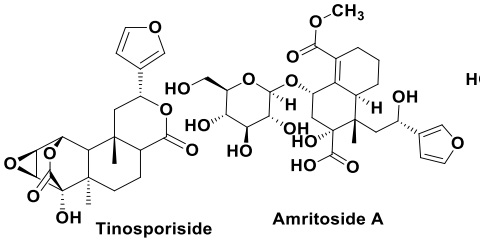
Tinosporiside

Amritoside A

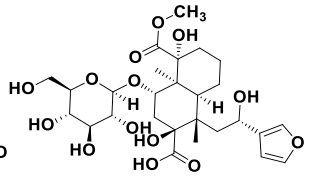
Amritoside B

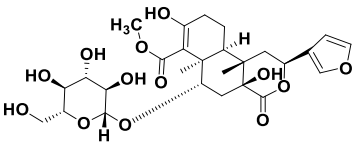
Amritoside C

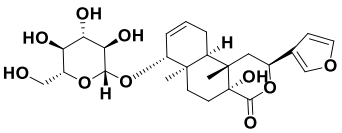
Amritoside D

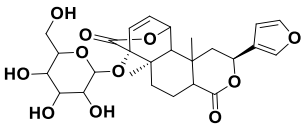
Palmitoside F

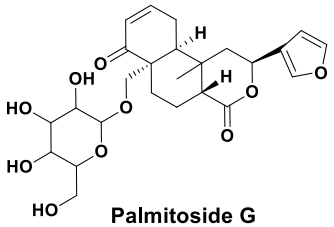

Palmitoside G

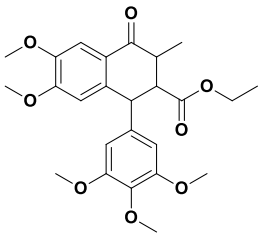

Lignan

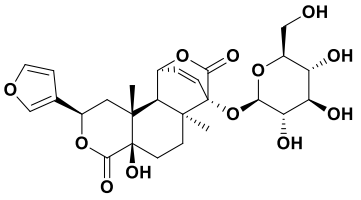

Tinosinenoside A

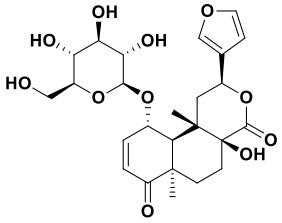

Tinosinenoside B

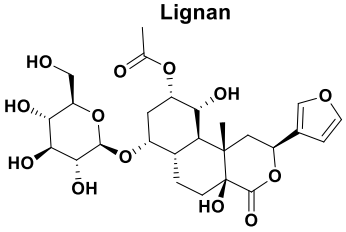

Tinosinenoside C

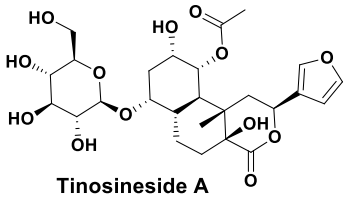

Tinosineside A

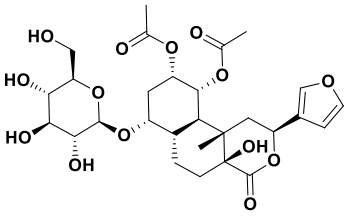

Tinosineside B

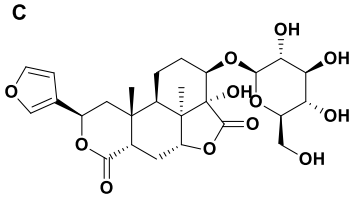

Borapetoside A

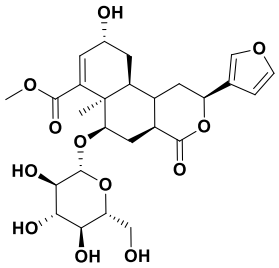

Borapetoside B

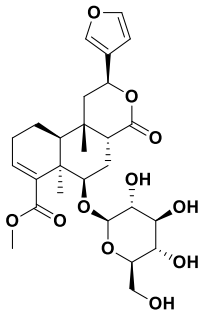

Borapetoside C

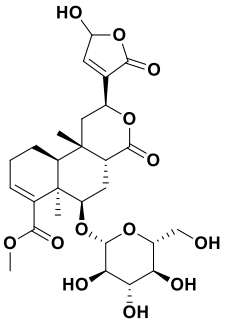

Rumphioside A

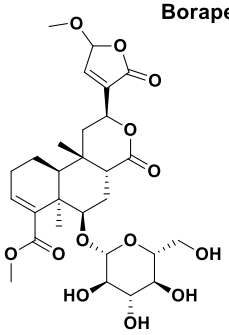

Rumphioside B

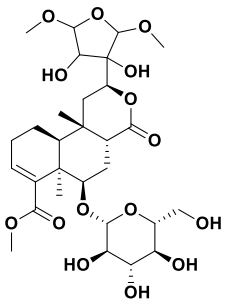

Rumphioside C

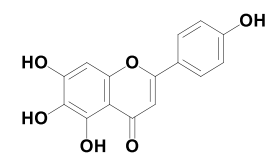

Scutellarein

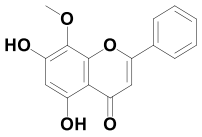

Wogonin

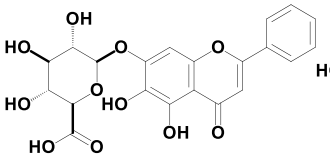

Baicalin

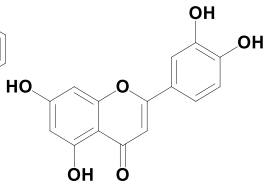

Luteolin

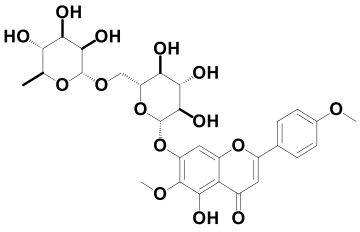

Pectolinarin

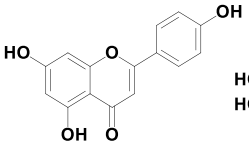

Apigenin

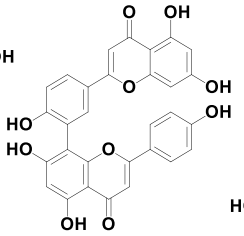

Amentoflavone

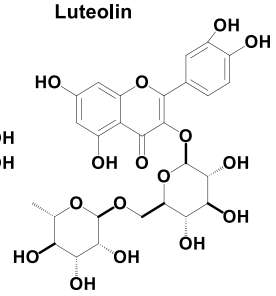

Rutin

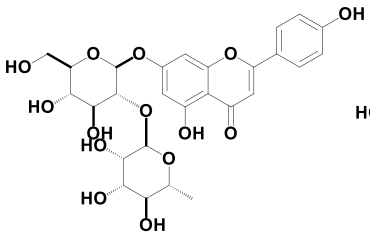

Rhoifolin

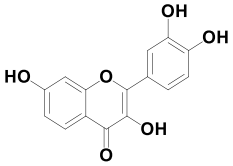

Fisetin

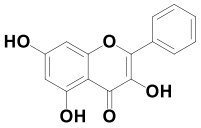

Galangin

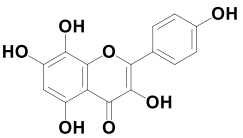

Herbacetin

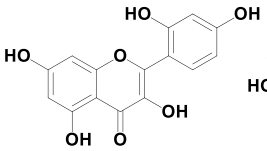

Morin

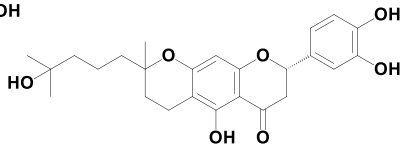

Tomentin A

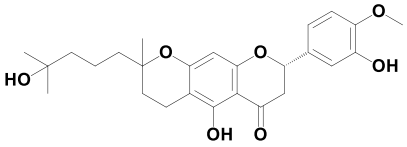

Tomentin B

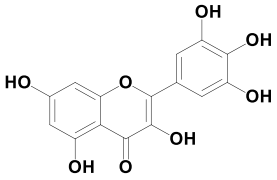

Myricetin

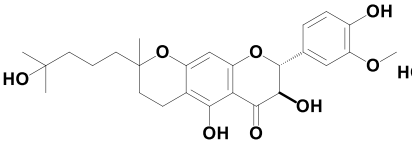

Tomentin E

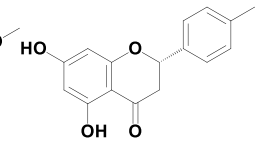

Naringenin

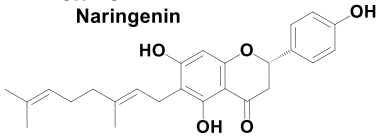

Mimulone

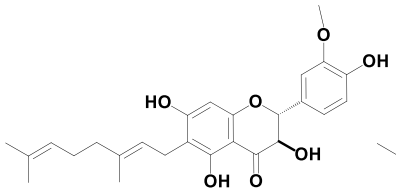

3'-O-Methyldiplacol

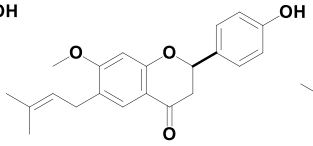

Bavachinin

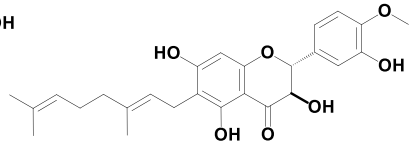

4'-O-Methyldiplacol

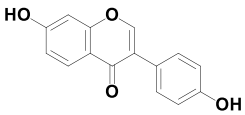

Daidzein

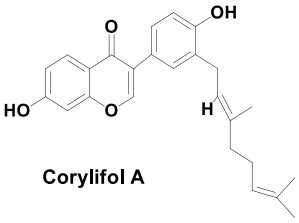

Corylifol A

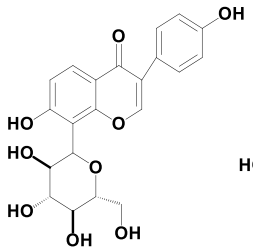

Puerarin

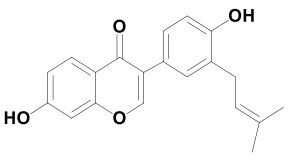

Neobavaisoflavone

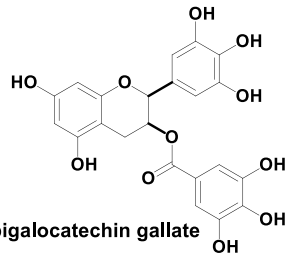

Epigalocatechin gallate

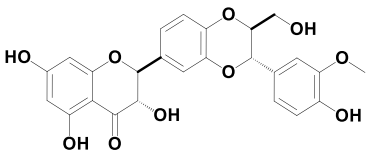

Silymarin

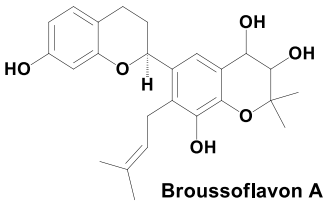

Broussoflavon A

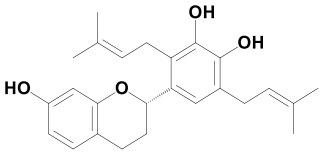

Kazinol A

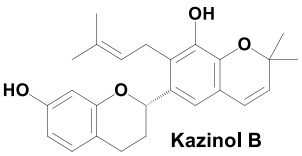

Kazinol B

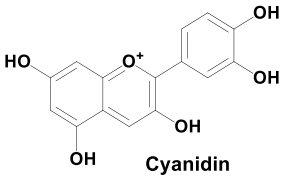

Cyanidin

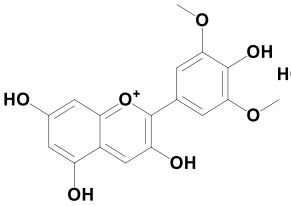

Malvidin

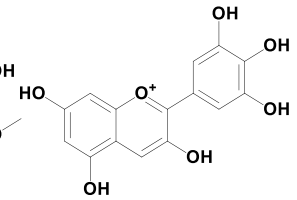

Delphinidin

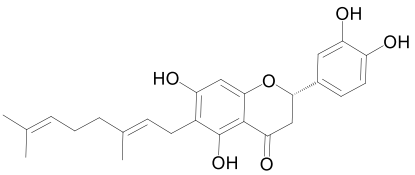

Diplacone

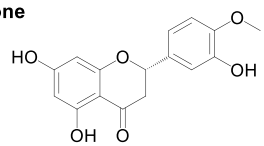

Hesperetin

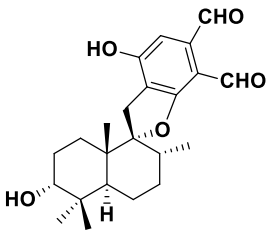

Stachybotrydial (Mer-NF5003F)

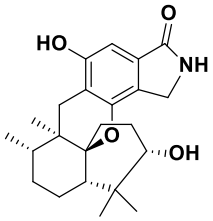

Stachyflin

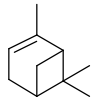

α–pinene

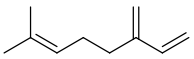

ß-myrcene

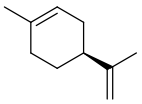

Limonene

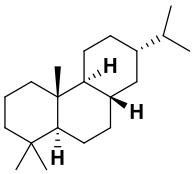

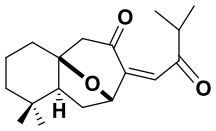

Norperovskatone

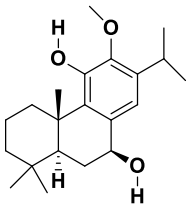

7ß-hydroxydeoxycryptojaponol

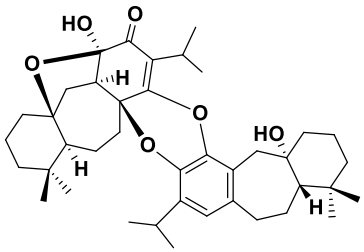

Biperovskatone

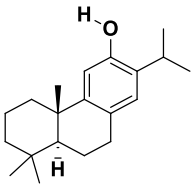

Ferruginol

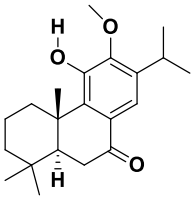

cryptojaponal

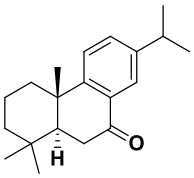

dehydroabieta-7-one

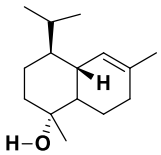

α-cadinol

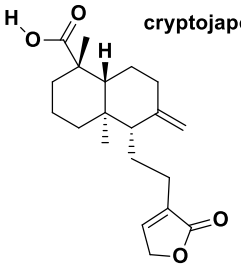

Pinusolidic acid

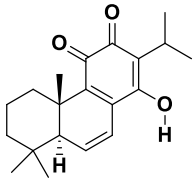

6,7-dehydroroyleanone

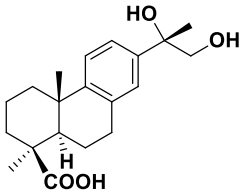

Jiadifenoic acid J

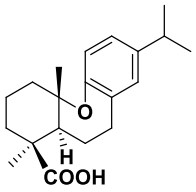

Jiadifenoic acid K

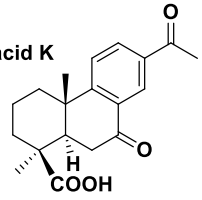

Jiadifenoic acid L

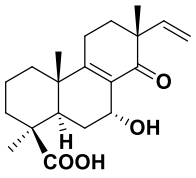

Jiadifenoic acid M

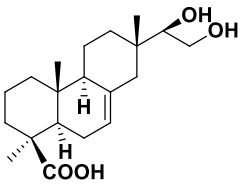

Jiadifenoic acid N

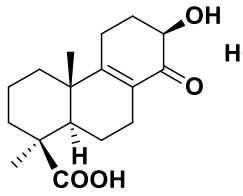

Jiadifenoic acid P

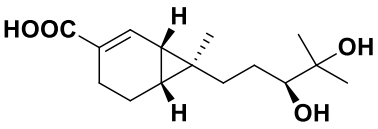

Sesquicaranoic acid A

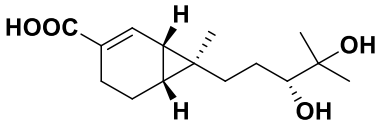

Sesquicaranoic acid B

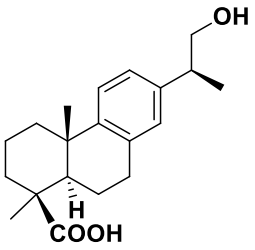

Majusanic acid E

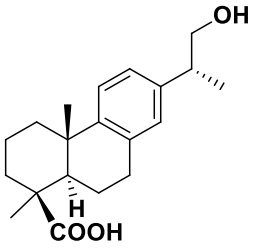

Majusanic acid F

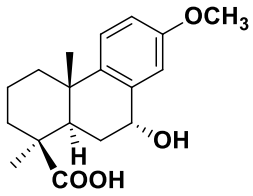

Jiadifenoic acid O

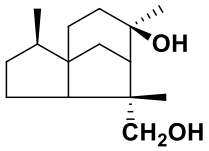

Cedrane-3beta,12-diol

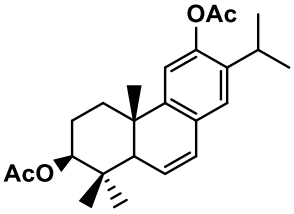

3ß,12-diacetoxyabieta-6,8,11.13-tetraene

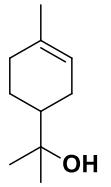

α-Terpineol

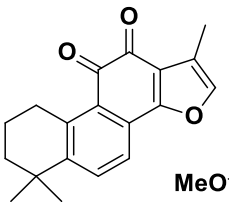

Tanshinone IIA

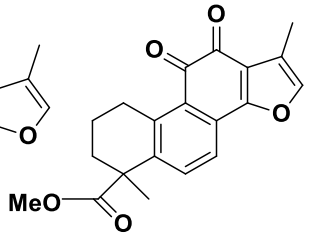

Methyl tanshionate

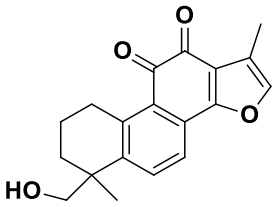

Tanshinone IIB

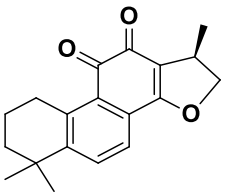

Cryptotanshinone

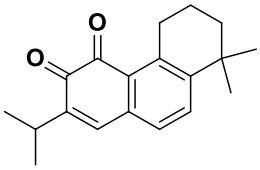

Rosmariquinone

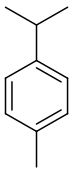

p-cymene

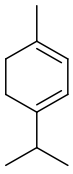

α-Terpinene

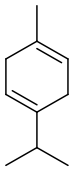

γ-Terpinene

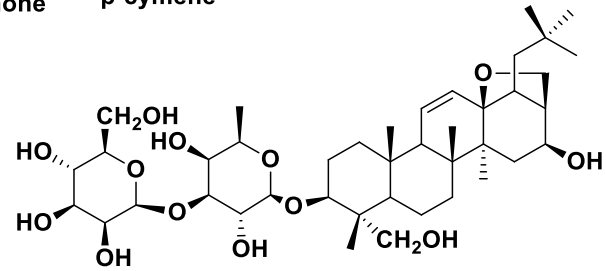

Saikosaponin A

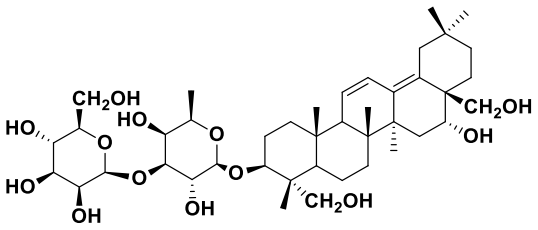

Saikosaponin B2

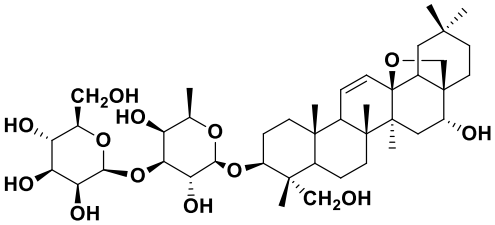

Saikosaponin D

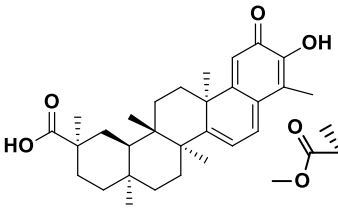

Celastrol

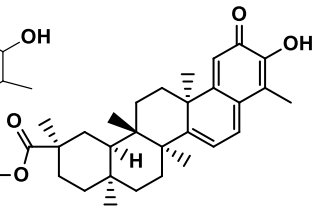

Pristimerin

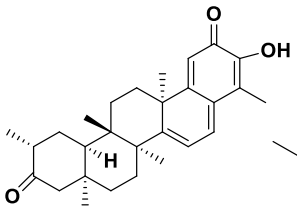

Tingenone

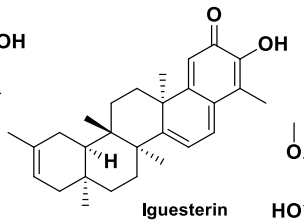

Iguesterin

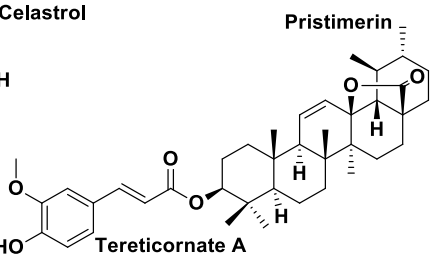

Tereticornate A

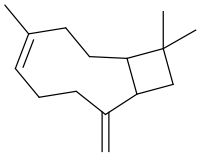

Beta-caryophyllene

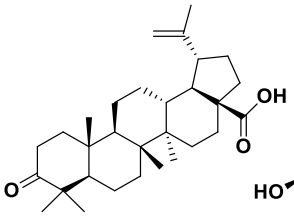

Betulonic acid

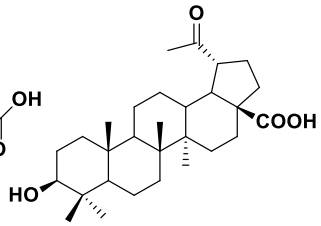

Betulinic acid

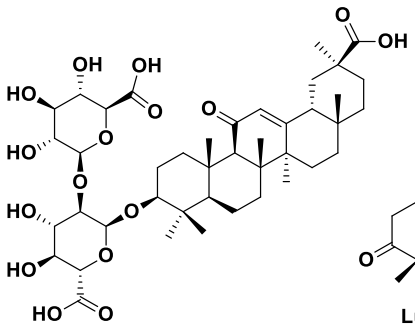

Glycyrrhizin

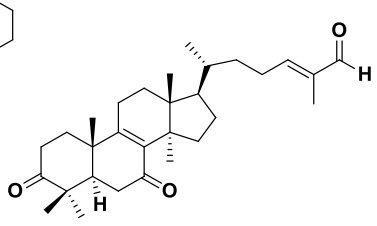

Lucialdehyde B

Annex F1 : Structures of selected plant-based secondary metabolites

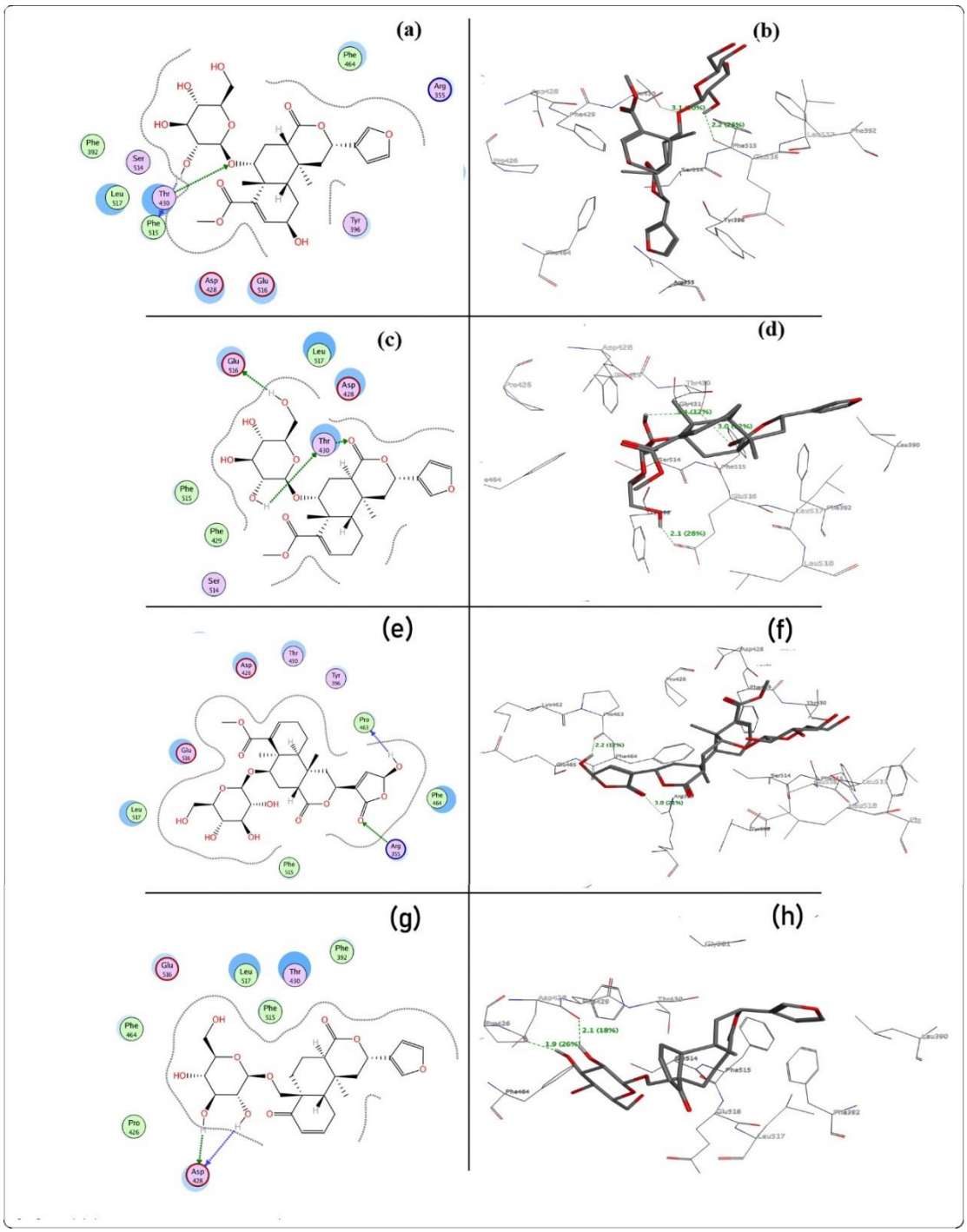

Appendix F2: a) 2D and **b)** 3D interaction of borapetoside B with spike protein (Fitness score 54.52); **c)** 2D and **d)** 3D interaction of borapetoside C with spike protein (Fitness score 53.68); **e)** 2D and **f)** 3D interaction of palmitoside G with spike protein (Fitness score 50.80); **g)** 2D and **h)** 3D interaction of rumphioside A with spike protein (Fitness score 50.77).

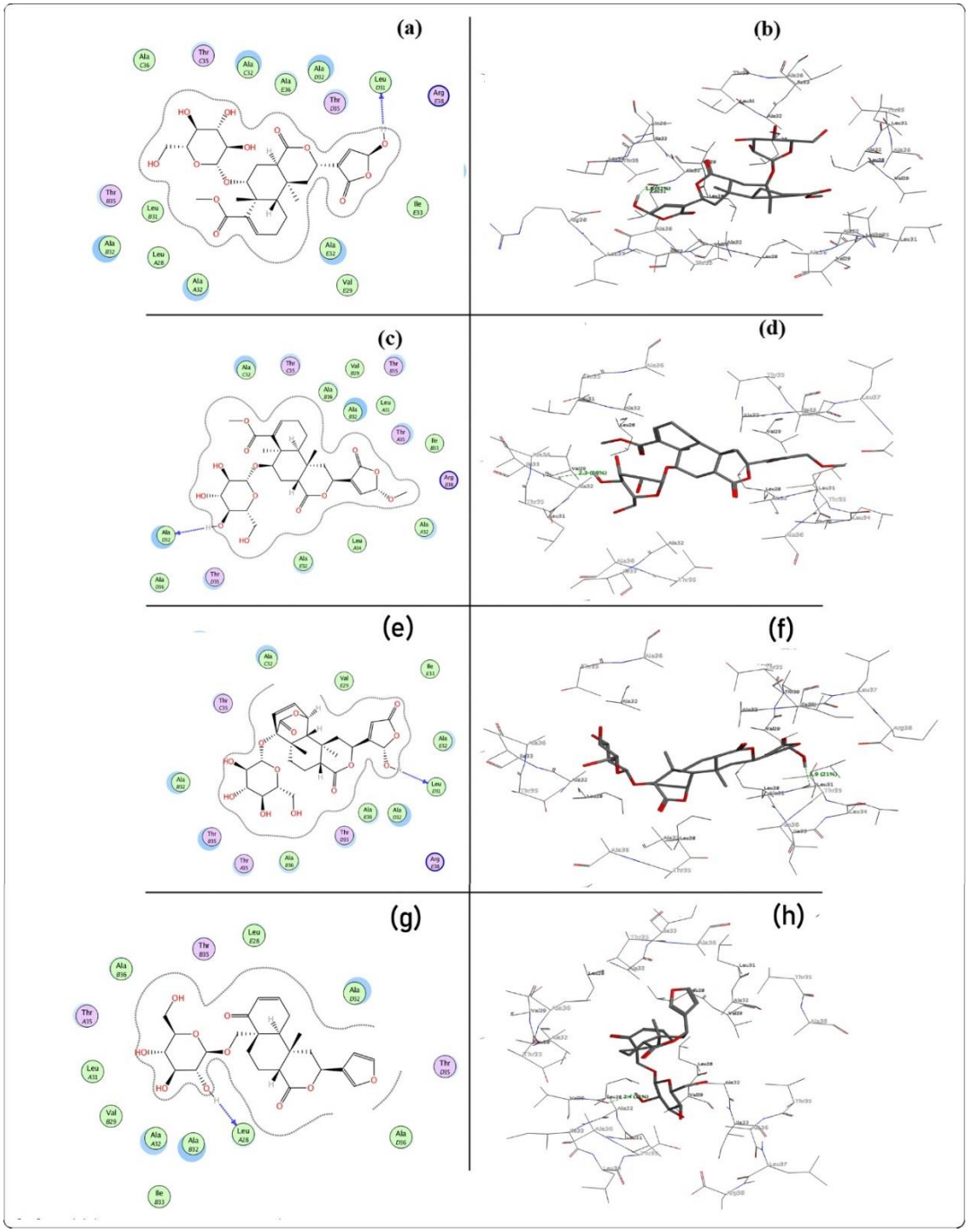

Appendix F3: a) 2D and **b)** 3D interaction of rumphioside B with spike protein (Fitness score 57.87); **c)** 2D and **d)** 3D interaction of rumphioside A with spike protein (Fitness score 55.87); **e)** 2D and **f)** 3D interaction of cordifolide C with spike protein (Fitness score 53.08); **g)** 2D and **h)** 3D interaction of palmitoside G with spike protein (Fitness score 52.41).

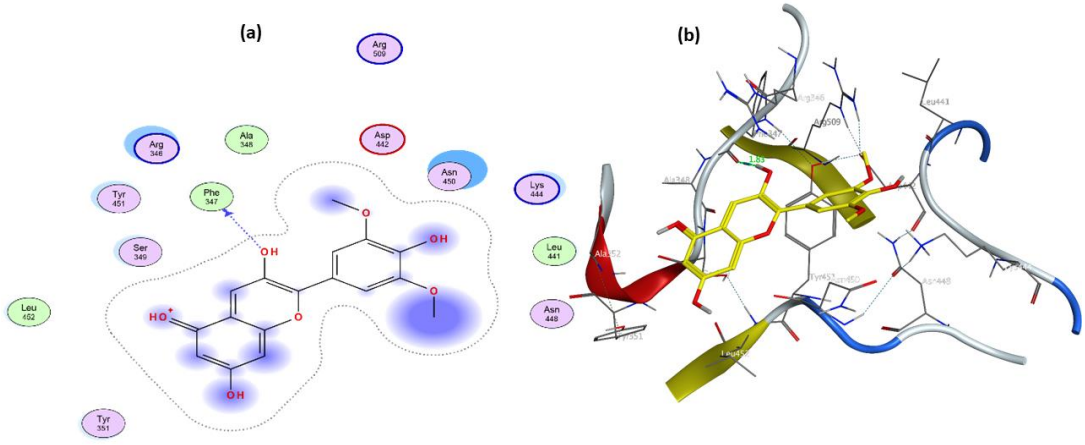

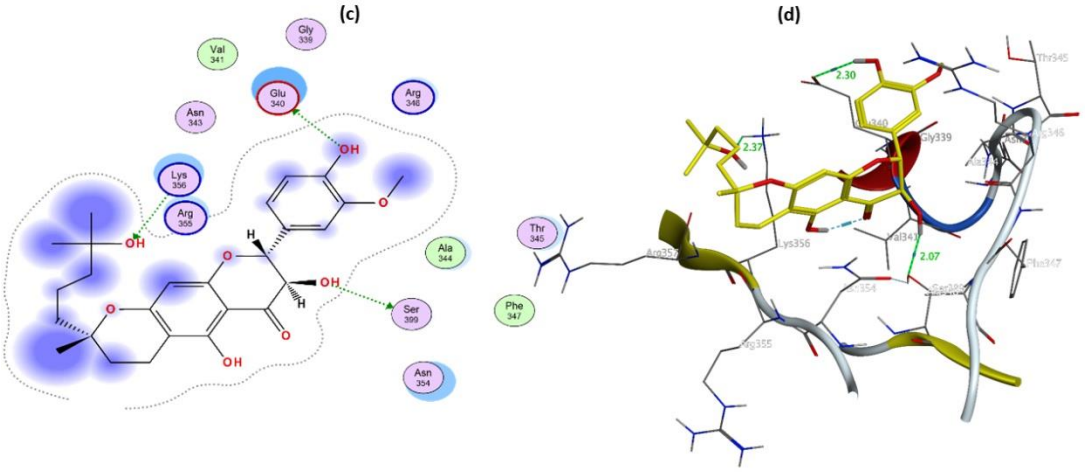

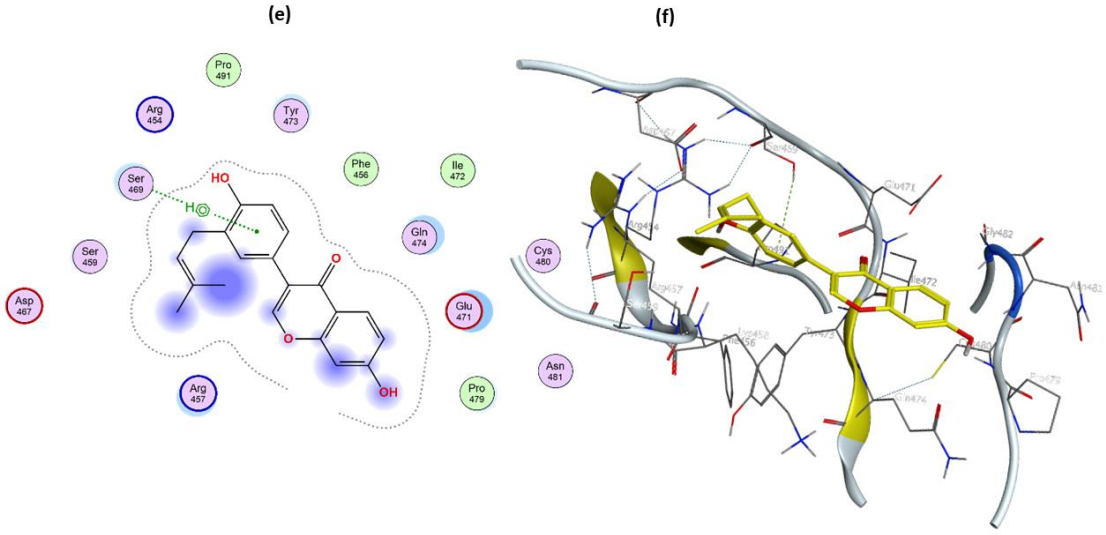

Appendix F4: 2D and 3D structures of Malvidin, Tomentin E, and Neobavaisoflavone complexed with SARS-CoV-2 spike protein.

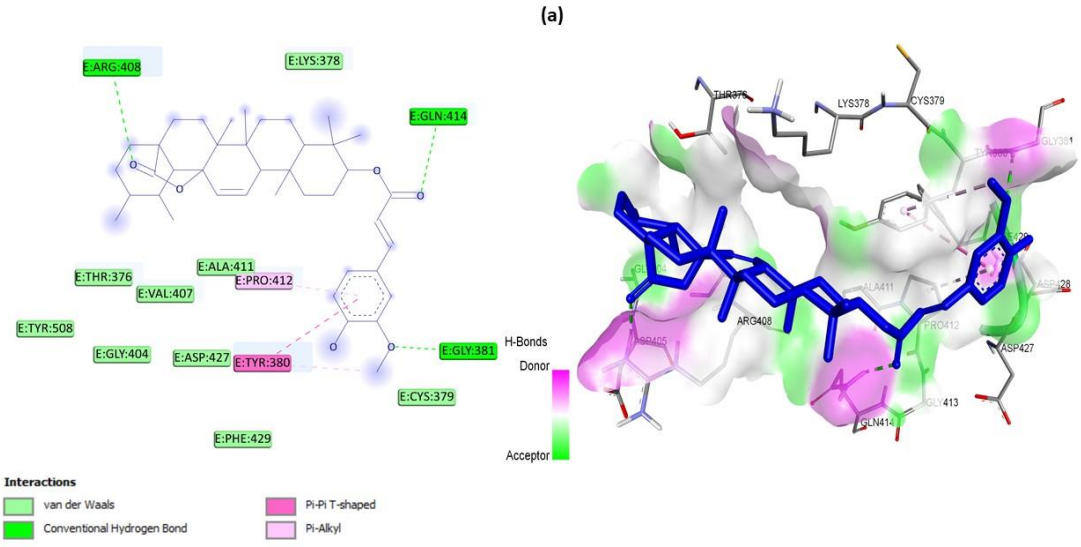

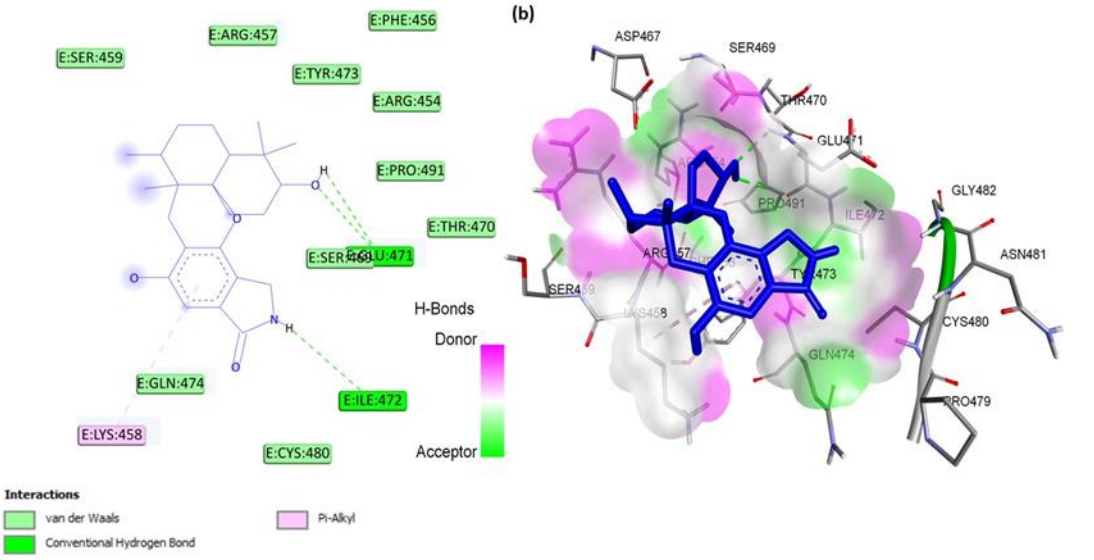
(b)
E:PHE:456
E:ARG:457
E:SER:459
E:TYR:473
E:ARG:454
E:PRO:491
E:THR:470
E:SER:469
E:GLU:471
E:GLN:474
E:ILE:472
E:LYS:458
E:CYS:480
H-Bonds
Donor
Acceptor
ASP467
SER469
THR470
GLU471
PRO491
ILE472
GLY482
ASN481
ARG457
TYR473
SER459
LYS458
CYS480
GLN474
PRO479
Interactions
van der Waals
Pi-Alkyl
Conventional Hydrogen Bond

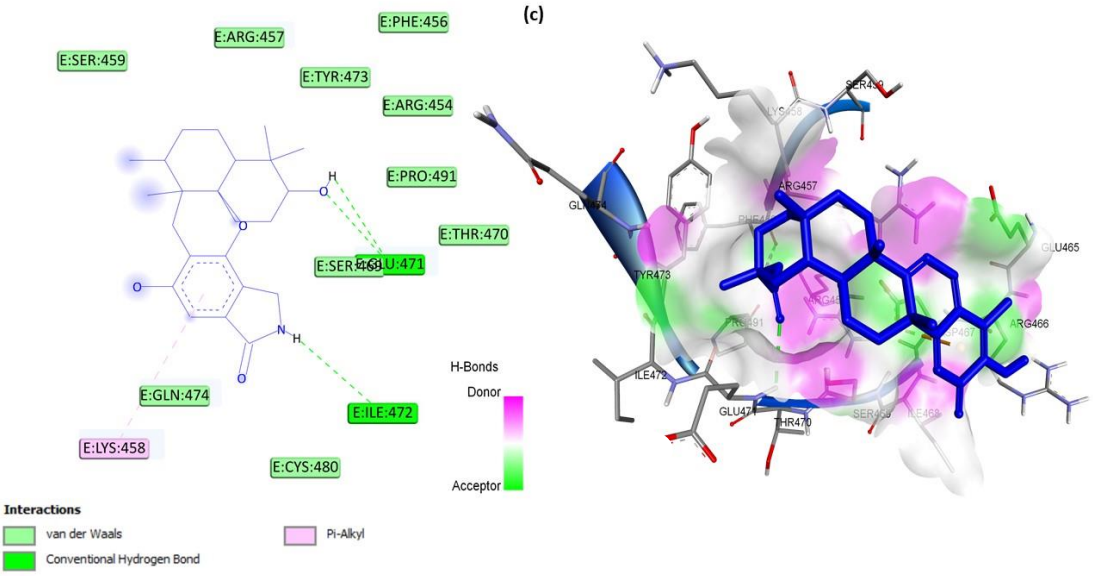
(c)
E:PHE:456
E:ARG:457
E:SER:459
E:TYR:473
E:ARG:454
E:PRO:491
E:THR:470
E:SER:469
E:GLU:471
E:GLN:474
E:ILE:472
E:LYS:458
E:CYS:480
H-Bonds
Donor
Acceptor
ARG457
TYR473
GLU465
ARG466
ILE472
GLU471
THR470
Interactions
van der Waals
Pi-Alkyl
Conventional Hydrogen Bond

Appendix F5: 2D and 3D structures of (a) tereticornate A; (b) stachyflin; and (c) pristimerin representing interaction with S1-RBD.

Appendix G: **Scientific Publications and Conference/Seminar Participation**

Appendix G1: List of Published Articles

- **A. Shrestha**, S. R. Upadhyaya, B. K. Raut, S. Bhattarai, K. R. Sharma, N. Parajuli, J. K. Sohng, B. P. Regmi, "In Silico and In Vitro Analyses of Multiple Terpenes Predict Cryptotanshinone as a Potent Inhibitor of the Omicron Variant of SARS-CoV-2", *Processes* **2024**, *12*, 230.

  https://doi.org/10.3390/pr12010230

- **A. Shrestha,** R. Marahatha, B. Regmi, S.R. Dahal, R.C. Basnyat, N. Parajuli, Molecular Docking and Dynamics Simulation of Several Flavonoids Predict Cyanidin as an Effective Drug Candidate Against SARS-CoV-2 Spike protein, Advances in Pharmacological and Pharmaceutical Sciences. Vol. 2022 (2022). https://doi.org/10.1155/2022/3742318

- S. Basnet, R. Marahatha, **A. Shrestha**, S. Bhattarai, S. Katuwal, K. R. Sharma, B.P. Marasini, S. R. Dahal, R. C. Basnyat, S.G. Patching, N. Parajuli. In Vitro and In Silico Studies for the Identification of Potent Metabolites of Some High-Altitude Medicinal Plants from Nepal Inhibiting SARS-CoV-2 Spike Protein. Molecules. 2022 Dec 15;27(24):8957.

  https://doi.org/10.3390/molecules27248957

- R. Marahatha, **A. Shrestha**, K. Sharma, B.P. Regmi, K.R. Sharma, P. Poudel, R.C. Basnyat, N. Parajuli, In Silico Study of Alkaloids: Neferine and Berbamine Potentially Inhibit the SARS-CoV-2 RNA-Dependent RNA Polymerase, Journal of Chemistry. 2022 (2022) 1–9. https://doi.org/10.1155/2022/7548802.

- S. Katuwal, S.R. Upadhyaya, R. Marahatha, **A. Shrestha**, B. P. Regmi, K. Khadayat, S. Basnet, R. C. Basnyat, N. Parajuli, "*In Silico* Study of Coumarins: Wedelolactone as a Potential Inhibitor of the Spike Protein of SARS-CoV-2 Variants", *Journal of Tropical Medicine*, vol.2023, Article ID 4771745, 19 pages, **2023**. https://doi.org/10.1155/2023/4771745

Appendix G2: Participation in Conference/Seminar

Oral and Poster Presentations at Conferences

1. **Shrestha A.,** Budhathoki R., Raut B. K., Parajuli N., (2023, September 28 – October 1). *Mass Spectrometry-based untargeted metabolomics study of Terminalia chebula* [Poster presentation]. FORCE-IICS-2023, Hyatt Regency, Kathmandu, Nepal.
2. **Shrestha A.,** Parajuli N., and Silwal M., (2023, July 9-14). *Alkaloids as Potential Phytochemicals for Inhibition of SARS-CoV-2: A Computational Approach* [Oral presentation]. 19th Asian Chemical Congress organized by Federation of Asian Chemical Societies (FACS), Istanbul Technical University, Istanbul, Turkey.
3. **Shrestha A.** and Parajui N., (2023, May 11-12). *Promising Terpenes and Terpenoids Inhibits Multiple Targets of SARS-COV-2: An In Silico Study* [Oral presentation] The First National Biotechnology Conference 2023, Kathmandu University, Nepal
4. **Shrestha A.** and Parajuli N., (2022, June 26-28). *Computational Investigation of Some Secondary Metabolites Against Spike Protein of SARS-CoV-2 Omicron Variant* [Oral presentation]. Nepal Academy of Science and Technology (NAST), 9th National Conference on Science and Technology, June 26-28, 2022, Kathmandu, Nepal
5. **Shrestha A.,** Basnyat R. C., and Parajuli N., (2022, April 4-5). *Pharmacokinetics and Molecular Docking Analysis of Some Secondary Metabolites from Natural Products for the Inhibition of SARS-CoV-2 S-RBD* [Oral presentation]. Himalayan Knowledge Conclave 2022, the 8th Graduate Conference, Surkhet, Nepal.

Seminar

- One-Day Seminar on " COVID-19 Research Project" held on 28th December 2021, Central Department of Chemistry, Tribhuvan University, Kathmandu, Nepal
- Research Project Dissemination Seminar, 27th December 2022, Central Department of Chemistry, Tribhuvan University, Kathmandu, Nepal
- One-Day Seminar on " Drug Discovery and Metabolomics" held on 11th August 2023, NIST Higher Education, Lainchour, Kathmandu, organized by UGC Research Project, Central Department of Chemistry, TU.

Training

- Trainer in the Advanced Training on Pharmacognosy, Phytochemistry, and Pharmacology held in the Department of Plant Resources, Thapathali, Nepal on March 23-29, 2022.
- Trainer in molecular docking and molecular dynamics simulation, DAV College, Sanepa, Lalitpur, Nepal

Future-Oriented Research Conferences and Exhibitions

Interdisciplinary Initiatives in Chemical Sciences

(FORCE-IICS 2023)

Sept. 28 – Oct. 01, 2023 @Hyatt Regency, Kathmandu, Nepal

ROYAL SOCIETY OF CHEMISTRY

FORCE-IICS Interdisciplinary Initiative in Chemical Sciences 2023

G20 भारत 2023 INDIA

Certificate of Participation

This is to certify that **Ms. Asmita Shrestha**, Tribhuvan University, Nepal, participated and presented a '**Brainstorming Session Poster**' in the '**FORCE IICS 2023**' conference held at **Hyatt Regency, Kathmandu, Nepal** during **Sept. 28 – Oct. 01, 2023.**

Dr. Vishal Rai, *Professor*
Dept. of Chemistry, IISER Bhopal
Convener, FORCE-IICS 2023

TURKISH CHEMICAL SOCIETY

İTÜ 250

19TH ASIAN CHEMICAL CONGRESS
19ACC
JULY 9-14, 2023 / ISTANBUL TECHNICAL UNIVERSITY, ISTANBUL, TÜRKİYE
21ST GENERAL ASSEMBLY OF THE FEDERATION OF ASIAN CHEMICAL SOCIETIES | JULY 8, 2023

CERTIFICATE OF ATTENDANCE

This is to certify that

Asmita Shrestha

has participated in the
19th Asian Chemical Congress

Mustafa Culha

Congress Chairman
Mustafa Culha

JULY 9-14, 2023
ISTANBUL TECHNICAL UNIVERSITY
ISTANBUL, TÜRKİYE


20 years
National BIOTECHNOLOGY CONFERENCE 2023
CERTIFICATE
OF APPRECIATION
The certificate is presented to
Asmita Shrestha
in recognition of their ORAL PRESENTATION
contributions as a Member of the Organizing Committee of the First National Biotechnology Conference 2023, held at Kathmandu University on May 11-12, 2023. Your dedicated efforts are highly appreciated. We value what you have done and what you will do in the years to come.
Dr. Dhurva P. Gauchan
Convener
NBC-2023
Prof. Dr. Subodh K. Upadhyaya
Co-chairperson
NBC-2023
Prof. Dr. Janardan Lamichhane
Chairperson
NBC-2023
HELIX
eppendorf
WTC


Nepal Academy of Science and Technology (NAST)
CERTIFICATE OF PARTICIPATION
Awarded to
Asmita Shrestha
for Presentation in Oral / ~~Poster~~ / ~~Participation~~ in the
9th National Conference on Science and Technology
June 26-28,2022 (Asar 12-14, 2079)
Khumaltar, Lalitpur, Nepal
Ms. Luna Vajra
Chief, Promotion Division
Prof. Dr. Mahesh K. Adhikari
Secretary
Dr. Sunil Babu Shrestha
Vice Chancellor

Eight Graduate Conference 2022

HIMALAYAN KNOWLEDGE CONCLAVE

Connecting Dots: Resources and Prosperity

Himalayan Knowledge Conclave

CERTIFICATE OF APPRECIATION

This certificate is awarded to

Asmita Shrestha

in recognition as a PRESENTER in the Eighth Graduate Conference held in Mid-West University, Birendranagar, Surkhet, Nepal on April 4-5, 2022.

Prof. Nanda Bahadur Singh, PhD
Patron
Vice-Chancellor
Mid-West University

Sudeep Thakuri, PhD
Convener
Dean, Faculty of Science and Technology
Mid-West University

Tribhuvan University
Institute of Science and Technology
Central Department of Chemistry
Kirtipur, Kathmandu

CERTIFICATE OF APPRECIATION

We present this to Mr./Mrs./Miss. Asmita Shrestha with appreciation and sincere thanks for attending the One-Day Seminar on "COVID-19 Research Project" held on 28th December 2021.

Prof. Dr. Niranjan Parajuli
President
Nepal Chemical Society

Dr. Pramod Poudel
Research Director, UGC
Special Guest

Prof. Dr. Dhyanendra Bahadur Rai
Principal, University Campus
Chief Guest

Prof. Dr. Ram Chandra Basnyat
Head CDC and Principal Investigator
Chairperson

University Grants Commission Research Projects
Central Department of Chemistry
Tribhuvan University

CERTIFICATE
OF APPRECIATION

THIS IS PRESENTED TO

Mrs. Asmita Shrestha

for their presentation at the second
Research Project Dissemination Seminar
held at the Central Department of Chemistry, Tribhuvan University
on
December 27, 2022

Pramod Poudel, Ph.D.
Special Guest
Research Director
University Grants Commission

Prem Sagar Chapagain, Ph.D.
Chief Guest
Executive Director
Research Directorate
Professor
Central Department of Geography
Tribhuvan University

Jagadeesh Bhattarai, Ph.D.
Chair
Professor & Head
Central Department of Chemistry
Tribhuvan University

Certificate of Appreciation

Granted to

Asmita Shrestha

in recognition for given an oral presentation in
one day seminar on

"DRUG DISCOVERY & METABOLOMICS"

Organized by UGC Supported Research Project, Central Dept. of Chemistry, TU
Co-organized by
NIST HIGHER EDUCATION
National Model College for Advance Learning, Lainchaur, Kathmandu
(11 August 2023)

Prof. Dr. Jagadeesh Bhattarai
Head of Department
Central Department of Chemistry
Tribhuvan University

Prof. Dr. Niranjan Parajuli
Principal Investigator
UGC Research Project
Tribhuvan University

Dr. Madhav Prasad Baral
Chief Guest
Chairman, NIST Foundation

CERTIFICATE
OF PARTICIPATION

This certificate is presented to

Asmita Shrestha

in recognition of oral presentation in

BIOLOGICAL CHEMISTRY RESEARCH SEMINAR

organized by

UGC Supported Research Project,
Central Department of Chemistry, Tribhuvan University

Prof. Dr. Paras Nath Yadav
Special Guest
Executive Director
Curriculum Development Center
Tribhuvan University

Prof. Dr. Jagadeesh Bhattarai
Chairman
Head of Department
Central Department of Chemistry
Tribhuvan University

Prof. Shankar Prasad Bhandari
Chief Guest
Secretary Member
University Grants Commission

SRTN

D.A.V. COLLEGE
Affiliated to TU

CERTIFICATE OF PARTICIPATION

This Certificate is Awarded to

Prof./Dr./Mr./Ms. Asmita Shrestha (Trainer)

for the successful completion of 2 days (April 6 to April 7)

Workshop on

"Homology Modeling, Flexible Docking and Molecular Dynamics in Drug Design"

organized by

BICID, SRTN and D.A.V. College

Mr. Shashi Bhushan Chaturwedi
Program Coordinator
D.A.V. College

Prof. Dr. Niranjan Parajuli
CDC, TU

Dr. Subin Adhikari
Trainer
SRTN